Effects of anle138b treatment on amyloid-β neurotoxicity

Dissertation

for the award of the degree

'Doctor rerum naturalium'

at the Georg-August-Universität Göttingen

within the

Georg-August University School of Science (GAUSS)

submitted by

Carolina Thomas

from La Plata, Buenos Aires, Argentina.

Göttingen, 2019

Supervisor

Prof. JeongSeop Rhee
Neurophysiology Group, Department of Molecular Neurobiology
Max Planck Institute for Experimental Medicine, Göttingen

Thesis Committee

Prof. Nils Brose
Department of Molecular Neurobiology
Max Planck Institute for Experimental Medicine, Göttingen

Prof. Christian Griesinger
Department of NMR-based Structural Biology
Max Planck Institute for Biophysical Chemistry, Göttingen

Prof. Ralf Heinrich
Department of Cellular Neurobiology
Schwann-Schleiden Research Centre, Göttingen

Members of the Examination Board

Reviewer: Prof. Nils Brose
Department of Molecular Neurobiology
Max Planck Institute for Experimental Medicine, Göttingen

Second Reviewer: Prof. Christian Griesinger
Department of NMR-based Structural Biology
Max Planck Institute for Biophysical Chemistry, Göttingen

Further members of the Examination Board:

Prof. Dr. Luis A. Pardo
Department of Molecular Biology of Neuronal Signals
Max Planck Institute for Experimental Medicine, Göttingen

Prof. Dr. Tiago Fleming Outeiro
Department of Experimental Neurodegeneration
University Medical Center Göttingen

Prof. Dr. Christine Stadelmann-Nessler
Institute for Neuropathology
University Medical Center Göttingen

Date of the oral examination: 14th August 2019.

I hereby declare that this thesis was written independently and with no other sources and aids than quoted.

Carolina Thomas

Göttingen, 15th July 2019.

Table of Contents

Abstract

Alzheimer's disease (AD), the leading etiology of dementia and the fifth cause of death worldwide, has been declared a public health priority by the World Health Organization in 2017. AD is incurable and no treatment can currently modify its natural history. Aberrant accumulation of soluble forms of the amyloid β (Aβ) peptide in AD mouse models has been associated with neuronal loss, hippocampal dysfunction and behavioral alterations, yet data about the underlying molecular synaptic changes are lacking. The novel small molecule anle138b has been found protective when orally administered, even at late stages, in an AD murine model. However, how this promising drug acts in the AD brain at a synaptic level remains unclear. One of the proposed mechanisms is the blockage of amyloid pores, a biophysical phenomenon mostly studied *in vitro*. Here, I established an *in vitro* model system of Aβ toxicity by means of incubating murine autaptic hippocampal cultures with synthetic Aβ oligomers, for functional and morphological characterization of AD-like synapses. Interestingly, I observed a marked deficit in synaptic function with no evidence of morphological or biochemical alterations. Furthermore, I preincubated the autaptic neurons with anle138b before Aβ exposure, as performed in other model membranes, to observe a putative inhibition of pore formation. In these experiments anle138b failed in protecting neurons from oligomer synaptotoxicity. In addition, I examined the membrane properties of Aβ-treated autaptic neurons. In contrast to previous literature, even though the oligomeric preparation that I used could induce pore formation in an artificial bilayer, no signs of loss of membrane integrity in neurons were found. Finally, experiments with the enantiomer AllD Aβ indicate that Aβ toxicity is stereospecific, a property that *in vitro* observed pores lack. In conclusion, I showed that Aβ oligomers impair synaptic glutamate release. These changes might be an early manifestation of AD and constitute a promising disease mechanism that requires further study and confirmation in another disease models. While anle138b failed as pore blocker, it is still possible that in the model system presented here, the autaptic glutamatergic neurons, it could act as an inhibitor of Aβ aggregation and further studies must be performed. Finally, these data suggest that pore formation is a phenomenon occurring mostly *in vitro*. This highlights the importance of carefully and comprehensively

examining the evidence from *in vitro* studies and the need for a validation in biologically relevant models when studying the mechanisms of human diseases.

Table of abbreviations

A	Amperes
AD	Alzheimer’s disease
ADAM-10	A disintegrin and metalloproteinase-10
ADDLs	Aβ-derived diffusible ligands
AFM	Atomic force microscopy
AHP	Afterhyperpolarization
AICD	APP intracellular domain
AIlD Aβ	Ent - amyloid-β peptide
AMPA	α-amino-3-hydroxy-5-methyl-4-isoxazolepropionic acid
ANOVA	Analysis of variance
APLP	Amyloid precursor like protein
ApoE	Apolipoprotein E
APP	Amyloid precursor protein
APP-CTF	APP carboxy-terminal fragment
ATP	Adenosine-5'-triphosphate
Aβ	Amyloid-β peptide
Aβ40	Amyloid-β peptide 1-40
Aβ42	Amyloid-β peptide 1-42
BACE-1	β-site APP cleaving enzyme-1
CA1	Cornu Ammonis area 1
CA3	Cornu Ammonis area 3
CaMKIV	Calcium/calmodulin-dependent protein kinase IV
CDK5	Cyclin-dependent kinase 5
CHO	Chinese hamster ovary
CN	Calcineurin
CNS	Central nervous system
DAPI	4',6-diamidino-2-phenylindole
DG	Dentate gyrus
DiphyPC	Diphytanoyl phosphatidylcholine
DIV	Day *in vitro*
DMN	Default mode network
DOPC	1,2-dioleoyl-sn-glycero-3-phosphocholine
EDTA	Ethylenediaminetetraacetic acid
EGTA	ethylene glycol-bis (β-aminoethyl ether)-N,N,N',N'-tetraacetic acid
EM	Electron microscopy
F-actin	Filamentous actin
FcγRIIb	Fc region of IgG receptor IIb
Fig.	Figure
FRET	Förster resonance energy transfer
GABA	Gamma-aminobutyric acid
GSI	Gamma secretase inhibitor
GTP	Guanosine-5'-triphosphate
h	hours
HEK	Human embryonic kidney
HEPES	4-(2-hydroxyethyl)-1-piperazineethanesulfonic acid
HFIP	1,1,1,3,3,3-Hexafluoro-2-propanol
Hz	Hertz

kDa	Kilodalton
KO	Knock-out
LilrBII	Leukocyte immunoglobulin-like receptor BII
LTP	Long-term potentiation
M	Molar
MAP	Microtubule-associated protein
MCT	Multiple comparisons test
mEPSC	Miniature excitatory postsynaptic current
MES	2- (N-morpholino) ethanesulfonic acid
mGluR5	Metabotropic glutamate receptor 5
MOPS	3- (N-morpholino) propanesulfonic acid
ms	millisecond
NIA-AA	National Institute on Aging - Alzheimer's Association
NMDA	N-methyl-D-aspartate
NMR	Nuclear magnetic resonance
NSAIDs	Nonsteroidal anti-inflammatory drug
P0	Pellet at time = 0
PAGE	Polyacrylamide gel electrophoresis
PBS	Phosphate-buffered saline
PD	Parkinson's disease
PFA	Paraformaldehyde
PIP_2	Phosphatidyl Inositol (4,5) biphosphate
PirB	Paired immunoglobulin-like receptor B
PLL	Poly-L-lysine
POPE	1-palmitoyl-2-oleoyl-*sn*-glycero-3-phosphoethanolamine
POPS	1-palmitoyl-2-oleoyl-sn-glycero-3-phospho-L-serine
PPF	Paired-pulse facilitation
PrP^C	Cellular prion protein
PS	Presenilin
PSD	Postsynaptic density
Pvr	Vesicular release probability
RRP	Readily releasable pool
S	Siemens
S0	Supernatant at time = 0
sAPP	Soluble APP
SC	Schaffer collateral
Sc or Scr	Scrambled
SDS	Sodium dodecyl sulfate
SEM	Standard error of the mean
Sh+	Shank2 Positive
SNARE	Soluble NSF attachment proteins (SNAP) receptor
Sum.	Summary
Syn.	Synaptic
TBS	Tris-buffered saline
TEM	Transmission electron microscopy
TIRF	Total internal fluorescence reflection
TTX	Tetrodotoxin
TwA	Two-way ANOVA
US FDA	United States Food and Drugs Administration

V	Volts
VG+	VGluT1 positive
Vm	Membrane Voltage
w/v	Weight/volume
WT	Wild type
α7-nAchR	α7-nicotinic acetylcholine receptor

List of figures

List of tables

1. Introduction

1.1. Alzheimer's disease and the amyloid cascade hypothesis

Memory, the ability to acquire, store and retrieve information, is an essential process that allows us to perform in our daily life and, in all its modalities, constitutes the basis of individuality. The loss of this vital brain function is the cardinal symptom of dementia, a devastating neuropsychiatric disorder that affects approximately 50 million people worldwide (WHO, 2017a). With an estimated incidence of one new case every three seconds and 58% of the people with dementia living in low-medium income countries (Prince *et al.*, 2015), dementia has been declared a public health priority by the World Health Organization in 2017 (WHO, 2017b, 2018). Clinically, dementia was defined in 2011 by the National Institute on Aging - Alzheimer's Association (NIA-AA) Workgroups as the presence of progressive and incapacitating cognitive decline affecting at least two of the following domains: ability to acquire and remember new information, reasoning and handling of complex tasks, visuospatial abilities, language function and/or changes in personality or comportment (McKhann *et al.*, 2011). The etiology of 60-70% of the cases of dementia is Alzheimer's disease (AD) (WHO, 2017b), a syndrome characterized by insidious onset of a multidomain cognitive decline, frequently with amnestic presentation (McKhann *et al.*, 2011). Histopathological AD diagnosis and staging have classically occurred postmortem and relied on the presence, quantity and distribution of amyloid plaques and neurofibrillary tangles (Hyman *et al.*, 2012). Amyloid plaques are extracellular deposits of amyloid β (Aβ), a 38-43 amino acid peptide that can aggregate into insoluble, β-pleated-sheet-rich fibrils. These fibrils are present in the so called dense-core or neuritic plaques, which are a specific finding of AD, in contrast with diffuse plaques that occur also in normally aged individuals (Delaère *et al.*, 1990; Serrano-Pozo *et al.*, 2011). Plaques are mainly distributed along the isocortex, while the allocortex and deep nuclei are compromised to a lesser extent and in later stages of the disease (Thal *et al.*, 2002). The histopathological burden of plaques correlates poorly with the presence of clinical symptoms (Arriagada *et al.*, 1992; Dickson *et al.*, 1992). Aβ deposits can also be found in the tunica media of small-medium size blood vessels constituting the pathological lesions called cerebral amyloid angiopathy,

found in ~80% of the AD patients (Jellinger, 2002). Neurofibrillary tangles are intracellular deposits of hyperphosphorylated and aggregated tau, a microtubule associated protein. The deposit of neurofibrillary tangles follows a predictable spatiotemporal distribution according to the staging by Braak and Braak, with initial compromise of limbic regions and later spreading towards associative cortical areas and subcortical nuclei (Braak and Braak, 1991). Aggregated tau deposition, unlike amyloid plaque accumulation, correlates with the magnitude of cognitive decline (Arriagada *et al.*, 1992). In addition to the "positive findings" that constitute Aβ and hyperphosphorylated tau deposition there are "negative findings", namely neuronal and synaptic loss. These negative findings, which match the topographical distribution of tangle deposition, are the best correlate of cognitive decline and are responsible for the atrophy of cortical areas in AD (Scheff, DeKosky and Price, 1990; Terry *et al.*, 1991; Gómez-Isla *et al.*, 1997; Ingelsson *et al.*, 2004).

With the advent of reliable biomarkers such as the detection of Aβ and tau in cerebrospinal fluid or positron emission tomography using Aβ and tau ligands, it is now possible to trace *in vivo* the progression of the histopathological lesions (Olsson *et al.*, 2016; Villemagne *et al.*, 2018). In this context, the 2018 NIA-AA Research Framework proposed a conceptual shift to defining AD as a bio-pathological entity, regardless of the clinical symptoms; '"Alzheimer's disease" refers to an aggregate of neuropathological changes and thus is defined *in vivo* by biomarkers and by postmortem histopathological examination, and not by clinical symptoms (Jack *et al.*, 2018). The authors explain that the clinical presentation has low sensitivity and specificity to detect AD and for this reason should not be considered necessary for the diagnosis, although the severity of the symptoms is used in the staging of AD (Serrano-Pozo *et al.*, 2014; Ossenkoppele *et al.*, 2015; Jack *et al.*, 2018). This new paradigm defines a pathological continuum ("Alzheimer's continuum") that begins with biomarker signs of Aβ deposition and progresses in later stages with tau accumulation and neuronal loss, regardless of the clinical presentation (Jack *et al.*, 2013, 2018). AD is now considered as the presence of an *in vivo* biomarker or postmortem histopathological evidence of concomitant Aβ and tau accumulation. There is a great advantage in such a radical change in the paradigm of the AD definition: this pathological rather than clinical conception of the disease includes in the Alzheimer's continuum stages of the illness that occur 15-20 years before the

onset of the symptoms. This opens the doors to the description and understanding of events happening at the beginning of the natural history of the disease and will facilitate the study and implementation of earlier therapeutic interventions (Jack *et al.*, 2018).

Although Aβ deposition appears early in the Alzheimer's continuum and correlates poorly with cognitive symptoms, great efforts and resources have been invested into researching its causative role in dementia (Arriagada *et al.*, 1992; Villemagne *et al.*, 2013). Solid evidence supports the so called "amyloid cascade hypothesis", which posits that accumulation of Aβ initiates the pathological events that end in hyperphosphorylated tau deposition and massive neurodegeneration (Hardy and Higgins, 1992; Hardy and Selkoe, 2002; Selkoe and Hardy, 2016). A first hint of a causal relationship is given by the fact that both patients carrying mutations in the genes related to the amyloid precursor protein (APP) and its processing into Aβ as well as individuals living with Down syndrome, who have an extra dose of the APP gene, develop a form of early onset dementia before the age of 60 years (St. George-Hyslop *et al.*, 1987; Tanzi and Bertram, 2005). Furthermore, the apolipoprotein E (ApoE), whose allele ε4 is the most important risk factor for late-onset AD, has been related to the regulation of Aβ clearance in the brain (Castellano *et al.*, 2011). Finally, although tau deposition can precede Aβ accumulation, the pathogenic mutations in the gene encoding for tau do not cause amyloid plaque deposition or AD (Jack *et al.*, 2013; Spillantini and Goedert, 2013). Overall, despite being a topic of heated debate, the amyloid cascade hypothesis with its variations and updates is still valid after more than 25 years (Herrup, 2015; Karran and De Strooper, 2016). In this context, considering that Aβ is responsible for tau deposition and ultimately for neurodegeneration, the question that has remained unanswered is what cellular and molecular events link them, *i.e.*, what the mechanism of toxicity is.

1.2. Physiology of APP and its cleavage products

1.2.1. APP structure

APP was first sequenced and localized to chromosome 21 in 1987 a few years after its proteolytic product, Aβ, was isolated from cerebrovascular deposits (Glenner and Wong, 1984; Goldgaber *et al.*, 1987; Kang *et al.*, 1987; Tanzi *et al.*, 1987). The APP gene can produce three isoforms of the single-pass

transmembrane protein of 695, 751 and 770 amino acids in length via alternative splicing (Matsui *et al.*, 2007). In addition, two more members of the APP family exist in mammals, the APP-like protein 1 and 2 (APLP-1 and -2) (Wasco *et al.*, 1992, 1993). For schematic representation of APP structure, see Figure 1. The extracellular portion of APP is composed of two folded domains, E1 and E2, separated by a flexible acidic region and a Kunitz-type protease inhibitor domain, the latter being absent in the shortest APP_{695} isoform. The intracellular domain is intrinsically disordered and is linked to the extracellular domain by the juxtamembrane - transmembrane regions (Coburger *et al.*, 2013; Müller, Deller and Korte, 2017). The structure of the entire protein has not been resolved yet, but data are available for the E1 subdomain, the E2 and the intracellular tail (Rossjohn *et al.*, 1999; Barnham *et al.*, 2003; Keil *et al.*, 2004; Wang and Ha, 2004; Dahms *et al.*, 2010). The APP extracellular domains can dimerize forming cis-, trans- or heparin-mediated interactions as well as heterodimers with other family members, in addition to binding components of the extracellular matrix (Kibbey *et al.*, 1993; Scheuermann *et al.*, 2001; Ho and Südhof, 2004; Soba *et al.*, 2005; Dahms *et al.*, 2010). These contacts have been shown to modulate APP neurotrophic and synaptogenic functions (Wang *et al.*, 2009). The E1 region also contains a copper-binding domain that is thought to act as a metal buffer, since knock-out (KO) mice lacking APP or APLP2 show increased copper

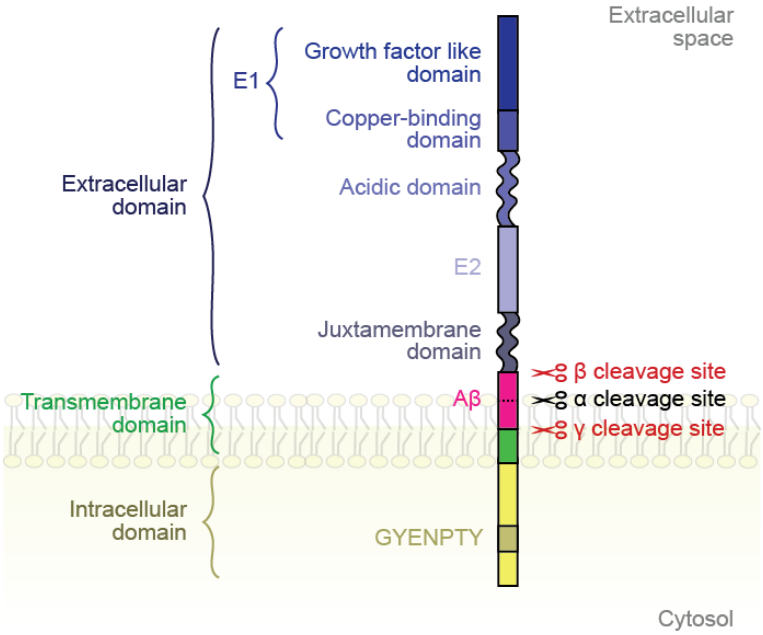

Figure 1. **APP structure and cleavage sites of the secretases.** The schematic represents a molecule of APP inserted into the plasma membrane, and its corresponding domains. The sites of cleavage by the secretases surrounding the Aβ region are indicated.

concentration in the cerebral cortex (White *et al.*, 1999). The intracellular domain contains a conserved GYENPTY sequence that plays an important role in trafficking and clathrin-mediated endocytosis of APP, which in turn can regulate Aβ production (Perez *et al.*, 1999). In addition, the cytoplasmic tail can bind adaptor molecules such as X11/Mint and Fe65 and it is required for the synaptogenic effects of APP (Borg *et al.*, 1996; Tamayev, Zhou and D'Adamio, 2009; Wang *et al.*, 2009). Finally, the transmembrane region contains in APP, but not in APLP-1 or -2, the Aβ peptide sequence, whose effects on synaptic transmission will be investigated in the present study.

1.2.2. APP synthesis and processing

APP is synthesized in the endoplasmic reticulum, trafficked to the trans-Golgi network and targeted to the plasma membrane in the secretory pathway (Weidemann *et al.*, 1989). In neurons, APP is modified by N- and O-glycosylation during its production and transported to both the axonal and somatodendritic compartments (Kins *et al.*, 2006; Laßek *et al.*, 2013). A set of α-secretases in the plasma membrane surface can shed the APP ectodomain releasing soluble APPα (sAPPα) and leaving the membrane-anchored fragment αAPP carboxy-terminal fragment (αAPP-CTF) (Sisodia, 1992; Parvathy *et al.*, 1999). The physiologically essential enzyme in the group of α-secretases is a disintegrin and metalloproteinase-10 (ADAM-10) (Kuhn *et al.*, 2010). The αAPP-CTF can be subsequently cleaved at the transmembrane region by the γ-secretase producing the extracellular p3 fragment and the APP intracellular domain (AICD) (Haass and Selkoe, 1993). The γ-secretase is a protein complex localized at the plasma membrane and endosomal compartment formed by four subunits: a presenilin (PS1 or 2) with the aspartyl-protease function essential for the intramembrane cleavage of substrates, the presenilin enhancer-2, anterior pharynx-defective phenotype-1 and nicastrin, which stabilizes the tripartite complex (De Strooper *et al.*, 1998; Kaether, Haass and Steiner, 2006; Zhao *et al.*, 2010). For schematic representation of the processing pathways see Figure 2. The α-secretase cleaves APP within the Aβ region, and therefore this processing pathway is described as non-amyloidogenic. Alternatively, if APP is endocytosed without passing through α-processing, sequential cleavage by the β- and γ- secretases occur in the acidic environment of endosomes generating intraluminal Aβ peptide

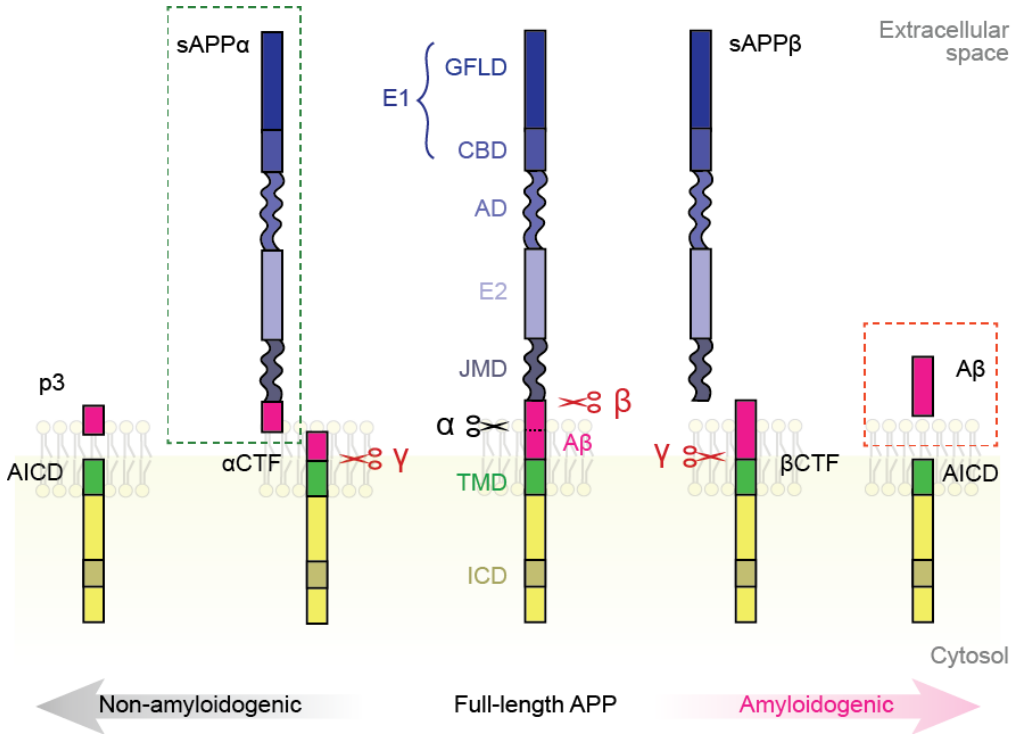

Figure 2. APP processing pathways and cleavage products. APP is cleaved in a first step by the α-secretase, ADAM10, in the non-amyloidogenic pathway (left), and by the β- secretase, BACE-1, in the amyloidogenic pathway (right). The α-shedding releases sAPPα (left, green dashed line), which is believed to be responsible for the physiological trophic effects attributed to APP. Sequential cleavage by BACE-1 and the γ-secretase produces Aβ (right, red dashed line), which accumulates extracellularly in AD and might be the culprit for neurodegeneration.

(Vassar *et al.*, 1999). There is only one β-secretase for APP named β-site APP cleaving enzyme-1 (BACE-1), which is most active in the endocytic compartment (Vassar *et al.*, 1999; Kaether, Haass and Steiner, 2006). At rest, dendritic BACE-1 is located in vesicles that do not contain APP (Sannerud *et al.*, 2011). However, under situations of increased neuronal activity, APP enters the endocytic pathway where APP and BACE-1 can be physically in contact (Das *et al.*, 2013, 2016). This amyloidogenic processing pathway produces the sAPPβ and AICD fragments in addition to giving rise to endosomal accumulation of Aβ, which once secreted is the main component of neuritic plaques, a hallmark of AD.

1.2.3. Effects of APP and APLPs genetic deletion on the murine central nervous system (CNS)

APP KO mice are viable and fertile but show a 15-20% body weight reduction, abnormal grip strength and altered locomotor activity when compared to wild-type (WT) littermates (Zheng *et al.*, 1995). Histological analysis reveals astrogliosis in several cortical areas, and reduced overall cell size and dendrite length has been reported in Cornu Ammonis area 1 (CA1) pyramidal neurons of

these animals (Zheng *et al.*, 1995; Seabrook *et al.*, 1999). Electrophysiological characterization of pyramidal neurons of the CA1 area shows a reduction in long-term potentiation (LTP) using acute hippocampal slices from aged mice (>12 months), with conserved membrane properties and unchanged paired-pulse facilitation (PPF) (Dawson *et al.*, 1999; Seabrook *et al.*, 1999). In turn, paired-pulse depression is reduced in APP KO gamma-aminobutyric acid (GABA) -ergic synapses in the CA1, and similar effects can be found in hippocampal and striatal APP KO GABAergic neurons in dissociated cultures, accompanied by increased expression levels of L-type calcium channels (Seabrook *et al.*, 1999; Yang *et al.*, 2009). The behavioral consequences of APP deletion consist of impaired learning and spatial memory in aged animals but not in young ones, as evidenced in the conditioned avoidance and water maze tests, as well as altered declarative long-term memory indicated by poor performance using a novel-object recognition test (Dawson *et al.*, 1999; Ring *et al.*, 2007; Zou *et al.*, 2016). Furthermore, biochemical abnormalities have also been found in tissue from APP KO animals, such as elevated copper concentrations in the brain and liver (White *et al.*, 1999), and increased brain levels of cholesterol and sphingomyelin (Grimm *et al.*, 2005). Another mouse line expressing a truncated form of APP has been generated (Müller *et al.*, 1994). Commissural alterations such as agenesis of the corpus callosum was observed in these mice, in addition to hypersensitivity to kainate-induced seizures (Steinbach *et al.*, 1998).

While single genetic deletion of APLP-1 or APLP-2 induces no striking phenotypes, combined KO of APLP-2 with either or both APP or APLP-1 results in a lethal perinatal phenotype, most likely due to alterations in the neuromuscular junction with normal brain morphology (von Koch *et al.*, 1997; Heber *et al.*, 2000; Wang *et al.*, 2005; Klevanski *et al.*, 2014). Finally, constitutive triple KO of APP, APLP-1, and APLP-2 also die after birth due to neuromuscular junction defects, but exhibit cortical dysplasia that resembles cobblestone lissencephaly with loss of Cajal-Retzius cells (Herms *et al.*, 2004).

Collectively, these data indicate that the members of the APP family are essential for the correct development of the CNS, neuronal, dendritic and spine growth, and adequate functioning of hippocampal synapses.

1.2.4. Role of APP cleavage products on neuronal morphology and function

While it is clear that APP plays an important role in CNS physiology, it is possible that its attributed functions are actually exerted by cleavage fragments produced in the amyloidogenic and non- amyloidogenic processing pathways (reviewed in Müller and Zheng, 2012; Andrew *et al.*, 2016; and Müller, Deller and Korte, 2017).

sAPPα, a secreted molecule produced by α- and γ-processing, is the main candidate that could mediate the neurotrophic effects of APP. Its expression is sufficient to rescue the lethal phenotype induced by knocking out both APP and APLP-2 genes, restoring the reduced grip force as well as the defective performance in the Morris water maze and Schaffer collateral (SC)/CA1 LTP deficits in aged animals (Ring *et al.*, 2007). Similar restorative effects can be observed on LTP at SC synapses when the aforementioned two genes are deleted specifically in the forebrain, and exogenous recombinant sAPPα is acutely applied in the artificial cerebrospinal fluid at low nanomolar concentrations (Hick *et al.*, 2015). Interestingly, higher concentrations of the homologous sAPPβ fragment, a molecule lacking the last 16 amino acids of sAPPα, fails to rescue the LTP defects in the forebrain-specific APP/APLP-2 double KO (Hick *et al.*, 2015). Furthermore, knocking in a gene encoding the sAPPα sequence can rescue the alterations in spine density and morphology in APP-KO CA1 neurons (Weyer *et al.*, 2014). In addition to the trophic effects on the KO backgrounds, exogenous recombinant sAPPα applied at low nanomolar concentrations enhances *in vivo* LTP in the dentate gyrus (DG) of anesthetized rats and N-methyl-D-aspartate (NMDA) -receptor mediated currents during high frequency stimulation on granule cells of acute hippocampal slices (Taylor *et al.*, 2008). sAPPα also interacts with the sushi1 subunit of the $GABA_B$ receptor, reducing the vesicular release probability (Pvr) in cultured murine hippocampal neurons and incrementing short term facilitation in acute hippocampal slices on SC/CA1 synapses (Rice *et al.*, 2019). Several lines of investigation have also indicated that sAPPα could play a role as a modulator of the processing pathway of its parent molecule, APP, and mitigate neurodegeneration. Obregon *et al.* demonstrated that sAPPα physically interacts with BACE1 *in vitro* and prevents APP cleavage in the amyloidogenic pathway, reducing Aβ deposition and neuritic plaques in the hippocampus and cortex of transgenic $APP_{Swe}/PS1_{\Delta E9}$ mice (for description of the $APP_{Swe}/PS1_{\Delta E9}$ mutation, see section 1.3.2) (Obregon *et al.*,

2012). Additionally, Deng *et al.* showed that sAPPα reduces tau phosphorylation by enhancing phosphorylation, and thus inactivation, of glycogen synthase kinase 3 β in SH-SY5Y cells and transgenic $APP_{Swe}/PS1_{\Delta E9}$ mice (Deng *et al.*, 2015). Finally, overexpression of sAPPα rescues behavioral, morphological and biochemical changes in $APP_{Swe}/PS1_{\Delta E9}$ transgenic mice, possibly by enhancing microglial function (Fol *et al.*, 2016).

α- or β- proteolysis of APP releases APP-CTFs. A wide range of neurotoxic effects are associated with increased concentrations of these peptides either by intraventricular injection, transgenic introduction in a murine model or by inhibiting the γ-secretase (Nalbantoglu *et al.*, 1997; Song *et al.*, 1998; Bittner *et al.*, 2009; Mitani *et al.*, 2012; Tamayev *et al.*, 2012). Reduced density and altered shape of spines as well as astro- and microgliosis are morphological and histopathological consequences of APP-CTFs accumulation (Nalbantoglu *et al.*, 1997; Bittner *et al.*, 2009). In addition, mice with increased brain concentrations of APP-CTFs exhibit reduced performance in spatial memory tests like the Morris water maze and the Y-maze, and in a contextual memory test (Nalbantoglu *et al.*, 1997; Song *et al.*, 1998; Mitani *et al.*, 2012). Regarding the electrophysiological consequences, LTP impairment has been associated with increased APP-CTFs in the hippocampus (Nalbantoglu *et al.*, 1997). Moreover, recently these peptides have been shown to modulate presynaptic function via regulation of synaptotagmin-7 expression (Barthet *et al.*, 2018). Accumulation of APP-CTFs in acute hippocampal slices of PS1/2 conditional double-KO reduces presynaptic facilitation and synaptic vesicle replenishment as well as synaptotagmin-7 concentrations in the mossy fiber/CA3 synapses (Barthet *et al.*, 2018).

In addition to the canonical APP processing pathways, novel cleaving enzymes have been described whose products could modulate synaptic function. Namely, the proteolytic products of the η-secretase, in particular the Aη-α has been shown to impair LTP in SC synapses and to reduce neuronal CA1 activity *in vivo* (Willem *et al.*, 2015). In an alternative cleavage path, the successive proteolysis of CTFs by caspases -3, -6 and -8 and γ- secretase produces an intracellular fragment denominated JCasp (Fanutza *et al.*, 2015). The peptide binds *in vitro* to release machinery proteins such as synaptotagmin-2 and synaptobrevin-2, and its intracellular application reduces basal synaptic transmission and Pvr in APP-

containing synapses of the CA1 region of acute hippocampal slices (Fanutza *et al.*, 2015).

1.2.5. Physiological role of Aβ at the synapse

Aβ, the APP product used in this study, is produced as a consequence of normal neuronal metabolism in the 40 amino acid variant, and its production is increased with neuronal activity (Haass *et al.*, 1992; Mori *et al.*, 1992; Seubert *et al.*, 1992; Shoji *et al.*, 1992; Kamenetz *et al.*, 2003; Cirrito *et al.*, 2005). Toxic effects aside, only few studies have been performed to decipher the physiological role of Aβ on synapses, most of them concluding that it enhances synaptic transmission (see Table 1). Experiments where picomolar concentrations of "aged" Aβ 1-42 (Aβ42) were injected into mouse hippocampi showed that the peptide enhanced LTP in the CA1 and improved performance in the Morris water maze in a mechanism dependent on the α7 nicotinic acetylcholine receptor (α7-nAchR) (Puzzo, Privitera, Leznik, Fà, Staniszewski, Palmeri and Arancio, 2008; Puzzo *et al.*, 2011). Similar effects were found by visualizing anti-synaptotagmin-1 antibody uptake in rat neuronal cultures treated with thiorphan, an inhibitor of neprilysin and Aβ degradation, or with application of exogenous Aβ at high picomolar concentration (Lazarevic *et al.*, 2017). The latter experiment showed that Aβ increases the open time of α7-nAchR, enhances the activity of calcineurin (CN) and reduces cyclin-dependent kinase 5 (CDK5) activation, thus enlarging the recycling pool of synaptic vesicles and in turn diminishing the resting pool (Lazarevic *et al.*, 2017). Using a similar approach, experiments on mouse hippocampal neurons using the fluorescent membrane dye FM 1-43 to image

Table 1. Summary of physiological effects of Aβ at the synapse.

Effect	Mechanism	Citation
↑ CA1 LTP ↑ Memory formation (performance in Morris water maze)	α7-nAchR dependent	Puzzo *et al.* 2008
↑ Recycling pool of vesicles ↓ Resting pool of vesicles ↑ Pvr	α7-nAchR dependent ↑ CN - ↓ CDK5	Lazarevic *et al.* 2017
↑ Pvr - Switch synapses from low pass to high-pass filter function	↑ APP homodimers ↑ Ca^{2+} transients	Abramov *et al.* 2009 Fogel *et al.* 2014
↑ mEPSC frequency and ↑ LTP with unchanged active synapses	Actin polimerization - p38MAPK dependent	Koppensteiner *et al.* 2016

synaptic activity indicated that elevated Aβ concentrations within picomolar range increase the Pvr and switch synapses from a high-pass to a low-pass filter mode (Abramov *et al.*, 2009). Furthermore, using APP- Förster resonance energy transfer (FRET) on similar settings, *i.e.* on mouse hippocampal neurons exposed to picomolar Aβ concentrations, it was shown that APP dimerization is necessary for the enhancement of Pvr in a G-protein mediated mechanism that involves an increase in calcium transients (Fogel *et al.*, 2014). An alternative mechanism has also been proposed in which short exposure to high picomolar Aβ42 concentrations enhances LTP and miniature excitatory postsynaptic currents (mEPSC) frequency in an actin-dependent manner, with no change in the number of active synapses (Koppensteiner *et al.*, 2016). Interestingly, some of the studies mentioned above have indicated additionally that longer exposures or higher concentrations of Aβ are detrimental to synaptic transmission, in most of the cases inhibiting LTP accompanied by a poor performance on memory tests (Puzzo, Privitera, Leznik, Fà, Staniszewski, Palmeri and Arancio, 2008; Koppensteiner *et al.*, 2016).

Taken together these data point to a hormetic behavior of Aβ at the synapse, with picomolar concentrations exerting trophic functions, and nanomolar concentrations being synaptotoxic. This highlights the importance of fine-tuning Aβ concentrations at the synapse and predicts catastrophic effects for its dysregulation.

1.3. Physiopathology of Aβ and models to study AD

1.3.1. Aβ aggregation, preparations to model synaptotoxicity and the controversy of the toxic species

Aβ belongs to the group of amyloid proteins which are characterized by its propensity to adopt an alternative β-sheet-rich conformation to its native one and aggregate into large, insoluble and thermodynamically stable fibrils, structurally characterized by in-register parallel cross-β (Soto, 2003; Petkova *et al.*, 2005; Lu *et al.*, 2013; Xiao *et al.*, 2015; Soto and Pritzkow, 2018). The aggregation process of monomeric Aβ starts with a conformational change from the random coil structure into a β-strand (Hou *et al.*, 2004). Aβ primary structure is one of the factors with greatest influence in this interconversion. Using biochemical and imaging tools, Bitan *et al.* observed that Aβ 1-40 (Aβ40) and Aβ42 aggregate in

a different fashion, inducing the formation of distinct oligomeric species (Bitan *et al.*, 2003). A potential explanation for the difference in aggregation propensity between the isoforms comes from nuclear magnetic resonance (NMR) spectroscopic studies, in which an increased rigidity was observed in the C-terminus of Aβ42 which contains the extra isoleucine-alanine residues not present in the Aβ40 (Yan and Wang, 2006). In addition, several APP mutations within the Aβ region, in the vicinity of the α-cleavage site, result in enhanced amyloidogenicity (see section 1.3.2). Truncations in the Aβ N-terminus have also been observed in the AD brain, which can enhance the aggregation propensity *in vitro* (Pike *et al.*, 1991; Schieb *et al.*, 2011). Additionally, several posttranslational modifications have been reported in AD (reviewed in Kummer and Heneka, 2014). One of the most extensively studied modifications is pyroglutamylation, which enhances Aβ amyloidogenicity (He and Barrow, 1999). Pyroglutamate-3 Aβ displays a similar neurotoxic profile to Aβ42 and can be found in brains from several AD mouse models (Kawarabayashi *et al.*, 2001; Tekirian *et al.*, 2002; Christensen *et al.*, 2008; Jawhar *et al.*, 2011).

Fibrils of Aβ constitute the core of the neuritic plaques found in the brains of patients suffering from AD. Despite representing a pathognomonic feature of the disease, accumulation of plaques correlates poorly with the symptoms of dementia (see section 1.1). This observation led to questioning the toxicity of fibrils *per se* and to hypothesize that the soluble oligomeric species generated during aggregation could be the culprit for neurodegeneration. Pioneering studies using human brain tissue demonstrated that soluble Aβ concentrations serve to correctly classify and distinguish between AD patients, controls and high-pathology controls, *i.e.* non demented individuals with great load of neuritic plaques (Lue *et al.*, 1999; McLean *et al.*, 1999). But “Aβ oligomers” are far from being a unique, structurally well-defined species (Benilova, Karran and De Strooper, 2012). On the contrary, the nature of the toxic oligomer depends on the system used for its production and the tools to characterize its structural properties. Several criteria can therefore be used to classify oligomeric Aβ, namely the method of obtention (brain-derived, naturally secreted, recombinant or synthetic) (reviewed in Benilova, Karran and De Strooper, 2012; and Masters and Selkoe, 2012), whether they are intermediates in the production of fibrils (“on-” or “off-pathway”) (reviewed in Roychaudhuri *et al.*, 2009) and their binding to

conformation-specific antibodies (A11 or OC positive, among others) (Kayed *et al.*, 2010).

One of the most widely used oligomeric species are dimers - trimers of Aβ naturally secreted by the 7PA2 line of Chinese hamster ovary (CHO) cells, which stably express the APP_{Ind} (see section 1.3.2) and were developed in the Selkoe lab to investigate Aβ toxicity (Walsh *et al.*, 2002; Shankar *et al.*, 2007, 2008). Another toxic oligomeric form obtained using synthetic Aβ42 by the Klein lab are the Aβ-derived diffusible ligands (ADDLs), mostly of globular structure and proposed to be off-pathway intermediates (Lambert *et al.*, 1998; Zempel *et al.*, 2010). Within the group of brain-derived oligomers is the Aβ*56, a dodecamer which has been purified from Tg2576 mice brains (Lesné *et al.*, 2006). All of the mentioned oligomeric species induce cognitive impairment in mice or rats and have been related to tau phosphorylation, N-methyl-D-aspartate receptor-mediated toxicity, changes in synaptic transmission and cytotoxicity in neuronal hippocampal cultures (reviewed in Benilova, Karran and De Strooper, 2012).

The main advantage of *in vitro* generation of Aβ oligomers is the possibility of controlling many of the factors that modulate aggregation. Synthetic peptides allow the use of a single, well-defined and pure Aβ isoform and additionally, the buffer composition, pH, temperature, agitation conditions and salt content can be manipulated to control the kinetics of aggregation. One of the critical steps in synthetic Aβ species preparation is the peptide dissolution (Teplow, 2006). It is possible that aggregates are formed during Aβ synthesis, especially in the case of the more amyloidogenic Aβ42, which can later act as nucleation seeds (Nilsson, 2004). In order to avoid rapid and uncontrolled aggregation, several strategies have been utilized to remove large, pre-formed aggregates like dissolution in organic solvents or alkaline solutions, size-exclusion chromatography and centrifugation (Fezoui *et al.*, 2000; Teplow, 2006; Jan, Hartley and Lashuel, 2010). Once a monomeric solution is obtained, the aggregation process must be monitored and it is necessary to characterize the yielded preparation using biochemical and morphological tools in order to correlate the oligomers structure to putative toxic effects (Jan, Hartley and Lashuel, 2010). However, criticism has been raised concerning the *in vitro* Aβ preparations. While naturally produced dimers-trimers or recombinant oligomers are toxic at nanomolar concentrations, usually micromolar concentrations are

needed to reach a similar effect using synthetic peptides (Townsend, Mehta and Selkoe, 2007; Finder *et al.*, 2010). Additionally, the question remains, as to whether the *in vitro* generated species are a faithful representation of the *in vivo* situation, and therefore the experimental results can be translated to the human AD brain.

Finally, it is worth highlighting that still the nature of the "toxic oligomeric species" has neither been fully elucidated nor validated in the human situation. The concept of oligomeric Aβ toxicity arose, as stated before, with the failure of Aβ fibril deposition to correlate with and explain cognitive decline. In order to avoid a superficial description of circumstantial phenomena, it is highly desirable that studies of Aβ toxic effects always include a thorough description of the preparation used.

1.3.2. Considerations about murine models of AD

In order to study the disease progression and mechanisms, several attempts of recapitulating AD in a murine model have been made and currently up to 169 different mouse lines are available (*Research Models Search* | *ALZFORUM*, 2019). In principle, a good murine model must exhibit the histopathological features of AD, namely synaptic and neuronal loss accompanied by the presence of amyloid plaques and neurofibrillary tangles in the areas affected in patients and within a time frame that incorporates the impact of aging but also provides a therapeutic window for drug testing (Götz, Bodea and Goedert, 2018). Furthermore, these histopathological alterations must be accompanied by progressive behavioral deficits that recapitulate the cognitive decline typical of AD. Mice do not develop AD endogenously and their Aβ sequence differs from the human in three amino acids, which is sufficient to prevent aggregation. For this reason, it is necessary to induce the expression of human Aβ in order to reproduce an AD-like pathology (Esquerda-Canals *et al.*, 2017). The most widely used mouse models are transgenic, *i.e.* they have been created by random incorporation of one or multiple human genes of interest in the murine genome, such as mutant forms of APP or PS1 (Götz, Bodea and Goedert, 2018). To date, 53 APP mutations have been reported, 31 of which are known to be pathogenic (*Mutations Search* | *ALZFORUM*, 2019). APP mutations can be grouped according to their position with respect to the cleavage sites of the secretases

within the molecule (Haass *et al.*, 2012). Mutations around the α- site, such as the Dutch (E693Q) and Arctic (E693G) mutations, are contained within the Aβ region and are pathogenic in that they enhance amyloidogenicity, *i.e.* Aβ propensity to misfold and aggregate (Levy *et al.*, 1990; Nilsberth *et al.*, 2001). Mutations close to the cleavage site of the β-secretase, of which the Swedish mutation (K670/M671L) is an example, enhance the APP-BACE interaction and therefore the amyloidogenic processing, increasing the Aβ concentration (Mullan *et al.*, 1992). Finally, the mutations nearby the γ-site, such as the Indiana mutation (V717F), alter the γ-cleavage increasing the Aβ42/Aβ40 ratio (Murrell *et al.*, 1991). Some examples of transgenic mouse models carrying these mutations are the PDAPP, the first AD mouse model developed, which expresses the APP Indiana mutation under the platelet-derived growth factor-β promoter; the Tg2576 that carries the APP Swedish mutations; or the J20, which combines the Indiana and Swedish mutations and displays and earlier onset of AD-like pathology, among others (Games *et al.*, 1995; Hsiao *et al.*, 1996; Mucke *et al.*, 2000).

In addition, there are a great number of mutations in the PSEN1 gene (<200) most of which are pathogenic. The most frequently introduced mutations in AD murine models are the M146V, M146L, L286 and ΔE9, all of which increase the Aβ42/Aβ40 ratio (Esquerda-Canals *et al.*, 2017). In order to recapitulate the AD pathology, these mutations have to be co-expressed with APP mutants as in the case of the $APP_{Swe}/PS1_{\Delta E9}$ or the 5xFAD ($APP_{Swe,Lnd,Flo}$ /$PS1_{M146V,\ L286}$) mice, accelerating Aβ deposition and the onset of cognitive decline (Jankowsky *et al.*, 2001; Oakley *et al.*, 2006).

The mouse models expressing pathogenic variants of human APP alone or accompanied by PS1 mutations exhibit functional defects like impaired LTP and basal synaptic transmission starting at 6 months of age, which is accompanied by poor performance in hippocampal-dependent tasks that can appear even earlier depending on the animal model (Spires-Jones and Knafo, 2012). Interestingly, none of these models show deposition of hyperphosphorylated tau in neurofibrillary tangles, thus not recapitulating the whole spectrum of AD pathology (Götz, Bodea and Goedert, 2018). In order to model tau deposition, transgenic mouse models have been combined, such as the case of the 3xTg mice, which carry the APP_{Swe} together with $PS1_{M146V}$ and tau_{P301L} (Oddo *et al.*,

2003). Finally, knock-in and KO mice have also been developed to model the effects of protein variants which act as risk factors for late-onset AD such as ApoE and triggering receptor expressed on myeloid cells 2, among others (reviewed in Götz, Bodea and Goedert, 2018).

1.3.3. Consequences of Aβ accumulation on central synapses

Several alterations in synapse quantity, structure and function have been described associated with Aβ accumulation (see Table 2).

1.3.3.1. Alterations of synapse number and morphology

A reduction in the number of synapses is one of the hallmarks of the AD brain and was proposed to be the most relevant neuropathological correlate of cognitive impairment more than twenty years ago (Scheff, DeKosky and Price, 1990; Terry *et al.*, 1991; Ingelsson *et al.*, 2004; Duyckaerts, Delatour and Potier, 2009; Serrano-Pozo *et al.*, 2011). More recently, a study using the J20 and $APP_{swe}/PS1_{\Delta E9}$ mouse models of AD associated synapse loss with abnormal synapse pruning by phagocytic microglia activation (Hong *et al.*, 2016). In addition, a meta-analysis of 22 publications utilizing human tissue confirmed that synapses were reduced in AD-brain-affected areas and a larger loss of presynaptic markers was found in an additional review including 67 synaptic proteins (de Wilde *et al.*, 2016). However, this concept has been challenged by a study including samples from a large cohort (171 patients spread in five degrees of cognitive status) in which a reduction in synaptic proteins was poorly correlated with cognitive decline, and the correlation was found mostly in the late

Table 2. Summary of Aβ synaptotoxic effects.

Morphological alterations	Functional alterations	Network alterations
Presynapse ↓ Total vesicle pool ↓ Presinaptic markers (immunohistochemistry) **Postsynapse** ↓ Dendritic spines ↓ Dendritic branching ↓ Total synapses	**Hippocampal slices** Impaired basal synaptic transmission ↓ LTP ↑ LTD **Cultured neurons** ↓ mEPSC frequency ↓ RRP size ↓ Pvr	Impaired deactivation of the DMN Hiper- and later hippo-activation of task related areas Hypersynchrony with ↑ risk of seizures ↓ γ power

stages of dementia (Poirel *et al.*, 2018). Despite this recent controversy, the hypothesis that synapse loss contributes to impaired memory in AD remains widely accepted.

In addition to the gross reduction in synapse quantity, Aβ accumulation has also been linked to morphological anomalies in synapses. Postsynaptic changes associated with Aβ pathology include a simplification of the dendritic tree and a loss of dendritic spines. A reduction of spine density in the hippocampus has been observed in transgenic mouse models of AD such as the J20 and $APP_{swe}/PS1_{\Delta E9}$ (Moolman *et al.*, 2004). In addition, Tg2576 mice showed a loss of spines near amyloid plaques in the cerebral cortex (<15 µm away) with no changes in spine morphology (Spires *et al.*, 2005). Conversely, further studies in mice carrying this mutation indicated that the spine loss preceded plaque formation in the DG, which was accompanied by reduced freezing in fear conditioning tests (Jacobsen *et al.*, 2006). Regarding dendritic arborization, a reduction in apical dendrite branching in the somatosensory cortex was observed in aged (11-months old) Tg2576 mice. Furthermore, cultured cortical neurons from these mice showed a reduced number of dendritic crossings in Sholl analysis (Wu *et al.*, 2010). Although the pathogenic role of plaques remains controversial, the data obtained using AD mice models strengthen the inverse association between Aβ accumulation and spine number.

Similar effects to those found in murine models are observed upon increasing extracellular Aβ concentration in hippocampal slices by means of APP overexpression, incubation with naturally secreted oligomers or application of Aβ species purified from brains of patients suffering from AD (Tsai *et al.*, 2004; Shankar *et al.*, 2007, 2008; Wei *et al.*, 2010). These effects on spine density have been associated with reduced NMDA currents, loss of surface α-amino-3-hydroxy-5-methyl-4-isoxazolepropionic acid (AMPA) receptors and activation of the CN - cofilin pathway (Hsieh *et al.*, 2006; Lacor *et al.*, 2007; Shankar *et al.*, 2007; Wu *et al.*, 2010). Additionally, a direct interaction of Aβ oligomers with postsynaptic densities (PSD) has been described, accompanied by a reduction in PSD-95 staining and spine shrinkage observed in cell cultures as well as in murine and human brain tissue (Lacor *et al.*, 2004; Koffie *et al.*, 2009).

Axons and presynaptic terminals are also altered in AD. Aβ accumulation has been detected within axons and axonal terminals of patients suffering from AD

with immunolabelling and electron microscopy (EM) (Kokubo *et al.*, 2005). In addition, in synaptosomes purified from brains of AD patients, Aβ colocalizes preferentially with the remaining VGluT1-positive terminals (Sokolow *et al.*, 2012). An impaired vesicle trafficking through the axon and altered formation of presynaptic boutons induced by chemical LTP have additionally been reported upon Aβ exposure in cultured rat hippocampal neurons (Park *et al.*, 2017). In accordance with these data, incubation of mouse hippocampal neurons with high nanomolar concentrations of synthetic Aβ40 for 24 hours has been associated with a reduction in the total vesicle pool evidenced by EM and decreased expression of pre- and postsynaptic proteins in Western blots (Parodi *et al.*, 2010).

1.3.3.2. Alterations in synaptic transmission

The functional correlates of the structural changes described in the previous section include a reduced basal synaptic transmission with lower Pvr and altered short-term plasticity, impaired LTP and enhancement of long-term depression, which have been linked to a lack of memory formation in behavioral tests. In mouse models of AD, loss of LTP at SC/CA1 synapses is the earliest sign of electrophysiological hippocampal dysfunction, affecting animals as young as 2-3 months of age (Larson *et al.*, 1999; Gong *et al.*, 2004; Trinchese *et al.*, 2004; Ma *et al.*, 2010; reviewed in Spires-Jones and Knafo, 2012). After 6 months of age, basal synaptic transmission is additionally impaired in the AD mouse lines most frequently used in basic research (Chapman *et al.*, 1999; Fitzjohn *et al.*, 2001; Oddo *et al.*, 2003; Gong *et al.*, 2004; Trinchese *et al.*, 2004; Kimura and Ohno, 2009; Kimura, Devi and Ohno, 2010). Regarding short-term plasticity, only the PDAPP line shows a reduced PPF, which is observed in 4-5 months old mice. Since these animals do not exhibit amyloid deposition, the authors propose that oligomeric Aβ or other soluble APP product could alter presynaptic calcium and disrupt the mechanisms of transmitter release (Larson *et al.*, 1999). Conversely, PPF is enhanced in acute hippocampal slices from aged 27-29 month old mice form the same mouse line, which exhibit a striking loss of synapses but, surprisingly, the remaining ones display a normal function with no presynaptic alterations (Larson *et al.*, 1999).

An equivalent phenotype to that induced by transgenic expression of human APP can be triggered by exogenous application of Aβ aggregates. Altered LTP induction has been found in organotypic slice cultures exposed to exogenous oligomeric Aβ and also in *in vivo* recordings from rats injected with Aβ (Lambert *et al.*, 1998; D. M. Walsh *et al.*, 2002; Hsieh *et al.*, 2006). Similarly, a failure in LTP induction at SC/CA1 synapses was the most frequently reported functional defect in murine WT acute hippocampal slices exposed to high Aβ concentrations in the nanomolar range (Shankar *et al.*, 2008; S. Li *et al.*, 2011; Ripoli *et al.*, 2013). Furthermore, basal synaptic transmission can additionally be affected in acute slices by exposure to exogenous Aβ concentrations as low as 50 nM, as indicated by a progressive reduction of the slope of field excitatory postsynaptic potentials in the CA1 region (Talantova *et al.*, 2013). Finally, dissociated mass and autaptic hippocampal neurons exposed to high nanomolar (200 – 500 nM) extracellular Aβ concentrations for 24 hours showed a reduced evoked response accompanied by a smaller readily releasable pool (RRP) and decreased mEPSC frequency (Parodi *et al.*, 2010; Ripoli *et al.*, 2013). Interestingly, when Aβ was allowed to diffuse through the patch pipette, *i.e.* applied intracellularly, an increased paired pulse ratio was observed indicating a possible reduction in the Pvr (Ripoli *et al.*, 2014).

1.3.3.3. Neuronal network dysfunction

In association with the changes mentioned in the previous sections and possibly as their consequence, AD affects the functioning of neuronal networks (reviewed in Palop and Mucke, 2016). Using functional magnetic resonance imaging, it has been observed that patients with high amyloid deposition, mild cognitive impairment or carriers of AD associated mutations showed hippocampal hyperactivation and reduced deactivation of the default mode network (DMN) during memory encoding tasks, which has been associated with poor memory formation in healthy individuals (Bookheimer *et al.*, 2000; Sperling *et al.*, 2009, 2010; Quiroz *et al.*, 2010; Bakker *et al.*, 2012; Sepulveda-Falla, Glatzel and Lopera, 2012). Conversely, patients at later stages of AD continued suffering from a deactivation deficit of the DMN but displayed hippocampal hypoactivation (Celone *et al.*, 2006). The role of the hippocampal hyperactivation in the early stages of AD is not yet clear, but growing evidence suggests that it might be part of the pathophysiology of AD (Bakker *et al.*, 2012). Network hypersynchrony is

another dysfunction associated to amyloid accumulation and AD-related mutations observed in mouse models, for which expression of WT soluble tau is a requisite (Palop *et al.*, 2007; Roberson *et al.*, 2007; Minkeviciene *et al.*, 2009; Bezzina *et al.*, 2015; Siwek *et al.*, 2015). As a consequence of this network abnormality, patients suffering from AD have a 7-8-fold increase in the incidence of seizures when compared to controls, which is especially higher in patients suffering from early-onset AD (Amatniek *et al.*, 2006; Imfeld *et al.*, 2013; Vossel *et al.*, 2013). In addition, AD is associated with an impairment of interneuron function. Inhibitory interneurons, especially parvalbumin-positive cells, are responsible of the generation of gamma oscillations in the brain and regulate cross-frequency interactions, both of which are necessary for effective memory encoding (Sederberg *et al.*, 2006; Tort *et al.*, 2009). Several lines of evidence indicate that the power of gamma oscillations and gamma-theta coupling are impaired in AD murine models and human patients (Ittner *et al.*, 2010; Verret *et al.*, 2012; Goutagny *et al.*, 2013; Gurevicius, Lipponen and Tanila, 2013). The impairment of inhibitory interneuron function could explain the deactivation deficits in the DMN, but evidence supporting this hypothesis is still missing.

1.3.3.4. Summary of pathological changes induced by Aβ

On the whole, a great body of evidence supports the hypothesis that Aβ exposure at non-physiological concentrations has deleterious consequences on synapse number, morphology and function. Reduced number of synapses, loss of dendritic spines and morphologically aberrant axon terminals can only lead to an impaired synaptic transmission, plasticity and network function. The most prominent defects are observed in basal synaptic transmission and LTP, which are necessary for memory formation. At the network level, these mentioned phenomena and possibly others, result in abnormal activation-deactivation, network hypersynchrony and impaired oscillatory rhythms associated with dysfunction of inhibitory interneurons. The large number of models used to study Aβ-related changes can partly explain the diversity in the observed synaptotoxic effects. However, it is possible that this multiplicity of toxic effects coexists in the human AD brain acting as building blocks for cognitive decline, indicating that several pathogenic mechanisms can be activated simultaneously by Aβ accumulation.

1.3.4. Proposed mechanisms of Aβ toxicity

Although there is a consensus about the main consequences of Aβ deposition in the human and murine brain, the underlying mechanisms of toxicity have not been yet fully elucidated. However, a number of hypotheses have been proposed based on the observed Aβ interactions and biochemical, morphological and functional alterations in neurons upon treatment (Figure 3).

1.3.4.1. Aβ receptors

Several cell surface molecules interact with Aβ (reviewed in Sakono and Zako, 2010; and Kam, Gwon and Jung, 2014). However, the best candidates are those "receptors" that bind oligomeric over monomeric species of Aβ with nanomolar or higher affinity and have been validated by the absence of Aβ toxicity in several models upon its genetic deletion (Smith and Strittmatter, 2017). One of the most prominent candidates is the cellular prion protein (PrP^C), a glycophosphatidylinositol-anchored protein located at postsynaptic sites that binds Aβ oligomers with nanomolar affinity (Laurén *et al.*, 2009). Moreover, PrP^C null mice are protected from Aβ-induced LTP impairment and age-related cognitive decline in murine models (Laurén *et al.*, 2009; Gimbel *et al.*, 2010). It has been proposed that the metabotropic glutamate receptor 5 (mGluR5) acts as a coreceptor with PrP^C, which upon Aβ-oligomer binding mediate the activation of neuronal Fyn (Um *et al.*, 2012, 2013). The activation of mGluR5-Fyn then would lead to a transient increase of surface NMDA receptor with excitotoxicity, followed by a reduction of surface receptors and spine loss (Um *et al.*, 2012). The Leukocyte immunoglobulin-like receptor subfamily B2 (LilrB2) and its murine homolog, paired Ig-like receptor B (PirB), were initially described as receptors for the major histocompatibility complex class I. Both proteins were subsequently found to be expressed in neurons and it was proposed that they play a role in stabilizing neural circuits (Syken *et al.*, 2006). LilrB2/PirB constitute nanomolar-affinity receptors for oligomeric Aβ and PirB KO mice are resistant to functional and behavioral amyloid-induced defects (Kim *et al.*, 2013). As activated cofilin is not found in PirB KO mice, it has been suggested that Aβ oligomers binding to PirB would be necessary to activate cofilin, an actin depolymerizing factor that promotes spine retraction (Kim *et al.*, 2013). Likewise, the lack of IgG Fcγ receptor II-b (FcγRIIb) and erythropoietin-producing hepatocellular A4

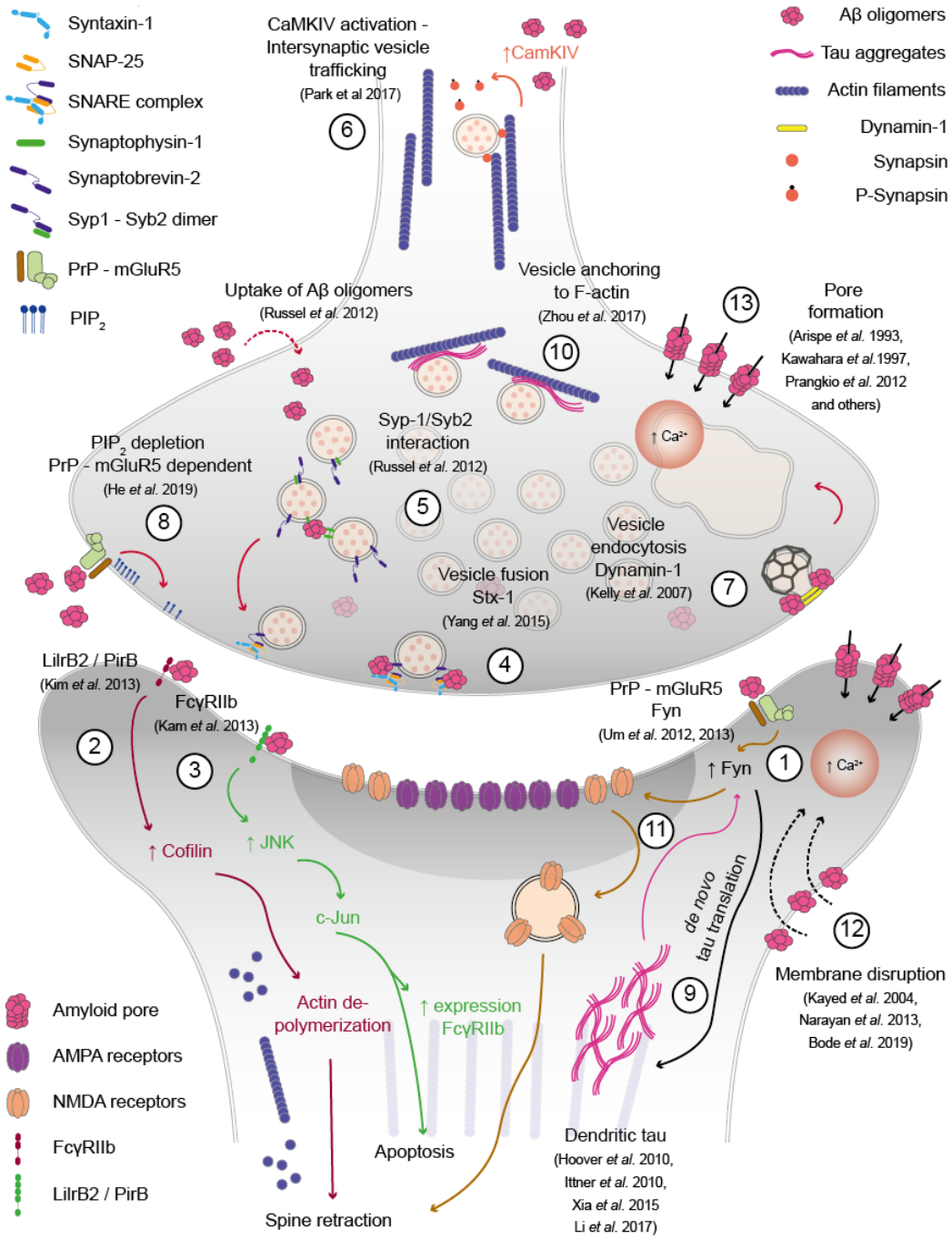

Figure 3. Mechanisms of Aβ synaptotoxicity. The schematic shows the synaptic alterations induced by oligomeric Aβ. **1)** Binding of Aβ oligomers to PrP and mGluR5 activates Fyn kinase, leading to loss of surface NMDA receptors. **2)** Interaction of Aβ oligomers with LilrB2/PirB induces cofilin activation, actin depolymerization and spine retraction. **3)** Interaction of oligomeric Aβ with the FCγRIIb receptor enhances JNK activity, which results in c-Jun mediated transcription of pro-apoptotic genes. **4)** Oligomeric Aβ binds syntaxin-1a and blocks vesicle fusion. **5)** Synaptophysin-1 interaction with Aβ oligomers disrupts the binding of the former with synaptobrevin-2, which at first enhances Pvr but leads to missorting of synaptobrevin-2 at a later stage. **6)** Oligomeric Aβ activates CaMKIV, which phosphorylates synapsin and impairs its interaction with the actin cytoskeleton, altering synaptic vesicle trafficking. **7)** Aβ oligomers reduce dynamin-1 cellular concentrations, impairing vesicle endocytosis. **8)** mGluR5 activation by Aβ oligomers activates phospholipase C, which leads to PIP2 depletion and Pvr reduction. **9)** Oligomeric Aβ induces *de novo* translation of mislocalized tau in a Fyn-dependent mechanism.**10)** Tau cross-links synaptic vesicles, reducing their mobility and the release rate at the terminal. **11)** Dendritic tau induces Fyn activation. **12)** Oligomeric Aβ interacts with the plasma membrane and disrupts its integrity and **13)** organizes within the membrane forming ion permeable pores, leading to calcium dyshomeostasis.

prevent Aβ toxicity *in vitro* and in mouse models (Kam *et al.*, 2013; Fu *et al.*, 2014). Some other cell surface molecules have been extensively studied in the context of AD, such as p75 neurotrophin receptor ($p75^{NTR}$), the neuronal insulin receptor and the receptor for advanced glycation endproducts (Rabizadeh *et al.*, 1994; María Frade, Rodríguez-Tébar and Barde, 1996; Kuner and Hertel, 1998; Deane *et al.*, 2003; Zhao *et al.*, 2008; Vodopivec *et al.*, 2009). Although the binding to Aβ and toxicity through a variety of intracellular cascades has been proposed, the role of these receptors has not yet been validated by strategies of genetic deletion. Finally, some surface molecules can bind monomeric Aβ with picomolar affinity, such as the α7-nAchR. These receptors most likely mediate the physiological functions of Aβ described in the section 1.2.4.

1.3.4.2. Aβ interaction with presynaptic proteins and lipids

Aβ also interacts with proteins within the presynaptic terminal (reviewed in Ovsepian *et al.*, 2018). A reduction in soluble N-ethylmaleimide-sensitive factor attachment protein receptor (SNARE) complexes has been observed in $APP_{swe}/PS1_{\Delta E9}$ mice brains accompanied by a normal concentration of the individual SNARE proteins (Sharma, Burré and Südhof, 2012; Yang *et al.*, 2015). Moreover, an interaction between the SNARE motif of syntaxin-1a and Aβ oligomers has been shown, accompanied by a defect in fusion in a vesicle content-mixing assay, with unmodified docking *in vitro* (Yang *et al.*, 2015). In addition to the syntaxin-1a interaction, Aβ oligomers are internalized by dissociated hippocampal rat neurons when applied extracellularly and bind synaptophysin-1, disrupting its interaction with synaptobrevin-2 (Russell *et al.*, 2012). This effect has been linked to an increase in the RRP in the short term, but the authors argue that a chronic sequestration of synaptophysin-1 by Aβ oligomers alters the sorting and endocytosis of synaptobrevin-2, leading to long-term deficits in transmitter release. Additionally, Aβ oligomers may alter intersynaptic vesicle trafficking by means of disrupting the actin - synapsin interaction, as a consequence of synapsin phosphorylation by activated calcium/calmodulin-dependent protein kinase type IV (CaMKIV) (Park *et al.*, 2017). Exposure to oligomeric Aβ induced a reduction in dynamin 1 at transcriptional and posttranscriptional levels in a NMDA-calpain dependent manner, which has been correlated with deficits in endocytosis at the presynaptic terminal and depletion of the RRP in cultured rat hippocampal neurons (Kelly,

Vassar and Ferreira, 2005; Kelly and Ferreira, 2006, 2007). Finally, increased amounts of Aβ reduced the concentration of phosphatidylinositol-4,5-diphosphate (PIP_2) in acute hippocampal slices from AD mice as well as in WT slices and WT dissociated neurons treated with 400 nM oligomeric Aβ (He *et al.*, 2019). The loss of PIP_2 at the neuronal membrane led to a reduction of Pvr, in a process that required mGluR5 and PrP^C.

1.3.4.3. Tau mediated effects

Tau is an amyloid protein itself and can also act as a downstream toxic effector of Aβ. In its random-coil native conformation, tau fulfills its neuronal physiological function in the axon, binding to and stabilizing the microtubule cytoskeleton (reviewed in Guo, Noble and Hanger, 2017). However, under pathological conditions it can be relocated via hyperphosphorylation (Hoover *et al.*, 2010; Xia, Li and Götz, 2015; Amar *et al.*, 2017) and also synthesized *de novo* in the somatodendritic compartment through an Aβ-Fyn-dependent mechanism (Li and Götz, 2017). Hyperphosphorylated tau has been shown to inhibit microtubule assembly and affect the cytoskeleton stability by binding MAP (microtubule associated protein) 2 and normal tau (Li *et al.*, 2007). In addition, oligomeric tau has been linked to memory loss *in vivo* and neuronal death with a reduction of synaptic markers in the injected areas (Lasagna-Reeves *et al.*, 2011). Upon mislocalization, tau present at the presynaptic terminal can impair neurotransmitter release by anchoring synaptic vesicles to filamentous actin (F-actin) and restricting their mobility (Zhou *et al.*, 2017). On the postsynaptic side, dendritic tau increases the level of Fyn in spines, enhancing Aβ-mediated transient excitotoxicity and later loss of NMDA receptors (Ittner *et al.*, 2010). Importantly, tau has been shown to be required for Aβ-mediated LTP impairment, since hippocampal slices from tau KO mice were protected from Aβ toxicity (Shipton *et al.*, 2011).

1.3.4.4. Effects on the plasma membrane, pore formation and calcium dyshomeostasis

As a hydrophobic peptide, Aβ can interact with lipids at the plasma membrane. Disruption of membrane integrity has been proposed as toxicity mechanism and related to ion dyshomeostasis (Narayan *et al.*, 2013). In artificial phospholipidic membranes, soluble Aβ oligomers (as well as oligomers from other amyloid

proteins) reduced the dielectric barrier for ions and increased membrane conductance (Kayed *et al.*, 2004). Moreover, a detergent-like effect has been demonstrated for Aβ42 oligomers on mica-supported lipid bilayers and large unilamellar vesicles using atomic force microscopy (AFM) and EM (Bode *et al.*, 2019). In the same study the authors showed that fibrillar Aβ only interacted with the membrane leaflet that is exposed to the peptide, with less deleterious consequences when compared to its oligomeric counterparts (Bode *et al.*, 2019). Alternatively, Aβ oligomers have been proposed to cross the lipidic membranes, accompanied by an influx of calcium ions (Drews *et al.*, 2016). As Aβ can bind artificial bilayers directly, specific lipids have been proposed as candidates to facilitate the Aβ - plasma membrane interaction. For example, the monosialotetrahexosylganglioside ganglioside (GM1) binds Aβ42 oligomers with great affinity and is necessary for Aβ-induced LTP impairment and calcium dyshomeostasis (Ariga *et al.*, 2001; Hong *et al.*, 2014; Evangelisti *et al.*, 2016). In addition, subpopulations of cells in PC12, GT1-7 and primary rat neuronal cultures susceptible to Aβ toxicity expose phosphatidylserine on their surface, and its levels are correlated with Aβ binding (Simakova and Arispe, 2007).

Besides the described transient binding or crossing, Aβ oligomers can additionally assembly within membranes and span them forming ion-conducting pores. Channel-like activity was first described in artificial palmitoyl-oleoyl phosphatidylethanolamine (POPE)/ phosphatidylserine (POPS) bilayers exposed to Aβ-containing liposomes (Arispe, Rojas and Pollard, 1993). The formation of these amyloid pores was further investigated using other techniques like double-dip (Arispe, Pollard and Rojas, 1993) and excised patches of hypothalamic GT1-7 cells (Kawahara *et al.*, 1997). These studies described Aβ40 or Aβ42 channels with multiple conductance levels ranging from 300 to 3500 pS, that were cation-selective and could be blocked by zinc and aluminum, among other substances (Arispe, Pollard and Rojas, 1993, 1996; Kawahara *et al.*, 1997). In an attempt to correlate cytotoxicity with Aβ aggregation states and pore formation, a multivariate analysis was performed using Aβ40 and Aβ42, analyzing the mentioned parameters over the course of 20 days of Aβ aggregation (Prangkio *et al.*, 2012). This study concluded that oligomeric isoforms of both Aβ40 and Aβ42 could induce pore formation in artificial bilayers and displayed concomitantly the highest cytotoxicity. In another set of experiments, seeking to describe the impact of amyloid pore formation in

neuronal membranes, cell-attached recordings were performed in human embryonic kidney (HEK) 293 cells, and the same oligomeric preparation was applied to rat primary hippocampal neurons (Sepúlveda *et al.*, 2014). The authors showed that intra-pipette oligomeric Aβ induced a progressive increase in HEK 293 cells membrane permeability, in a "perforated-patch-like" effect, with no evidence of discrete pore formation. Subsequently, Aβ oligomers were applied to hippocampal neurons from the patch pipette together with a fluorescent glucose analog during cell-attached recordings. The authors described that after 30 minutes the membrane perforations grew in size enough to allow the glucose analog entry into the cytoplasm. Similarly, cell-attached recordings on HEK 293 cells described amyloid pore formation with an initial cation selectivity, which shifted towards an ohmic behavior at the end of the experiments. In the same set of experiments, cultured hippocampal neurons incubated with a similar preparation of oligomers as used the for patch-clamp experiments displayed a loss of synaptobrevin-2 puncta, which was interpreted as a morphological correlate of amyloid pore toxicity (Sepúlveda *et al.*, 2014). In order to visualize the amyloid pores, AFM was combined with florescence microscopy. These experiments showed that artificial vesicles reconstituted with Aβ42, in whose surface Aβ could be observed by AFM, displayed an increased calcium influx that could be blocked by zinc application (Rhee, Quist and Lal, 1998). Moreover, AFM at high resolution revealed globular doughnut-shaped oligomers on Aβ40-reconstituted lipid bilayers (Quist *et al.*, 2005). These same aggregates induced channel-like behavior in Aβ-reconstituted dioleoyl-glycero-phosphocholine (DOPC) membranes. In support of an Aβ pores-mediated ion dyshomeostasis, intracellular calcium was increased in hypothalamic GT1-7 cells exposed to 10 μM Aβ40 in the course of minutes, as revealed by fluorescence intensity measurements using the calcium dye Fura2-AM (Kawahara *et al.*, 2000). Furthermore, imaging of transmembrane calcium currents of *Xenopus laevis* oocytes with a different fluorescent calcium indicator, Fluo4, and total internal reflection fluorescence (TIRF) microscopy revealed similar channel-like behavior to the described electrophysiological observations for Aβ42, with multiple permeability levels, voltage dependence and variable open probabilities (Demuro, Smith and Parker, 2011). Finally, a recent study on excised patches from HEK 293 cells showed that only Aβ42 oligomers (and not Aβ40) could induce channel-like behavior, with discrete open and closed states and multiple

conductance levels between 300 - 1000 pS (Bode, Baker and Viles, 2017). The channels described in these experiments do not display cation selectivity. Interestingly, for the first time since pore formation was observed, the authors stated the success rate of Aβ42 pore formation, which they observed in only ~35% of the cases, although Aβ had been applied at concentrations that would theoretically saturate the patch membrane.

By means of its varied effectors, calcium is a potent second messenger that controls manifold cellular processes ranging from exocytosis to cell death (reviewed in Brini *et al.*, 2014). Among other mechanisms, disruption of the plasma membrane as an ionic barrier and dysfunction of endoplasmic reticulum calcium receptors (Ferreiro, Oliveira and Pereira, 2004) induced by Aβ can lead to calcium dyshomeostasis with deleterious consequences to neuronal function, such as calpain and calcineurin activation leading to enhanced long-term depression, impaired LTP and cytoskeleton alterations with spine retraction (reviewed in Bezprozvanny, 2009).

1.3.4.5. Conclusions about Aβ toxicity mechanisms

In conclusion, despite the large amount of work on the molecular toxicity mechanisms of Aβ, the described findings are not yet conclusive. The role of the putative Aβ downstream molecules and pathways has to be pondered over in the context of the human disease and ultimately be validated by clinical trials showing the prevention, detention, or reversion of cognitive decline by modulating the proposed targets.

1.4. Therapeutic strategies in AD

A cure for AD has been intensively searched for in the last decades. With each hypothesis that aimed to explain AD physiopathology, corresponding drugs were developed to target and correct the putative toxic changes (see Table 3). Due to the hypothesis of cholinergic imbalance (Davies and Maloney, 1976), the first drugs approved by the United States Food and Drug Administration (US FDA) to treat AD were the acetylcholinesterase inhibitors. Within this group are tacrine, approved in 1993 but almost not used to date due to its hepatotoxicity; donepezil, approved in 1996 to treat all the clinical stages of AD; and rivastigmine -

Table 3. Current therapeutic strategies for AD.

	Therapeutic strategy		Active compound	Status
FDA approved therapies	Acetylcholinesterase inhibitors		tacrine donepezil rivastigmine galantamine	FDA approved
	NMDA blockers		memantine	FDA approved
Anti Aβ	Immunization	Active	AN1792	discontinued (adverse events)
			CAD 106	phase III
		Passive	solanezumab	phase III
			crenezumab	phase II
			gantenerumab	phase II
			BAN 2401	phase III
			aducanumab	discontinued (futility)
	γ-secretase inhibitors	non -selective	semagacestat	discontinued (adverse events)
		cleavage-site modulators	R-flurbiprofen	discontinued (futility)
			tarenflurbil	
		APP selective /Notch sparing	avagacestat	discontinued (adverse events)
	BACE1 inhibitors		elenbecestat	phase III
			CNP520	phase II/III
Anti tau	Reduction of tau expression		antisense oligonucleotides	phase I
	Postraslational modifications	Phosphorylation	selenate (PP2A)	phase I
			tideglusib (GSK3β)	discontinued (futility)
		Acetylation	salsalate (p300)	phase I
	Inhibition of tau aggregation		methylene blue	phase II
	Microtubule stabilization		TPI 287	phase I
	Immunization	Active	ADDvac-1	phase II
			ACI 35	phase I
		Passive	BMS986168 C2N-8E12 LY330033560	phase II
Novel small molecules	Inhibition of amyloid aggregation (?) Amyloid pore blocker (?)		anle138b	Not tested in AD patients

galantamine, approved in 2000 and 2001 respectively to treat mild to moderate AD (reviewed in Aisen, Cummings and Schneider, 2012). Although they have

different modes of action for cholinesterase inhibition, all acetylcholinesterase inhibitors are equally effective for the treatment of mild to moderate AD and have a good safety profile, with gastrointestinal side effects being the most commonly found (Birks, 2006). Memantine, an uncompetitive NMDA channel blocker, is the remaining drug approved by the US FDA to treat AD (Chen and Lipton, 2006). It can prevent Aβ-associated toxicity in animal models and has been proven effective and well-tolerated in patients at moderate to severe stages of the disease, alone or in combination with donepezil (Martinez-Coria *et al.*, 2010; McShane *et al.*, 2019).

Since 1992, when the amyloid cascade hypothesis was posited, Aβ secretion, aggregation, deposition and clearance have been targeted for drug development. The main approaches used to date have been active and passive immunization to enhance Aβ clearance and impair aggregation, and the use of β- and γ-secretase inhibitors to reduce its production (Schenk, Basi and Pangalos, 2012; Panza, Lozupone, Logroscino, *et al.*, 2019). Active immunization is the exposure to an Aβ-antigen that can trigger an immune response in the host. Pre-aggregated Aβ42 was applied together with an adjuvant in a vaccine named AN-1792. Immunization with this preparation reduced greatly the amyloid deposits in AD patients (Holmes *et al.*, 2008). However, it did not improve the cognitive decline and 6% of the treated patients suffered from meningoencephalitis (Gilman *et al.*, 2005; Holmes *et al.*, 2008). Currently, only one vaccine is in a phase III trial, CAD106, whose antigen is composed by multiple copies of Aβ 1-6 plus a carrier adjuvant. A study in mice and a phase I trial indicated that this vaccine displays a good safety profile (Wiessner *et al.*, 2011; Winblad *et al.*, 2012). CAD106 is being evaluated in the Generation S1 study, which targets cognitively healthy homozygous APOE*ε4 carriers (US National Library of Medicine. ClinicalTrials.gov, 2019e). Passive immunization with monoclonal or polyclonal humanized or recombinant human antibodies against Aβ species has been widely studied in the past decade. Unfortunately, most of the clinical trials on mild to moderate AD patients have shown passive immunization to be ineffective (reviewed in Panza, Lozupone, Logroscino, *et al.*, 2019). The ongoing phase II and phase III trials have sought to target patients with evidence of brain Aβ deposition in early stages of the AD spectrum such as mild AD patients, aged individuals at risk for memory loss or individuals at risk for early onset AD. The list of the currently actively tested antibodies include: 1) solanezumab, given to

aged individuals in the A4 study (sponsored by US National Library of Medicine. ClinicalTrials.gov, 2019k) and early-onset AD patients in the DIAN-TU (Dominantly Inherited Alzheimer Network Trial Unit) together with gantenerumab (US National Library of Medicine. ClinicalTrials.gov, 2019l); 2) crenezumab, which is being evaluated in presymptomatic carriers of the PSEN1 E280A mutation (US National Library of Medicine. ClinicalTrials.gov, 2019g); and 3) the protofibril-specific BAN2401 antibody, currently studied in a phase III trial in early AD patients (US National Library of Medicine. ClinicalTrials.gov, 2019i). Gantenerumab is also being tested in early AD in the GRADUATE 1 and GRADUATE 2 trials (US National Library of Medicine. ClinicalTrials.gov, 2019m, 2019r). Aducanumab, a promising human recombinant IgG1 antibody that exhibits 10,000 higher affinity for fibrils in comparison to monomers, successfully reduced Aβ deposits accompanied by an improvement in cognitive status in a phase Ib trial (Sevigny *et al.*, 2016). Recently, despite the early encouraging results, the company Biogen halted the ENGAGE and EMERGE trials due the lack of improvement in the primary outcome measure of efficacy (US National Library of Medicine. ClinicalTrials.gov, 2019p, 2019o).

In late-onset AD, impaired clearance of plaques has been proposed as a mechanism of Aβ accumulation (Mawuenyega *et al.*, 2010). In order to reach a production-elimination equilibrium and mitigate Aβ deposition, inhibition of the secretases has been attempted. The γ-secretase inhibitors (GSI) are classified by their mechanism of action into non-specific, which block the active site and therefore every kind of proteolytic activity, cleavage-site modulators, and the APP-selective/Notch-sparing inhibitors (Schenk, Basi and Pangalos, 2012). Semagacestat was the most studied non-selective GSI, but unfortunately failed in phase III trials in patients with probable AD, where it was found to worsen cognition and increase the incidence of skin cancer and infections (Doody *et al.*, 2013). Among the modulators of the cleavage site, which belong to the family of non-steroidal anti-inflammatory drugs (NSAIDs), are R-flurburprofen and tarenflurbil. They display a good safety profile but failed in altering the plasma levels of Aβ42 and did not produce any cognitive improvement in mild AD patients (Galasko *et al.*, 2007; Green *et al.*, 2009). Finally, a representative member of the group of APP-selective/Notch-sparing inhibitors is avagacestat, which is 193-fold more selective for APP versus notch cleavage (Gillman *et al.*, 2010). Despite its theoretically improved safety profile, a high number of gastrointestinal adverse

events and increased incidence of skin cancer were reported in a trial for prodromal AD with avagacestat, in addition to a higher number of individuals who progressed to dementia and/or suffered from brain atrophy (Coric *et al.*, 2015). There are no ongoing clinical trials with GSI to date.

Inhibitors of the β-secretase have also been utilized to target the early steps of the amyloid cascade, since they act upstream of Aβ production and could prevent its toxic consequences. Although BACE1 KO mice showed no gross phenotype, when translated to humans, pharmacological BACE1 inhibition was not exempt from adverse effects and studies on drugs from this group have been discontinued due to a lack of improvement, or even worsening in cognition accompanied by whole brain and hippocampal volume reduction as well as elevation of liver enzymes (Luo *et al.*, 2001; reviewed in Panza, Lozupone, Logroscino, *et al.*, 2019). Currently elenbecestat and CNP520 are the only BACE inhibitors in phase II and/or III clinical trials in patients at risk or with early AD (US National Library of Medicine. ClinicalTrials.gov, 2019e, 2019f, 2019b, 2019c).

Given that many anti-Aβ therapies have failed in protecting from cognitive decline, great interest has arisen in tau, a putative Aβ downstream effector, as a therapeutic target in AD. A high number of strategies are currently under study that cover almost every step of tau physiopathology (reviewed in Congdon and Sigurdsson, 2018). Since tau KO mice do not display gross abnormalities, inhibiting tau production by antisense oligonucleotides has been considered as an attractive therapeutic measure (Ke *et al.*, 2012). Successful results have been reported with this strategy in a mouse model of tauopathy and a phase I trial has been initiated to treat patients with mild AD (DeVos *et al.*, 2017; US National Library of Medicine. ClinicalTrials.gov, 2019q). At the core of tau toxicity lay its posttranslational modifications, which impair tau binding to microtubules and facilitate aggregation. Phosphorylation and acetylation are targeted respectively by sodium selenate, which activates the phosphatase PP2A, and salsalate, an NSAID dimer of salicylic acid that inhibits the p300 acetyltransferase (Corcoran *et al.*, 2010; Min *et al.*, 2015). Both compounds are currently being tested as therapy for mild to moderate AD (Australian New Zealand Clinical Trials Registry, 2019; US National Library of Medicine. ClinicalTrials.gov, 2019s). Tideglusib, another modifier of tau phosphorylation by inhibition of glycogen synthase kinase 3 β, has already been tested in mild to moderate AD showing good tolerance, but

unfortunately it did not produce any clinical improvement (Lovestone *et al.*, 2015). The phenothiazine methylene blue strain/compound binds tau monomers and exerts its therapeutic effects by preventing their aggregation (Wischik *et al.*, 1996). This compound was tested in mild to moderate AD patients with no signs of beneficial effects (Gauthier *et al.*, 2016). However, it is currently in a phase III trial that includes patients with early AD (US National Library of Medicine. ClinicalTrials.gov, 2019s). Stabilizers of microtubules are also being utilized to restore the cytoskeletal abnormalities caused by altered tau function. Currently, the drug TPI287 is in a phase I clinical trial as treatment for AD (US National Library of Medicine. ClinicalTrials.gov, 2019d). Finally, immunization against tau is also being intensively studied. Concerns have been expressed as to what tau region or conformational isomer to target, and whether antibodies will reach tau intracellularly (reviewed in Congdon and Sigurdsson, 2018). Active immunization in the P301L tau mouse model has already shown to successfully remove tau deposits and improve behavioral abnormalities without inducing autoimmunity (Asuni *et al.*, 2007). There are currently two vaccines against tau, ADDvac-1 and ACI-35, in phase II and phase I trials respectively (International Clincal Trials Registry Platform., 2019; US National Library of Medicine. ClinicalTrials.gov, 2019a). Regarding passive immunization, there are a considerable number of antibodies targeting different regions of tau in phase II trials directed to patients with early AD, such as BMS986168, C2N-8E12, and L43303560, among others (US National Library of Medicine. ClinicalTrials.gov, 2019h, 2019j, 2019n).

The negative results yielded by the trials with aducanumab, summed to the large body of failures with anti-amyloid strategies reinforced the criticisms to the amyloid cascade hypothesis (Herrup, 2015; Karran and De Strooper, 2016; Panza, Lozupone, Dibello, *et al.*, 2019; Panza, Lozupone, Logroscino, *et al.*, 2019). However, the body of evidence supporting this hypothesis, with the current focus shifted to Aβ oligomers as toxic species, is also large and the failed studies might have included patients far too advanced in the natural history of the disease. Therefore, an invaluable insight to test the validity of the amyloid hypothesis will come from the results of the current clinical trials targeting patients in earlier phases of the AD spectrum (Selkoe, 2019). Targeting tau has opened new avenues in the therapeutic for AD, sparing toxicity (reviewed in Panza *et al.*, 2016; and Congdon and Sigurdsson, 2018). With the completion of the ongoing clinical trials in the next years, not only will the medical and scientific community

learn how to treat AD but also gain insight about its underlying physiopathological mechanisms. Likewise, as our understanding on how neurodegeneration occurs in AD deepens and expands, novel therapies can and will emerge.

1.4.1. Novel diphenylpyrazole derivatives in AD and other neurodegenerative diseases

Misfolding and aggregation seem to be common features of multiple neurodegenerative disorders, with soluble intermediate oligomeric species putatively mediating the toxic effects, as explained in section 1.3.1 (Soto, 2003; Soto and Pritzkow, 2018). In the context of the development of therapeutic strategies this would imply that inhibiting or modulating aggregation could be beneficial to halt the physiopathological cascade triggered by toxic oligomers. In 2013, Wagner *et al.* carried out a high throughput screening of 20,000 small molecules by testing their ability to inhibit PrP aggregation both *in vitro* and *in vivo* (Wagner *et al.*, 2013). As a result, they discovered the novel leading compound diphenylpyrazole as an inhibitor of PrP aggregation. Further screening experiments indicated that the derivative with the highest protective effects in prion and Parkinson's disease (PD) models was anle138b. This small molecule prolonged the survival of prion-infected mice to an extent that no other compound had achieved before, was as effective as hemivagotomy in preventing motor symptoms in the oral rotenone model of PD and extended significantly the disease-free survival of A30P mice, a transgenic mouse model of PD (Wagner *et al.*, 2013). Interestingly, the authors also showed in sucrose gradients of whole-brain homogenates from the A30P mice a reduction of oligomeric forms at expense of an increase in monomers, with no changes in the overall concentration of synuclein. This suggests that anle138b exerts its protective effects by modulating protein aggregation. Furthermore, the compound has an excellent oral bioavailability and blood-brain barrier penetration, which enable oral administration (Wagner *et al.*, 2013). Recently, in a novel mouse model of PD that expresses a truncated form of α-synuclein, MI2 mice, anle138b restored striatal release of dopamine, reduced neuronal loss in the substantia nigra pars compacta and improved the gait pattern, even when the treatment had started at 9 months of age after the onset of synuclein pathology (Wegrzynowicz *et al.*, 2019). In addition, direct stochastic optical reconstruction microscopy confirmed that anle138b treatment reduced the number of large α-synuclein aggregates

while increasing non-clustered α-synuclein (Wegrzynowicz *et al.*, 2019). Further experiments performed in murine models of tauopathy and multiple system atrophy rendered similar results, with anle138b administration ameliorating the symptoms, reversing histopathological changes and reducing the accumulation of large amyloid deposits (Wagner *et al.*, 2015; Heras-Garvin *et al.*, 2018).

AD pathology has also been targeted with anle138b. A comprehensive study was published in 2018 in which electrophysiological and behavioral tools accompanied by transcriptome analysis were applied to characterize the changes in $APP_{Swe}/PS1_{\Delta E9}$ mice upon anle138b administration (Martinez Hernandez *et al.*, 2018). The authors showed that anle138b restored hippocampal synaptic transmission as evidenced by an improvement in CA1-LTP measurements in acute slices in pre-plaque mice with treatment initiated at 2 months of age as well as in post-plaque animals with treatment initiated at 6 months of age. The electrophysiological effects were accompanied by an enhanced performance in both groups in the Morris water maze test when compared to untreated transgenic animals, although the post-plaque group could not reach the WT levels in the probe trial (Martinez Hernandez *et al.*, 2018). A hippocampal transcriptome analysis was performed to characterize the alteration and restoration of gene expression in both the pre-plaque and post-plaque mice, and also upon anle138b treatment. From a total of 202 dysregulated genes in the pre-plaque group, only 27 remained altered in the anle-treated group. Importantly, APP and PS1 expression was not altered by the treatment (Martinez Hernandez *et al.*, 2018). In the post-plaque group, expression of 220 genes was altered and a pathway analysis associated these changes with neuroinflammation. Remarkably, anle138b treatment did not prevent the expression these genes, indicating that the beneficial effects on the post-plaque group are not mediated by a reduction of neuroinflammatory processes. Moreover, histological examination using thioflavin S revealed a decreased plaque deposition in the cortex and hippocampus of anle138b-treated mice. When analyzed in the context of the previous studies of anle treatment in murine models of neurodegenerative diseases, the experiments on the AD model suggest that anle138b exerted its protective effects by acting as an anti-amyloid aggregation molecule. Besides undergoing misfolding and aggregation, another common feature of amyloid proteins is their ability to interact with lipid bilayers and assemble into ion-conducting pores (Quist *et al.*, 2005). Interestingly, in

addition to restoring functional and behavioral defects in the $APP_{Swe}/PS1_{\Delta E9}$ mice, anle138b was found to restrict the formation of Aβ42 pores in artificial phospholipidic bilayers and to protect cultured hippocampal neurons from Aβ40-induced perturbation of membrane integrity (Martinez Hernandez *et al.*, 2018). Taken together, these data indicate that anle138b could protect hippocampal neurons from amyloid toxicity by a dual mechanism, preventing Aβ aggregation into toxic oligomers and also inhibiting the formation of amyloid pores.

1.5. Aims of the present study

AD is the most prevalent neurodegenerative disease and the main cause of dementia worldwide. Several lines of evidence indicate that accumulation of soluble aggregates of the Aβ peptide play a causative role in AD, a concept summarized in the amyloid cascade hypothesis more than 25 years ago. To date a large body of studies have associated the accumulation of Aβ in AD mouse models to learning and memory deficits. Moreover, these behavioral changes are often accompanied by aberrant dendrite and spine number and morphology. In addition, altered synaptic transmission in the hippocampus has been studied, most frequently utilizing LTP and field recordings. However, little is known about Aβ synaptotoxicity at the single-cell and molecular levels, which might represent the earliest event in AD. Therefore, in this study I aim to gain insight into the effects of Aβ exposure on neurotransmission by means of establishing an *in vitro* model system of amyloid toxicity. In a first step, I will establish a reproducible method to prepare putative synaptotoxic Aβ aggregates, which will be characterized thoroughly with multiple techniques. Next, I plan to take advantage of electrophysiological recordings on autaptic neuron cultures, which have been widely used in my host laboratory in the study of the physiology of transmitter release, to describe the molecular mechanisms that fail at the glutamatergic synapse upon Aβ incubation. In addition, I will examine whether putative Aβ synaptotoxic effects correlate or depend on morphological alterations of the autaptic neurons.

AD is currently an incurable disease and after manifold efforts in the past decades, the field has seen promising therapeutic strategies fail in phase III clinical trials. The novel small molecule anle138b has been shown to positively modify the natural history of multiple neurodegenerative diseases in animal

models, including AD mice. Moreover, its mechanism of action is unconventional, in that it does not modify physiological processes like other therapeutic agents. The available information on anle138b in AD has revealed that treated mice show a restoration in behavioral and electrophysiological parameters, decreased amount of amyloid plaques and less gene deregulation. Yet the exact cellular and molecular causes of this phenotype amelioration remain unclear. In addition, there is currently no information available about synaptic function and neuronal morphology in the presence of anle138b. Furthermore, the lack of a clear mechanism of action impedes the prediction and anticipation of unwanted side effects upon treatment with anle138b in AD patients. In this context, I aim to get a better understanding of the protective effects of the small molecule anle138b. For this purpose, Aβ-treated autaptic cultures used as a model of AD-related synaptotoxicity will be exposed to anle138b and its physiological properties will be characterized by performing electrophysiological recordings.

In the last part of my work I will focus on the formation of amyloid pores as mechanism of Aβ toxicity, a highly debated hypothesis in the field of AD. Amyloid pores have been observed in artificial bilayers and patches from cells grown as immortalized lines or primary cultures. *in vitro* evidence indicate that anle138b could exert its protective effects blocking these pores. Still, how the *in vitro* findings relate to neurotoxicity at the cellular and synaptic levels remains an open question. Hence, I aim to elucidate whether Aβ pores could relate to and also underlie the synaptotoxicity observed in autaptic neuronal cultures. In a first effort to observe pores, I will perform electrophysiological recordings from artificial bilayers to later move to the study of pore formation and its consequences on autaptic hippocampal cultures. Finally, I will make use of the enantiomeric Aβ42 and compare its toxicity on autaptic hippocampal cultures to the WT peptide, since it has been hypothesized that the formation of Aβ pores is independent of any stereospecific interaction.

2. Materials and Methods

2.1. Materials

2.1.1. Reagents

Table 4. Reagents.

Reagent	Provider
1,1,1,3,3,3-hexafluoro-2-propanol (HFIP)	Merck
2-morpholinoethanesulphonic acid (MES)	Merck
3-(1,3-Benzodioxol-5-yl)-5-(3-bromophenyl)-1H-pyrazole, 5-(1,3-Benzodioxol-5-yl)-3-(3-bromophenyl)-1H-pyrazole (Anle138b)	A. Leonov and S. Ryazanov (NMR Based Structural Biology Department, Max Planck Institute for Biophysical Chemistry)
3-(N-morpholino) propanesulfonic acid (MOPS)	Biomol
4-(2-hydroxyethyl)-1-piperazineethanesulfonic acid (HEPES)	Roth
4',6-Diamidino-2-Phenylindole, Dihydrochloride (DAPI)	Thermo-Fisher
Acetic acid, glacial	Merck
Adenosine 5'-triphosphate (ATP) magnesium salt	Sigma-Aldrich
Agarose type IIa, medium	Sigma-Aldrich
Ammonia 32%	Merck
Amyloid-β peptide, 1-42	Bachem (Cat. N. 4014447)
Amyloid-β peptide, 1-42 scrambled	Bachem (Cat. N. 4064853)
Amyloid-β peptide, 42-1 ("reverse" Aβ42)	Bachem (Cat. N. 4027991)
Aprotinin	Roth
Aqua-Poly/Mount	Polysciences, Inc.
B27 serum - free supplement (50X)	Gibco
Bovine serum albumin	Sigma-Aldrich
Bradford reagent	Bio-Rad
Bromophenol blue	Pierce
Calcium chloride ($CaCl_2$)	Sigma-Aldrich
Chloroform	Sigma-Aldrich
Collagen 1, rat tail	Becton Dickinson GmbH
Creatine phosphokinase from rabbit muscle	Sigma-Aldrich
Deuterium hydroxide	Deutero
Dimethyl sulfoxide	Sigma-Aldrich
Diphytanoyl phosphatidylcholine (DiphyPC)	Avanti Polar Lipids
Disodium hydrogen phosphate ($Na_2HPO_4.2H_2O$)	Merck
Dry milk (skimmed milk)	Reforma
Dulbecco's modified eagle medium	Gibco
Enhanced chemiluminescence reagents (Solutions I and II)	GE Healthcare

Ent - amyloid-β peptide (AllD Aβ42)	Bachem (Cat. N. 4037836)
Ethanol	Sigma-Aldrich
Ethylendiaminetetraacetic acid (EDTA)	Sigma-Aldrich
Ethylenglycoltetraacetic acid (EGTA)	Sigma-Aldrich
Fetal bovine serum	Gibco
GlutaMAX	Gibco
Glutamic acid	Sigma-Aldrich
Glycerin	Merck
Glycerol	Sigma-Aldrich
Glycine	Sigma-Aldrich
Goat serum	Sigma-Aldrich
Guanosine triphosphate (GTP) sodium salt	Sigma-Aldrich
Hank's balanced salt solution	Gibco
Hoechst solution	Thermo Fisher
Hydrochloric Acid 37%, fuming (HCl)	Merck
L-aspartic acid	Sigma-Aldrich
L-cysteine	Sigma-Aldrich
Leupeptin	Peptide Institute
Magnesium chloride ($MgCl_2$)	Merck
MemCode® Reversible Protein Stain Kit	Thermo Fisher
Methanol	J.T.Baker
MITO + serum extender	Becton Dickinson GmbH
n-decane	Merck
Neurobasal A	Gibco
Oxidized cholesterol	Prof. Roland Benz
Papain	Worthington Biomedical Corp.
Paraformaldehyde (PFA)	Serva
Penicillin / streptomycin	Gibco
Phenylmethylsulfonylfluoride	Roche
Phosphocreatine disodium salt hydrate	Sigma-Aldrich
Poly-D-lysine	Sigma-Aldrich
Poly-L-lysine (PLL)	Sigma-Aldrich
Potassium chloride (KCl)	Merck
Potassium D-gluconate	Sigma-Aldrich
Potassium dihydrogen phosphate (KH_2PO_4)	Merck
Protein molecular weight standards - PageRuler®	Thermo-Fischer
Protein molecular weight standards - SeeBlue 2®	Invitrogen
Silver nitrate ($AgNO_3$)	Merck
Sodium azide (NaN_3)	Merck
Sodium carbonate (Na_2CO_3)	Merck
Sodium chloride (NaCl)	Merck

Sodium dihydrogen phosphate ($NaH_2PO_4.H_2O$)	Merck
Sodium dodecyl sulfate (SDS)	GERBU GmBH
Sodium hydroxide (NaOH)	Merck
Sodium pyruvate	Sigma-Aldrich
Sodium thiosulphate ($Na_2S_2O_3$)	Merck
Sucrose	Merck
Tetrodotoxin (TTX)	Tocris Bioscience
Thioflavin T (ThT)	Sigma-Aldrich
Tris base	Sigma-Aldrich
Triton X-100	Roche
Trypsin inhibitor	Sigma-Aldrich
Trypsin-EDTA (0.05% (wt/vol)	Gibco
Tween 20	Sigma-Aldrich
Uranyl acetate	SPI Supplies

2.1.2. Solutions

- Phosphate buffered saline solution (PBS): 136 mM NaCl, 2.68 mM KCl, 6.4 mM NaH_2PO_4, 1.76 mM KH_2PO_4, pH= 7.40.

- Phosphate buffer: 23.1 mM $Na_2HPO_4.2H_2O$, 16.9 mM $NaH_2PO_4.H_2O$, pH= 7.00.

2.1.2.1. Solutions for electrophoretic separation of proteins and Western blot

- Glycine buffer: 0.1 M glycine, 0.05% sodium azide, pH= 8.

- Laemmli sample buffer: 10% glycerol, 50 mM Tris HCl, 2 mM EDTA, 2% SDS, 0.05% bromophenol blue).

- MES buffer: 50 mM MES, 50 mM Tris base, 1 mM EDTA, 0.1% SDS, pH= 7.3.

- MOPS buffer: 50 mM MOPS, 50 mM Tris base, 1 mM EDTA, 0.1% SDS pH= 7.7.

- Transfer buffer: 25 mM Tris base, 190 mM Glycine, 20% Methanol.

- Tris-buffered saline (TBS): 50 mM Tris HCl (pH= 7.50), 150 mM NaCl.

- TBS-T: 50 mM Tris HCl (pH= 7.40), 150 mM NaCl, 10% Tween 20.

- PBS-T: PBS + 0.1% Tween 20.

- Buffer A: 20 mM Tris-HCl pH= 7.5, 150 mM NaCl, 1 mM EDTA-NaOH, 1 mM DTT, 0.2 mM phenylmethylsulfonylfluoride, 1 µg/mL aprotinin, 0.5 µg/mL leupeptin.

- Buffer B: 20 mM Tris-Cl pH= 7.5, 150 mM NaCl, 0.2% (w/v) Triton X-100, 1 mM EDTA-NaOH pH= 8, 1 mM DTT, 0.2 mM phenylmethylsulfonylfluoride, 1 µg/mL aprotinin, 0.5 µg/mL leupeptin.

2.1.2.2. Solutions for neuron culture

- Papain stock solution: 0.2 mg/mL cysteine, 1 mM $CaCl_2$, 0.5 mM EDTA in Dulbecco's Modified Eagle's Medium.

- Papain working solution: 20 UI of papain dissolved in 1 mL papain stock solution. In order to solubilize the papain, the solution was saturated with carbogen (95% oxygen, 5% carbon dioxide) and sterilized by filtering (0.22 µm syringe filter).

- Stop solution: 2.5 mg/mL bovine serum albumin (BSA), 2.5 mg/mL trypsin inhibitor and 10% fetal bovine serum in Dulbecco's Modified Eagle's Medium.

- Neurobasal plus supplements: 500 mL Neurobasal A, 5 mL GlutaMAX, 10 mL B-27 supplement, 1 mL penicillin/streptomycin.

2.1.2.3. Solutions for electrophysiology

- External solution ("Base Plus"): 140 mM NaCl, 4 mM $CaCl_2$, 4 mM KCl, 10 mM HEPES, 24 mM $MgCl_2$, 10 mM Glucose (pH=7.3, ~ 310 mOsm/L).

- Intracellular solution (for voltage-clamp recordings): 136 mM KCl, 17.8 mM HEPES, 15 mM phospho creatine, 1 mM EGTA, 0.6 mM $MgCl_2$, 0.3 mM Na-GTP, 4 mM Mg-ATP, 5 U/mL creatine phosphokinase (pH= 7.4, ~320 mOsm/L).

- Intracellular solution – Low chloride (for current-clamp recordings): 20 mM KCl, 10 mM HEPES, 0.1 mM EGTA, 0.3 mM Na-GTP, 4 mM Mg-ATP (pH= 7.4, ~320 mOsm/L).

- Solution for recordings from artificial bilayers: 1 M KCl, 10 mM HEPES, pH= 7.0.

2.1.3. Antibodies

Table 5. Secondary antibodies.

Antibody	Host	Dilution	Provider	Use
Chicken – Alexa Fluor 633	Goat	1:2000	Thermo Fischer	Immunocytochemistry
Guinea pig - Alexa Fluor 488	Goat	1:2000	Mobitec	Immunocytochemistry
Mouse - horse radish peroxidase (HRP) - Affinity purified	Goat	1:10,000	Dianova	Western Blot - Enhanced chemiluminescence
Mouse - IRDye 680 RD	Goat	1:5000	LI-COR	Western Blot - LI-COR Odyssey®
Rabbit - Alexa Fluor 555	Goat	1:2000	Thermo Fischer	Immunocytochemistry
Rabbit - IRDye 800 CW	Goat	1:5000	LI-COR	Western Blot - LI-COR Odyssey®

Table 6. Primary antibodies.

Antibody	Host	Dilution	Provider	Use
Actin	Rabbit	1:250	Sigma	Western Blot - LI-COR Odyssey®
Aβ peptide 1-16 (6E10)	Mouse	1: 7500	Biolegend	Western Blot - HRP
CAPS1	Mouse	1:500	BD Biosciences	Western Blot- LI-COR Odyssey®
GAPDH	Rabbit	1:1000	Abcam	Western Blot- LI-COR Odyssey®
GluA2	Rabbit	1:1000	Synaptic Systems	Western Blot- LI-COR Odyssey®
MAP2	Chicken	1:1000	Novus Biologicals	Immunocytochemistry
Munc13-1	Rabbit	1:1000	Synaptic Systems	Western Blot- LI-COR Odyssey®
PSD95	Mouse	1:50,000	Neuromab	Western Blot- LI-COR Odyssey®
Shank2	Guinea pig	1:500	Synaptic Systems	Immunocytochemistry
Synaptophysin-1	Mouse	1:10,000	Synaptic Systems	Western Blot- LI-COR Odyssey®
Synaptotagmin-1	Mouse	1:1000	Synaptic Systems	Western Blot- LI-COR Odyssey®
VGluT1	Rabbit	1:1000	Synaptic Systems	Immunocytochemistry

2.2. Methods

2.2.1. Aβ42 monomerization and in vitro aggregation

2.2.1.1. Dissolution by 0.5% ammonium hydroxide

The first Aβ dissolution method that I tested was a modified version of a published protocol (Ryan *et al.*, 2013) provided by Prof. Dr. Tiago Outeiro (personal communication). First, 1 mg of Aβ42 peptide was suspended in 100 µL PBS.

Afterwards, ammonium hydroxide was added to a final concentration of 0.5%, which led to a clear solution indicating a successful peptide dissolution. Finally, PBS was added to 1 mL for a final peptide concentration of 1 mg/mL. All steps were performed at 4°C.

2.2.1.2. HFIP / 100 mM NaOH two-step dissolution

The second Aβ dissolution protocol used in this study combined the use of the polyfluorinated alcohol HFIP with alkaline solution in 100 mM NaOH. In a first step, Aβ42 was dissolved in HFIP at a concentration of 2 mg/mL. After at least 60 minutes of incubation at room temperature, the solution was lyophilized for 2 hours to evaporate and remove the HFIP. In the second step, 100 mM NaOH was added to the lyophilized powder to a concentration of 2 mg/mL. After 3 hours of incubation at room temperature, the solution was aliquoted and stored at -80°C until use.

2.2.1.3. In vitro preparation of oligomeric enriched Aβ42 solutions

In order to prepare aggregates for the study of Aβ toxicity, phosphate buffer was added to an aliquot of monomerized Aβ42 and the pH was corrected to 7.40 with 0.5 or 0.1 M HCl. The initial pH was >11.00. After pH correction, Sartorius water was added to a final Aβ42 concentration of 0.5 mg/mL and 20 mM phosphate buffer. The sample was centrifuged for 10 minutes at 23,000x g and 4°C. Supernatant and pellet were separated and both dissolved to the same final volume. The supernatant was then incubated at 37°C and 800 revolutions per minute in a Thermomixer®. For oligomerization and use in toxicity experiments the supernatant was incubated for 40 minutes. For characterization of the aggregation kinetics, samples were taken at several time points during 72 hours incubation.

2.2.2. Characterization of Aβ42 preparation

Aβ preparations were characterized taking samples at increasing incubation periods by means of ThT fluorescence measurements, negative staining for electron microscopy and Western blot or silver staining.

2.2.2.1. Measurement of protein concentration in the monomeric solution

Protein concentration of the monomeric solution was calculated by measuring absorbance in a Nanophotometer (Implen) with 5 µL samples, using the equation for Beer's law:

$$A_{280} = \varepsilon IC$$

where A_{280} is absorbance at 280 nm, ε is the Aβ42 molar extinction coefficient (1490 $cm^{-1}M^{-1}$), I is the path length (for the Nanophotometer using 10 mm lid, I = 0.1 cm) and C is the concentration. This procedure is described in the protocol by Jan *et al* (Jan, Hartley and Lashuel, 2010).

2.2.2.2. ThT fluorescence measurements

Sample preparation and ThT fluorescence upon Aβ binding was measured as described previously by others (Jan, Hartley and Lashuel, 2010). In brief, a 100 µM ThT stock solution was prepared, kept in the dark at 4°C and discarded after 7 days. Prior to fluorescence measurement, the sample was prepared by dissolving ThT to 5 µM or 50 µm in glycine buffer and adding 10 µl of sample or blank solution. Samples were measured by duplicates in a Quanta Master fluorometer, with excitation at 450 nm and emission detected at 480 nm for 60 seconds.

2.2.2.3. NuPAGE® polyacrylamide gel electrophoresis

Aβ samples containing ~4 µg of protein were dissolved in Laemmli sample buffer and stored at -80°C. For electrophoretic separation, samples were loaded without boiling on NuPAGE® 4-12% Bis-Tris gradient gels. Samples ran in parallel with the protein molecular weight standards SeeBlue2® at constant voltage (110 V) in MES running buffer for ~ 2 hours.

2.2.2.4. Western blot

After gel electrophoresis, proteins were transferred onto a nitrocellulose membrane in transfer buffer by constant current at 250 mA for 2 hours. Membranes were blocked with 5% skimmed milk and 5% goat serum in TBST for one hour. Next, the membrane was incubated for one hour with the 6E10 anti-Aβ peptide at 1: 7,500 in blocking buffer. After three washes with blocking buffer, a

HRP-conjugated secondary antibody was added to 1:10,000 and incubated for one hour. After incubation with the secondary antibody, the membrane was washed four times in TBST-5% skimmed milk. Two last washing steps using TBST and TBS were performed before detecting the signal on the membrane with the enhanced chemiluminescence system.

2.2.2.5. Silver staining

Silver staining was performed according to a modified protocol by Dr. O. Jahn and D. Hesse from Blum, Beier and Gross (Blum, Beier and Gross, 1987). In brief, gels were fixed for 2 hours in 40% ethanol and 10% acetic acid, washed two times with 30% ethanol and once with Sartorius water for 20 minutes. 0.012% sodium thiosulfate was used to sensitize the gels for 1 minute, followed by three 20-second washes in Sartorius water. Afterwards, the gel was impregnated in 0.2% silver nitrate, 0.05% formaldehyde solution and washed again three times for 20 seconds with Sartorius water. Finally, the gel was developed in 3% sodium carbonate, 0.05% formaldehyde solution for 2-10 minutes. Once the staining reached the expected intensity, the developing reaction was stopped by placing the gel in 5% acetic acid for 10 minutes followed by three 10-minutes washes with Sartorius water.

2.2.2.6. Transmission electron microscopy (TEM)

In order to visualize the Aβ aggregates, 10 µL of peptide sample was incubated for 20 minutes on glow discharged, PLL pretreated, Formvar coated copper grids at room temperature. After three washes with Sartorius water, the grid was contrasted by a 60-second incubation with 1% uranyl acetate. The grid was dried using filter paper, left to air-dry and stored until visualization. Images were taken with a LEO 912AB Omega TEM (Zeiss) in collaboration with Dr. Benjamin Cooper and Lydia Maus.

2.2.2.7. Mass spectrometry and NMR spectroscopy

Mass spectrometry was performed on Aβ42 and AllD Aβ42 samples dissolved in HFIP at 1 mg/mL by Uwe Pleßmann and Prof. Henning Urlaub (Bioanalytical Mass Spectrometry Research Group, Max Planck Institute for Biophysical Chemistry). For NMR spectroscopy, Aβ42 and AllD Aβ42 were dissolved in HFIP, lyophilized and dissolved in 100 mM NaOH, as described previously (see section

2.2.1.2). pH was adjusted to 7.20 and deuterium oxide was added to 10%. Afterwards, the sample was sonicated for 1 minute and incubated it in the cold room with gentle agitation for 30 minutes. NMR spectroscopic registers were performed by Kris Runge and Dr. Nasrollah Rezaei-Ghalleh (NMR Based Structural Biology Department, Max Planck Institute for Biophysical Chemistry).

2.2.3. Dissolution of anle138b for application to primary hippocampal neurons

Anle138b is a lipophilic compound (see Figure 4). For dissolution in hippocampal neuronal medium, a 200 mM anle138b stock solution in DMSO was prepared in a first step. Next, anle138b in DMSO was dissolved in fetal bovine serum (FBS) to a theoretical concentration of 660 µM. The measured concentration of this anle138b in DMSO/FBS solution was 484 µM (Sergey Ryazanov, personal communication). Using this corrected value, anle138b was applied to neurobasal medium plus supplements at 7 or 10 µM to treat the primary hippocampal neurons for electrophysiological experiments.

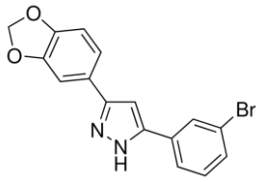

Figure 4. Anle138b chemical formula.

2.2.4. Preparation of dissociated mass and autaptic cultures of murine hippocampal neurons

Hippocampal neurons were prepared as described by Burgalossi *et al.* (Burgalossi *et al.*, 2012). In brief, following postnatal day 0 mice decapitation, hippocampi were dissected in ice-cold Hank's balanced salt solution, followed by enzymatic digestion at 37°C for 60 minutes in papain working solution with mild agitation (450 revolutions per minute). After discarding the papain working solution, the hippocampi were incubated in stop solution for 15 minutes, followed by three washes with Neurobasal-A medium plus supplements. In order to dissociate the cells, the digested hippocampi were triturated by pipetting using a 200 µL filter tip. Neurons were counted in a Neubauer chamber and plated at 20,000 / cm^2, grown as mass cultures on PLL coated glass coverslips for quantification of picnotic nuclei and synaptic proteins. For autaptic cultures,

neurons were seeded at ~400 / cm^2 on glass coverslips previously stamped with poly-D-lysine and collagen where astrocytes were grown forming microislands. In the context of this work and in agreement with the conventions in the field of Electrophysiology this culture system was considered as *in vitro*.

2.2.5. Quantification of picnotic nuclei upon Aβ treatment

Picnotic nuclei were quantified by a modified protocol from Ripamonti *et al.* (Ripamonti *et al.*, 2017). In order to analyze chromatin condensation, neuronal mass cultures grown on PLL-coated glass coverslips were treated with 10 µM Aβ42 or vehicle buffer on day *in vitro* (DIV) 8. After 72 hours of treatment, the neurons were incubated for 30 minutes with Hoechst 33342 at 2 µg/mL, mounted with Aqua-Poly/Mount without fixation and imaged 15 minutes afterwards on a Zeiss Apotome microscope. Since these cells were not fixed and the quality of the staining varied within each coverslip, the exposure time was optimized for each image. The total nuclei number was obtained by manual count. The number of picnotic nuclei, which displayed a better signal to noise ratio due to the chromatin condensation, was automatically quantified by manually setting a threshold for each image and applying a custom-made macro based on the FIJI "Analyze Particles" built-in function (Schindelin *et al.*, 2012). The criteria for including the nuclei within the picnotic group were: size= 50-1000, circularity= 0.50-1.00, with a pixel size of 258 nm. Imaging and nuclei quantification were performed blinded to treatment condition.

2.2.6. Quantification of synaptic proteins by Western blot- LI-COR Odyssey

In order to measure putative differences in the concentration of synaptic proteins upon Aβ42 treatment, primary hippocampal neurons were grown on PLL-coated 6-well plates. After 8 days *in vitro*, neurons were treated with 10 µM Aβ42 or the vehicle buffer as control. 72 hours later, on DIV 11, the neurons were washed two times with buffer A, briefly incubated with ~30 µL / well of buffer B, collected and stored at -80°C. Prior to electrophoretic separation, the Bradford protein assay was used to measure absorbance of the samples at 595 nm and the protein concentration was calculated by extrapolation from a standard curve generated by measurements of BSA samples at increasing concentrations. Samples were subsequently diluted in Laemmli buffer at 0.8 µg/µL. After 5 minutes of boiling at 95°C, the samples were loaded into a NuPAGE Bis-Tris 4-

12% gel, along with protein molecular weight standards (PageRuler), and let run in MOPS buffer for ~3 hours at constant voltage of 100 V. Once optimal separation was achieved, the proteins were transferred onto a nitrocellulose membrane for 16 hours at 4°C, at a constant current of 40 mA. Later the membrane was dyed with the MemCode Reversible Protein Stain and imaged for later normalization of the immunolabelled protein bands to the lane signal. After MemCode destaining, the membrane was blocked for 1 hour with LI-COR blocking buffer diluted 1:2 in PBS and incubated with the primary antibodies for 16 hours at 4°C. The primary antibodies used correspond to multiple synaptic proteins enumerated in Table 6 (labeled as LI-COR Odyssey) and in LI-COR blocking buffer with PBS-T. Afterwards, three 5-minutes washes with PBS-T were performed and the membrane was incubated for 2 hours with the secondary antibodies mentioned in Table 5 in LI-COR:PBS-T buffer. After washing three more times with PBS-T, the membrane was imaged using the Odyssey Infrared Imaging System (LI-COR). Protein band quantification was achieved with Image-Studio software (Odyssey System). MemCode signal quantification was performed with FIJI (Schindelin *et al.*, 2012) and used to normalize the fluorescence band signal to the total amount of protein in the lane.

2.2.7. Immunocytochemistry for quantification of synaptic puncta and Sholl analysis

Immunocytochemistry was performed following a protocol kindly provided by Dr. Ali Shaib (Neurobiology Department, Max Planck Institute for Experimental Medicine). To observe the morphological signs of toxicity induced by amyloid aggregates, primary autaptic hippocampal cultures were treated on DIV 8 with 10 μM Aβ42 or the corresponding vehicle control. After 24 or 72 hours of treatment, the Neurobasal-A medium was removed and neurons were washed two times with PBS and fixed with 4% PFA in PBS at room temperature for 20 minutes. PFA was discarded and the neurons were washed three times with PBS and kept at 4°C until immunostaining was performed.

Before starting the immunolabelling, the PBS was removed and samples were quenched with 50 mM glycine in PBS for 10 minutes. Afterwards, cells were permeabilized with 0.1% Triton X-100/ 2.5% goat serum in PBS for 30 minutes. Neurons were subsequently washed two times with 2.5% goat serum in PBS for

5 minutes. The primary antibodies were diluted in 2.5% goat serum in PBS and are listed in Table 6. The autaptic cultured neurons were incubated on top of a ~200 µL drop of the solution with the primary antibodies for 60 minutes at room temperature in a wet chamber. When the incubation was complete, the neurons were washed with 2.5% goat serum in PBS three times for 5 minutes. Next, the neuronal cultures were incubated for 45 minutes on a ~200 µL drop of solution containing the secondary antibodies and DAPI in a 1:2000 dilution in a wet dark chamber. Finally, neurons were washed five times with 1% Triton X-100/ 2.5% goat serum in PBS for 5 minutes, three times with PBS for 5 minutes and mounted using Aqua-Poly/Mount mounting medium. The fixed and immunolabelled neurons were stored at 4°C in a closed coverslip holder until imaging.

2.2.8. Fluorescence microscopy

Images from autaptic hippocampal neurons were acquired using a Leica TCS SP2 or in collaboration with Dr. Ali Shaib on a Leica TCS SP5 confocal microscope, using the 40x oil-immersion objective, with image format= 1024 x 1024, zoom=1.05, voxel size= 360.75 nm x 360.75 nm x 300 nm. Z-stacks of images from autaptic neurons were acquired with a step size of 280 – 300 nm (17-22 slices per neuron). Power, gain and offset of lasers were adjusted at the beginning of each session and kept constant across images for that session. Equal number of images were obtained during each session for all the conditions to be compared. Image acquisition was performed blinded to experimental condition.

2.2.9. Image analysis

2.2.9.1. Sholl analysis

In order to study dendritic branching, Sholl analysis was performed as described in previous publications (Ripamonti *et al.*, 2017). In brief, a manual threshold was applied on the MAP2 signal to obtain a binary image. Any remaining isolated background signal was manually removed. A circle was drawn around the cell somata and its center was automatically detected by a custom-made function. The “Sholl analysis” plugin for FIJI was used for characterization of dendritic arborization using the following analysis parameters: starting radius = 5 µm away

from the center of neuronal somata, ending radius = 250 µm away from the center of neuronal somata, radius step = 5 µm. The outcome values analyzed were: total number of intersections, enclosing radius and number of intersections at increasing distance from the cell center.

2.2.9.2. Synapse count

In order to investigate putative changes in synapse number, image analysis was performed by modifying a protocol published by Ripamonti *et al.* (Ripamonti *et al.*, 2017). In a first step, background signal from astrocytes was deleted from the image stack by manually selecting the area containing the MAP2, VGluT1 and Shank2 signals and applying the “Clear Outside” FIJI built-in function. Then, background signal was subtracted using a custom-made macro provided by Dr. Ali Shaib and Prof. Ute Becherer. In order to restrict the area of analysis and to minimize the amount of noise detected, regions of interest (ROIs) containing synaptic signal were generated by the “WEKA Trainable Segmentation” plugin (Arganda-Carreras *et al.*, 2017). To this aim, 10 random image stacks were selected from the data sets, and the slice with the largest area of signal from each stack was detected and duplicated by a custom-made function. The 10 images were used as data set for training the WEKA classifier using the following segmentation settings: Classifier = FastRandomForest, Training features = Gaussian blur, Hessians, Membrane projections, Laplacian, entropy, sobel filter, Difference of gaussians, structure and neighbors, Minimum thickness = 1, Membrane Patch size = 19, Minimum sigma = 1. The classifier was trained by manually selecting representative regions of the signal and the background on the training data set. Once optimal segmentation was accomplished, the classifier was saved and then applied to the image stack. A ROI containing the signal detected by the classifier was generated and juxtaposed to the preprocessed stack (raw stack after astrocyte signal deletion and background subtraction). The “Clear Outside” function was applied to remove the signal not detected by the classifier. A manual threshold was then applied to the stack and number of puncta were detected by using the “3D Object Count” plugin (Bolte and Cordelieres, 2006). Particles were then reclassified and those larger than 80 voxels were counted as two synaptic puncta. This process was executed independently for the VGluT1 and the Shank2 channels. To obtain the number of puncta positive for both VGluT1 and Shank2, which were considered as a proxy

for synapse number, the Shank2 signal was converted into a ROI and enlarged by 1 pixel. This ROI was applied to the VGluT1 channel and the VGluT1 signal outside the ROI was deleted. The manual threshold was applied again to the Shank-corrected VGluT1 channel and the number of objects per stack was obtained with the 3D Object Count plugin, as described before.

The representative images in the Results section are maximum intensity projections of a stack for a representative neuron for each condition. The brightness and contrast settings optimized for visualization used are identical for the compared conditions.

2.2.10. Electrophysiology

2.2.10.1. Whole-cell recordings of autaptic hippocampal neurons

In order to study effects of Aβ42 and anle138b on synaptic transmission, autaptic hippocampal neurons were treated after at least 7 days *in vitro* and recorded between DIV11 and DIV13. Electrophysiological recordings were performed as described previously (Burgalossi *et al.*, 2012; Ripamonti *et al.*, 2017). Neurons were transferred from the culture medium into a recording chamber containing Base Plus at room temperature. A glass pipette with tip resistance between 2 and 3.5 MΩ was back-filled with intracellular solution and, after gigaseal formation, the membrane patch was ruptured to perform whole-cell recordings. The membrane potential was voltage-clamped at -70 mV using an EPC9 (HEKA) amplifier. Recordings were performed only if the series resistance was below 12 MΩ during the experiment. In order to record evoked EPSCs, neurons were depolarized by a 2-millisecond (ms) square pulse to 0 mV at 0.2 Hz. To study short-term plasticity, neurons were stimulated with the same square pulse but at a frequency of 10 Hz for 5 seconds. External solutions were gravity-based applied for chemical or pharmacological stimulation as puffs onto the autaptic neuron in a precisely regulated manner by a Trigger Interface TIB 14S (HEKA), which controlled the opening and closing of valves and also the position of perfusion micro-pipes. A 6-second application of 0.5 M sucrose in Base Plus was utilized to record the size of the RRP. Spontaneous release as mEPSCs were recorded in the presence of 300 nM TTX diluted in Base Plus. Finally, a 5-second pulse of 100 µM glutamate in Base Plus was applied in order to study the population size

of AMPA receptors, since NMDA currents are blocked by the presence of high magnesium concentration in the Base Plus solution.

For current clamp experiments, the glass pipettes were backfilled with intracellular solution containing low chloride. After gigaseal formation and membrane rupture, the neuron was voltage-clamped at -70 mV and a single EPSC was recorded. The recording mode was immediately switched to current clamp. Subsequently, five hyperpolarizing square pulses from -100 pA to 0 pA were applied in 20 pA increments, followed by depolarizing pulses from 0 pA and 10 pA increments. The depolarizing pulses were applied until the current pulse was three times the value of the rheobase.

The obtained data were imported into Igor Pro (Wavemetrics). Igor waves were converted using the ABF Utilities Software into Axograph-readable files. Data analysis was performed in Axograph (AxoGraph Scientific). For the current clamp results, the junction potential was calculated using an extension contained in the Patcher's Power Tools package for Igor Pro, and corrected offline.

The following parameters were obtained from the recordings:

Voltage-clamp mode:

- EPSC amplitude: minimum value in the EPSC after baseline correction.

- RRP size: integral of the response to sucrose application, when baseline was corrected to the last part of the sucrose response.

- Pvr: ratio of EPSC integral over the RRP, expressed as percentage.

- Paired-pulse ratio: ratio of the amplitude of the second over the amplitude of the first event in a high frequency train of stimuli.

- Depression ratio: ratio of the average amplitude of the last ten EPSCs over the amplitude of the first in a high frequency train of stimuli.

- mEPSC frequency: number of mEPSCs per second. For mEPSC detection, a template-matching method was applied using the following parameters: amplitude= -20 pA, rise time = 0.5 ms, decay time = 3 ms.

- mEPSC amplitude: the minimum current value of a model mEPSC obtained by averaging all the events detected in 100 seconds.

- Response to exogenous glutamate: minimum current value within the initial phase of the response to glutamate application.

Current-clamp mode:

- Membrane resting potential (Vm): voltage value with no current injected, immediately after switching to current clamp mode.

- Input resistance (Rin): slope of the linear fit when plotting voltage vs current from the negative current injections.

- Rheobase: the amount of current injected to elicit the first AP.

- Number of action potentials per second: the number of AP elicited by the first stimulus after the rheobase.

- Action potential threshold (as calculated with the method of third derivative): membrane potential value in the original trace at the time of the first peak of the third derivative.

- Action potential overshoot: maximum value of the AP.

- Action potential amplitude: maximum value of the AP when threshold was subtracted.

- Action potential width: time between two cursors at AP threshold.

- Action potential half width: time between two cursors at half amplitude.

- Afterhyperpolarization amplitude: minimum value of the AP when value after HP was subtracted.

- Afterhyperpolarization half-decay time: period between time of minimum peak to its half.

2.2.10.2. Preparation and recordings from artificial bilayers

Recordings from artificial bilayers exposed to Aβ42 isomers were performed in collaboration with Prof. Roland Benz (Jacobs University), following published protocols (Benz *et al.*, 1978; Martinez Hernandez *et al.*, 2018). In brief, 0.3 mm^2 planar bilayers were formed by spreading a solution of 1% oxidized cholesterol or 1% diphyPC in n-decane using a Teflon loop over a hole in a wall that divided two chambers of a Teflon cell. Currents were measured, digitized and voltage

clamped by a pair of Ag/AgCl electrodes using a Multiclamp 700 (Axon Instruments). After a 5-minutes baseline, Aβ42 or its isomers were added into one side of the chamber at 10 µM. Recordings were performed at varying holding potentials for at least 20 minutes. The recorded data were analyzed using Axograph (AxoGraph Scientific).

2.2.11. Statistics and graphic design software

Data were collected, organized and stored in Microsoft Excel sheets. Statistical analysis was performed using Prism 6 (GraphPad). In a first step, descriptive statistics for each data set were obtained in order determine the distribution of the data. Normally distributed data were analyzed using parametric statistical tests (t-test, one-way ANOVA), whereas not normally distributed data or small data sets were analyzed using non-parametric (Mann-Whitney test, Kruskall-Wallis test) tests depending on the number of groups and variables to compare. For all tests the critical significance level α was 0.05. All data are represented as mean ± standard error of the mean (SEM). The distribution of the data points is depicted by the scatter plots.

All figures were generated using Adobe Illustrator.

3. Results

3.1. Aβ42 species preparation and characterization

Unlike non-amyloid proteins, the effects of *in vitro* preparations of amyloids depend not only on the concentration but also on their aggregation state (Dahlgren *et al.*, 2002; Deshpande, 2006). In aqueous solutions that mimic physiological conditions of temperature and pH, Aβ is prone to fold into hairpin-like structures and its low-entropy C-terminus, to adopt a β conformation (Yan and Wang, 2006; Lim *et al.*, 2007). These two structural features favor intermolecular aggregation into increasingly larger oligomeric species up to insoluble, thermodynamically-stable amyloid fibrils (Lim *et al.*, 2007; Rezaei-Ghaleh *et al.*, 2011). The kinetics of the aggregation process depend on the temperature, agitation, peptide concentration, and presence of aggregate seeds in the starting material, among other factors (reviewed in Thal *et al.* 2015 and Tycko 2015). The dissolution of commercially available protein powder into an aqueous solution of monomers used in aggregation experiments is of critical importance to ensure reproducibility in the effects of the resulting Aβ species solution (Teplow, 2006). In the present study, I initially compared two dissolution methods to disrupt and minimize the presence of large insoluble aggregates that could act as seeding material and bring the Aβ peptide to its monomeric conformation. The solution obtained using a two-step dissolution protocol was further incubated to generate aggregates that were biochemically and morphologically characterized and utilized for investigation of Aβ toxic effects on hippocampal neurons. All experiments were performed with Aβ42, hereafter Aβ.

3.1.1. Characterization of Aβ species yielded by dissolution in HFIP / NaOH followed by in vitro aggregation

In an initial approach, I used an alkaline treatment in which the Aβ peptide was first dissolved in sterile PBS and subsequently ammonia was added to 0.5%. Despite the high pH of the initial solution (>10.5), this method did not remove the large aggregates as evidenced by the presence of smear in the Western blot between 28 and 62 kDa (Figure 5A). In addition, incubation for up to 96 hours did

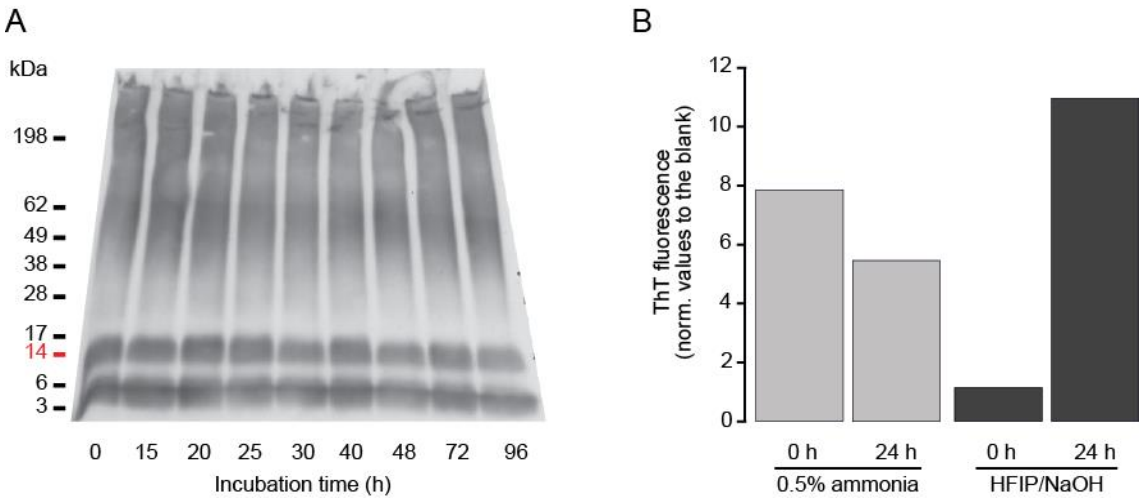

Figure 5. **Dissolution with 0.5% ammonia could not reduce the concentration of seeding material. (A)** Samples of Aβ taken at increasing time points after dissolution with 0.5% ammonia. **(B)** Normalized ThT fluorescence emission of the 0.5% ammonia dissolved sample and the sample dissolved with the two-step method, immediately after dissolution ("0 h") and after 24 hours of incubation ("24h").

not modify the relative concentration of aggregates. Moreover, using ThT fluorescence measurements I observed that the emission of the Aβ solution upon dissolution was eight times higher than the blank, indicating the presence of large aggregates (Figure 5B).

On the next attempt to monomerize the peptide, I used a two-step method involving the organic solvent HFIP and the alkaline solution 100 mM NaOH. Upon dissolution ("0 h"), the ThT emission values were 1-2 times the blank, and these values increased ~10 times after 24 hours (Figure 5B, Figure 6A). The Western blot of the initial supernatant ("S0") showed that 50% of the peptide formed species smaller than 28 kDa (monomers to pentamers) and less than 20% was larger than 98 kDa (Figure 6B). The initial pellet ("P0") showed 50% less signal than the S0, indicating a low concentration of insoluble species (Figure 6B ii). In addition, in the pellet the proportion of species larger than 98 kDa was higher than in the supernatant (Figure 6B ii). These data demonstrated that the two-step method successfully reduced the presence of large aggregates upon dissolution.

In order to describe the aggregation kinetics, samples were taken at increasing incubation periods and analyzed using ThT, Western blot, and TEM. Already at the first time point evaluated after dissolution ("0.6 h"), protofibrillar structures were present evidenced by a 10-fold increase in the ThT emission values, a reduction of the <28-kDa fraction to 20% and an increase in the concentration of

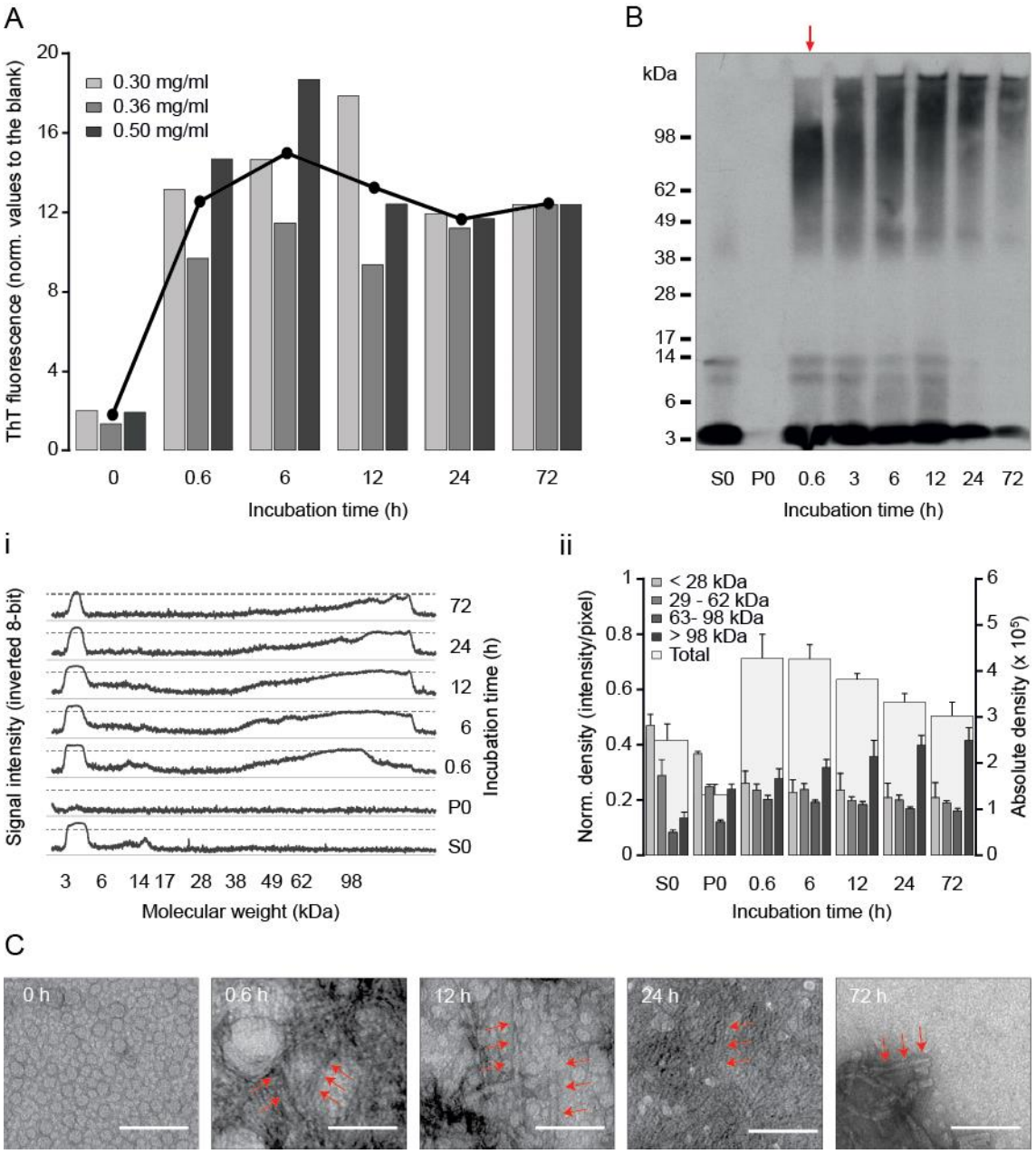

Figure 6. Characterization of Aβ aggregation upon dissolution with HFIP/ NaOH. (A) ThT fluorescence intensity measured at increasing intervals after dissolution, at three different concentrations of Aβ. The values were normalized to the blank for each time point. Note that initially the fluorescence was minimal and increased after 40 minutes of incubation. A plateau was reached after 6 hours of incubation. No lag phase was present. **(B)** Representative Western blot of Aβ samples at increasing incubation intervals at 0.5 mg/ml. The aggregation state of the samples used in the electrophysiological and morphological experiments is indicated by the red arrow. **(i)** Profile of gray intensities versus molecular weight in kDa. Each lane represents a time point after dissolution. Solid and dashed lines represent the 0 and 255 values respectively. **(ii)** Analysis of the normalized signal density per lane. Each narrow bar represents a fraction of the lane corresponding to a range of molecular weights in kDa. The initial supernatant (S0) was composed mostly of Aβ monomers (~0.5 < 28 kDa) although some aggregates between 29 and 62 kDa could be found (~0.3). The proportion of larger aggregates increased with incubation and after 72 hours most of the sample was in protofibrillar/ fibrillar state (0.40 > 62 kDa and 0.42 > 98 kDa). The monomeric fraction was also reduced and was minimal after 72 hours (0.21 < 28 kDa). Thick bars represent the total density per lane in absolute values (n= 3 Aβ preparations). Error bars represent the SEM. **(C)** TEM images of negatively stained samples at increasing times of incubation (20,000x). The red arrows indicate protofibrillar / fibrillar aggregates. Brightness and contrast have been adjusted in the EM images to improve visualization. Scale bars= 100 nm.

species larger than 63 kDa to up to ~50% in the Western blot (Figure 6A, B). Analysis of the successive samples showed that monomers were consumed and in turn the proportion of large aggregates increased (Figure 6B). No lag phase was found in the ThT emission measurements (Figure 6A), indicating that despite the efforts to eliminate the seeding material, some fibrils remained thus accelerating the aggregation process.

The respective TEM grids were smothered with protofibrils of 200-nm length and 10-nm width (Figure 6C) already at 0.6 hours. At the last time point evaluated ("72 h"), a large part of the TEM grid was empty, only covered by contrasting material and isolated accumulation of protofibrils or mature fibrils were occasionally found. Despite the reproducibility in the aggregation patterns evidenced by ThT measurements and Western blot, the morphology of the aggregates by TEM displayed some variation between preparations (Figure 7). At 0 hours in two of the grids no aggregates could be visualized, whereas in

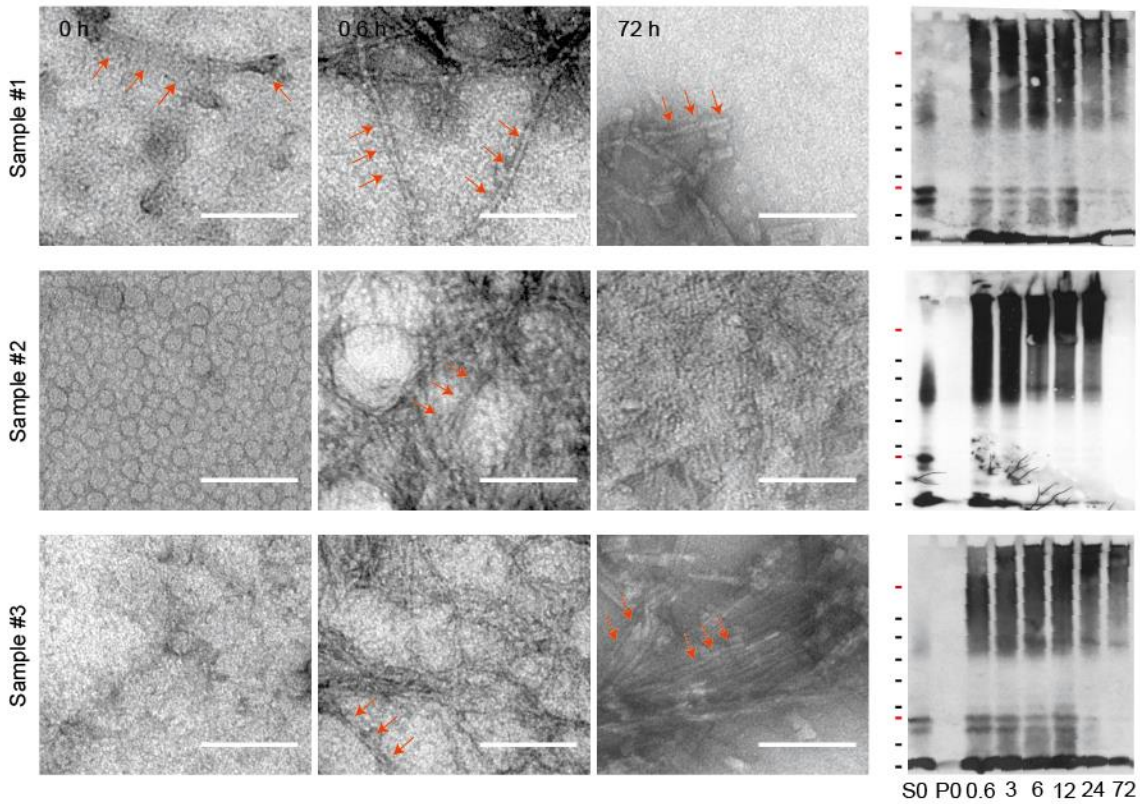

Figure 7. TEM reveals conformational variability among aggregates with identical Western blot patterns. TEM images at 20,000X of aggregates at selected incubation time points to compare the morphology of three sets of samples (left) and the corresponding Western blots (right). Although the blots showed similar patterns of aggregation the relative amount of protofibrils and fibrils seemed to vary. The red arrows indicate protofibrillar / fibrillar aggregates. Brightness and contrast have been adjusted in the EM images to improve visualization. Scale bars= 100 nm. Molecular weight markers as in Fig.6.

sample #1 there were globular or short protofibrillar structures (red arrows). Although all samples showed protofibrillar aggregates at 0.6 hours, their density on the grid varied. Similarly, at 72 hours isolated clusters of protofibrils or fibrils were observed, with variation in the density across samples.

Taken together, these data showed that the two-step dissolution method successfully minimized the presence of fibrils in the initial solution of monomers which aggregated in a reproducible manner, despite some variation in the conformational state of the aggregates in the EM images.

3.2. Effects of Aβ treatment on survival, synaptic function and morphology of hippocampal neurons

Once its reproducibility was established, I used the product of the protofibrillar Aβ preparations at different concentrations and treatment durations to study toxic effects on primary hippocampal neurons. The aggregation process was stopped after 0.6 hours of incubation, the time point at which the solution contained ~50% of high molecular weight oligomeric aggregates (protofibrils according to the EM data) and ~20% monomeric Aβ. The concentrations mentioned in the following experiments correspond to monomeric equivalents since protein concentration could only be measured before starting the *in vitro* aggregation.

3.2.1. Effects of 10 μM Aβ treatment for 72 hours

3.2.1.1. Analysis of cell death upon 72-hour Aβ treatment

On DIV 8, 10 μM Aβ (“Aβ”) or equal volume of phosphate buffer (“Vehicle”) was added to primary hippocampal neurons cultured at a high density. After 72 hours of treatment, the coverslips were stained with Hoechst dye and approximately 20 images of neuronal nuclei per coverslip were immediately acquired without fixation (Figure 8A). Although the total nuclei per image were nearly identical in both groups (Figure 8B i), I found an increase in the fraction of picnotic nuclei from 27.5% in the vehicle to 35.6% in the Aβ-treated neurons (Figure 8B ii) reflecting a mild increase in cell death, in accordance to data published by others (Jan *et al.*, 2008). It has been shown that synaptic dysfunction precedes neuronal death and that loss of synapses is the best correlate with cognitive decline (see section 1.3.3). Since I aimed to model Aβ synaptotoxicity *in vitro*, this mild

reduction in neuronal survival did not prevent or interfere with the study of synaptic function in the remaining neurons.

3.2.1.2. Effects of 72-hour Aβ exposure on synaptic transmission

AD has been described as a “synaptic failure” already decades ago (Selkoe, 2002). However, the exact nature of synaptic dysfunction is still not completely understood. In the next set of experiments, I aimed to describe the effects of Aβ exposure on glutamatergic synaptic transmission, which might underlie the symptoms of early-stage dementia before gross alterations occur. Hippocampal autaptic neurons were grown at low density on astrocytic feeder islands and treated with 10 µM Aβ or vehicle on DIV 8. After 72 hours Aβ-treated neurons showed a 60% reduction in EPSC amplitude compared to vehicle-treated neurons (Figure 9A). The RRP size of Aβ-treated neurons was also decreased to 48% compared to vehicle-treated neurons (Figure 9B). No change in Pvr was observed (Figure 9C). Previously it had been reported that Aβ could induce synapse loss, which could explain the reduced evoked response (reviewed in Spires-Jones and Hyman 2014). However, in these experiments the response to exogenous glutamate application of the Aβ-treated neurons was moderately reduced to 80% the value of the vehicle-treated neurons (Figure 9D). Since 95%

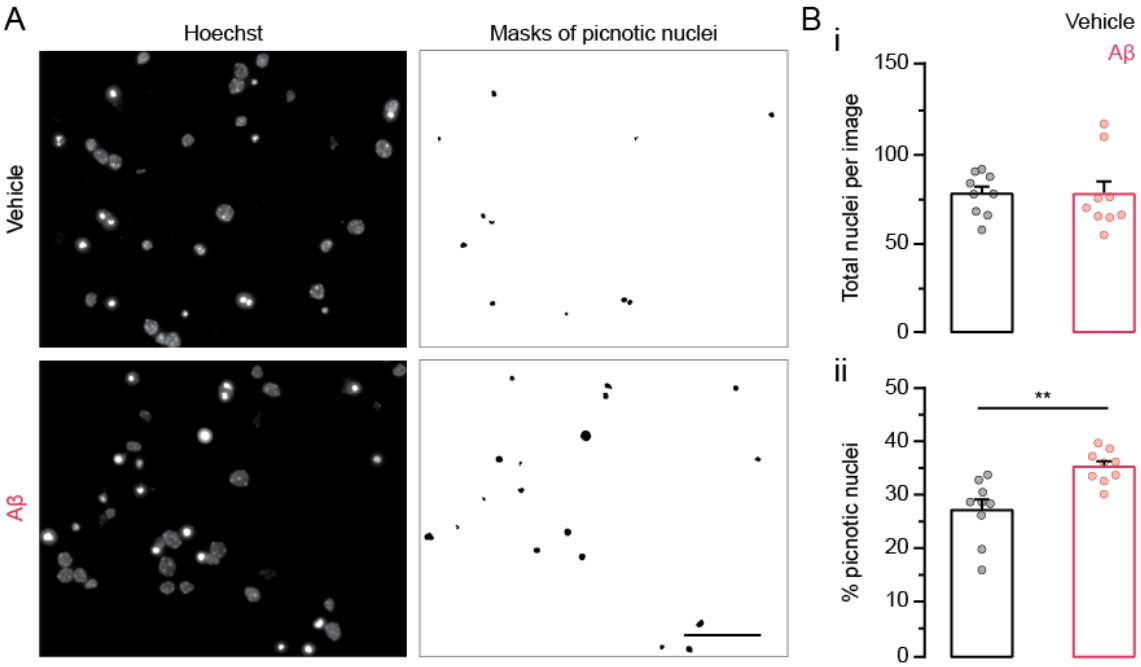

Figure 8. Mild increase in picnotic nuclei count upon Aβ treatment. (A) Representative images of Hoechst-stained neuronal nuclei from vehicle- or Aβ-treated cultures and the respective masks of picnotic nuclei. Scale bar= 50 µm. **(B)** Quantification of **(i)** total nuclei per image and **(ii)** percentage of picnotic nuclei with respect to the total (n= 9 coverslips, from N= 3 cultures and Aβ preparations; unpaired t-test, **p= 0.002). Bars represent the mean and error bars, the SEM.

of the AMPA receptors are localized at postsynaptic sites, these data indicate that the release defect was most likely due to an alteration in presynaptic function, unless AMPA receptors had been relocated to extrasynaptic sites (Lee *et al.*, 2017). In accordance with this, a reduction in mEPSC frequency with no change in the amplitude in the Aβ-treated neurons compared to the vehicle-treated neurons was observed (Figure 9E). Short-term plasticity was not affected as shown by unchanged paired-pulse ratio and depression ratio (Figure 9F).

3.2.1.3. Quantification of synapse number and dendritic branching in 72-hour Aβ-treated neurons

To further investigate the cause of the presynaptic defects in Aβ-treated neurons, I performed a morphological analysis on autaptic neurons treated identically to those used for electrophysiological experiments. After 72 hours of treatment, the neurons were fixed and later immunolabelled against MAP2, VGluT1, and Shank2.

Sholl analysis of binarized MAP2 signal was used to quantify and analyze the distribution of dendrites in vehicle- or Aβ-treated neurons (Figure 10A). A plot of the average number of intersections versus the distance from the center of the cell soma showed that the spatial distribution of dendrites was similar in both groups, but suggested that the Aβ-treated neurons had a reduced number of branches (Figure 10B). To quantify these putative effects, I first compared the radius of the largest circle that could contain the complete dendritic tree ("enclosing radius"), an indicator of the cell size, which was not modified by Aβ exposure (Figure 10C i). Subsequently, I analyzed the sum of all intersections from a neuron, a proxy measurement for dendritic branching, which showed a 20% reduction in the Aβ-treated neurons (Figure 10C ii). These changes in the number of dendrites could explain the reduction in the response to exogenous glutamate application seen in electrophysiological experiments. Finally, the intersections were grouped in bins to analyze the effects in branching at increasing distances from the cell soma (Figure 10C iii). Although not statistically significant, the Aβ-treated neurons showed a tendency towards a reduction in the number of intersections at distances between 40-80 µm (Mann-Whitney test, p= 0.0603) and 85-250 µm (Mann-Whitney test, p= 0.0673) from the center of the cell somata.

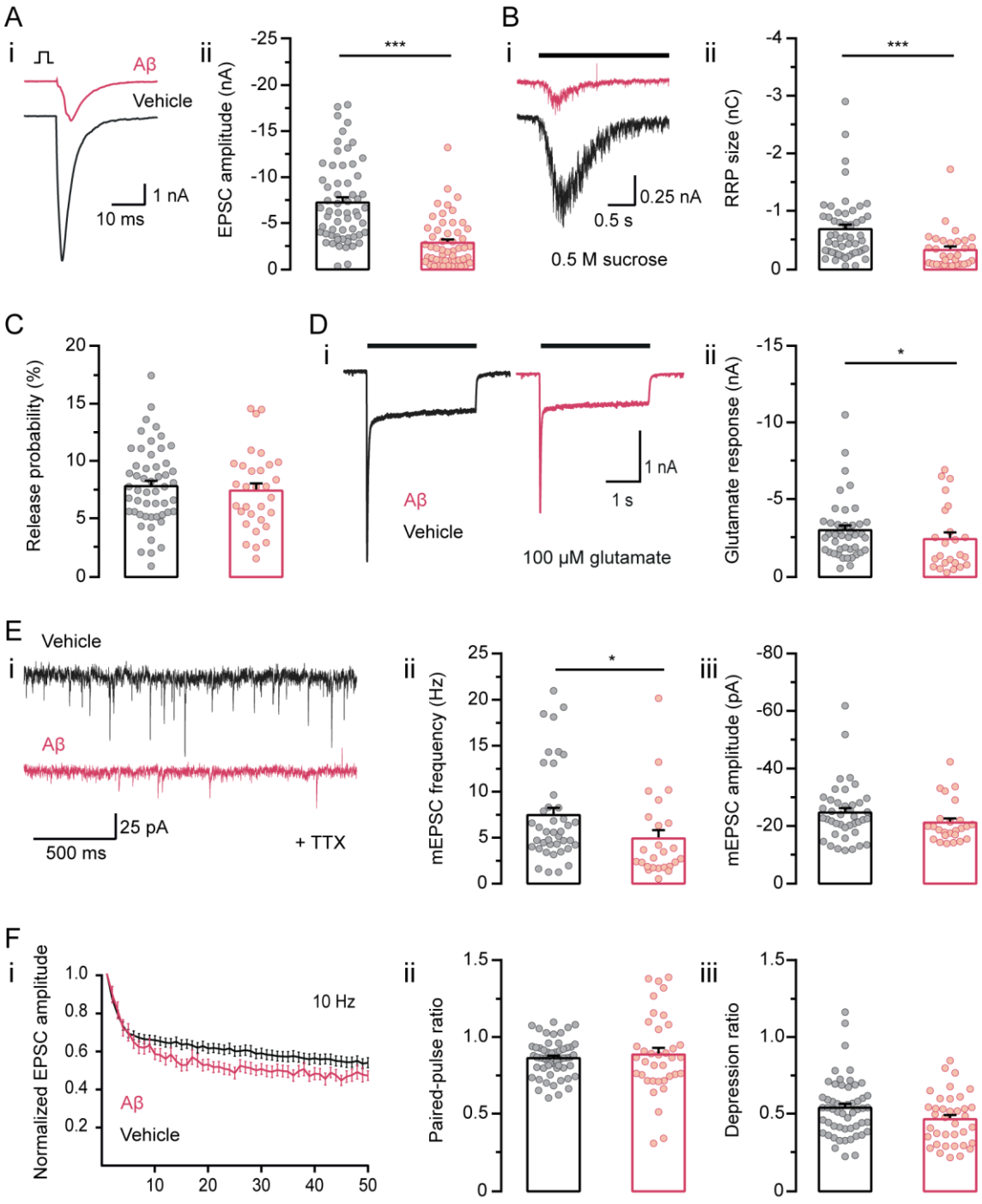

Figure 9. 72-hour Aβ treatment reduces evoked and spontaneous glutamate release. (A) (i) Representative traces and **(ii)** quantification of EPSCs evoked by a 2-ms depolarizing pulse (n= 52-60 neurons, from at least N= 3 cultures and Aβ preparations; Mann-Whitney test, ***p< 0.001). **(B) (i)** Representative traces and **(ii)** quantification of RRP evoked by application of 0.5 M sucrose (n= 31-52, N= 3; Mann-Whitney test, ***p< 0.001). **(C)** Quantification of Pvr. **(D) (i)** Representative traces and **(ii)** quantification of postsynaptic response to the application of 100 μM glutamate (n= 24-42, N= 3; Mann-Whitney test, *p= 0.038). **(E) (i)** Representative traces and **(ii)** quantification of mEPSCs amplitude and **(iii)** frequency of events recorded in the presence of 300 nM TTX (n= 25, N= 3; Mann-Whitney test, *p= 0.009). **(F) (i)** Normalized amplitudes of the first 50 EPSCs in a train of stimuli at 10 Hz. **(ii)** Ratio between the 2nd to the 1st EPSCs in the train ("Paired-pulse ratio") and **(iii)** the 41th- 50th to the 1st EPSCs ("Depression ratio"). Bars represent the mean. Error bars represent SEM. Vehicle, black bars; Aβ, pink bars.

I also compared VGluT1 and Shank2 puncta as well as puncta with juxtaposed VGluT1 and Shank2 signal ("VG+/Sh2+") between the Aβ- and vehicle-treated neurons (Figure 10A). The quantitative analysis of these markers showed no differences between the groups (Figure 10B i-iii). These results indicated a conserved number of pre- and postsynaptic structures as well as entire synapses upon Aβ exposure. In addition, the mean intensity of VGluT1 puncta did not differ between the Aβ- and vehicle-treated neurons, suggesting that the number of vesicles in the presynaptic terminals was not modified by the presence of Aβ (Figure 10B iv).

A summary of the results of 10 μM Aβ treatment for 72 hours on cell death, synaptic transmission and neuronal morphology can be found in Table 7.

3.2.1.4. Effects of 72-hour exposure to Aβ on synaptic protein composition

Given that Aβ markedly impaired glutamate release in hippocampal neurons with no gross alterations in their morphology, I hypothesized that a change in the protein composition at synapses could underlie these effects. Autaptic cultures

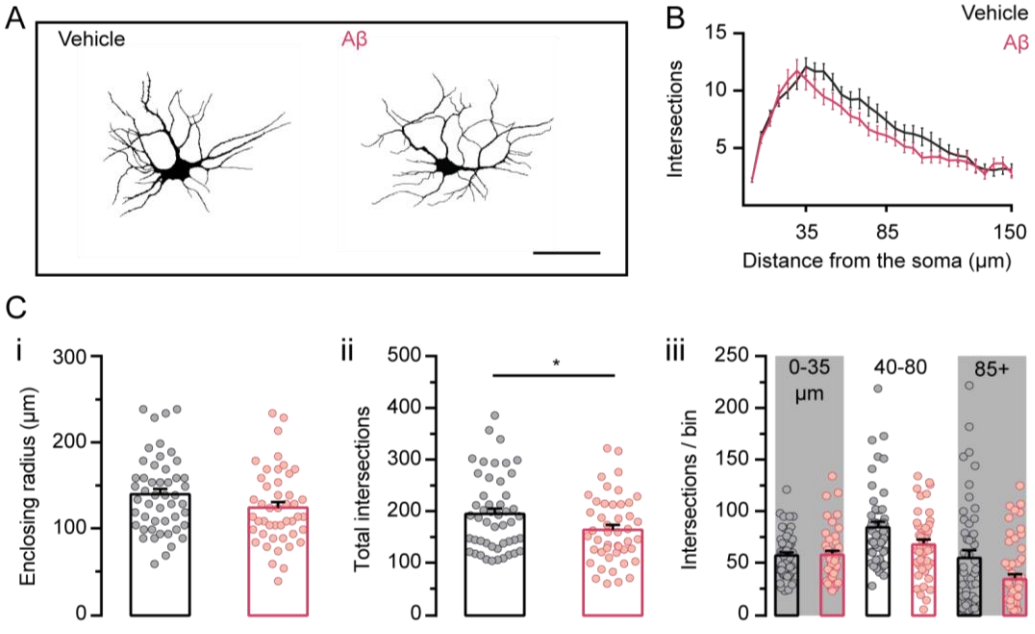

Figure 10. Aβ treatment reduces dendritic branching. (A) Representative images of skeletonized MAP2 signal for Sholl analysis from vehicle- or Aβ-treated neurons. Scale bar= 50 μm. **(B)** Distribution of intersections with respect to the distance from the cell soma. A similar profile of dendrite distribution was found in both groups. **(C) (i)** Enclosing radius. **(ii)** Total intersections per neuron (n= 46-49 neurons from N= 6 cultures and Aβ preparations; unpaired t-test, *p= 0.033). **(iii)** Total intersections grouped in bins by distance from the center of cell soma. Bars represent the mean. Error bars represent SEM. Vehicle, black bars; Aβ, pink bars.

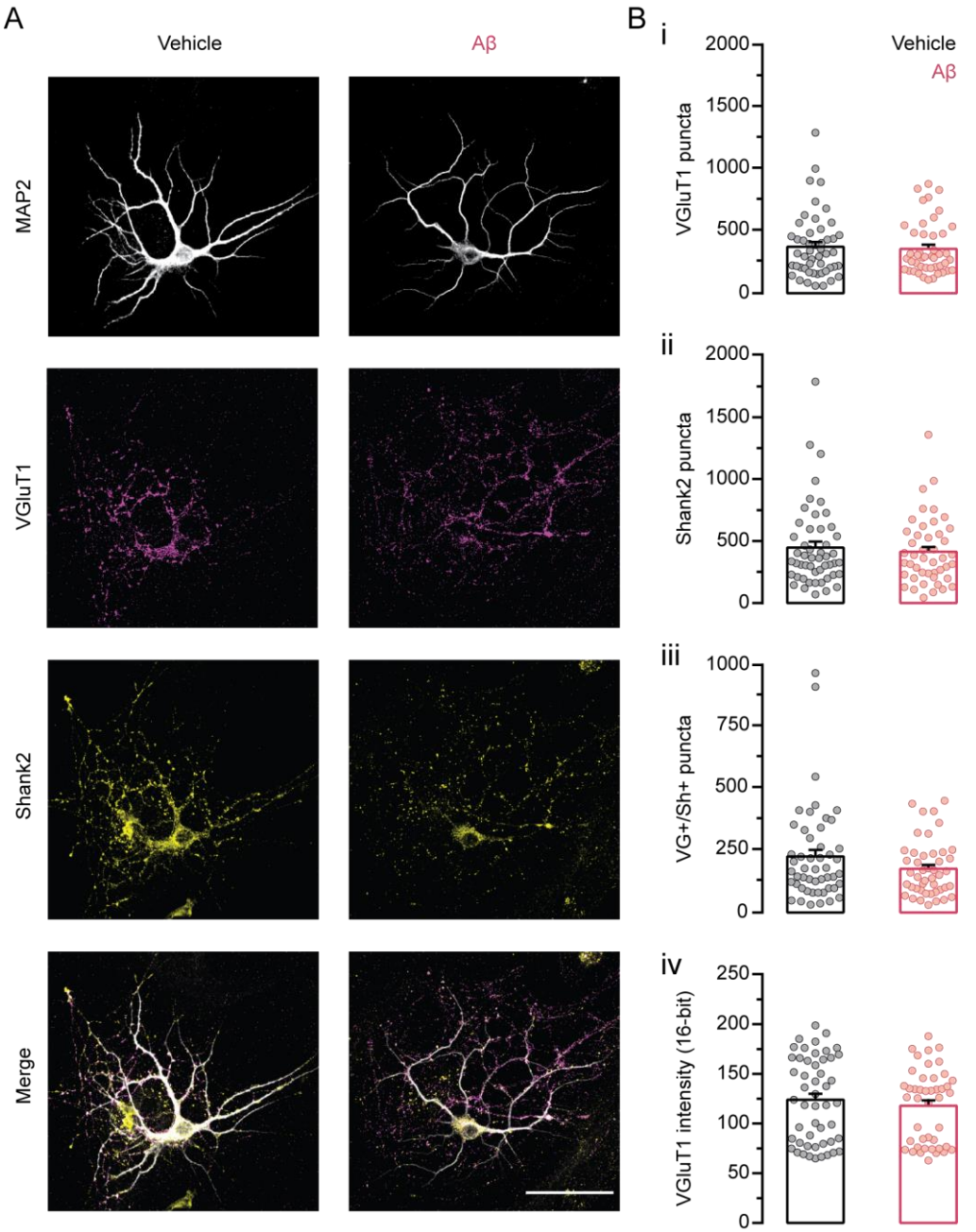

Figure 11. Conserved morphology and number of synapses in 72-hour Aβ-treated neurons. (A) Representative images of neurons fluorescently labelled with antibodies against MAP2, VGluT1 and Shank2. Scale bar= 50 µm. **(B)** Quantification of puncta per image of **(i)** VGluT1, **(ii)** Shank2 and **(iii)** puncta positive for both VGluT1 and Shank2. **(iv)** The mean gray intensity for VGluT1-positive puncta was also quantified and compared. Bars represent the mean. Error bars represent SEM. Vehicle, black bars; Aβ, pink bars.

could not be used to test this hypothesis because of their low density and consequently low yield of protein sample; and also due to the presence of supporting glial cells, which would contaminate the neuronal lysate. I therefore cultured hippocampal neurons at high density and treated them in the same way as the cultures for electrophysiological and morphological experiments. On DIV

Table 7. Summary of effects of 72-hour treatment with 10 μM Aβ on hippocampal neurons.

Fig.	Parameter	Vehicle			Aβ			p value	Summary	Test
		Mean	SEM	n	Mean	SEM	n			
	Cell death (mass cultures)									
8B i	Total nuclei	77.610	3.955	9	77.460	7.104	9	0.986	n.s.	t test
8B ii	% picnotic nuclei	27.480	1.945	9	35.590	1.024	9	0.002	**	t test
	Electrophysiology (autaptic cultures)									
9A ii	EPSC (nA)	-7.277	0.569	60	-2.918	0.373	52	< 0.001	***	Mann-Whitney
9B ii	RRP (nC)	-0.703	0.007	52	-0.341	0.006	31	< 0.001	***	Mann-Whitney
9C	Pvr (%)	7.902	0.472	52	7.523	0.616	31	0.626	n.s.	Mann-Whitney
9D ii	Glutamate-induced current (nA)	-3.067	0.307	42	-2.475	0.436	24	0.038	*	Mann-Whitney
9E ii	mEPSC frequency (Hz)	7.446	0.812	41	4.918	0.920	25	0.009	**	Mann-Whitney
9E iii	mEPSC amplitude (pA)	-24.7	1.571	41	-21.24	1.456	25	0.071	n.s.	Mann-Whitney
9F ii	Paired-pulse ratio	0.8682	0.016	54	0.893	0.042	37	0.538	n.s.	t test
9F iii	Depression ratio	0.5455	0.025	54	0.470	0.027	37	0.057	n.s.	Mann-Whitney
	Sholl - syn. puncta (autaptic cultures)									
10C i	Enclosing radius (μm)	141.0	6.327	49	125.7	6.426	46	0.091	n.s.	t test
10C ii	Total intersections	197.0	10.48	49	166.3	9.559	46	0.033	*	t test
11B i	VGluT1 puncta	377.5	36.78	50	360.50	31.97	45	0.924	n.s.	Mann-Whitney
11B ii	Shank2 puncta	450.2	47.04	50	414.90	40.05	45	0.802	n.s.	Mann-Whitney
11B iii	VG+/Sh2+ puncta	227	27.11	50	177.00	16.70	45	0.313	n.s.	Mann-Whitney
11B iv	VGluT1 intensity (16-bit)	124.4	6.060	50	118.40	5.598	44	0.474	n.s.	Mann-Whitney

11, after 72 hours of treatment with either Aβ or the equivalent vehicle volume, the cells were lysed and samples were collected. Later, the lysates were processed using SDS-PAGE and Western blot to mark a battery of synaptic proteins. Overall, no biologically relevant changes between the conditions were found and only a 20% reduction in the presynaptic protein synaptotagmin-1 was statistically significant (Figure 12, values summarized in Table 8).

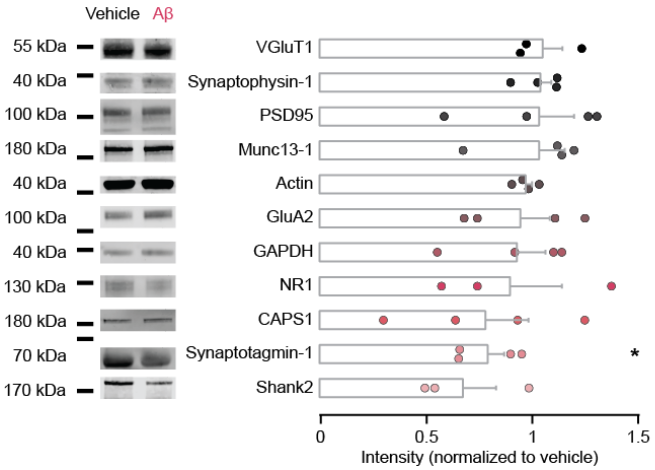

Figure 12. Protein composition of Aβ-treated synapses is unchanged upon 72-hour treatment. Representative Western blot bands for the corresponding synaptic proteins and band signal normalized to the values of samples from vehicle-treated neurons (n= 3-4 cultures, N= 1-2 Aβ preparations; Kolmogorov-Smirnov test, *$p_{Synaptotagmin-1}$= 0.028).

3.2.2. Effects of 10 μM Aβ treatment for 24 hours

After having established a model for chronic toxicity with the 72-hour treatment, I explored the effects of a shorter exposure to Aβ, aiming to find earlier alterations which could be potentially reverted. In this set of experiments, autaptic hippocampal neurons were treated on DIV 10 with 10 μM Aβ for 24 hours. With this shorter exposure I expected to find a milder but still similar phenotype to the 72-hour treatment. Surprisingly, the 24-hour Aβ-treated neurons displayed a 59% increase in EPSC amplitudes (Figure 13A), and a trend towards larger RRPs (Figure 13B), although the latter were not statistically significant. Additionally, the Pvr increased from an average of 8.1% in the control neurons to 11.26% upon Aβ treatment (Figure 13C). Neither the response to exogenous glutamate application (Figure 13D) nor the amplitude of mEPSCs (Figure 13E ii) were

Table 8. Summary of the Western blot results of synaptic proteins from neurons treated with 10 μM Aβ for 72 hours.

Fig.	Protein	Mean	SEM	n	p value	Summary	Test
12	VGluT1	1.054	0.092	3	0.590	n.s.	t test
12	Syphy1	1.043	0.051	4	0.433	n.s.	t test
12	PSD95	1.036	0.166	4	0.835	n.s.	t test
12	Munc13	1.036	0.120	4	0.772	n.s.	t test
12	Actin	0.972	0.026	4	0.353	n.s.	t test
12	GluA2	0.948	0.139	4	0.722	n.s.	t test
12	GAPDH	0.931	0.134	4	0.629	n.s.	t test
12	NMDAR-1	0.899	0.243	3	0.702	n.s.	t test
12	CAPS1	0.782	0.202	4	0.325	n.s.	t test
12	Synaptotagmin-1	0.794	0.078	4	0.039	*	t test
12	Shank2	0.677	0.156	3	0.108	n.s.	t test

modified, indicating a functionally conserved postsynaptic site as well as unchanged quantal size. Despite the increase in Pvr, there was no change in mEPSC frequency (Figure 13E iii) or in short term plasticity as reflected by unaltered paired-pulse ratio and depression ratio (Figure 13F). The results from this section are summarized in Table 9.

3.2.3. Comparison of the joint effects of development and Aβ exposure on neuronal morphology

The duration of the exposure to Aβ was found to be a factor that not only defined the magnitude of the effects but also the type of the electrophysiological changes in the treated neurons. EPSC amplitudes were reduced in the 72-hour treatment, whereas both EPSC amplitude and Pvr increased upon exposure for 24 hours. Since opposing effects were found in synaptic transmission depending on the time of Aβ exposure, I compared the morphological effects of the chronic, 72-hour Aβ exposure to the shorter, 24-hour treatment. While electrophysiological recordings were performed on neurons of the same age (DIV 11), this morphological analysis was performed on cells at different developmental stages. Specifically, autaptic neurons were treated on DIV 8 with 10 µM Aβ or equivalent volume of the vehicle and later, on DIV 9 a group of coverslips was fixed to investigate effects at 24 hours and another, on DIV 11 after 72 hours of exposure. Immunolabelling of the autaptic neurons, quantification of synaptic puncta, and Sholl analysis were performed as described previously for the 72-hour treatment (see section 3.2.1.3). In this experiment, two-way ANOVA was used for statistical analysis of the influence of “duration of exposure” and “treatment” as categorical independent variables on the tested morphological parameters. Additionally, the interaction between these variables was analyzed. As previously described, the complexity of the dendritic tree was investigated in all the groups using Sholl analysis of the binarized MAP2 signal (Figure 14A). The profile of the dendrite distribution (Figure 14B) showed that the vehicle treated neurons at 72 hours of exposure (DIV 11) presented a higher number of branches at longer distances from the center of the cell soma than the neurons of the same condition at 24 hours (DIV 8), describing normal dendritic development of autaptic neurons *in vitro*. This process seemed to be impaired in the 72-hour Aβ-treated neurons. Neither the duration of exposure to Aβ nor the treatment as independent factors showed a significant effect on the enclosing radius (Figure 13C i) or total sum of

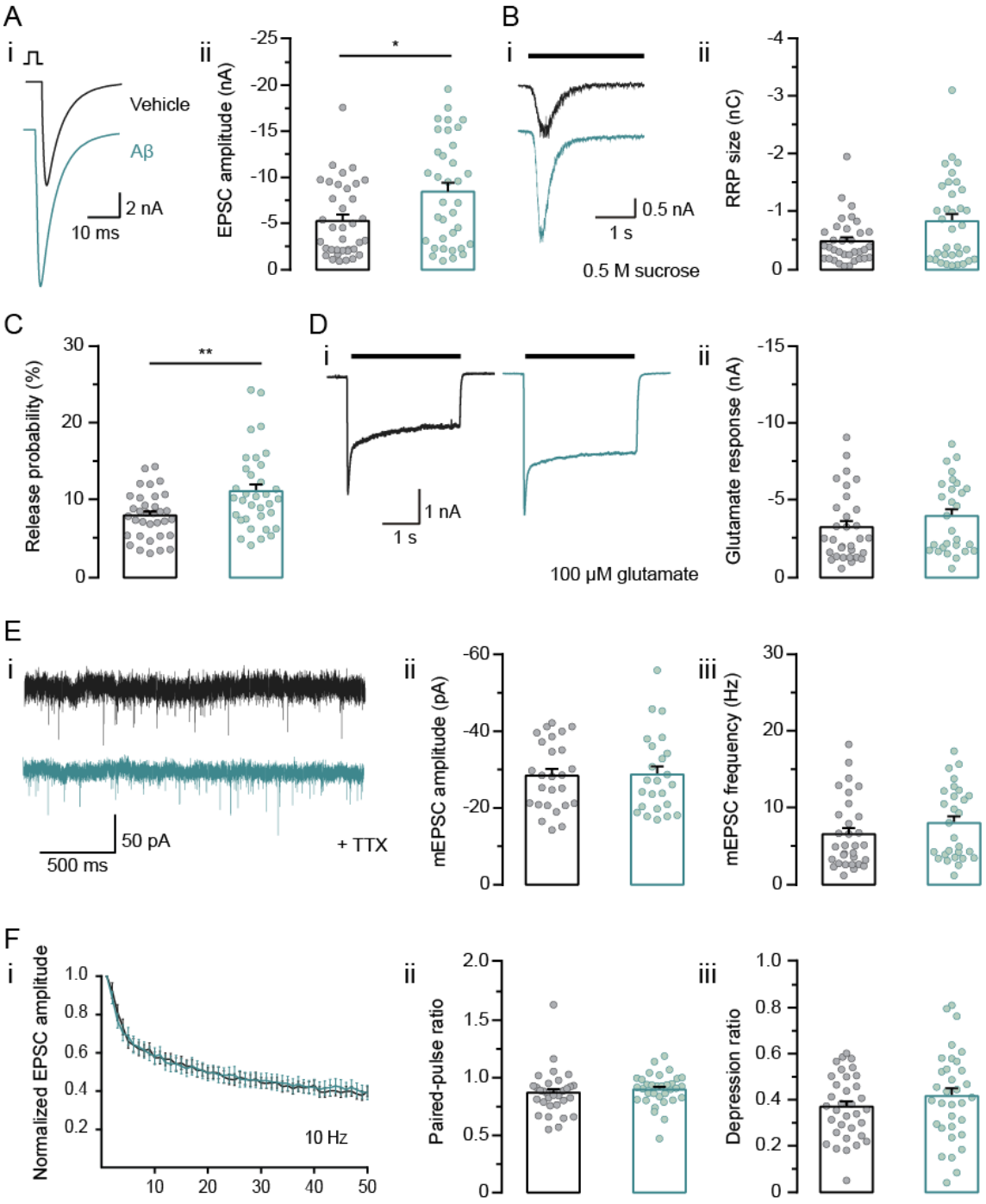

Figure 13. 24-hour Aβ treatment enhances evoked glutamate release with no change in postsynaptic response or short-term plasticity. (A) (i) Representative traces and **(ii)** quantification of EPSC amplitude (n= 35-36, N=3 cultures and Aβ preparations; Mann-Whitney test, *p= 0.015). **(B) (i)** Representative traces of the response evoked by 0.5 M sucrose application. **(ii)** Quantification of RRP size. **(C)** Quantification of Pvr. (n= 34, N= 3; Mann-Whitney test, **p= 0.007). **(D**) **(i)** Representative traces and **(ii)** quantification of postsynaptic response to exogenous glutamate application. **(E) (i)** Representative traces and quantification of **(ii)** amplitude and **(iii)** frequency of mEPSCs recorded in the presence of TTX. **(F) (i)** Normalized amplitudes of the first 50 EPSCs in a train of stimuli at 10 Hz. Quantification of **(ii)** paired-pulse ratio and **(iii)** depression ratio. Bars represent the mean. Error bars represent SEM. Vehicle, black bars; Aβ, green bars.

Table 9. Summary of the electrophysiological effects of 24-hour treatment with 10 µM Aβ on autaptic hippocampal neurons.

Fig.	Parameter	Vehicle			Aβ			p value	Summary	Test
		Mean	SEM	n	Mean	SEM	n			
13A ii	EPSC (nA)	-5.323	0.670	36	-8.492	0.969	35	0.015	*	Mann-Whitney
13B ii	RRP (nC)	-0.497	0.006	34	-0.844	0.012	34	0.146	n.s.	Mann-Whitney
13C	Pvr (%)	8.10	0.521	34	11.26	0.879	34	0.007	**	Mann-Whitney
13D ii	Glutamate-induced current (nA)	-3.292	0.408	28	-4.014	0.446	31	0.210	n.s.	Mann-Whitney
13E ii	mEPSC amplitude (pA)	-28.46	1.739	26	-28.72	2.114	24	0.843	n.s.	Mann-Whitney
13E iii	mEPSC frequency (Hz)	7.483	1.245	26	6.752	1.110	24	0.925	n.s.	t-test
13F ii	Paired-pulse ratio	0.867	0.032	34	0.895	0.024	33	0.144	n.s.	Mann-Whitney
13F iii	Depression ratio	0.371	0.023	34	0.418	0.033	33	0.258	n.s.	t-test

intersections (Figure 13C ii). However, a statistically significant reduction in the interaction p-value for both the enclosing radius and total intersections confirmed the observation from the Sholl profile that branching increases over the course of the experiment in the control group, while this process is impaired in neurons exposed to Aβ, and even dendritic loss may occur.

VGluT1 and Shank2 immunoreactive puncta, as well as co-labeled puncta were quantified and compared in Aβ and vehicle-treated groups at DIV 9 and DIV 11 (Figure 14A). No changes were found between the tested groups (Figure 14B i-iii). Since the 24-hour treated neurons showed larger EPSCs, I decided to evaluate the fluorescence intensity of the VGluT1 puncta as an indicator of the quantity of vesicles in the synapses (Figure 14B iv). Similarly, this parameter showed no differences among the experimental groups.

When analyzed together, these morphological data described no major changes in autaptic neurons upon the 24-hour Aβ treatment, even though the electrophysiological measurements showed an altered glutamate release. In addition, these experiments confirmed the findings of section 3.2.1.3 of a moderate deleterious Aβ effect in dendrite development, which becomes more evident when analyzed over time.

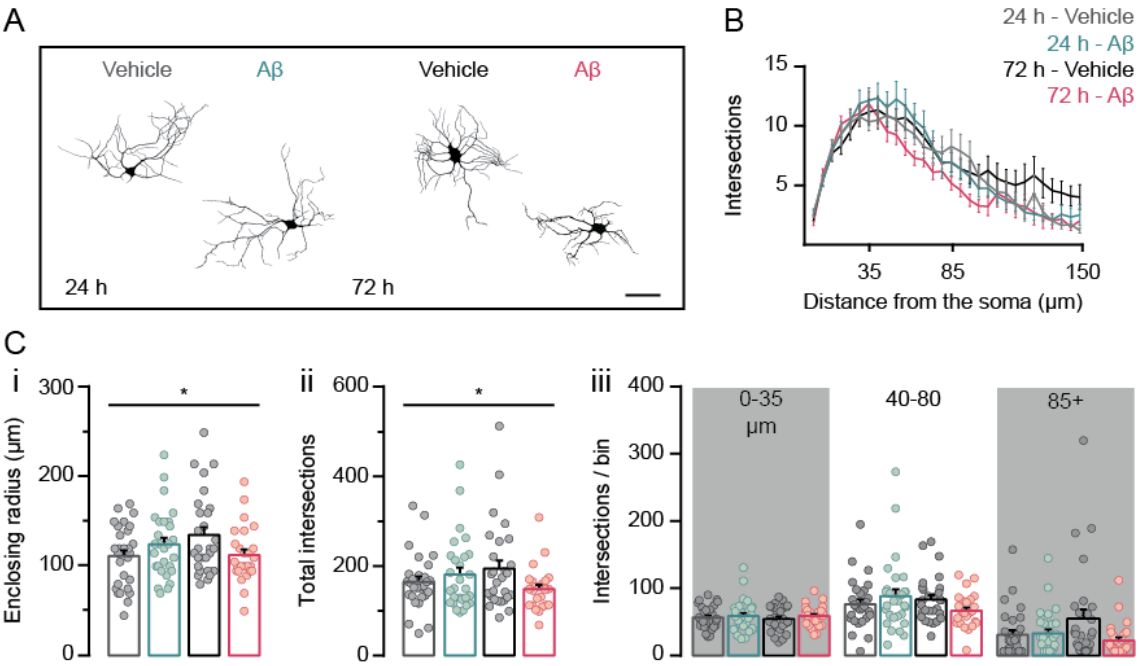

Figure 14. Aβ detrimental effects on dendritic development. (A) Representative images of skeletonized MAP2 signal for Sholl analysis from vehicle- or Aβ-treated neurons after 24 or 72 hours of exposure. Scale bar= 50 μm. **(B)** Distribution of intersections with respect to the distance from the center of the cell soma. **(C) (i)** Enclosing radius (n= 26-28, N= 3; two-way ANOVA; interaction "duration of exposure" x "treatment": $F_{(1,106)}$= 5.956, *p= 0.001). **(ii)** Total intersections per neuron (n= 26-28, N= 3; two-way ANOVA; interaction "duration of exposure" x "treatment": $F_{(1,106)}$= 4.631, *p= 0.0337). **(iii)** Total intersections grouped in bins by distance from the cell soma. Bars represent the mean. Error bars represent SEM. 24 h - Vehicle, gray bars; 24 h - Aβ, green bars, 72 h - Vehicle, black bars; 72 h - Aβ, pink bars.

The descriptive statistics for the data set corresponding to each condition are summarized in Table 10. The results of the two-way ANOVA analysis can be found in Table 11.

3.2.4. Analysis of 72-hour Aβ treatment concentration dependence

In the previous experiments I observed that the duration of the exposure to the Aβ peptide was a factor that determined the magnitude of the impairment of synaptic transmission in the autaptic neurons, as indicated by reduced EPSC amplitudes, among other effects. Next, I wanted to investigate whether a correlation existed between the concentration of Aβ in the culture medium and putative neurotoxicity. To this aim, I cultured and treated autaptic hippocampal neurons as described before, but in these experiments utilizing 200 nM and 1 μM (in monomeric equivalent concentrations) in addition to the vehicle and 10 μM Aβ, which were used as negative and positive controls for toxicity respectively. After 72 hours of treatment, the neurons were used for patch-clamp recording of their synaptic activity. EPSCs were evoked as before by a 2-ms depolarizing pulse (Figure 15A i) and the amplitudes were compared between groups (Figure

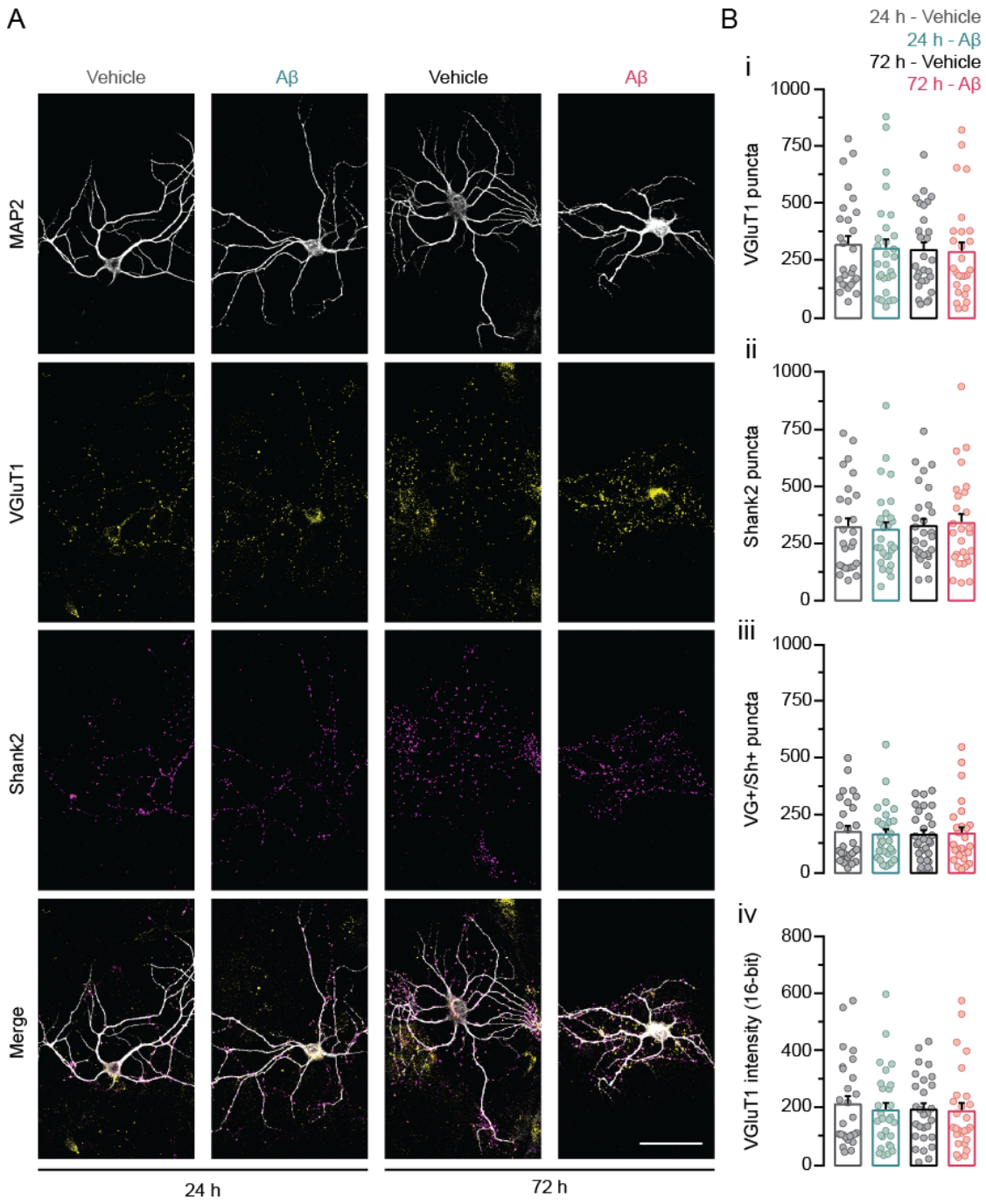

Figure 15. Conserved number of synapses in 24-hour and 72-hour Aβ-treated neurons. (A) Representative images of vehicle or Aβ-treated neurons after 24 or 72 hours of exposure, fluorescently labelled with antibodies against MAP2, VGluT1 and Shank2. Scale bar= 50 µm. **(B)** Quantification of puncta per image of **(i)** VGluT1, **(ii)** Shank2 and **(iii)** puncta positive for both VGluT1 and Shank2. **(iv)** The mean gray intensity for VGluT1-positive puncta was also quantified and compared between the groups. Bars represent the mean. Error bars represent SEM. 24 h - Vehicle, gray bars; 24 h - Aβ, green bars, 72 h - Vehicle, black bars; 72 h - Aβ, pink bars.

15A ii). No statistically significant differences were found, but still the tendency remained for the 10 µM Aβ-treated neurons to have smaller amplitudes compared to the vehicle-treated neurons, and a trend was observed of larger EPSCs with increasing Aβ concentrations below 10 µM. To investigate the size of the RRP, 0.5 M sucrose was applied (Figure 15B i), with no changes observed between

Table 10. Summary of morphological changes induced by Aβ on dendrite development

Fig.	Parameter	24 h - Vehicle			24 h - Aβ			72 h - Vehicle			72 h - Aβ		
		Mean	SEM	n	Mean	SEM	n	Mean	SEM	n	Mean	SEM	n
14C i	Enclosing radius (µm)	111.8	7.223	28	124.6	6.588	28	135.4	8.599	28	112.9	6.128	26
14C ii	Total intersections	165.4	15.42	28	181.9	12.03	28	194.8	18.46	28	149.3	9.311	26
15B i	VGluT1 puncta	322.2	39.66	27	306	40.97	28	299.4	34.05	28	294	43.4	26
15B ii	Shank2 puncta	323.1	37.64	27	311.5	33.43	28	327.6	31.52	28	345.5	41.23	26
15B iii	VG+/Sh2+ puncta	183.7	26.79	27	169.8	23.37	28	169.1	20.33	28	173.7	27.66	26
15B iv	VGluT1 intensity (16-bit)	485.6	19.29	27	456.6	14.83	28	467.5	16.27	28	465.7	19.71	26

Table 11. Two-way ANOVA comparison of morphological changes induced by Aβ on dendrite development.

Fig.	Parameter	TwA - main effect Duration of exposure		TwA - main effect Treatment		TwA - Interaction		MCT
		F value	p value	F value	p value	F value	p value	Tukey's post-hoc test
14C i	Enclosing radius	$F_{(1, 106)}$ = 0.665	0.416	$F_{(1, 106)}$ = 0.441	0.508	$F_{(1, 106)}$ = 5.956	0.016 **(*)**	n.s.
14C ii	Total intersections	$F_{(1, 106)}$ = 0.012	0.912	$F_{(1, 106)}$ = 1.016	0.315	$F_{(1, 106)}$ = 4.631	0.033**(*)**	n.s.
15B i	VGluT1	$F_{(1, 105)}$ = 0.193	0.661	$F_{(1, 105)}$ = 0.074	0.785	$F_{(1, 105)}$ = 0.019	0.890	n.s.
15B ii	Shank2	$F_{(1, 105)}$ = 0.286	0.593	$F_{(1, 105)}$ = 0.007	0.930	$F_{(1, 105)}$ = 0.168	0.682	n.s.
15B iii	VG+/Sh2	$F_{(1, 105)}$ = 0.047	0.827	$F_{(1, 105)}$ = 0.035	0.851	$F_{(1, 105)}$ = 0.142	0.706	n.s.
15B iv	VGluT1 intensity	$F_{(1, 105)}$ = 0.063	0.800	$F_{(1, 105)}$ = 0.764	0.384	$F_{(1, 105)}$ = 0.594	0.442	n.s.

TwA: two-way ANOVA
MCT: multiple comparisons test.

the groups (Figure 15B ii). The calculated Pvr (Figure 15C) was not changed in the 10 µM Aβ-treated neurons as seen in the previous experiments. The neurons exposed to Aβ concentrations lower than 10 µM showed a trend of a directly proportional increase in Pvr with respect to the Aβ concentration. Glutamate was applied exogenously and the postsynaptic response was similar in all groups (Figure 15D). Spontaneous release in the presence of TTX was additionally recorded (Figure 15E i). No alterations were observed in the mEPSC frequency (Figure 15E ii) or in the amplitude (Figure 15E iii) in any of the groups exposed to Aβ. Finally, short-term plasticity was evaluated by high-frequency stimulation at 10 Hz (Figure 15F i). Despite the changes observed in Pvr, the paired pulse ratio

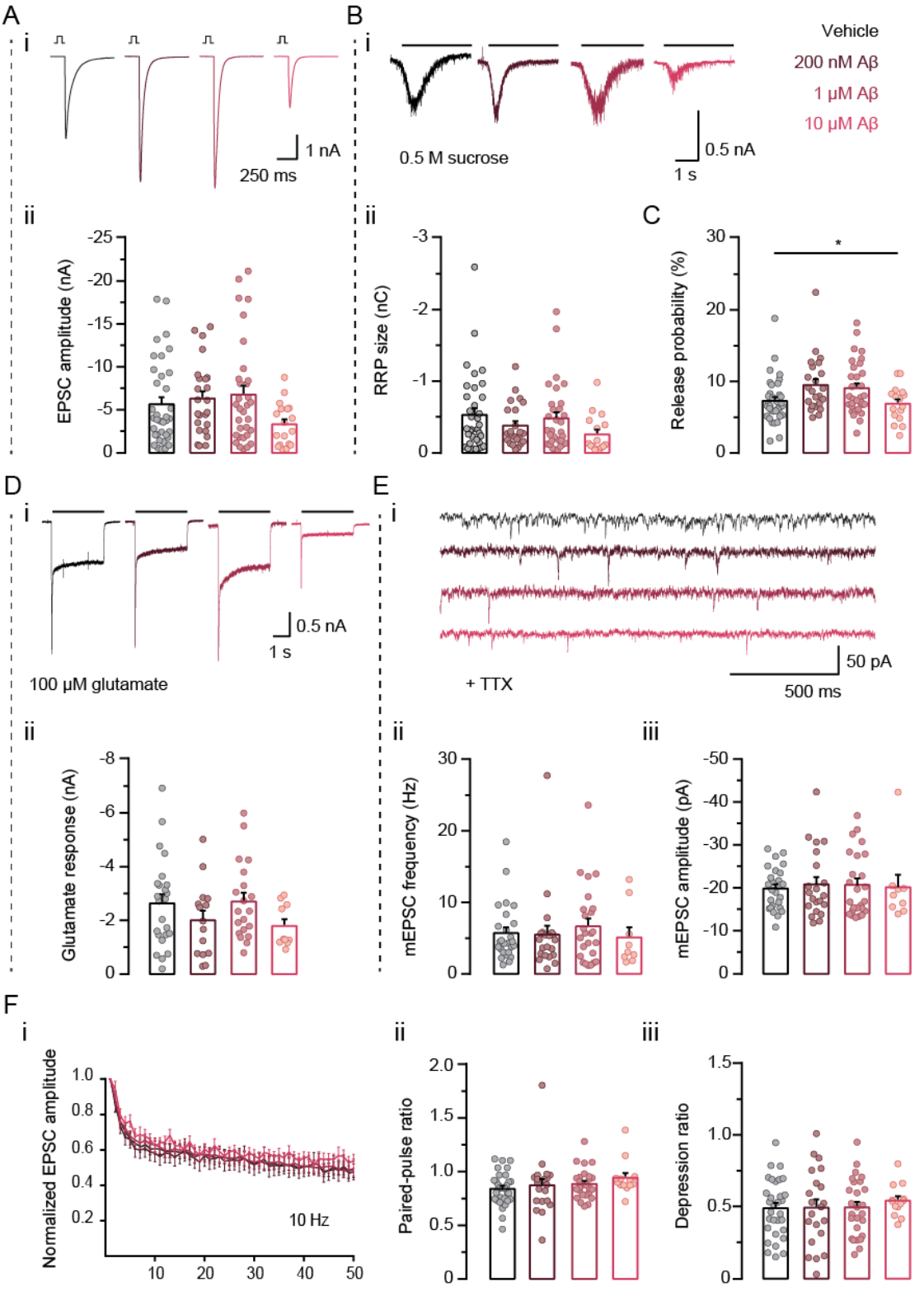

Figure 16. Analysis of concentration dependence of the 72-hour Aβ treatment. (A) (i) Representative traces and **(ii)** quantification of EPSCs amplitude. **(B) (i)** Representative traces and **(ii)** quantification of RRP size evoked by application of 0.5 M sucrose. **(C)** Quantification of Pvr (n= 16-35 neurons, from at least N= 3 cultures; Kruskal-Wallis test, *p < 0.032, post-hoc Dunn's multiple comparisons test: n.s.). **(D) (i)** Representative traces and **(ii)** quantification of postsynaptic response to the application of 100 μM glutamate. **(E) (i)** Representative traces and **(ii)** quantification of frequency and **(iii)** amplitude of mEPSCs recorded in the presence of TTX. **(F) (i)** Normalized amplitudes of the first 50 EPSCs in a train of stimuli at 10 Hz. Quantification of **(ii)** paired-pulse ratio and **(iii)** depression ratio. Bars represent the mean. Error bars represent SEM. Vehicle, black bars; 200 nM Aβ, dark brown bars; 1 μM Aβ, light brown bars; 10 μM Aβ, pink bars.

(Figure 15F ii) and depression ratio (Figure 15F iii) were conserved between the groups. These results are summarized in Table 12.

Table 12. Summary of Aβ concentration dependent electrophysiological effects at 72 hours.

Fig.	Parameter	Vehicle			200 nM Aβ			1 µM Aβ			10 µM Aβ			p value	Sum.	Test	MCT
		Mean	SEM	n	Mean	SEM	n	Mean	SEM	n	Mean	SEM	n				Dunn's
15A ii	EPSC (nA)	-5.683	0.818	36	-6.331	0.865	24	-6.790	1.066	32	-3.330	0.593	18	0.124	n.s.	Kruskall-Wallis	n.s.
15B ii	RRP (nC)	-0.532	0.092	35	-0.383	0.006	23	-0.485	0.008	31	-0.263	0.006	16	0.181	n.s.	Kruskall-Wallis	n.s.
15C	Pvr (%)	7.278	0.538	35	9.506	0.813	23	9.052	0.670	31	6.877	0.627	16	0.032	*	Kruskall-Wallis	n.s.
15D ii	Glutamate-induced current (nA)	-2.642	0.341	24	-2.009	0.354	15	-2.71	0.323	20	-1.797	0.251	10	0.188	n.s.	Kruskall-Wallis	n.s.
15E ii	mEPSC amplitude (pA)	-19.87	0.958	26	-20.84	1.732	21	-20.75	1.474	25	-20.2	2.881	9	0.978	n.s.	Kruskall-Wallis	n.s.
15E iii	mEPSC frequency (Hz)	5.726	0.784	26	5.513	1.223	21	6.664	1.079	25	5.109	1.421	9	0.752	n.s.	Kruskall-Wallis	n.s.
15F ii	Paired-pulse ratio	0.839	0.027	31	0.873	0.058	21	0.886	0.027	26	0.942	0.0451	13	0.347	n.s.	Kruskall-Wallis	n.s.
15F iii	Depression ratio	0.493	0.036	31	0.496	0.058	21	0.497	0.039	26	0.545	0.031	13	0.834	n.s.	Kruskall-Wallis	n.s.

Sum.; summary; MCT: multiple comparisons test.

3.3. Effects of anle138b on morphology and synaptic physiology of hippocampal autaptic neurons

Great efforts have been made in the last decades to find an effective treatment for AD and its devastating consequences (Guerrero-Muñoz, Castillo-Carranza and Kayed, 2014). In this context, the diphenylpyrazole compound and its derivatives were discovered as modulators of aggregation that inhibit oligomer formation and have been proven effective in ameliorating the symptoms in mouse models of a variety of neurodegenerative disorders such as prion disease, Parkinson's Disease and tauopathies, among others (Wagner *et al*., 2013, 2015). Within this group of compounds, anle138b was the most effective in preventing oligomer formation (Wagner *et al.*, 2013) and, importantly, neuroprotective effects were found in transgenic mouse models of AD (Martinez Hernandez *et al.*, 2018). I therefore aimed to investigate whether this compound might also ameliorate the synaptic defects triggered by Aβ in hippocampal autaptic neurons.

However, before performing the combined treatment with anle138b and Aβ, I characterized the effects of anle138b *per se* on the physiology and morphology of autaptic neurons.

3.3.1. Effects of 96-hour exposure to 10 µM anle138b

In a first set of experiments, I treated hippocampal autaptic neurons on DIV 7 with 10 µM anle138b, which was the highest concentration that could be dissolved in the neuronal culture medium, or equivalent volume of the vehicle. After 96 hours of treatment whole-cell patch-clamp experiments were performed as described in the previous sections. Unexpectedly, the neurons exposed to anle138b showed a 40% reduction in their EPSC amplitudes (Figure 17A) as well as a 35% reduction in the RRP size (Figure 17B). The Pvr was not changed (Figure 17C) and the application of exogenous glutamate induced similar postsynaptic currents in both groups (Figure 17D). I also recorded spontaneous glutamate release in the presence of TTX (Figure 17E). The frequency of mEPSCs was reduced by 30% after 96 hours of exposure to anle138b, which correlated to the reduction in the RRP size (Figure 17E ii). In addition, mEPSC amplitudes were 5% smaller in the anle138b-treated group with respect to the control (Fig. 13E iii). The analysis of short-term plasticity (Figure 17F) did not evidence any changes between groups, neither in the paired-pulse ratio (Figure 17F ii) nor in the depression ratio (Figure 17F iii). These data indicated that 96-hour treatment with 10 µM anle138b had negative effects *per se* on synaptic transmission in the autaptic hippocampal neurons and therefore this concentration was not used in further experiments.

3.3.2. Effects of 96-hour exposure to 7 µM anle138b

Since the goal of the use of anle138b was to prevent the synaptotoxicity of Aβ oligomers, the direct effects of anle138b on synaptic transmission *per se* represented a confounding factor. Therefore, I decided to further seek for a maximal concentration of anle138 that would not exert negative effects on synaptic properties. To this aim, autaptic neurons were treated with 7 µM anle138b or equivalent vehicle volume on DIV 7 and used for recordings on DIV 11, as described in the previous sections. The synaptic responses were found to be similar in both groups (Figure 18A). The RRP size evoked by application of 0.5 M sucrose (Figure 18B) as well as the calculated Pvr (Figure 18C) were

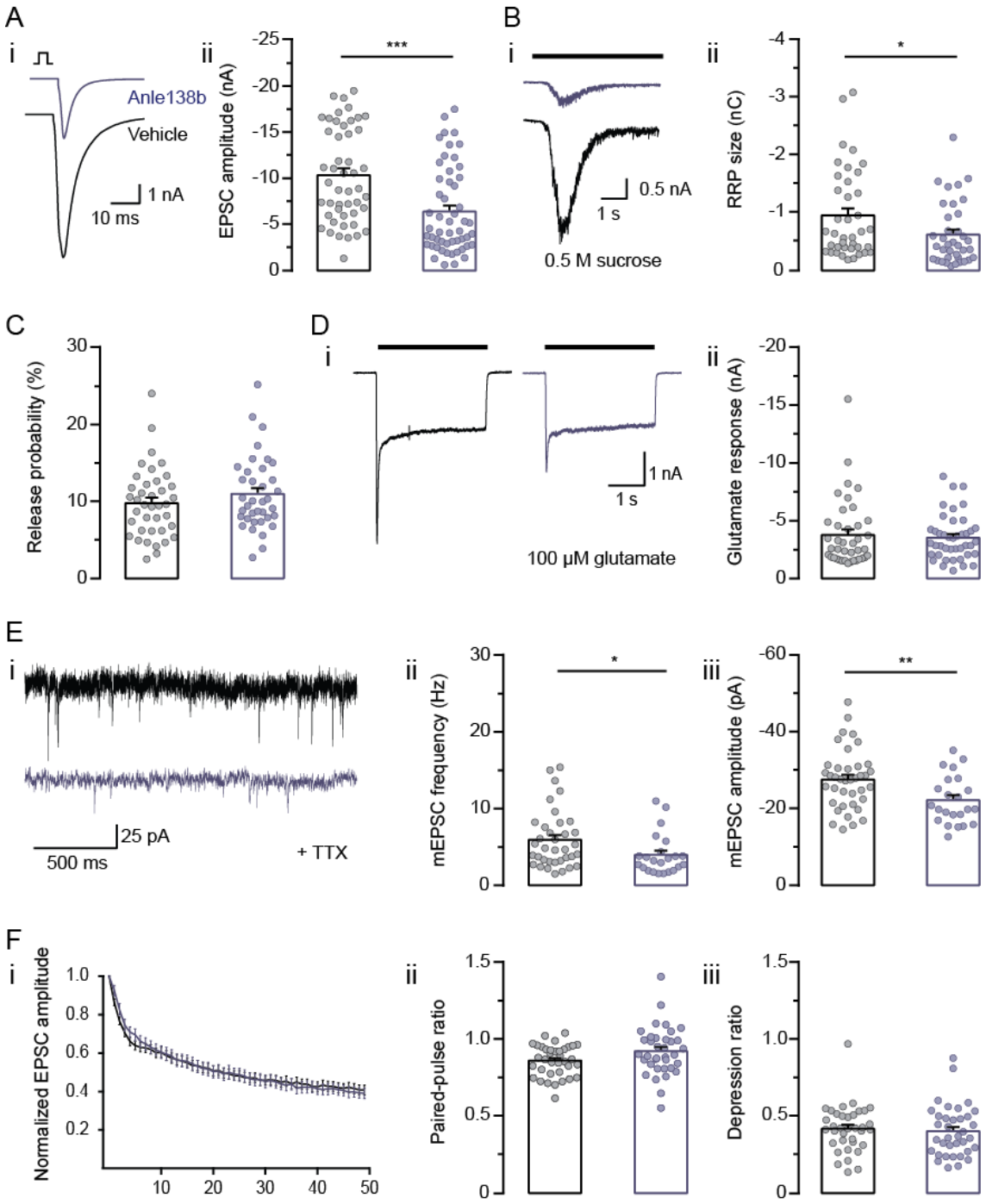

Figure 17. 10 µM anle138b treatment alters synaptic physiology on hippocampal autaptic neurons. (A) (i) Representative traces and **(ii)** quantification of EPSC amplitude (n= 48-53 neurons, from at least N= 3 cultures; Mann-Whitney test, ***p< 0.001). **(B) (i)** Representative traces of the response evoked by 0.5 M sucrose application. (ii) Quantification of RRP size (n= 37-39, N= 3; Mann-Whitney test, *p= 0.024). **(C)** Quantification of the calculated Pvr. **(D) (i)** Representative traces and **(ii)** quantification of postsynaptic response to exogenous glutamate application. **(E) (i)** Representative traces of mEPSCs recorded in the presence of TTX. **(ii)** Quantification of mEPSC frequency (n= 24-26, N= 3; Mann-Whitney test, *p= 0.016). **(iii)** Quantification of mEPSC amplitudes (n= 24-26, N= 3; Mann-Whitney test, **p= 0.006). **(F) (i)** Normalized amplitudes of the first 50 EPSCs in a train of stimuli at 10 Hz. Quantification of (ii) paired-pulse ratio and **(iii)** depression ratio. Bars represent the mean. Error bars represent SEM. Vehicle, black bars; Anle138b, purple bars.

unchanged. In addition, the exposure to 7 µM anle138b did not affect the postsynaptic response to exogenous glutamate application (Figure 18D) nor the

spontaneous activity recorded in the presence of TTX (Figure 18E), as indicated by a conserved mEPSC frequency (Figure 18E ii) and amplitude (Figure 18E iii). Finally, the response to high-frequency stimulation at 10 Hz (Figure 18F) was not modified by the anle138b treatment, with similar values of paired-pulse ratio (Figure 18F ii) and depression ratio (Figure 18F iii). In conclusion, all electrophysiological parameters tested remained unmodified by the 96-hour exposure to 7 µM anle138b, thus indicating the absence of detectable deleterious effects at this concentration.

The results of 96-hour exposure to 7 µM and 10 µM anle138b are summarized in Table 13.

3.4. Effects of anle138b as protective pretreatment against Aβ toxicity

To investigate the putative neuroprotective effects of anle138b, I performed a combined treatment together with Aβ using the protocols described in the previous sections. 7µM anle138b or equal volume of the vehicle was added to the culture medium of hippocampal autaptic neurons on DIV 7. After 24 hours, on DIV 8, the neurons were treated with 10 µM Aβ (or equivalent volume of the vehicle). Later, on DIV 11, electrophysiological recordings were performed. The results for the tested parameters were analyzed using two-way ANOVA to evaluate the effects of anle138b and Aβ independently, as well as the result of their interaction. This last parameter was used to test whether the pretreatment with anle138b could modify the changes induced by Aβ. The exposure to anle138b, when considered as a main variable, showed no effects on the EPSCs (Figure 19A). Aβ exposure induced a statistically significant reduction in the amplitude of EPSCs, akin to the effects described in section 3.2.1. Since anle138b had been shown to rescue memory deficits in a mouse model of AD and restored the changes in LTP induced by Aβ accumulation (Martinez Hernandez *et al*., 2018), I expected a statistically significant interaction between the treatments on EPSC amplitude, provided that the pretreatment with anle138b could protect from Aβ-induced toxicity and normalize the evoked release. This hypothesis was not verified, since the EPSCs of neurons pretreated with anle138b and later exposed to Aβ were as reduced in amplitude as the vehicle pretreated ones. Similarly, the RRP size was reduced in all the groups of Aβ-treated neurons (Figure 19B). In addition to the Aβ-dependent changes,

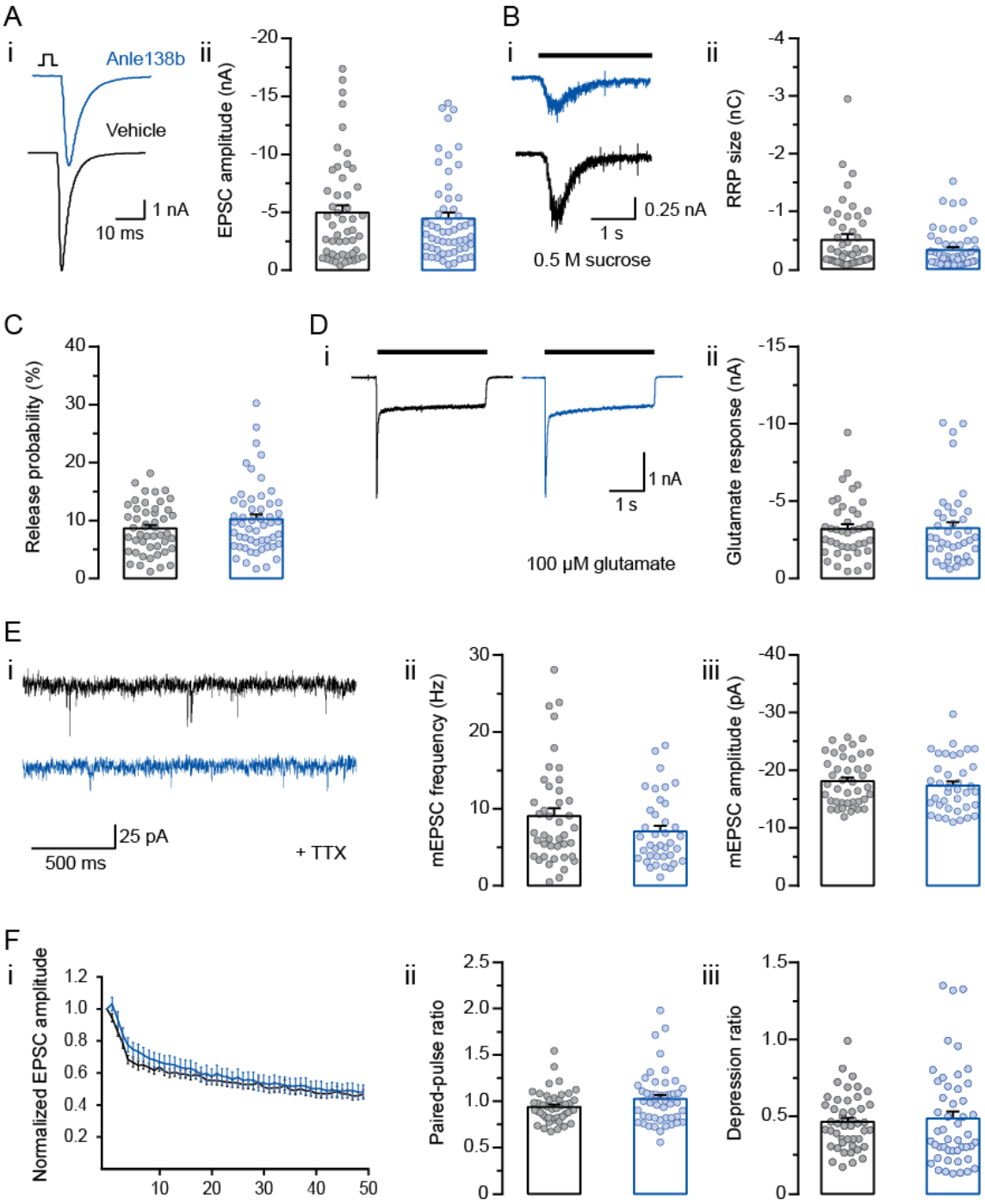

Figure 18. Exposure to 7 µM anle138b has no effects on synaptic transmission in hippocampal autaptic neurons. (A) (i) Representative traces and **(ii)** quantification of EPSC amplitude. **(B) (i)** Representative traces of the response evoked by 0.5 M sucrose application and **(ii)** quantification of RRP size. **(C)** Quantification of Pvr. **(D) (i)** Representative traces and **(ii)** quantification of postsynaptic response to exogenous glutamate application**. (E) (i)** Representative traces and quantification of **(ii)** amplitude and **(iii)** frequency of mEPSCs recorded in the presence of TTX. **(F) (i)** Normalized amplitudes of the first 50 EPSCs in a train of stimuli at 10 Hz. Quantification of **(ii)** paired-pulse ratio and **(iii)** depression ratio. Bars represent the mean. Error bars represent SEM. Vehicle, black bars; Anle138b, blue bars.

anle138b effects were also found to be statistically significant in the analysis of the RRP size, suggesting a mild toxicity of the anle compound which had not been detected in the previous experiments of section 3.3.2. The interaction

Table 13. Summary of the electrophysiological effects of 96-hour treatment with 10 µM and 7 µM anle138b.

Fig.	Parameter	Vehicle			Anle138b			p value	Summary	Test
		Mean	SEM	n	Mean	SEM	n			
	10 µM anle138b									
16A ii	EPSC (nA)	-10.38	0.737	48	-6.429	0.641	53	< 0.001	***	Mann-Whitney
16B ii	RRP (nC)	-0.960	0.012	39	-0.626	0.088	37	0.024	*	Mann-Whitney
16C	Pvr (%)	9.838	0.724	39	11.01	0.783	37	0.304	n.s.	Mann-Whitney
16D ii	Glutamate-induced current	-3.801	0.461	40	-3.552	0.302	42	0.600	n.s.	Mann-Whitney
16E ii	mEPSC frequency (Hz)	5.937	0.624	36	3.967	0.554	42	0.016	*	Mann-Whitney
16E iii	mEPSC amplitude (pA)	-27.57	1.24	39	-22.17	1.314	42	0.006	**	t test
16F ii	Paired-pulse ratio	0.863	0.016	36	0.925	0.026	36	0.050	n.s.	t test
16F iii	Depression ratio	0.420	0.025	36	0.404	0.027	36	0.524	n.s.	Mann-Whitney
	7 µM anle138b									
17A ii	EPSC (nA)	-5.005	0.635	50	-4.497	0.505	55	0.888	n.s.	Mann-Whitney
17B ii	RRP (nC)	-0.506	0.008	48	-0.333	0.004	53	0.160	n.s.	Mann-Whitney
17C	Pvr (%)	8.673	0.617	48	10.28	0.835	53	0.371	n.s.	Mann-Whitney
17D ii	Glutamate-induced current	-3.226	0.299	41	-3.276	0.387	41	0.590	n.s.	Mann-Whitney
17E ii	mEPSC frequency (Hz)	4.53	0.504	42	3.526	0.362	38	0.394	n.s.	Mann-Whitney
17E iii	mEPSC amplitude (pA)	-18.12	0.645	42	-17.35	0.757	38	0.200	n.s.	Mann-Whitney
17F ii	Paired-pulse ratio	0.943	0.025	46	1.030	0.041	29	0.177	n.s.	Mann-Whitney
17F iii	Depression ratio	0.469	0.026	46	0.490	0.045	48	0.447	n.s.	Mann-Whitney

between anle138b and Aβ treatments was also analyzed for the RRP size. The absence of statistical significance indicated that 7 µM anle138b could not rescue the Aβ-induced reduction of the RRP. No changes in Pvr were found with either of the treatments or with their combination. The Aβ effects on the exogenous glutamate-evoked response could not be rescued by anle138b. Spontaneous glutamate release was recorded during the application of TTX (Figure 19E). Neither the frequency (Figure 19E ii) nor the amplitude (Figure 19E iii) of mEPSCs were modified in any of the treated groups. No interaction between the treatments was found on these parameters. Regarding short-term plasticity, no differences were observed between the experimental groups or their interaction (Figure 19F ii). However, the ratio between the responses at the end of the train (41th-50th) and the 1st EPSC was found to be reduced as an Aβ-dependent effect (Figure 19F iii). Interestingly, the Tukey's post-hoc test indicated that the neurons pretreated with anle138b and subsequently with Aβ exhibited larger

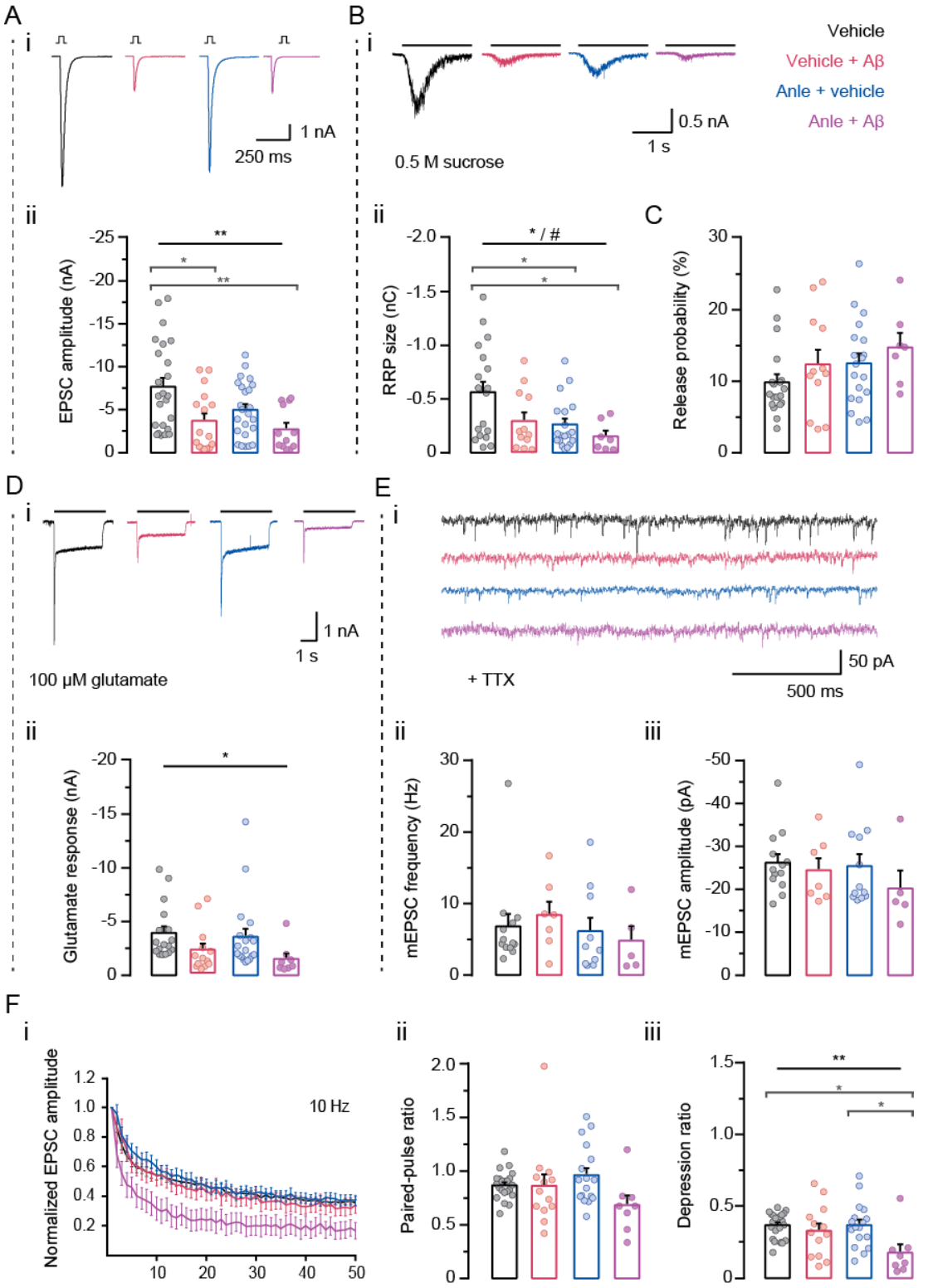

Figure 19. Pretreatment with 7 μM anle138b does not modify Aβ toxic effects on synaptic transmission in autaptic hippocampal neurons. (A) (i) Representative traces and **(ii)** quantification of EPSC amplitude (n= 12-24 neurons from at least N= 3 cultures and Aβ preparations; two-way ANOVA; main effect Aβ: $F_{(1, 72)}$= 11.09, **p= 0.001; Tukey's post-hoc test, Vehicle vs Vehicle+Aβ: *p= 0.012, Vehicle vs Anle+Vehicle: **p= 0.003). **(B) (i)** Representative traces of the response evoked by 0.5 M sucrose application and **(ii)** quantification of RRP size (n= 7-19, N= 3; two-way ANOVA; main effect Aβ: $F_{(1, 53)}$= 4.652, *p= 0.035; main effect anle138b: $F_{(1, 53)}$= 5.948, *p= 0.018; Tukey's post-hoc test, Vehicle vs Anle+Vehicle: *p= 0.023, Vehicle vs Anle+Aβ: *p= 0.021). **(C)** Quantification of Pvr. **(D) (i)** Representative traces and **(ii)** quantification of postsynaptic response to exogenous glutamate application (n= 8-19, N= 3; two-way ANOVA; main effect Aβ: $F_{(1, 51)}$= 6.812, *p= 0.011; Tukey's post-hoc test: n.s.). **(E) (i)** Representative traces

and quantification of **(i)** amplitude and **(ii)** frequency of mEPSCs recorded in the presence of TTX. **(F) (i)** Normalized amplitudes of the first 50 EPSCs in a train of stimuli at 10 Hz. Quantification of **(ii)** paired-pulse ratio and **(iii)** depression ratio (n= 8-22, N= 3; two-way ANOVA; main effect Aβ: $F_{(1, 56)}$= 8.488, **p= 0.005; Tukey's post-hoc test, Vehicle vs Vehicle+Aβ: *p= 0.014, Vehicle vs Anle+Vehicle: **p= 0.010. Bars represent the mean. Error bars represent SEM. Vehicle, black bars; Vehicle +Aβ, pink bars; Anle138b+Vehicle, blue bars; Anle138b+Aβ, purple bars. Black lines represent the two-way ANOVA results. Stars represent the main Aβ effect. Hash marks represent the anle138b main effect. Gray lines and stars represent the Tukey's post-hoc test results.

depression in the EPSC amplitudes at the end of the train when compared with the neurons not exposed to anle138b. This suggested that the combination of anle138b pretreatment together with exposure to Aβ could alter ability of the autaptic neurons to sustain an efficient release over the course of milliseconds-seconds rather than affecting the rapid initial plasticity.

When analyzed altogether, these results showed that the anle138b pretreatment failed in protecting against Aβ-induced synaptic toxicity, mostly indicated by an absence of significant interaction between the treatments. The descriptive statistics for the compared data sets are summarized in Table 15. The two-way ANOVA values are presented in Table 14.

3.5. Pore formation as toxicity mechanism of Aβ

In the previous sections I described changes in neuronal function and morphology induced by exposure to the Aβ peptide. In the final part of my work, I aimed to explain the cellular and molecular causes for the toxic effects of Aβ, focusing on the hypothesis of amyloid pore formation.

3.5.1. Effects of Aβ treatment on artificial bilayers

The phenomenon of pore formation by amyloid proteins was described initially by means of recordings of the occurrence of currents steps on artificial bilayers (Arispe, Rojas and Pollard, 1993). In an effort to replicate those findings and to further characterize the effects of the protofibrillar aggregates described in section 3.1., I performed electrophysiological recordings from lipid bilayers exposed to Aβ. Two different Aβ isomers were used as negative controls for these experiments: the reverse Aβ peptide ("Aβ 42-1") and the scrambled Aβ42 ("scr Aβ"), which has an identical amino acid composition to Aβ42 but a randomized primary structure (De Felice et al., 2009; Gilson et al., 2015). Voltage-clamp recordings were performed on membranes formed using two kinds of lipids: 1% (w/v) oxidized cholesterol in n-decane and 2% (w/v) diphyPC in n-decane. In the

Table 14. Two-way ANOVA comparison of the effects of anle138b and Aβ combined treatment.

Fig.	Parameter	Vehicle			Vehicle+Aβ			Anle+Vehicle			Anle+Aβ		
		Mean	SEM	n	Mean	SEM	n	Mean	SEM	n	Mean	SEM	n
19A	EPSC (nA)	-7.694	1.049	24	-3.729	0.863	16	-5.021	0.664	24	-2.752	0.735	12
19B	RRP (nC)	-0.564	0.097	19	-0.290	0.081	12	-0.264	0.053	19	-0.150	0.053	7
19C	Pvr (%)	9.850	1.131	19	12.380	2.036	12	12.520	1.358	19	14.750	2.003	7
19D	Glutamate-induced current (nA)	-3.955	0.608	17	-2.165	0.592	13	-3.592	0.758	19	-1.537	0.499	8
19E ii	mEPSC amplitude (pA)	-26.230	2.019	13	-24.470	2.820	7	-25.420	2.810	12	-20.230	4.217	5
19E iii	mEPSC frequency (Hz)	6.825	1.744	13	8.391	1.873	7	6.146	1.861	10	4.806	2.036	5
19F ii	Paired-pulse ratio	0.869	0.028	22	0.864	0.106	13	0.962	0.067	17	0.684	0.090	8
19Fiii	Depression ratio	0.371	0.019	22	0.332	0.050	13	0.371	0.038	17	0.179	0.058	8

Table 15. Summary of the effects of anle138b and Aβ combined treatment.

Figure	Parameter	TwA - main effect anle138b		TwA - main effect Aβ		TwA - Interaction		MCT
		F value	p value	F value	p value	F value	p value	Tukey's
19A	EPSC (nA)	$F_{(1, 72)}$ = 3.802	0.055	$F_{(1, 72)}$ = 11.09	0.001 **(**)**	$F_{(1, 72)}$ = 0.820	0.368	Vehicle vs Vehicle+Aβ *p=0.012 Vehicle vs Anle+Vehicle **p=0.003
19B	RRP (nC)	$F_{(1, 53)}$ = 5.948	0.018 **(*)**	$F_{(1, 53)}$ = 4.652	0.035 **(*)**	$F_{(1, 53)}$ = 0.800	0.375	Vehicle vs Anle+Vehicle *p=0.023 Vehicle vs Anle+Aβ *p=0.021
19C	Pvr (%)	$F_{(1, 53)}$ = 2.274	0.138	$F_{(1, 53)}$ = 2.025	0.16	$F_{(1, 53)}$ = 0.008	0.928	n.s.
19D	Glutamate-induced current (nA)	$F_{(1, 51)}$ = 0.351	0.556	$F_{(1, 51)}$ = 6.812	0.011 **(*)**	$F_{(1, 51)}$ = 0.057	0.811	n.s.
19E ii	mEPSC amplitude (pA)	$F_{(1, 33)}$ = 0.705	0.407	$F_{(1, 33)}$ = 1.342	0.255	$F_{(1, 33)}$ = 0.325	0.572	n.s.
19E iii	mEPSC frequency (Hz)	$F_{(1, 31)}$ = 1.067	0.310	$F_{(1, 31)}$ = 0.003	0.956	$F_{(1, 31)}$ = 0.495	0.487	n.s.
19F ii	Paired-pulse ratio	$F_{(1, 6)}$ = 0.370	0.545	$F_{(1, 56)}$ = 3.883	0.053	$F_{(1, 56)}$ = 3.613	0.063	n.s.
19Fiii	Depression ratio	$F_{(1, 56)}$ = 3.728	0.059	$F_{(1, 56)}$ = 8.488	0.005 **(**)**	$F_{(1, 56)}$ = 3.681	0.060	Anle+Vehicle vs Anle+Aβ *p=0.014 Vehicle vs Anle+Aβ *p=0.010

Vehicle: Neurons treated with vehicle for anle138b on DIV7 and vehicle for Aβ on DIV 8.
Vehicle+Aβ: Neurons treated with vehicle for anle138b on DIV7 and 10 μM Aβ on DIV 8.
Anle+Vehicle: Neurons treated with 7 μM anle138b on DIV7 and vehicle for Aβ on DIV 8.
Anle+Aβ: Neurons treated with 7 μM anle138b on DIV7 and vehicle for Aβ on DIV 8.
TwA: two-way ANOVA
MCT: multiple comparisons test.

first set of experiments, oxidized cholesterol membranes were formed and after 5 minutes of recording a stable baseline at 20 mV, Aβ or Aβ 42-1 were added to one of the chambers at a concentration of 10 µM (Figure 20A i). Both isomers induced current steps after a latency period, which were accompanied by an increased standard deviation of the baseline current. However, the latency period for the activity induced by Aβ was shorter, and in two out of three recordings the total charge transferred was two to four times the Aβ 42-1 induced charge (Figure 20A ii). Similar experiments were conducted on diphyPC membranes but using higher holding potentials of 50 mV and 100 mV (Figure 20B i-ii). In the case of these phospholipidic membranes, no current steps were found at either of the holding potentials, and the transferred charge was equally low upon exposure to both peptides when compared to the effects in oxidized cholesterol membranes (Figure 20B iii).

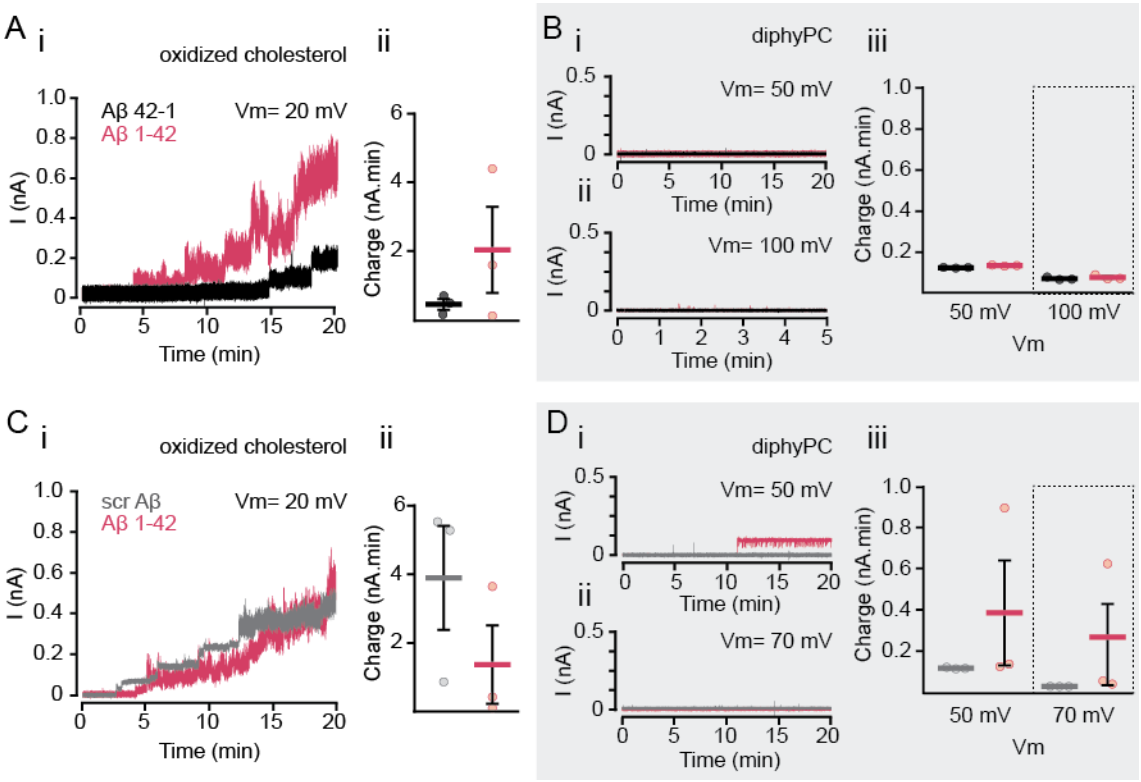

Figure 20. Aβ treatment disrupts the integrity of oxidized cholesterol membranes but has no effects on diphyPC membranes.(A) (i) Representative recordings from oxidized cholesterol membranes treated with Aβ42 or Aβ 42-1 at 20 mV and **(ii)** quantification of the charge transferred in 20 minutes. **(B)** Representative recordings from diphyPC membranes treated with Aβ42 or Aβ 42-1 **(i)** at 50 mV and **(ii)** 100 mV. **(iii)** Quantification of transferred charge in 20 minutes at 50 mV and 5 minutes at 100 mV. **(C) (i)** Representative recordings from oxidized cholesterol membranes treated with Aβ42 or scr Aβ at 20 mV and **(ii)** quantification of the charge transferred in 20 minutes. **(D) (i)** Representative recordings from diphyPC membranes treated with Aβ42 or scr Aβ **(i)** at 50 mV and **(ii)** 70 mV. **(iii)** Quantification of transferred charge in 20 minutes at 50 mV and 70 mV. Thick lines represent the mean. Error bars represent SEM. Aβ42, pink lines; Aβ 42-1, black lines; scr Aβ, gray lines.

The scr Aβ was used as negative control for the next set of experiments on oxidized cholesterol at 20 mV (Fig. 16C i). Both Aβ and scr Aβ at 10 μM induced current steps with similar latency periods, but the scr Aβ was active in two out of three recordings showing large charges, while Aβ showed activity only in one case (Figure 20C ii). Next, diphyPC membranes were used for recordings at 50 mV and 70 mV (Figure 20D i-ii). Almost no activity was found with either of the peptides as evidenced by no changes in the charge transferred, except for one recording in which a single and stable step in the baseline was found (Figure 20D iii).

These data highlight the importance of the lipidic composition of the membrane in the formation of Aβ pores, since the oxidized cholesterol membranes were more easily perforated than the diphyDPC ones, which resemble cell membranes biologically relevant in the context of this study. Surprisingly, both peptides used as negative controls could induce current steps indicating that either they can form active, pore-forming oligomeric species or that the Aβ-membrane interaction and pore formation does not depend on the aggregation state.

3.5.2. Effects of Aβ treatment on the plasma membrane of hippocampal autaptic neurons

Since membrane composition was found to be an important factor determining the formation of amyloid pores in the experiments of the previous section, I performed the subsequent measurements on the plasma membrane of autaptic hippocampal neurons, a biologically more relevant membrane model for a human disease like AD.

3.5.2.1. Use of GABA-induced currents recorded in cell-attached configuration to investigate perforated patch-like effects of 10 μM intrapipette Aβ

One of the major technical challenges of the study of amyloid pore formation was to set an experimental design that would allow me to distinguish the signal derived from the insertion of actual discrete pores from noise generated by the spontaneous, partial rupture of the neuronal membrane during the recording. Unlike classical pores constituting defined subunits in channels or receptors, amyloid pores had been reported to be only transiently located in the membrane and to have multiple conductance levels. For this reason, their electrical signal

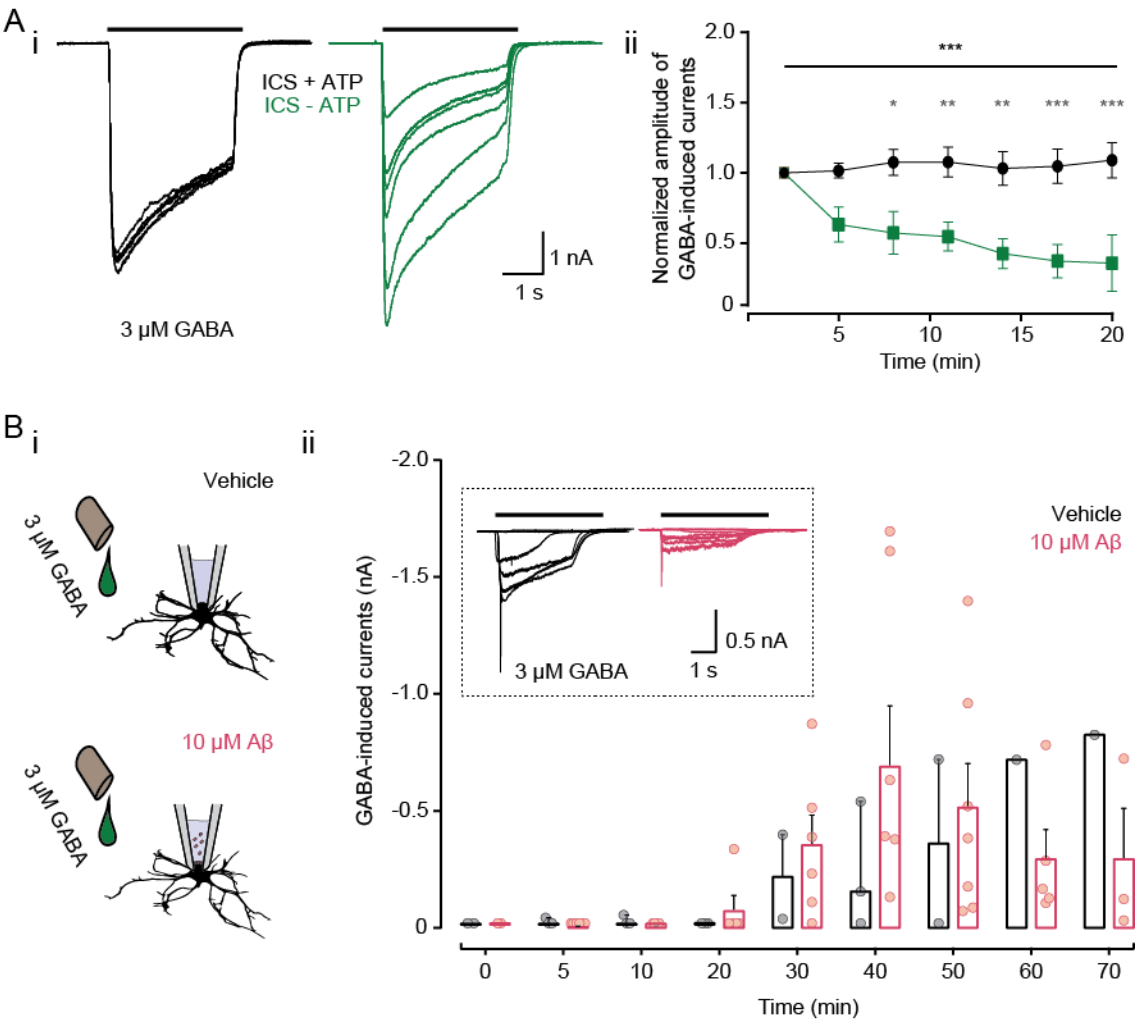

Figure 21. Measurements of GABA currents and perforated patch-like configuration using 10 µM intrapipette Aβ. (A) Whole-cell recordings of GABA-induced currents over time using hippocampal intracellular solution with or without ATP. Low access resistance (series resistance <15 MΩ) was maintained over the course of the experiments. **(i)** Representative traces of GABA-induced currents. A faster rundown was found in the neurons dialyzed with intracellular solutions without ATP. **(ii)** Quantification of GABA amplitudes over time. (n= 6-7, from at least N=3 different cultures and Aβ preparations; two-way ANOVA, main effect "intracellular solution": $F_{(1,60)}$= 71.87, ***p< 0.001; interaction: $F_{(6,60)}$= 2.861, *p= 0.0162; Sidak's multiple comparisons test: see table 10). Black stars represent the effect of intracellular solution as main effect using two-way ANOVA. The gray stars represent the results of Sidak's multiple comparisons test. **(B) (i)** Schematic of the experimental design for the cell-attached/perforated patch experiments. Recordings were performed on cell-attached configuration using intracellular solution without ATP, with 10 µM oligomeric Aβ or equivalent volume of the vehicle in the patch pipette. Pulses of 3 µM GABA were applied every 10 minutes. **(ii)** Quantification of GABA-induced currents over time in cell attached configuration with 10 µM Aβ or vehicle within the patch pipette. Inset: representative traces of GABA-induced currents over time. Symbols in A ii and bars in B ii represent the mean. Error bars represent SEM.

would be very similar to recording artifacts found if the tightness of the membrane seal were lost during the experiment (Arispe, Pollard and Rojas, 1993). In this context, I performed cell-attached recordings of autaptic hippocampal neurons combined with measurements of the rundown of GABA-induced currents over time when an ATP-free intracellular solution was utilized.

Initially, I performed whole-cell recordings on hippocampal autaptic neurons and applied pulses of 3 µM GABA every 3-4 minutes. Regular intracellular solution or a modified ATP-free intracellular solution were used to dialyze the neuronal cytoplasm, provided that the access resistance was low for the duration of the entire experiment (<15 MΩ). When compared over time, the amplitudes of GABA-induced currents measured in the absence of ATP showed a marked rundown that was not observed in the control condition (Figure 21A i-ii, Table 16).

Afterwards, I used the GABA rundown effect as an indicator of dialysis of the cytoplasm in the study of Aβ pore formation. I hypothesized that Aβ might form pores that would provide electrical access to the neuron without physically permitting the dialysis, thus allowing the recording of increasingly larger GABA-induced currents as more pores were added to the membrane, with no rundown, in a perforated patch-like configuration (Figure 21B i). Aβ oligomers were freshly prepared before the recordings and dissolved in the ATP-free intracellular solution at 10 µM. Unlike the protocols for the Aβ treatments described so far, Aβ was applied for a shorter period (40-70 minutes) only onto a small patch of the neuronal plasma membrane at the tip of the pipette, in cell-attached configuration. No GABA-induced currents were found in either of the experimental groups in the first 20 minutes of recordings indicating a tight membrane seal and the absence of pores (Figure 21B ii). After 20 minutes, the GABA-induced current amplitudes increased in both groups, but more markedly in the Aβ-exposed patches. However, after reaching a peak at 40 minutes, the GABA-induced currents showed a decreasing pattern similar to the rundown found when the tight seal was purposely broken to gain access to the whole cell. These results suggested that a partial rupture of the membrane patch could be responsible of the gain of electrical access to the cell rather than the formation of discrete pores.

Table 16. Validation of GABA rundown effect with ATP free intracellular solution.

ANOVA table	Main effect Time		Main effect Presence of ATP		Interaction		Sidak's MCT		
							Time	p value	Summary
	F value	P value	F value	P value	F value	P value	2	>0.999	n.s.
GABA-induced current	$F_{(6,60)}$ = 1.912	0.093	$F_{(1,60)}$ = 71.87	<0.001 **(***)**	$F_{(6,60)}$ = 71.87	0.016 **(*)**	5	0.060	n.s.
							8	0.020	*
							11	0.006	**
							14	0.002	**
TwA: two-way ANOVA, MCT: multiple comparisons test.							17	>0.001	***
							20	>0.001	***

3.5.2.2. Analysis of membrane properties of hippocampal autaptic neurons upon Aβ treatment

Next, I tested the effects of Aβ exposure for 72 hours on the passive and active membrane properties of hippocampal autaptic neurons. The electrical membrane properties depend largely on its population of ionic channels. I therefore hypothesized that membrane properties would be altered if amyloid pores were present, since they would allow aberrant movements of ions. In these experiments, the cultured neurons were treated on DIV 8-9 and recordings were performed on DIV 11-12 in current-clamp mode. The first parameter tested was the resting membrane potential (Figure 22A), which indicated that membranes from Aβ-treated cells were slightly hyperpolarized when compared to the controls, although this difference was not statistically significant. Afterwards I stimulated the neurons by injecting a series of 1-second hyperpolarizing pulses of current from -100 pA to -20 pA (Figure 22B i). The voltage responses to these steps were used to calculate the membrane input resistance, which was similar in both Aβ-treated and control neurons (Figure 22B ii). I also utilized a series of 1-second depolarizing pulses of current to trigger action potentials, in order to observe their properties upon Aβ treatment. Square pulses of 10 pA were used and the number of steps applied were either three times the rheobase or up to a maximum of 400 pA (Figure 22C). The rheobase, defined as the minimum amplitude of a current pulse that could elicit an action potential, was not changed in Aβ-treated neurons (Figure 22D). The frequency of action potential firing measured as the number of action potentials triggered by a voltage step 10 pA larger than the rheobase, was conserved upon exposure to Aβ (Figure 22E). The first action potential triggered by a current pulse was used to analyze the kinetics of the depolarization and hyperpolarization (Figure 22F). The action potential threshold was calculated as the voltage in the raw trace that coincided with the peak of the third derivative of the raw trace (Figure 22G). No changes were observed in the action potential threshold in neurons exposed to Aβ. To characterize the depolarizing phase, the action potential overshoot was measured as the voltage amplitude from 0 mV to the maximum voltage reached (Figure 22H i) and the amplitude, as the value of the maximum voltage reached when the baseline was adjusted to the action potential threshold (Figure 22H ii). Interestingly, the neurons treated with Aβ showed a 15% reduction in the

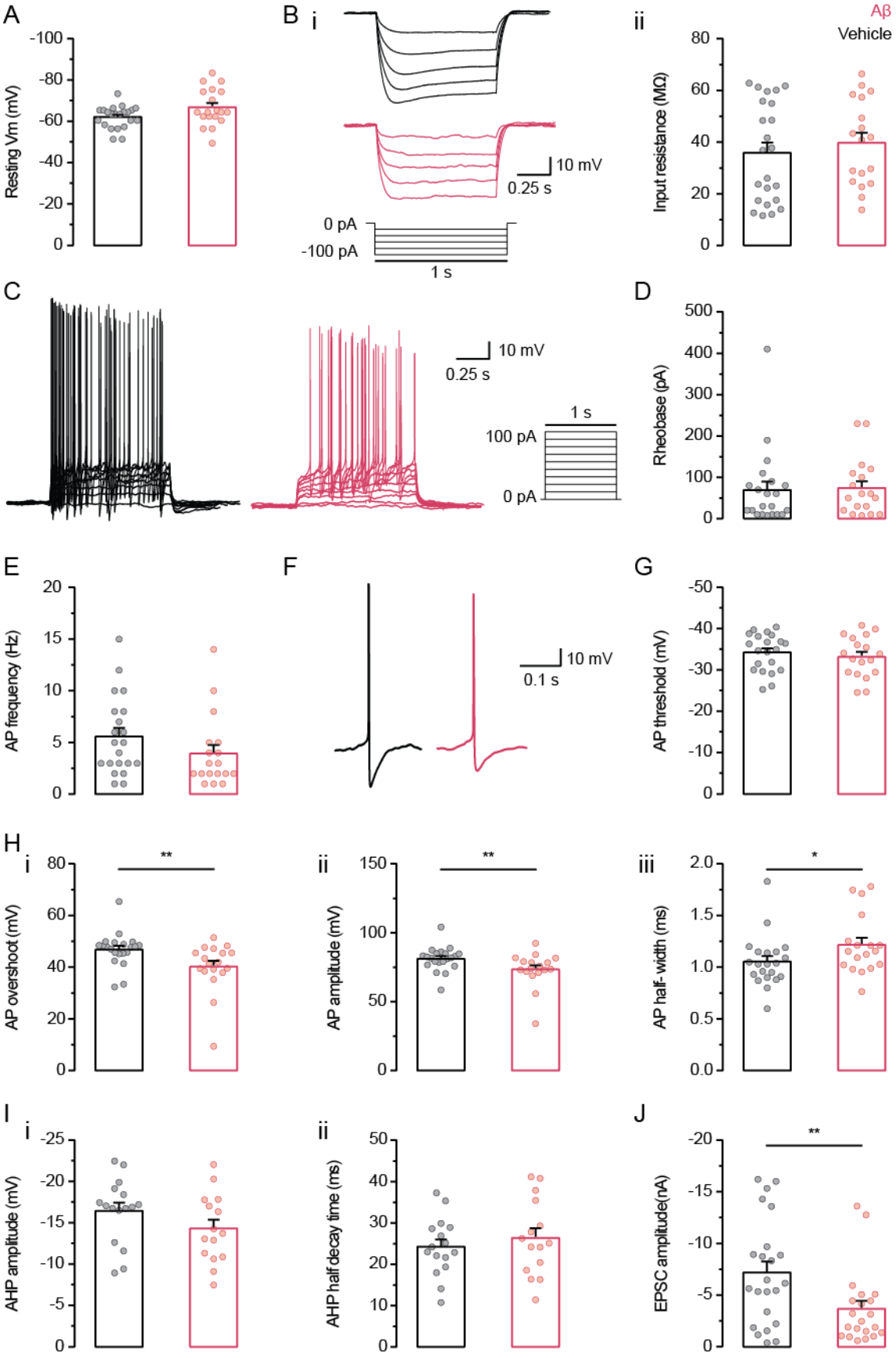

Figure 22. Changes in membrane properties and action potential shape in Aβ-treated neurons. (A) Resting membrane potential. **(B) (i)** Representative traces of voltage responses to 1-second steps of hyperpolarizing currents. **(ii)** Input resistance calculated from the traces in (i). **(C)** Representative traces of voltage responses to the injection of depolarizing currents. **(D)** Rheobase. **(E)** Frequency of action potential firing at a current step 10 pA larger than the rheobase

(F) Representative traces of isolated action potentials. **(G)** Action potential threshold. **(H)** Action potential depolarizing phase. **(i)** Action potential overshoot. (n= 18-21 neurons from N=2 cultures; Mann-Whitney test, **p= 0.004). **(ii)** Action potential amplitude (n= 18-21, N=2 cultures; Mann-Whitney test, **p= 0.008). **(iii)** Action potential half-width (n= 18-21, N=2 cultures; Mann-Whitney test, *p= 0.015). **(I)** Action potential afterhyperpolarization. **(i)** Amplitude. **(ii)** Half decay time. **(J)** EPSC amplitude. (n= 21-23, N=2; Mann-Whitney test, **p= 0.008). Bars represent the mean. Error bars represent SEM. Vehicle, black bars; Aβ, pink bars.

overshoot and a 10% reduction in the amplitude. The action potential half-width was measured as the duration of the peak when the voltage was half the value of the amplitude. A 15% increase in half-width duration was observed when neurons were exposed to 10 μM Aβ for 72 hours (Figure 22 H iii). The properties of the afterhyperpolarization (AHP) phase were also characterized. The AHP amplitude was measured as the voltage between the threshold and the minimum value of the action potential after the depolarization peak (Figure 22I i) and the AHP half-decay time as the duration of the action potential at a voltage half the AHP amplitude (Figure 22I ii). No changes were observed in the AHP phase upon Aβ treatment. Finally, recordings of EPSCs in voltage-clamp were obtained from each cell as a control for Aβ toxicity on synaptic transmission (Figure 22J). As observed in previous sections, the Aβ treatment induced a 50% reduction in the EPSC amplitude. Taken together, these results suggest that the conductance to potassium might be increased in the Aβ-treated neurons, which could explain a mild hyperpolarization and the reduction in the action potential amplitude.

A summary of the results from this section is presented in Table 17.

3.5.3. Comparison of toxicity of Aβ and its stereoisomer AllD

In this final set of experiments, I compared the deleterious effects on hippocampal autaptic neurons of the “wild type” L-Aβ42 peptide versus the artificial stereoisomer AllD Aβ42, which is composed of D- amino acids. These experimental settings allowed me to define whether stereospecific Aβ-membrane interactions were involved in the occurrence of the previously observed toxic effects.

3.5.3.1. AllD Aβ showed identical structural properties and aggregated with similar kinetics to Aβ, with different stereospecificity

A set of experiments were performed to compare the structural properties of AllD Aβ and Aβ monomers. In collaboration with Uwe Pleßmann and Prof. Henning Urlaub (Bioanalytical Mass Spectrometry Research Group, Max Planck Institute

for Biophysical Chemistry), a mass spectrometric analysis (Figure 23A i-ii) showed that the monomerized Aβ and AllD Aβ had the same molecular weight. Together with Kris Runge and Dr. Nasrollah Rezaei-Ghalleh (NMR Based Structural Biology Department, Max Planck Institute for Biophysical Chemistry), two-dimensional homonuclear NMR experiments were performed and ^{1}H-TOCSY spectra were obtained from Aβ and AllD Aβ (Figure 23B). The spectra from both stereoisomers highly overlapped, indicating that the primary structures of both peptides were identical.

In order to compare the aggregation kinetics between the Aβ and AllD Aβ, the peptides were monomerized and incubated at 37°C with external agitation at 800 rpm, as described in section 3.1. In addition to the AllD Aβ and Aβ, the aggregation of scr Aβ was also characterized in this experiment. Samples were taken at increasing incubation time points, then separated using SDS-PAGE and labelled with silver staining (Figure 23C). The gel images showed that Aβ and AllD Aβ were dissolved and aggregated in a similar fashion, but with differences in the relative concentration of species at each given time point. At S0, the Aβ solution was mostly composed by species smaller than 17 kDa, whereas a smear

Table 17. Summary of membrane properties and action potential shape changes in hippocampal autaptic neurons treated with 10 μM Aβ for 72 hours.

Fig.	Parameter	Vehicle			Aβ			p value	Summary	Test
		Mean	SEM	n	Mean	SEM	n			
21A	Resting Vm (mV)	-62.13	1.125	22	-66.87	2.051	19	0.052	n.s.	t-test
21B ii	Input resistance (MΩ)	35.88	4.016	23	39.73	3.896	18	0.366	n.s.	Mann-Whitney
21D	Rheobase (pA)	69.52	20.17	21	73.89	16.37	18	0.56	n.s.	Mann-Whitney
21E	AP frequency (Hz)	5.571	0.826	21	3.944	0.822	18	0.089	n.s.	Mann-Whitney
21G	AP threshold (mV)	-34.27	0.981	21	-33.22	1.171	18	0.497	n.s.	t-test
21H i	AP overshoot (mV)	46.88	1.436	21	40.22	2.267	18	0.004	**	Mann-Whitney
21H ii	AP amplitude (mV)	81.14	1.889	21	73.45	2.91	18	0.008	**	Mann-Whitney
21H iii	AP half-width (ms)	2.098	0.075	21	2.488	0.135	18	0.015	*	Mann-Whitney
21I i	AHP amplitude (mV)	-16.45	0.992	16	-14.32	1.075	15	0.154	n.s.	t-test
21I ii	AHP half decay time (ms)	24.25	1.751	16	26.33	2.371	15	0.481	n.s.	t-test
21J	EPSC amplitude (nA)	-7.205	1.063	23	-3.691	0.775	21	0.008	**	Mann-Whitney

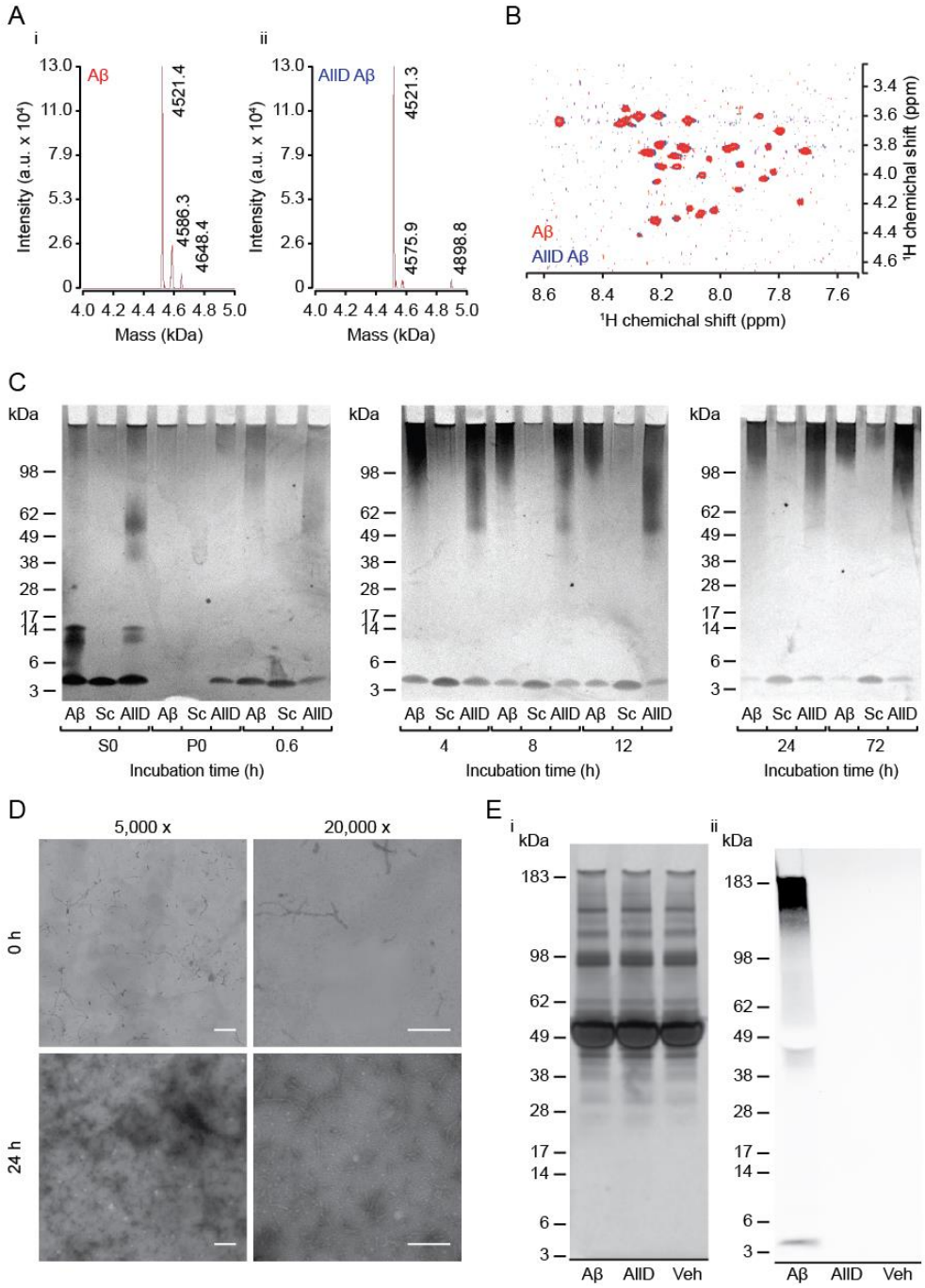

Figure 23. AIID Aβ has identical structural properties and aggregates with similar kinetics to Aβ, but with different stereospecificity. (A) Deconvoluted mass spectrum of **(i)** Aβ and **(ii)** AIID Aβ. **(B)** Juxtaposed ^{1}H-TOCSY spectra of Aβ and AIID Aβ. **(C)** Silver staining of Aβ, AIID Aβ and scr Aβ samples taken at increasing incubation times. **(D)** TEM images of AIID Aβ. Scale bars at 5,000x = 500 nm; at 20,000x = 250 nm. **(E)** Samples from hippocampal autaptic neuronal culture medium treated with Aβ, AIID Aβ or vehicle were loaded by duplicates and separated using SDS-PAGE. **(i)** Silver staining of one half of the gel. The bands correspond to serum proteins from the culture medium. **(ii)** Western blot of the remaining half of the gel using the 6E10 anti-Aβ antibody.

could be found between 49 and 62 kDa in the AIID Aβ sample. At later time points, however, Aβ formed high molecular aggregates larger than 98 kDa, while species between 62 and 98 kDa could be found until the end of the experiment in the case of the AIID Aβ solution. The scr Aβ remained mostly in monomeric state

until the end of the experiment, but surprisingly, some species larger than 98 kDa could be found after 72 hours of incubation. In addition to silver staining, TEM grids were prepared and imaged, showing that upon dissolution some fibrillar aggregates could be found in the AllD Aβ solution. After 24 hours of incubation the most abundant species were protofibrillar aggregates (Figure 23D). Finally, the culture medium of hippocampal neurons was collected after 72 hours of treatment with 10 μM Aβ, 10 μM AllD Aβ or the vehicle. Duplicate samples were loaded on a SDS-PAGE gel. After separation, the gel was cut in half to be processed by silver staining and Western blot. Multiple bands were found in the silver staining which corresponded to serum proteins from the neuronal culture medium (Figure 23E i). The signal corresponding to the Aβ peptides could not be distinguished from the serum protein bands and it was also possible that the concentration was too low to be detected by silver staining. The remaining half of the gel was processed for Western blotting using the sequence specific anti-Aβ antibody 6E10 (Figure 23E ii). As expected, bands were found only in the lane loaded with Aβ, with no signal in the AllD Aβ or the vehicle lanes.

These results confirmed that Aβ and AllD Aβ are structurally identical and they aggregated with similar kinetics, but had opposite stereospecificity.

3.5.3.2. AllD Aβ did not share the toxic properties of Aβ on synaptic transmission and morphology of hippocampal autaptic neurons

In this last set of experiments, I compared the effects of the stereoisomers Aβ and AllD Aβ on neuronal morphology and synaptic transmission. Autaptic hippocampal neurons were treated on DIV 8 with 10 μM oligomerized Aβ, 10 μM oligomerized AllD Aβ or equivalent volume of the vehicle. After 72 hours of exposure to the peptides, the cultures were fixed to study neuronal morphology or used to obtain electrophysiological recordings.

After fixation on DIV 11, the cultures were immunolabelled with antibodies against MAP2, VGluT1, and Shank2 to quantify dendritic branching and the number of synaptic puncta. Sholl analysis was performed on binarized images from the MAP2 signal as before (Figure 24A). The plot of the number of intersections versus the distance from the cell soma showed a similar distribution of dendritic branches for all the experimental groups (Figure 24B). The enclosing radius (Figure 24C i) and total number of intersections (Figure 24C ii) were also

compared, with no statistically significant differences found between the treatments. However, there was a trend in both Aβ-treated groups towards a smaller enclosing radius (n= 36-38 neurons from at least N=3 cultures and Aβ preparations; one-way ANOVA, p= 0.071).

VGluT1 and Shank2 signals were used to label and quantify synaptic structures (Figure 25A). When compared, neither the number of VGluT1-positive presynaptic puncta (Figure 25B i), the postsynaptic Shank2-positive puncta (Figure 25B ii), or the number of puncta positive for both markers used as a proxy for synapse number (Figure 25B iii) were modified by exposure to either of the Aβ peptides. The fluorescence intensity of the VGluT1 signal was used as a measurement of the number of synaptic vesicles per presynaptic terminal (Figure 25B iv). No changes were found in this parameter between the compared groups. After establishing that the exposure to AllD Aβ did not induce any obvious changes in neuronal morphology, electrophysiological recordings were performed to investigate putative synaptic functional defects induced by AllD Aβ. On DIV 11, after 72 hours of exposure to 10 μM Aβ, 10 μM AllD Aβ, or the vehicle, synaptic transmission was studied using whole-cell recordings. As found in other sections of this study, the exposure to Aβ induced a 58% reduction in the EPSC amplitude (Figure 26A i-ii). In contrast, no changes were found in AllD Aβ-treated neurons.

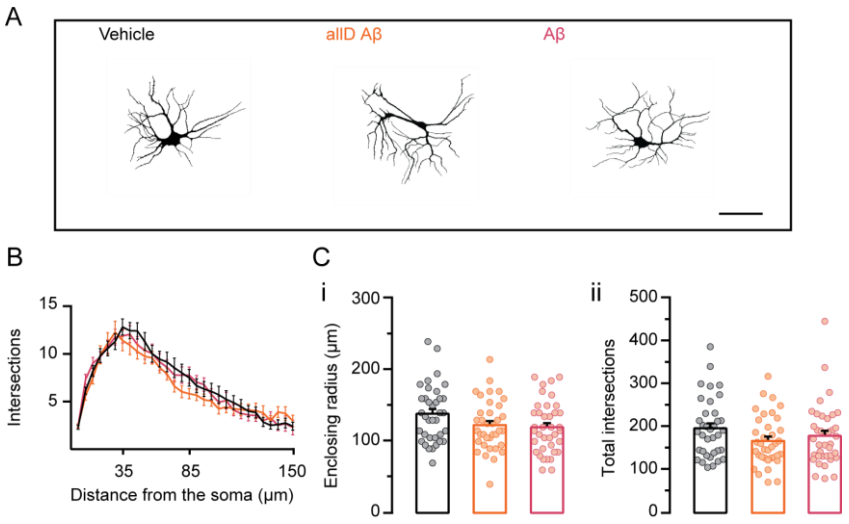

Figure 24. AllD Aβ treatment did not alter dendritic branching. **(A)** Representative images of the skeletonized MAP2 signal used for Sholl analysis to describe dendritic branching. **(B)** Distribution of dendrite number versus distance from the center of the cell somata. **(C)** Comparison of **(i)** the enclosing radius and **(ii)** the total number of intersections per neuron measured from vehicle, AllD Aβ- or Aβ-treated neurons. Bars represent the mean. Error bars represent SEM. Vehicle, black bars; AllD Aβ, orange bars. Aβ, pink bars.

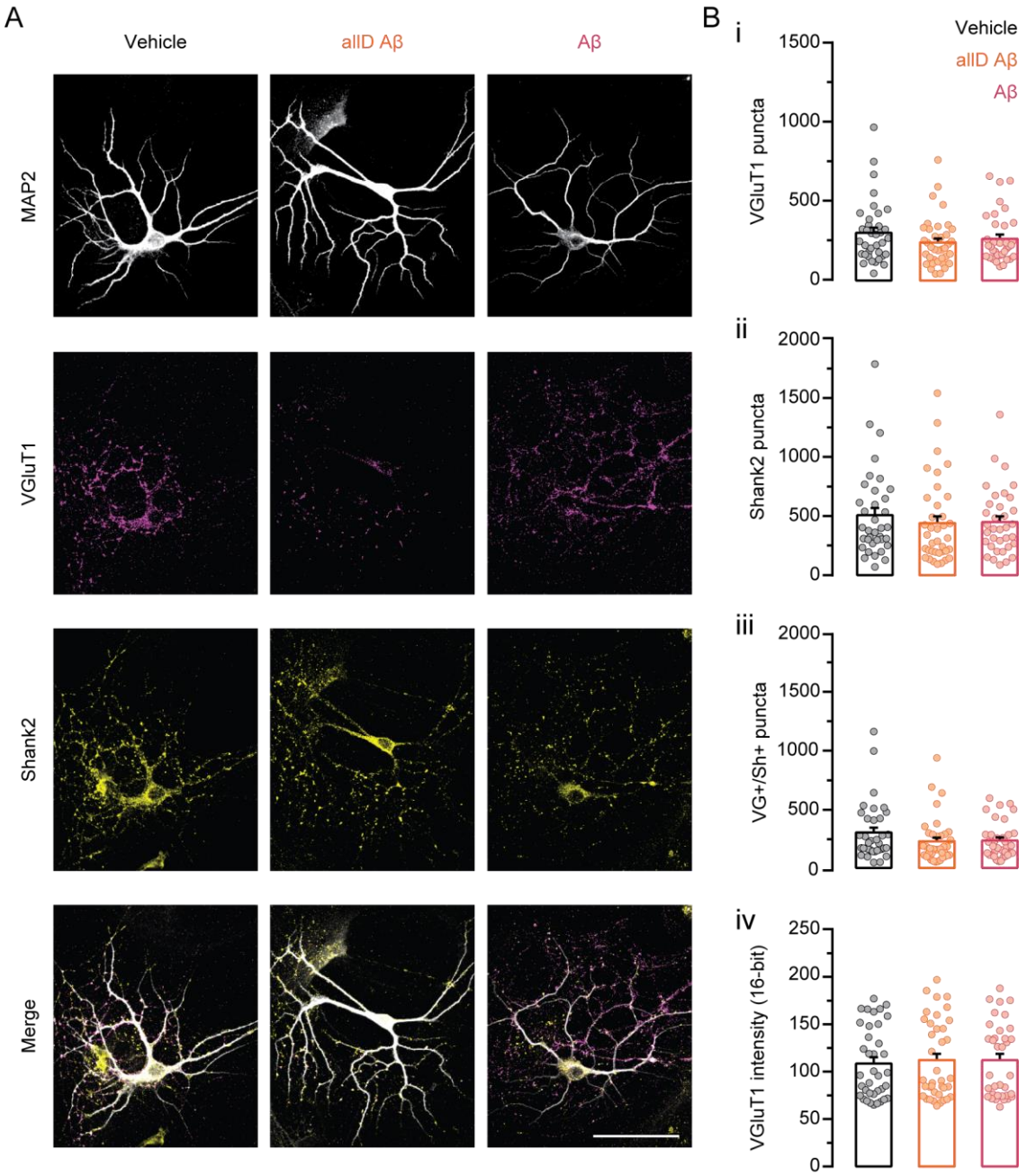

Figure 25. AllD Aβ treatment did not modify the number of synaptic puncta. (A) Representative images of autaptic hippocampal neurons fluorescently labelled against MAP2, VGluT1 and Shank2. **(B)** Quantification of **(i)** VGluT1 puncta, **(ii)** Shank2 puncta and **(iii)** puncta with juxtaposed VGluT1 and Shank2 signal. **(iv)** Comparison of the VGluT1 intensity between groups. Bars represent the mean. Error bars represent SEM. Vehicle, black bars; AllD Aβ, orange bars. Aβ, pink bars.

Similarly, the RRP size evoked by application of 0.5 M sucrose showed a 46% reduction in the Aβ-treated neurons whereas a conserved RRP was observed in the AllD Aβ exposed group (Figure 26B i-ii). No changes were observed in the Pvr (Figure 26C). A pulse of 100 µM glutamate was applied to study the postsynaptic response, which was similar in all experimental groups (Figure 26D i-ii). Recordings of mEPSCs in the presence of TTX were obtained (Figure 26E i). Both the frequency (Figure 26E ii) and the amplitude (Figure 26E iii) of the

mEPSCs were conserved between the groups, with a trend towards a reduced frequency in the Aβ-treated group. Finally, a train of depolarizing stimuli at 10 Hz was applied (Figure 26F). Neither the calculated paired-pulse ratio nor the depression ratio were changed upon treatment with the Aβ peptides.

In summary, the lack of morphological or functional effects of the AllD Aβ peptide suggested that the Aβ toxicity depended on molecular interactions that were stereospecific, such as the ligand-receptor binding.

A summary of these results can be found in Table 18.

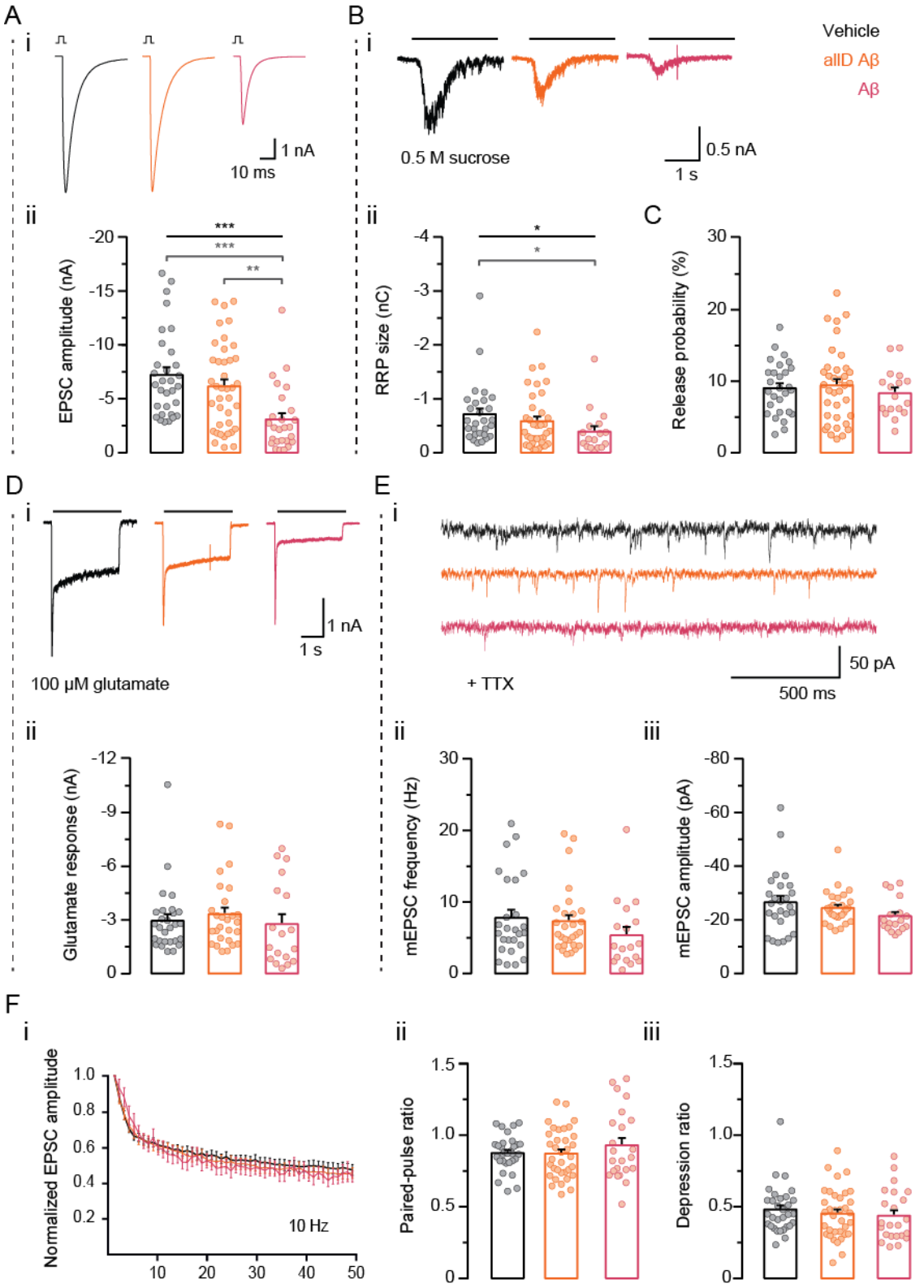

Figure 26. AllD Aβ treatment induced no toxic effects on synaptic transmission. (A) (i) Representative traces of EPSCs upon stimulation with a 2-ms depolarizing pulse. **(ii)** Comparison of EPSC amplitudes (n= 26-39 neurons from at least N=3 cultures and Aβ preparations; Kruskal-Wallis test, ***p<0.001; post-hoc Dunn's multiple comparisons test: Vehicle vs Aβ: ***p<0.001, AllD Aβ vs Aβ: **p= 0.002) **(B) (i)** Representative traces of the RRP evoked by application of 0.5 M sucrose **(ii)** Quantification of RRP size (n= 17-36,N=3; Kruskal-Wallis test, *p=0.024; post-hoc Dunn's multiple comparisons test: Vehicle vs Aβ: *p=0.020). **(C)** Comparison of the calculated Pvr. **(D) (i)** Representative traces and **(ii)** quantification of glutamate-induced currents. **(E) (i)** Representative recordings of spontaneous activity measured in the presence of TTX. **(ii)** Quantification of mEPSC frequency and **(iii)** amplitude. **(F) (i)** Short term plasticity induced by application of a train of stimuli at 10 Hz. **(ii)** Paired pulse ratio and

(iii) depression ratio. Bars represent the mean. Error bars represent SEM. Vehicle, black bars; AllD Aβ, orange bars. Aβ, pink bars.

Table 18. Statistical analysis of AllD Aβ versus Aβ effects on hippocampal neurons.

Fig.	Parameter	Vehicle			AllD Aβ			Aβ			p value	Summary	Test
		Mean	SEM	n	Mean	SEM	n	Mean	SEM	n			
Sholl - synaptic puncta (autaptic cultures)													
23C i	Enclosing radius (µm)	138.9	6.616	36	122.9	5.937	36	120.1	5.872	38	2.702	n.s.	one-way ANOVA
23C ii	Total intersections	197.8	11.6	36	168.3	9.82	36	180.1	11.68	38	0.176	n.s.	one-way ANOVA
24B i	VGluT1 puncta	404.8	43.69	36	321.4	33.59	38	348.9	34.84	36	0.330	n.s.	Kruskall-Wallis
24B ii	Shank2 puncta	510.3	60.96	36	445.8	56.41	38	446.3	46.12	36	0.531	n.s.	Kruskall-Wallis
24B iii	VG+/Sh2+ puncta	250.6	34.77	36	180.2	23.54	38	185.9	19.53	36	0.148	n.s.	Kruskall-Wallis
24B iv	VGluT1 intensity (16-bit)	109.2	6.395	36	112.6	6.756	38	112.8	6.625	35	0.925	n.2.	Kruskall-Wallis
Electrophysiology (autaptic cultures)													
25A ii	EPSC (nA)	-7.263	0.722	31	-6.192	0.643	39	-3.11	0.593	26	< 0.001	***	Kruskall-Wallis
25B ii	RRP (nC)	-0.719	0.108	28	-0.588	0.088	36	-0.394	0.100	17	0.024	*	Kruskall-Wallis
25C	Pvr (%)	9.027	0.696	28	9.408	0.875	36	8.337	0.800	17	0.343	n.s.	one-way ANOVA
25D ii	Glutamate-induced current (nA)	-2.963	0.349	28	-3.314	0.371	27	-2.763	0.556	18	0.252	n.s.	Kruskall-Wallis
25E ii	mEPSC frequency (Hz)	7.793	1.117	26	7.303	0.868	28	5.374	1.128	18	0.159	n.s.	Kruskall-Wallis
25E iii	mEPSC amplitude (pA)	-26.54	2.33	26	-24.46	1.16	28	-21.45	1.487	18	0.125	n.s.	Kruskall-Wallis
25F ii	Paired-pulse ratio	0.876	0.021	31	0.871	0.028	35	0.930	0.051	23	0.432	n.s.	one-way ANOVA
25F iii	Depression ratio	0.482	0.029	31	0.453	0.029	35	0.438	0.037	23	0.481	n.s.	Kruskall-Wallis

EPSC amplitude: Dunn's multiple comparisons test; Vehicle vs. Aβ: ***p< 0.001; AllD Aβ vs. Aβ: **p=0.002.
RRP size: Dunn's multiple comparisons test; Vehicle vs. Aβ: *p= 0.020

4. Discussion

4.1. Overview.

After more than 25 years since the amyloid cascade hypothesis was formulated to explain the role of Aβ in AD, many questions have been answered but central ones remain open (Selkoe and Hardy, 2016). The original hypothesis has been reformulated, shifting the focus from plaque deposition to the accumulation of soluble oligomeric aggregates. In addition, the use of standardized biomarkers and the widespread use of passive immunization in phase II/III clinical trials will hopefully generate in the near future new evidence that will help to finally explain the molecular nature of Aβ toxicity.

A still open question that I aimed to answer in the present study is how an excess of Aβ peptide in the surroundings of neurons can induce deleterious effects in synaptic function, focusing on the amyloid pore hypothesis and intending to set the stage for testing putative protective effects of the novel small molecule anle138b.

In the first part of my work I focused on establishing a reproducible method for obtaining synthetic Aβ oligomers that could be applied to diverse model systems. To this end, I utilized a two-step method for Aβ dissolution which yielded oligomer-enriched solutions, extensively characterized here using biochemical and imaging methods.

Later, I observed that the treatment of autaptic hippocampal cultures with Aβ oligomers impaired synaptic transmission, which was mostly caused by presynaptic dysfunction and devoid of gross accompanying morphological alterations, besides a small but statistically significant reduction in branching. This observation is in agreement with previous work by others and points to the presynaptic terminal as a target of Aβ toxicity. Further analysis of neurons exposed to Aβ oligomers for shorter periods pointed towards an enhancement in synaptic transmission, indicating that the quality of Aβ effects depend on the duration of treatment. In addition, I analyzed the efficacy of the small molecule anle138b, which could not prevent Aβ synaptotoxicity when applied as amyloid pore blocker. However, further experiments testing its properties as inhibitor of the amyloid aggregation might render different results.

Finally, I took advantage of several model bilayers to investigate the putative formation of pores by Aβ oligomers. Here I demonstrated that the same oligomer preparation that impaired presynaptic release failed in altering membrane properties in most of the models used or induced pore formation in a very low frequency (see Supplementary Material). Moreover, I could show that AIID Aβ, the enantiomer of the naturally occurring Aβ42, despite a similar aggregation propensity, lacks the toxicity of the L-counterpart. I therefore propose that the Aβ toxic effects on synaptic transmission that I observed in the *in vitro* model depend on a stereospecific molecular interaction yet to be elucidated, rather than on the formation of membrane perforations.

4.2. In vitro oligomeric preparations are a versatile tool to study Aβ toxicity

Recapitulating Aβ toxicity using *in vitro* generated oligomers offers several advantages. For example, a single isoform of synthetic or recombinant Aβ can be analyzed at a time and the aggregation conditions can be adjusted to obtain mixtures of well-characterized species, which minimizes the variability of the results. A key step in the preparation of toxic aggregates is the dissolution method (Teplow, 2006). In this study I tested two different methods for Aβ42 solubilization: an alkali-based using double-distilled water and 0.5% ammonia, and a two-step dissolution protocol comprising the initial application of 100% HFIP, a lyophilizing step and a final dissolution in 100 mM NaOH. Although the ammonia dissolution method has been validated by others, in the experiments reported here it failed to dissolve large Aβ aggregates and was therefore not further utilized (Ryan *et al.*, 2013). Conversely, HFIP could successfully dissolve the peptide in the first step. The use of HFIP to erase the peptide "structural history" was validated 15 years ago (Stine *et al.*, 2003). However, a recent study suggested that HFIP and film formation during lyophilization could induce the aggregation of Aβ into low-molecular weight oligomers, which were not detectable by TEM but were observed by dynamic light scattering in the literature reports. These low-molecular weight oligomers were linked to a faster rate of fibril formation evidenced by ThT fluorescence measurements and reduced toxicity when applied to PC12 cells (Ryan *et al.*, 2013). In the present study, HFIP was always followed by solubilization in 100 mM NaOH. It is therefore not possible to draw any conclusions about the effects of HFIP alone.

The two-step dissolution protocol yielded an Aβ solution that contained ~ 50% monomers to hexamers. This is in agreement with previous reports that Aβ monomers, even when purified by SEC, are readily in equilibrium with pentamers-hexamers (Bitan *et al.*, 2003). In addition, the monomer-enriched solution contained a percentage of aggregates larger than 63 kDa (~17%) which would theoretically correspond to 12-mers. This initial aggregation is almost unavoidable without using SEC at the Aβ concentrations used in these experiments. The presence of these aggregates that could act as seeds, correlate with the lack of a lag phase in the ThT fluorescence measurements and the presence of some isolated fibrillar aggregates observed in TEM.

By means of incubating the monomeric solution for 40 minutes at 37°C with external agitation, the content of oligomers larger than 12-mers was increased, and this corresponded with the emergence of protofibrillar structures evidenced by TEM. Unexpectedly, after 3 days of incubation no typical single, isolated mature fibrils were found. In turn, I observed an entangled accumulation of fibrillar aggregates, highly contrasted, from which single structures were not possible to be resolved (Figure 27, left). In addition, TEM also revealed lateral interaction of the fibrils (Figure 27, center) as reported by Tycko and collaborators for Aβ40 fibrils grown in agitation (Figure 27 right, from Petkova *et al.*, 2005. Reprinted with permission from AAAS. Licence number: 4622571423534). Given the unconventional morphology of these fibrillar species, it is possible that the oligomers described before represent “off-pathway” aggregates, *i.e.,* that they escape the amyloidogenic path towards fibril formation and remain in solution as oligomers.

In conclusion, I found here that the two-step protocol is more effective in disassembling preformed Aβ42 aggregates than a single solubilization step with

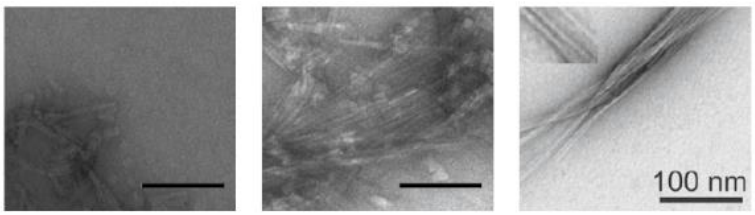

Figure 27. Fibrillar species observed by TEM grown under agitation. (Left) Accumulation of highly stained protofibrillar aggregates and (center) lateral interacting fibrils obtained using the Aβ42 preparation protocol described here. Aβ42 was incubated at 110.25 μM for 72 hours, with external agitation. (Right) Aβ40 fibrils with lateral interaction obtained by Tycko and collaborators by gentle circular agitation. Inset is 2x.

ammonia. Furthermore, the incubation conditions used here allowed for the rapid preparation of a protofibril-enriched solution that can be diluted in culture medium for the investigation of Aβ synaptotoxic properties.

4.3. Aβ effects on neuronal survival, physiology, morphology and development

4.3.1. 72-hour Aβ treatment mildly reduce neuronal viability without limiting the use of the surviving neurons for morphological and functional studies

Here I aimed to gain insight into Aβ-induced changes in synaptic transmission, which have been shown to occur before frank neuronal loss. Therefore, in a first set of experiments I sought to determine putative deleterious Aβ effects on neuronal survival, since a significant increase in neuronal death would not be compatible with functional and morphological studies. Hippocampal neurons grown in mass cultures at high density were exposed to 10 µM oligomeric Aβ aggregates for 72 hours. I observed a ~30% increase in cell death upon Aβ exposure with respect to the vehicle-treated condition, expressed as a higher count of picnotic nuclei. A limitation of this experiment was the use of the DNA-binding dye Hoechst to obtain the total number of nuclei per coverslip. It is possible that some of the counted nuclei corresponded to astrocytes, which occasionally are able to survive despite the growing conditions being optimized for nerve cells. It was not possible to immunolabel nuclei with a neuronal marker because the experiments were performed without permeabilization or fixation.

Whereas here I measured the excess of pyknotic nuclei as a proxy for cell death, Jan *et al.* used the count of NeuN-immunolabelled neuronal nuclei to determine the survival of rat hippocampal neurons in the presence of mixtures of synthetic Aβ species (Jan *et al.*, 2008). Interestingly, the authors could show that the preparation containing 10 µM protofibrillar Aβ42 induced a ~35% reduction of neuronal nuclei, whereas the mixture of 5 µM protofibrillar and 5 µM monomeric Aβ42 produced a ~50% reduction in the nuclei count. The Aβ species preparation that I established here yields a mixture of oligomeric and monomeric species of Aβ. Whereas here I observed a ~30% increase in picnotic nuclei, Jan *et al.* reported more than 50% of neuronal loss. I hypothesize that the main cause of this discrepancy is the exposure time to Aβ. Whereas I exposed the neurons to Aβ for 72 hours, Jan *et al.* extended their treatment for 7 days.

These results show that 72 hours are a convenient duration of treatment to study effects of Aβ on synaptic transmission, before the cultures have suffered an increase in neuronal death. In addition, considering its limitations, these results are in agreement with the findings in human AD patients, in which the accumulation of Aβ does not correlate with gross neuronal loss (Gómez-Isla *et al.*, 1997).

4.3.2. Aβ induced a prominent impairment of presynaptic function in autaptic cultures when applied for 72 hours, most likely mediated by interaction with proteins of the synaptic vesicle release machinery

The main open question I aimed to answer here was that of the nature of Aβ synaptic toxicity. In this context, I aimed to determine whether treatment of autaptic glutamatergic hippocampal neurons with 10 μM oligomeric Aβ for 72 hours could replicate *in vitro* the synaptotoxic effects reported in other AD models. My main finding was a drastic reduction in basal synaptic transmission. EPSC amplitude and RRP size showed a 60% and 48% decrease, respectively. There was a moderate but significant change in the response to exogenous glutamate application, which was reduced ~20% with respect to the vehicle-treated neurons, and mEPSC frequency showed a 35% reduction. In addition, I observed no changes in the Pvr. Importantly, the release of glutamate in an effective and temporally precise manner plays a central role in brain function as a whole, but is especially relevant in memory- and learning-related synaptic plasticity in the hippocampus (Basu and Siegelbaum, 2015). Therefore, the deficit in neurotransmitter release observed here would have devastating consequences in hippocampal function, if such Aβ-exposed neurons were integrated in its circuits. Several mechanisms could potentially explain the above described phenotype:

Synapse/ spine loss. Synapse and spine loss are hallmarks of AD neuropathology. Hence, they have been widely studied in relation to Aβ deposition (see section 1.3.3; Ripoli *et al.*, 2013). I consequently hypothesized that synapse loss could underlie the findings presented above, namely a reduction in evoked release and RRP. However, to cause the 60% EPSC amplitude reduction observed in Aβ-treated neurons, loss of synapses or dendritic spines should have resulted in reduced AMPA currents induced by

exogenous glutamate application to a much greater extent. Alternatively, it is also possible that synapses and spines were indeed reduced in number but with no change in surface extrasynaptic AMPA expression, which would explain the observed impairment of basal synaptic transmission accompanied by an almost normal glutamate-induced current. In order to determine whether the dendritic tree was altered and to investigate synaptic number, I performed immunostainings on Aβ-treated autaptic hippocampal neurons. In contrast with the findings by Ripoli *et al.,* immunocytochemistry of the treated neurons revealed an unchanged number of pre- and postsynaptic puncta by VGluT1 and Shank2 staining, as well as VGluT1/ Shank2 co-labelled puncta, with a mild reduction (~15 %) in dendritic branching. Altogether, the results I presented indicate that Aβ-treated neurons displayed a normal morphology, with no synapse loss, and consequently the electrophysiological results must be explained by ultrastructural or molecular Aβ-induced changes. Since the electrophysiological and imaging experiments were performed using different sets of cultures and Aβ preparations, further experiments could be done to directly correlate electrophysiology with fluorescence microscopy by biocytin-filling for fluorescent labelling of the autaptic neurons that have been used for recordings.

Alterations in the synaptic proteome. The loss of presynaptic proteins has been reported previously by others in Aβ-treated neurons (Parodi *et al.*, 2010; Ripoli *et al.*, 2013). Here protein quantification could not be performed using samples from autaptic cultures due to two factors: first, autaptic cultures are grown at low neuronal density (~400 / cm^2) and second, feeder astrocytes are used to support neuronal development. As a result, the protein yield would have been too low for Western blotting and also the sample would have been contaminated with proteins from the supporting glial cells. Therefore, in order to investigate whether Aβ incubation could change the protein composition of synapses, I used mass cultures for these experiments. In discrepancy with previous findings by others, using Western blot analysis I found no changes in the pre- or postsynaptic proteins tested with exception of Synaptotagmin-1, which was reduced by 20%. Previous studies with the Synaptotagmin-1 KO mouse line revealed that only homozygous KO animals displayed a lethal phenotype at birth, and cultured homozygous neurons showed a drastic reduction in synchronous release (Geppert *et al.*, 1994). These alterations were absent in heterozygous Synaptotagmin-1 animals and neurons, indicating that more than a 50%

decrease in in Synaptotagmin-1 protein expression is necessary to induce a funtional presynaptic defect. These results, if extrapolated to the experiments described here, indicate that it is highly unlikely that the observed Synaptotagmin-1 reduction induced by exposure of dissociated neurons to Aβ explains the electrophysiological alterations caused by the Aβ incubation in autaptic neurons.

Alterations of synaptic vesicle pools. Several studies that have addressed presynaptic alterations in Aβ-exposed neurons focused on the depletion of the total pool of synaptic vesicles as a putative mechanism of synaptic dysfunction. Parodi *et al.* observed that dissociated mass hippocampal neuronal cultures exposed to 500 nM Aβ40 for 24 hours showed more than a 50% reduction in the number of vesicles per area of the terminal using EM, which was accompanied by a reduction in AMPA mEPSCs (Parodi *et al.*, 2010). In order to study the size of the RRP, the authors applied a pulse of hypertonic sucrose solution and measured the miniature-current frequency, which was reduced in Aβ40-treated neurons. In addition, direct application of AMPA induced similar currents in both control and Aβ40-treated group, indicating an unchanged expression of surface AMPA receptors. Interestingly, the authors showed that acute application of 500 nM to 5 µM Aβ to the culture induced a transient increase in Ca^{2+} measured in selected regions of the cell somata, mediated by putative amyloid pores. Blockers of these pores such as the NA7 peptide could not only inhibit the Ca^{2+} influx but also prevented the decrease in mEPSC frequency observed after 24 hours of treatment. In another approach, Kelly *et al.* showed in neuronal cultures exposed to 2 µM Aβ for 24 hours that an NMDA-mediated enhancement of intracellular Ca^{2+} caused the activation of calpain, which in turn led to loss of dynamin-1 and impaired vesicle recycling (Kelly, Vassar and Ferreira, 2005; Kelly and Ferreira, 2006, 2007). More recently, Zhou *et al.* proposed that pathogenic tau can bind and cross-link synaptic vesicles and F-actin, reducing vesicular mobility and impairing vesicle release (Zhou *et al.*, 2017). In principle, a depletion of the total synaptic vesicle pool could explain the decrease in the size of EPSCs and RRPs as well as the reduced mini frequency that I observed in this study. However, I did not observe alterations in the intensity of VGluT1 puncta, suggesting that the number of vesicles per terminal was intact. Nevertheless, it is possible that using a higher resolution method, such as EM, changes in the vesicle distribution within Aβ-treated terminals could be revealed. With respect to the Aβ-mediated

impairment of vesicle recycling and mobility, such alterations would induce a larger depression of EPSC amplitudes in the final phase of high-frequency trains, as seen in dynamin-1 KO neurons, and also found as a consequence of tau accumulation in the work by Zhou *et al.* (Ferguson *et al.*, 2007; Zhou *et al.*, 2017). Conversely, I did not find any alteration in the refilling of the synaptic vesicle pool as indicated by an unchanged depression ratio in Aβ-treated neurons. Therefore neither a reduction in the total vesicle pool nor a refilling defect are likely to underlie the results presented here.

In addition, Park *et al.* showed that exposure of dissociated rat hippocampal neurons to soluble Aβ42 at 200 nM for 2 hours increased intracellular Ca^{2+} and impaired its clearance. Accumulation of Ca^{2+} led to activation of the Ca2+/calmodulin-dependent protein kinase IV, which in turn phosphorylated synapsin, inhibiting intersynaptic and axonal vesicle trafficking, impairing forskolin-induced LTP (Park *et al.*, 2017). In agreement with this, the authors showed that Aβ increased the resting vesicle pool, with no changes in the recycling pool. This same group had previously reported, using a similar approach, an increase in the RRP with a delayed recovery after high frequency stimulation (Park, Jang and Chang, 2013). The effects seen by Park *et al.* partly contradict the studies by Parodi *et al.* indicating that Aβ exposure depleted the total pool of vesicles. However, it is possible that acute exposure to soluble Aβ accompanied by a Ca^{2+} increase induces a temporary enlargement of the total pool of vesicles as seen in the work by Park *et al.*, whereas chronic exposure (longer than 24 hours), could deplete the pool as reported by Parodi *et al*. Regarding the data that I presented here, I observed a clear reduction in the RRP size when autaptic hippocampal neurons were exposed to 10 μM Aβ for 72 hours, which is in disagreement with the results by Park *et al.*

Altered Pvr. Recent work by He *et al.* pointed to a different mechanism of toxicity for soluble Aβ oligomers (He *et al.*, 2019). Using a short incubation of 20 minutes with 400 nM Aβ42 on dissociated hippocampal neurons, the authors found a reduction in mEPSC frequency accompanied by a depletion of PIP_2 that depended on phospholipase C activation, in an mGluR5-PrP dependent mechanism. The presynaptic changes observed in this study are mainly related to a reduction in Pvr linked to the loss of PIP_2 in contrast to the results presented here, in which neurons had no changes in Pvr or paired-pulse ratio.

Interaction of Aβ with proteins of the vesicle release machinery. Finally, another presynaptic mechanism of Aβ toxicity that has been proposed is the direct interaction between soluble oligomers and the H3 domain of syntaxin-1a, one of the SNARE proteins at the plasma membrane. This aberrant binding would cause the inhibition of vesicle membrane fusion without affecting docking, as shown mainly using *in vitro* membrane fusion assays (Yang *et al.*, 2015). Furthermore, it was recently demonstrated that expressing a syntaxin1-a point mutant of the H3 domain (syntaxin-1a^{A240V}) in the syntaxin-1a/b double KO background showed a similar phenotype to the generated by the syntaxin1a-Aβ binding, in which vesicle docking but not fusion can be rescued by the mutants (Vardar *et al.*, 2016). The mutant-infected neurons which expressed exclusively syntaxin-1a^{A240V} showed an almost complete arrest of evoked and spontaneous vesicle release. However, in the Aβ-syntaxin interaction scenario only a fraction of syntaxin molecules should have to be affected to explain a residual vesicle release as seen in the present study. In this context, to confirm the involvement of the Aβ-syntaxin interaction, it would be interesting to observe whether an overexpression of syntaxin-1a could protect autaptic neurons from Aβ-induced toxicity. This mechanism or a similar interaction of an oligomeric form of Aβ with a protein of the fusion machinery provides the most plausible explanation for the results that I presented in this study.

4.3.3. Shorter treatment with Aβ enhanced synaptic transmission in autaptic cultures

Since 72-hour treatment of neurons with 10 µM Aβ greatly reduced synaptic transmission, I aimed to induce milder effects that could represent an earlier and possibly reversible stage of Aβ-related toxicity. Consequently, I exposed autaptic hippocampal neurons to 10 µM Aβ, the concentration used previously, but for a shorter period of 24 hours. Surprisingly, instead of observing the expected milder version of the 72-hour treatment, I found the opposite effects. EPSCs were ~50% larger with a Pvr increased ~40%. No changes in paired-pulse ratio were observed, despite the increase in Pvr.

I posit two hypotheses to explain these results. First, I speculate that the enhancement in synaptic transmission and Pvr could be an effect of the remaining monomers present in the oligomer solution, which account for ~20%

of the Aβ species. As described by others, low Aβ concentrations in the picomolar range can enhance synaptic transmission. Abramov *et al.* showed more than a decade ago that Aβ exposure induces an increase in the Pvr (Abramov *et al.*, 2009). A later study by the same group explained that APP homodimerization and Ca^{2+} influx mediated this effect (Fogel *et al.*, 2014). Alternatively, Lazarevic *et al.* indicated that Aβ can bind α7-nAchR and increase the recycling of the synaptic vesicle pool in a CN-CDK5 dependent manner (Lazarevic *et al.*, 2017). A second possible explanation is that increased Pvr is part of the initial phase in the spectrum of Aβ toxic effects. Park *et al.* reported that exposure to 200 nM Aβ for 2 hours can enhance the Pvr, accompanied by an enlargement of the resting pool and a reduction of the recycling pool. However, this group also indicated that neurons that had been treated with Aβ for 72 hours showed also an increased Pvr. As discussed in the previous section, the results presented here suggest that oligomeric Aβ probably exert its toxic effects by binding to proteins of the fusion machinery and blocking membrane fusion, which would then result in the opposite to an increased Pvr.

More experiments are necessary to decipher the meaning of these puzzling findings. Pharmacological inhibition of the proposed pathways (α7-nAchR, CN-CDK5, p38MAPK) could be useful to discard or confirm a putative physiological enhancement of Pvr mediated by Aβ monomers or oligomers. In addition, addressing separately the effects of monomers and oligomers would clarify what species is responsible for the changes in Pvr. Finally, immunocytochemistry could reveal whether the electrophysiological effects are accompanied by morphological changes after 24 hours. On the whole, the question remains open as to whether the variation between the effects observed after 24 and 72 hours of treatment is a manifestation of the different biological activities of the Aβ species contained in the sample or it represent the evolution in stages of the same pathophysiological continuum.

4.3.4. Dendritic development is moderately altered by the exposure to oligomeric Aβ

As described in the previous sections, treatment with 10 μM Aβ for 72 hours impaired synaptic transmission on hippocampal autaptic neurons, whereas a shorter 24-hours exposure induced the opposite effects. I hypothesized that

similar time-dependent effects could be induced upon oligomeric Aβ treatment on neuronal morphology. In consequence, I exposed autaptic neurons to 10 µM Aβ on DIV 8 and fixed them after 24 and 72 hours of treatment. Using the two-way ANOVA test, I analyzed several morphological parameters considering duration and type of treatment as variables. Although the individual variables showed no significant changes in either of the analyzed parameters, the interaction between type and duration of treatment was statistically significant for enclosing radius and total number of intersections, which I interpreted as the Aβ treatment having effects in opposite directions over time. This observation is in agreement with the data obtained from the electrophysiology, and support the notion that two (or more) species of amyloid aggregates, which would exert opposing effects, are present at increasing time points upon treatment. It is possible that a longer duration of treatment might be required for the effects of Aβ in branching to become evident. In this context, performing a similar experiment extending the treatment duration and increasing the number of studied time points would provide a more accurate description of Aβ effects on the dendritic tree.

Although in this study I focused mostly on the presynaptic effects of exposure to Aβ, the morphological changes described in this section state that there is a postsynaptic component of amyloid toxicity which, according to the results presented here, occur at a later stage of treatment. It has been proposed that loss of presynaptic afferents in AD could result in simplification of the dendritic tree of the postsynaptic neuron (Anderton *et al.*, 1998; reviewed in Cochran, Hall and Roberson, 2014). However, recent evidence suggests that postsynaptic structures in most hippocampal synapses follow an autonomous path of development which is independent from neurotransmitter release, therefore indicating that possibly loss of presynaptic input does not induce the postsynaptic abnormalities observed here (Sando *et al.*, 2017; Sigler *et al.*, 2017).

Regardless of the initiating injury, the accumulation of tau in the neuronal somatodendritic compartment, a phenomenon briefly described above (see Section 1.3.4.3), has been directly related to neuritic dystrophy (reviewed in Cochran, Hall and Roberson, 2014; reviewed in Herms and Dorostkar, 2016). Tau mislocalization can be induced by phosphorylation in the microtubule-binding as well as in its proline-rich domain, among other mechanisms (Zempel *et al.*,

2010; Jin *et al.*, 2011; X. Li *et al.*, 2011; Mairet-Coello *et al.*, 2013). As a consequence, there is an increase in Fyn concentration at the synapse associated with NMDA-receptor mediated excitotoxicity, a cleavage of polyglutamylated microtubules and disruption of dendritic organization mediated by aberrant binding of tau to PSD-95 (Ittner *et al.*, 2010; Larson *et al.*, 2012; Zempel *et al.*, 2013). The mislocalization of tau as well as the activation of Fyn are attractive candidate mechanisms to explain the postsynaptic abnormalities depicted here and could be further studied in the autaptic cultures by means of immunostainings as well as Western blot (Li and Götz, 2017).

4.3.5. Aβ concentrations below 10 µM do not induce deleterious changes in synaptic function

Concentration has been reported as an important factor in defining Aβ physiological, trophic versus pathological, toxic effects on synaptic function (Puzzo *et al.*, 2008; Mucke and Selkoe, 2012). In order to study the concentration dependence of Aβ effects I treated autaptic hippocampal neurons with 200 nM and 1 µM Aβ for 72 hours. In addition, 10 µM Aβ and vehicle solution were used as positive and negative controls respectively. As reported here previously, the neurons exposed to 10 µM Aβ tended to display an impaired basal synaptic transmission, although statistical significance was not reached. Interestingly, neurons treated with lower Aβ concentrations of 200 nM and 1 µM showed a tendency towards larger EPSCs with respect to the untreated neurons and displayed a statistically significant increase in Pvr. Similar findings of an increased synaptic transmission upon exposure to low Aβ concentrations were reported by Puzzo and colleagues, who observed an enhancement of postetanic potentiation, hypothetically associated to α7-AchR activation and increased calcium entry during an action potential (Puzzo *et al.*, 2008). However, in the latter study, the lowest concentration used was in the picomolar range, which is thousand times smaller than the minimum Aβ concentrations applied here. As mentioned before, and also discussed by Puzzo *et al.*, it is likely that the actual concentration of the active species is lower than the measured monomeric concentration, because a mixture of aggregates coexists in solution (Puzzo *et al.*, 2008). This could partially explain the discrepancy between the results presented here and other reports from the literature.

4.4. Anle138b does not rescue the functional defects induced by Aβ treatment in the autaptic cultures

Anle138b is a novel small molecule that was shown to prevent AD related neuropathological and behavioral changes in murine models (Wagner *et al.*, 2013; Martinez Hernandez *et al.*, 2018). Despite the vast number of reports of anle138b protective effects in animal models of neurodegenerative diseases, the cellular and molecular effects underlying its benefits remain still unclear (Wagner *et al.*, 2013, 2015; Fellner *et al.*, 2016; Heras-Garvin *et al.*, 2018; Qin *et al.*, 2019; Wegrzynowicz *et al.*, 2019). Two main mechanisms of action have been proposed for anle138b, namely the inhibition of aggregation of Aβ and other amyloid proteins, and the blocking of amyloid pores. The latter mechanism has been mainly studied using artificial lipid bilayers reconstituted in the presence of anle138b and later exposed to Aβ applied to the recording chamber to induce pore formation. To compare these findings in bilayers with putative similar effects on autaptic cultures, I incubated the hippocampal neurons with anle138b for 24 hours before applying Aβ to the bath. Given anle138b liposolubility, I assumed that the compound would accumulate at the neuronal plasma membranes, where it could block the perforation by amyloid pores. Autaptic hippocampal neurons were initially treated with 10 µM anle138b, the maximum soluble concentration of the compound in our culture medium when dissolved in DMSO and FBS (Sergey Ryazanov, personal communication). After 96 hours of anle138b exposure, the autaptic neurons showed reduced EPSC amplitudes and RRP sizes, as well as a smaller mEPSCs amplitude and lower frequency. Conversely, no toxic effects have been reported in mice thus far. It is therefore possible that these synaptic effects constitute an artifact of the treatment in the *in vitro* model system. On the one hand, the concentration ranges used in the present work have been extrapolated from the anle138b concentrations measured in murine brain homogenates. This method for estimation of drug concentration in a certain tissue does not take into account the variation in lipid concentration in the different brain regions (Zhang *et al.*, 1996). Since anle138b is a highly lipophilic compound, it is possible that it gets “trapped” in the white matter and therefore the concentrations measured in the homogenates do not reflect the actual amount of drug present in the gray matter, and could overestimate it (Wagner *et al.*, 2013). On the other hand, in the model system that I used, namely autaptic neuronal cultures, the lipid fraction represented by the plasma membrane of

neurons and astrocytes constitutes only a minimum part of the total volume. In this case, if anle138b accumulates in the lipidic fraction it is possible that the actual concentration in the neuronal membrane is higher than the nominal concentration. Regarding the mechanisms of anle138b effects on autaptic cultures, it is possible that its accumulation in the neuronal membranes could modify the membrane's lipidic composition, which is tightly regulated at the presynaptic site, as well as the physical properties of the membrane altering the energy barrier for vesicle fusion.

Since it was not possible to measure the concentration of anle138b in the cellular fraction of the cultures because amounts of tissue in the range of grams would have been needed, I empirically searched for a concentration devoid of negative effects on the autaptic cultures. I thus tested whether 7 µM of the compound were still able to induce synaptic alterations. No statistically significant changes were observed after 96 hours of application and therefore this dose was used as putative protective treatment.

For the study of protective effects on synaptic function, anle138b was added to the culture medium of autaptic neurons on DIV 7, and 10 µM Aβ were added as co-treatment 24 hours later, on DIV 8. Electrophysiological recordings were performed after 72 hours of Aβ incubation, on DIV11. As reported previously, Aβ-treated neurons showed smaller EPSC amplitudes and RRP sizes. Surprisingly, anle138b-Aβ co-treated neurons displayed similarly reduced responses to the vehicle-Aβ treated. In addition, anle138b-Aβ co-treated neurons showed a decreased depression ratio accompanied by an increase, although not statistically significant, of Pvr.

There is a clear discrepancy between the lack of protective effects of anle138b when applied with Aβ to autaptic hippocampal cultures and the *in vivo* reported benefits of the compound. A limitation of the anle138b data set presented here is the low number of recordings in comparison to the rest of the data sets presented in other sections of this study. Further experiments must be performed to confirm these data, but the trend is very clear towards a lack of efficacy of anle138b in protecting from Aβ synaptotoxicity in this experimental setting. A potential explanation could be that anle138b would exert its protective effects on autaptic cultures by acting as an inhibitor of amyloid aggregation. If this were the case, anle138b and Aβ should be applied simultaneously to the culture medium, in

order for the compound to neutralize oligomerization. Another interpretation of these data could be that anle138b performs its protective effects on a cell type that is not present in autaptic cultures, like GABAergic neurons or microglia. Regarding microglial cells, there is a growing interest in the field about its role in neurodegeneration and AD (Sarlus and Heneka, 2017; Deczkowska *et al.*, 2018). However, Martinez Hernandez *et al.* reported that although anle138b was effective in protecting post-plaque AD mice from Aβ induced electrophysiological and behavioral changes, the transcriptome analysis revealed that most of the deregulated genes in this group were related to neuroinflammation and could not be modified by anle138b treatment (Martinez Hernandez *et al.*, 2018). It is therefore unlikely that anle138b protective effects are dependent on microglia or inflammation-related mechanisms.

Taken together, these data point to several directions to explore and experiments to perform, such as the study of GABAergic neurons or the application of anle138b together with Aβ in the medium, in order to better understand the mechanisms of the protective effects of this compound.

4.5. Pore formation does not explain the synaptic defects induced by exposure to Aβ

Pore formation is a potential mechanism of toxicity of Aβ that would mainly cause its downstream effects via deregulation of calcium homeostasis (Arispe, Rojas and Pollard, 1993; Arispe, Pollard and Rojas, 1996; Kawahara *et al.*, 1997; Demuro, Smith and Parker, 2011). The formation of amyloid pores could theoretically at least partially explain the electrophysiological alterations of autaptic cultures exposed to 10 µM Aβ for 72 hours. Therefore, I sought to investigate whether the oligomeric preparation that I used on hippocampal cultures could also induce pore formation. To this aim, I initially performed experiments on artificial bilayers exposed to Aβ or a control peptide for 20 minutes. The advantage of these model membranes to study pore formation is the absence of proteins or receptors, which can act as confounding factors in living cells, and the possibility of controlling the lipidic composition of the membrane. I initially utilized oxidized cholesterol membranes and exposed them to 10 µM of Aβ42 or two control peptides, the reverse Aβ 42-1 and the scrambled peptide, scr Aβ. In all the conditions tested, a stepwise current increase was

observed upon treatment, pointing to the assembly of conducting structures in the bilayer that could correspond to Aβ pores. However, when experiments were performed in phospholipid membranes (dyphyPC), a bilayer that resembles the neuronal plasma membrane in its lipidic composition, no induction of currents was observed. A limitation of these experiments is the use of the reverse and scrambled Aβ as negative controls. Recently, the group of Serpell and collaborators showed that both control peptides have a tendency to aggregate similar to the wild type Aβ42 peptide, although with less neurotoxic effects (Vadukul *et al.*, 2017). Therefore, if pore formation is a phenomenon that depends on aggregation and conformation, the Aβ 42-1 or scr Aβ are not valid as negative controls and have to be considered as potential amyloidogenic proteins. Another conclusion that can be drawn from these experiments is that Aβ aggregates show a great avidity to interact with cholesterol-enriched membranes, as has been reported before by Arispe and Doh (Arispe and Doh, 2002). Regarding the experiments with phospholipidic membranes, most of the experiments reported in the literature have included negatively charged phospholipids such as phosphatidylserine in their lipid mixture. In addition, some of the studies have even reconstituted the membranes after dissolving Aβ in the lipid mixture, thus skipping the insertion step (Arispe, Rojas and Pollard, 1993; Arispe, Pollard and Rojas, 1996; Rhee, Quist and Lal, 1998; Simakova and Arispe, 2007; Diaz *et al.*, 2009). These differences in membrane composition and preparation could explain the discrepancies between the absence of pore formation in the dyphyDPC membranes used here and the findings reported by others.

Next, I performed cell-attached recordings upon repetitive application of 3 µM GABA puffs and using an internal solution devoid of ATP. I had previously established that GABA currents would suffer a rundown if the cytoplasm was dialyzed and somatic ATP was removed. I hypothesized that observing a progressive increase of GABA currents when still in cell attached mode would be indicative of electrical access to the cell. Additionally, measurement of large GABA currents with absence of rundown would point to a perforated patch-like state, whereas GABA current rundown would be the outcome of patch rupture. During the first 20 minutes of these experiments, the GABA current increased only mildly in both control and Aβ-intrapipette exposed patches. This is already in contrast with previous reports by others in which pore formation occurred within the first 10 minutes of recording (Bode, Baker and Viles, 2017). However, some

studies have reported that at least 40 minutes are necessary to reach a perforated patch-like state (Sepúlveda *et al.*, 2010). Nevertheless, in later time points, after ~30 minutes of recording, both control and Aβ-treated patches showed increased GABA currents, with no rundown observed in the control patch. Since the control patch contained only the intracellular solution and phosphate buffer used as vehicle, it is highly unlikely that a perforated patch state had formed. This indicated that most likely a partial rupture of the patch with relatively high series resistance could simulate a perforated patch configuration. In the Aβ-intrapipette exposed patch, a GABA rundown current was observed after 50 minutes of recording, which could be explained by a total rupture of the patch regardless of pore formation, or due to an inadequate response of the neuron which had been in the recording chamber more than 40 minutes. The main conclusions that I drew from these experiments are that Aβ did not induce a perforated patch-like configuration during the first 20 minutes, and that cell attached recordings longer than 20 minutes have to be analyzed carefully, using proper negative controls.

Since I had observed that 10 μM Aβ altered synaptic transmission when applied for 72 hours to autaptic neurons, I next investigated whether these effects could relate to changes in membrane properties. I hypothesized that membrane alterations had to be present if aberrant pores would perforate the cell surface to an extent that triggered synaptic dysfunction. As in previous experiments, I exposed autaptic hippocampal neurons for 72 hours to 10 μM Aβ and performed electrophysiological recordings but in current clamp mode. To have a positive control for Aβ toxicity, I started the experiments by evoking an EPSC, which showed a reduced amplitude in Aβ-treated neurons, as reported before in this study. Importantly, the resting membrane potential and input resistance were not changed in Aβ-treated neurons, indicating that at rest the population of open channels was similar in both groups, and against the possibility that open amyloid pores are present and would induce toxicity. However, the Aβ-treated neurons displayed mild but statistically significant alterations in the shape of the action potential including a reduction in the amplitude and overshoot, and an increase in the half-width. These changes could be explained by an increase in the conductance to potassium. However, it is unlikely that altered conductance to potassium would not alter the resting membrane potential. In addition, this kind of ion specificity has not been observed in amyloid pores, which on the contrary

would be either cation selective or non-selective, and their effects on the plasma membrane would tend to be depolarizing. (Kawahara *et al.*, 1997; Bode, Baker and Viles, 2017). Alternatively, APP has been shown to modulate a potassium / chloride cotransporter in GABAergic neurons (Chen *et al.*, 2017). A potential explanation of the data presented here could be that Aβ retains the ability of APP of limiting potassium channel phosphorylation, thus increasing its membrane abundance. However, with no alteration in the resting membrane potential, these data have to be interpreted carefully.

Pore formation is believed to depend on the secondary structure of the amyloid aggregates, and it has been reported that many peptides with different primary structure can induce a similar pore-like behavior when applied to artificial bilayers (Quist *et al.*, 2005). In addition, the work by Cribbs *et al.* showed that the AllD stereoisomer of Aβ, which retained its aggregation properties, could also induce pore formation and cause neurotoxicity (Cribbs *et al.*, 1997). Moreover, Lal and collaborators used the AllD Aβ enantiomer to distinguish between a mechanism of toxicity dependent on intermolecular interactions, which would be stereospecific, and a conformation-dependent and unspecific mechanism, like membrane binding and amyloid pore formation (Capone *et al.*, 2012; Connelly *et al.*, 2012). In this context, in the last set of experiments I used the AllD Aβ enantiomer to investigate whether it retained the aggregation properties, and if its oligomers would induce similar electrophysiological deficits on autaptic neurons as its L- counterpart. In collaboration with colleagues from the Max Planck Institute for Biophysical Chemistry, we performed a mass spectrometric analysis and compared the NMR fingerprint regions of the TOCSY spectra of samples from both enantiomers. Both methods confirmed the identical primary structure of the enantiomers. Furthermore, I compared the aggregation kinetics of the peptides by analyzing samples taken at increasing incubation times using silver staining, which indicated a similar distribution of species for both stereoisomers. In addition, Western blot with the 6E10 antibody, which is specific for the L-Aβ showed no signal in the lane containing AllD Aβ. Finally, I exposed autaptic hippocampal neurons for 72 hours to Aβ or AllD Aβ and compared their morphology and electrophysiological properties. In agreement with the data presented in other sections, the morphology of the autaptic neurons was not changed. Surprisingly, although the L- isomer showed a marked reduction in EPSC amplitude and RRP size as seen previously, no changes were observed

in AllD-treated neurons, which displayed responses similar to the controls, indicating a requirement for stereospecific interactions in Aβ toxicity.

In sum, although pore formation could be reproduced in cholesterol bilayers and other membrane models at low frequency (see Supplementary Material, Figure 30 and Figure 31), I could not find evidence to support the hypothesis of amyloid pore toxicity in neuronal membranes.

5. Summary

AD is the most prevalent neurodegenerative disorder, characterized clinically by cognitive decline with amnestic presentation, and histopathologically by deposition of Aβ and hyperphosphorylated tau. Although a great number of studies in postmortem human tissue and in murine models have been performed, the cellular and molecular events leading to cognitive decline remain obscure. Moreover, the disease has still no treatment that can modify its natural history.

Here I aimed to study the mechanisms by which Aβ peptide induces deleterious effects on glutamatergic synapses. In a first part of my work, I successfully established a protocol to dissolve synthetic Aβ42 and to generate oligomer-enriched solutions in a reproducible manner. Later, I made use of the autaptic culture system and showed that Aβ42 impairs basal synaptic transmission and depletes the RRP, exerting synaptotoxic effects mainly by altering presynaptic function. Additionally, I observed moderate morphological changes in Aβ-treated neurons. I also studied a shorter exposure to Aβ aggregates, which resulted in a paradoxical increase in synaptic transmission.

In addition, Aβ-exposed neurons were used to explore putative protective effects of the small molecule anle138b, a novel therapeutic agent successfully utilized in multiple mouse models of neurodegenerative diseases. I unexpectedly found that anle138b can be toxic *per se* in a concentration dependent manner. Moreover, when applied in combination with Aβ, anle138b failed in protecting glutamatergic autaptic neurons from synaptotoxicity.

Finally, I took advantage of the oligomeric Aβ preparation to study whether synaptotoxic aggregates could also assemble as amyloid pores. No evidence of pore formation was found neuronal membranes, among other membrane types. Furthermore, by means of using the AllD Aβ, the D-Aβ42 enantiomer, I could show that Aβ deleterious effects on synapses require stereospecific interactions.

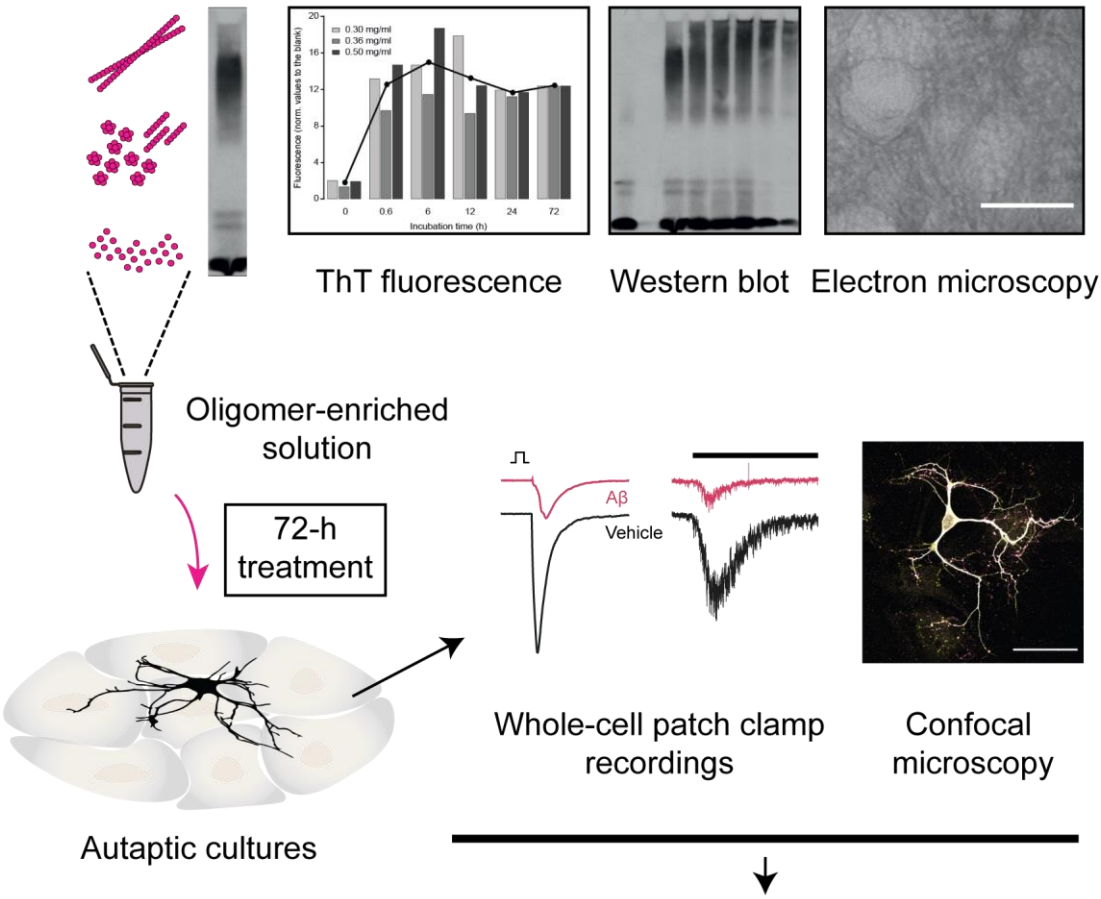

Reduced EPSC amplitude and RRP size → altered priming function
No changes in neuronal morphology → purely functional defect
No effects upon all-D Aβ treatment → chirality dependence
Normal resting membrane potential → unchanged population of membrane channels

- Pradoxical increase in EPSC amplitude with 24-h treatment
- No rescue with anle138b treatment

Figure 28. Graphical summary.

6. Supplementary Material

The data included in the present section was obtained after the submission and defense of the present work. Since it might be helpful to clarify some of the points discussed in the main body of the thesis I decided to attach them as a supplement.

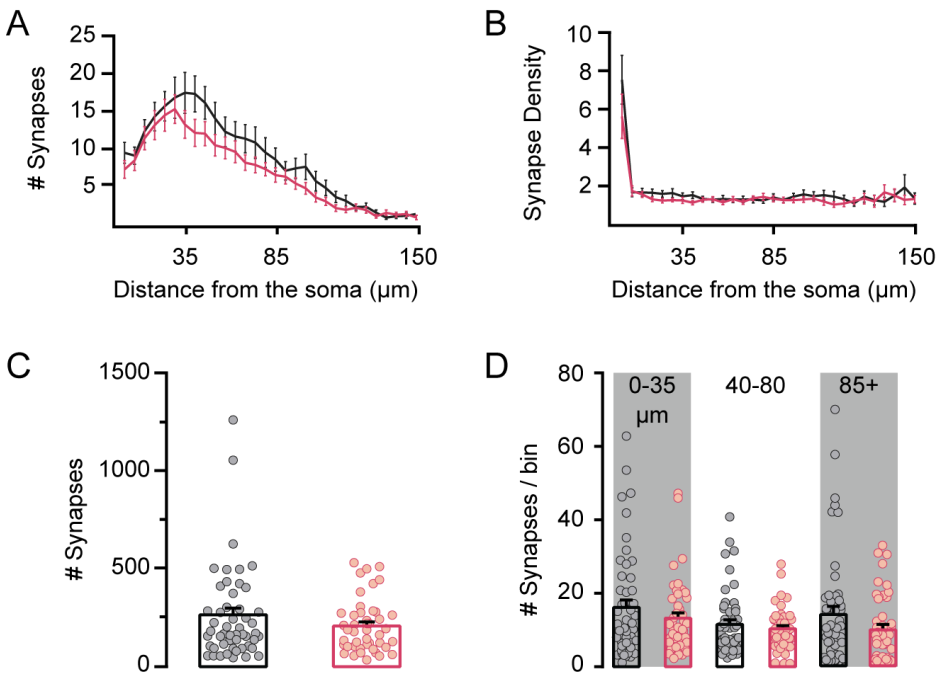

Figure 29. Synapse density is not altered in 72-hour Aβ-treated neurons. (A) Distribution of puncta with juxtaposed VGluT1 and Shank2 signal with respect to the center of the cell soma. **(B)** Distribution of synapse density calculated as the quotient between the number of synapses in a Sholl segment and divided by the number of dendritic crossings for that segment. **(C)** Number of synapses calculated from the maximum intensity projection images used for the calculation of synapse density. These results are in agreement with the data shown in Figure 11, where puncta positive for both VGluT1 and Shank2 were quantified in a z-stack using a 3D-particle counter. **(D)** The number of synapses analyzed in discrete bins of distance from the center of the cell soma shows no difference between the vehicle- and the 72-hour Aβ-treated neurons. In A and B the lines connect the means for given points of distance from the center of the cell soma and the error bars represent the SEM. In C and D, bars represent the mean and error bars represent SEM. Vehicle, black lines and bars; Aβ, pink lines and bars.

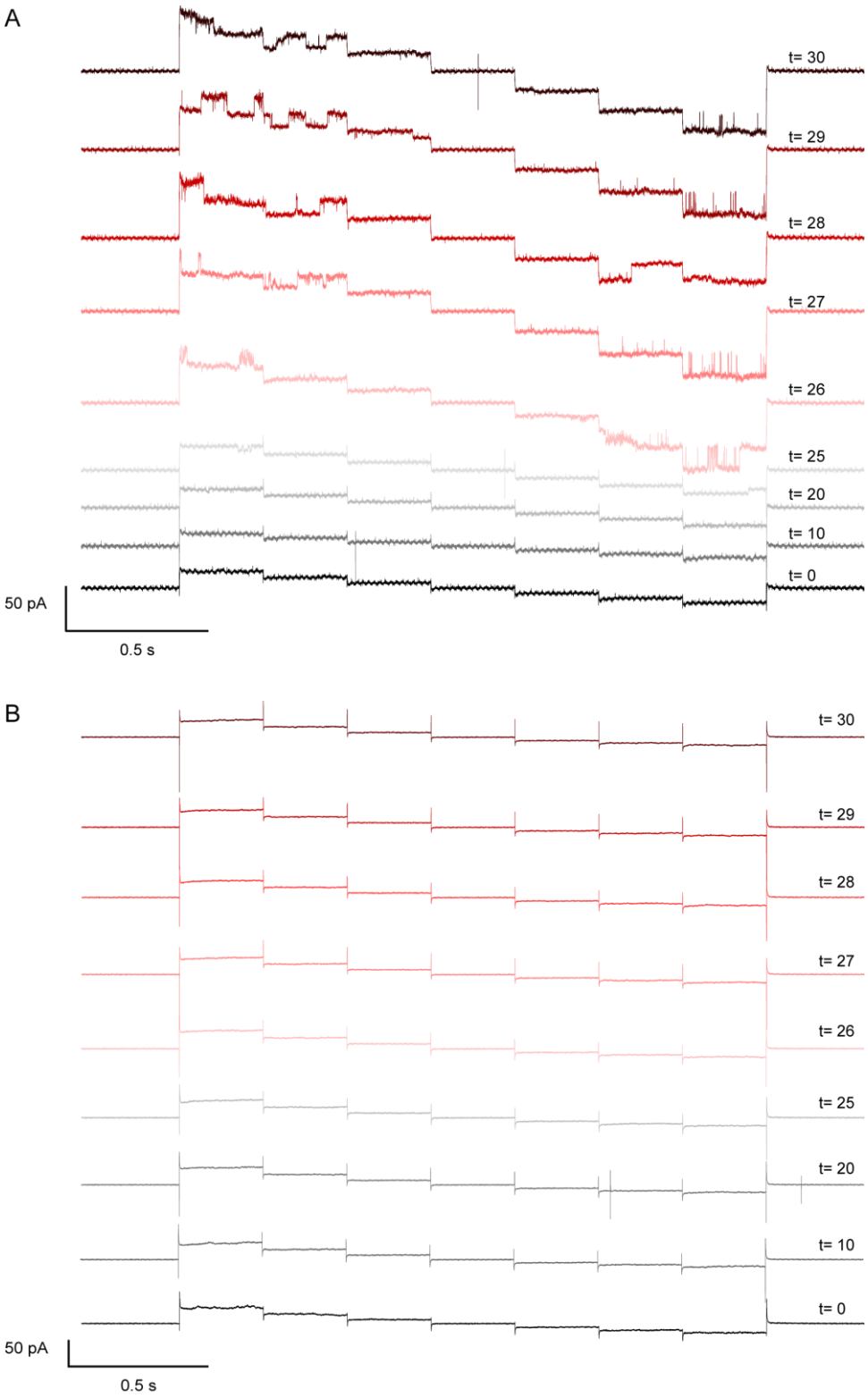

Figure 30. Pore formation could be observed in one out of 40 inside-out patches exposed to 5 µM Aβ. 80 inside-out patches were obtained from HEK cells in collaboration with Prof. JeongSeop Rhee and Prof. Luis Pardo under the same experimental conditions as in Bode, Baker and Viles 2017, with the exception of the use of a different method for the preparation of the oligomer-enriched Aβ solution. From these 80, 40 patches were exposed to 5 µM Aβ from within the patch pipette (data not shown). The remaining 40 patches were exposed to the vehicle solution and used as control. In the group of Aβ-exposed patches, only one showed pore-like activity. **(A)** Representative traces of the patch which showed electrophysiological activity resembling single-channel currents. Note that the pore-like activity started after 25 minutes after patch excision. **(B)** Representative traces of the remaining 39 Aβ-treated patches where no activity was observed. t= time of recording after patch excision.

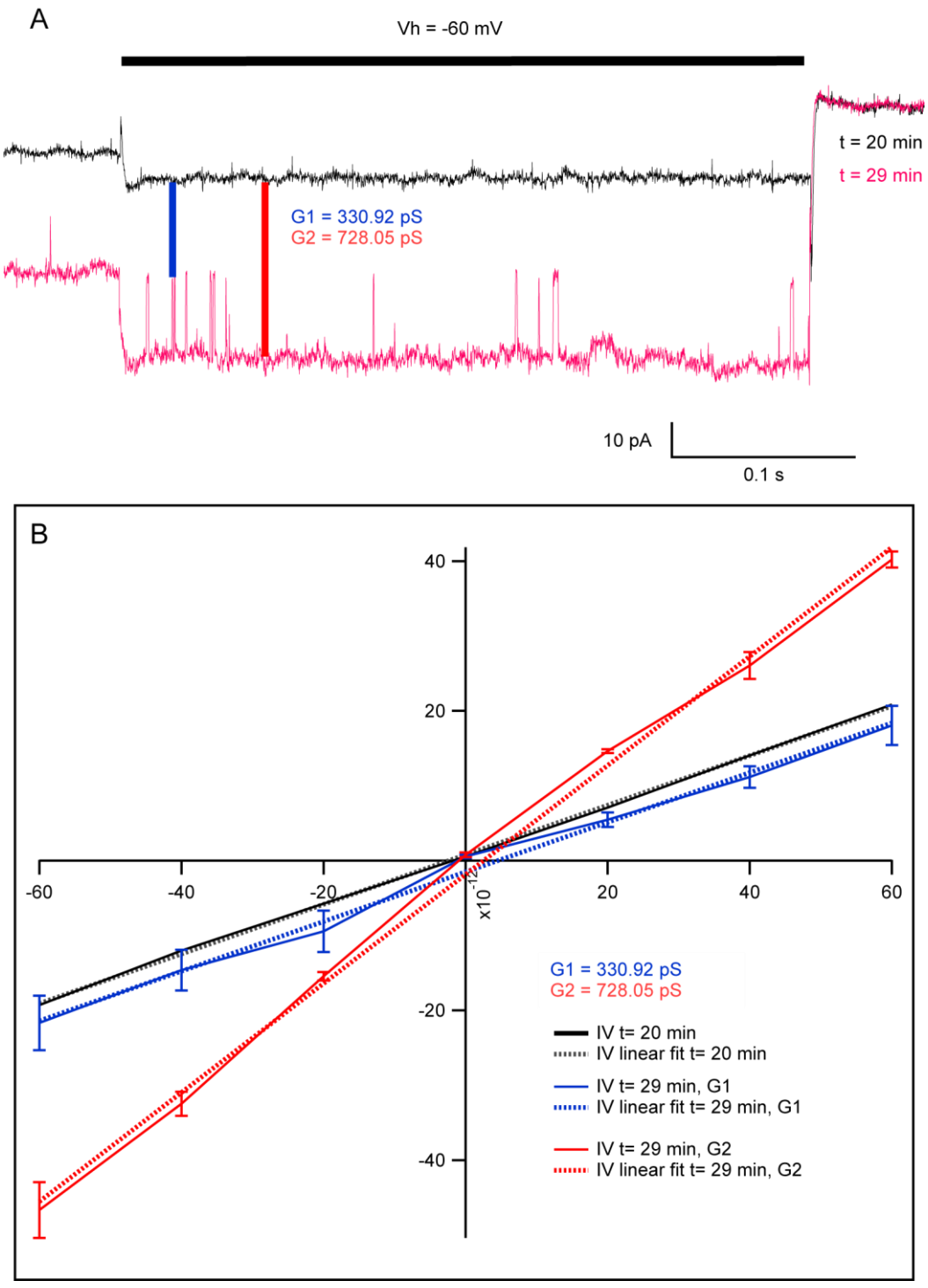

Figure 31. The Aβ-treated patch with pore-like activity displayed two levels of membrane permeability. (A) Comparison of juxtaposed traces of the patch with pore-like currents at 25 and 29 minutes after patch excision at -60 mV of holding potential. G1 is the calculated permeability for the first current step upon putative pore formation. G2 is the calculated permeability for the second current step. It is possible that the insertion of a second pore occurs, or that new molecules of Aβ are added to the existing pore. **(B)** Current/Voltage (IV) curves from the patch with pore-like activity at 20 and 29 minutes (solid lines) and linear-fitted curves (dashed lines) to calculate the membrane permeability. Black lines: 20 minutes after patch excision; blue lines: 29 minutes after patch excision, first current step; red lines: 29 minutes after patch excision, second current step. t= time after patch excision.

7. Bibliography

Abramov, E. *et al.* (2009) 'Amyloid-β as a positive endogenous regulator of release probability at hippocampal synapses.', *Nature Neuroscience*. Nature Publishing Group, 12(12), pp. 1567–1576. doi: 10.1038/nn.2433.

Aisen, P. S., Cummings, J. and Schneider, L. S. (2012) 'Symptomatic and nonamyloid/tau based pharmacologic treatment for Alzheimer disease.', *Cold Spring Harbor perspectives in medicine*. Cold Spring Harbor Laboratory Press, 2(3), p. a006395. doi: 10.1101/cshperspect.a006395.

Amar, F. *et al.* (2017) 'The amyloid-β oligomer Aβ*56 induces specific alterations in neuronal signaling that lead to tau phosphorylation and aggregation.', *Science signaling*. American Association for the Advancement of Science, 10(478), p. eaal2021. doi: 10.1126/scisignal.aal2021.

Amatniek, J. C. *et al.* (2006) 'Incidence and predictors of seizures in patients with Alzheimer's disease.', *Epilepsia*. John Wiley & Sons, Ltd (10.1111), 47(5), pp. 867–872. doi: 10.1111/j.1528-1167.2006.00554.x.

Anderton, B. H. *et al.* (1998) 'Dendritic changes in Alzheimer's disease and factors that may underlie these changes', *Progress in Neurobiology*. Elsevier Ltd, 55(6), pp. 595–609. doi: 10.1016/S0301-0082(98)00022-7.

Andrew, R. J. *et al.* (2016) 'A Greek tragedy: the growing complexity of Alzheimer amyloid precursor protein proteolysis.', *The Journal of Biological Chemistry*. American Society for Biochemistry and Molecular Biology, 291(37), pp. 19235–44. doi: 10.1074/jbc.R116.746032.

Arganda-Carreras, I. *et al.* (2017) 'Trainable Weka Segmentation: a machine learning tool for microscopy pixel classification', *Bioinformatics*. Edited by R. Murphy. Narnia, 33(15), pp. 2424–2426. doi: 10.1093/bioinformatics/btx180.

Ariga, T. *et al.* (2001) 'Characterization of high-affinity binding between gangliosides and amyloid β-protein.', *Archives of Biochemistry and Biophysics*. Academic Press, 388(2), pp. 225–230. doi: 10.1006/ABBI.2001.2304.

Arispe, N. and Doh, M. (2002) 'Plasma membrane cholesterol controls the cytotoxicity of Alzheimer's disease AβP (1–40) and (1–42) peptides.', *The FASEB Journal*. Federation of American Societies for Experimental Biology, 16(12), pp. 1526–1536. doi: 10.1096/fj.02-0829com.

Arispe, N., Pollard, H. B. and Rojas, E. (1993) 'Giant multilevel cation channels formed by Alzheimer disease amyloid beta-protein [AβP-(1-40)] in bilayer membranes.', *Proceedings of the National Academy of Sciences of the United States of America*, 90(22), pp. 10573–7. doi: 10.1073/pnas.90.22.10573.

Arispe, N., Pollard, H. B. and Rojas, E. (1996) 'Zn2+ interaction with Alzheimer amyloid beta protein calcium channels.', *Proceedings of the National Academy of Sciences of the United States of America*. National Academy of Sciences, 93(4), pp. 1710–5. doi: 10.1073/pnas.93.4.1710.

Arispe, N., Rojas, E. and Pollard, H. B. (1993) 'Alzheimer disease amyloid β protein forms calcium channels in bilayer membranes: blockade by tromethamine and aluminum.', *Proceedings of the National Academy of Sciences of the United States of America*. National Academy of Sciences, 90(2), pp. 567–571. doi: 10.1073/pnas.90.2.567.

Arriagada, P. V. *et al.* (1992) 'Neurofibrillary tangles but not senile plaques parallel duration and severity of Alzheimer's disease.', *Neurology*. Wolters Kluwer Health, Inc. on behalf of the American Academy of Neurology, 42(3 Pt 1), pp. 631–9. doi: 10.1212/WNL.42.3.631.

Asuni, A. A. *et al.* (2007) 'Immunotherapy targeting pathological tau conformers in a tangle mouse model reduces brain pathology with associated functional improvements.', *The Journal of neuroscience : the official journal of the Society for Neuroscience*. Society for Neuroscience, 27(34), pp. 9115–29. doi: 10.1523/JNEUROSCI.2361-07.2007.

Australian New Zealand Clinical Trials Registry (2019) *A phase IIa clinical trial of VEL015 (sodium selenate) in mild to moderate Alzheimer's Disease*. Available at: https://www.anzctr.org.au/Trial/Registration/TrialReview.aspx?id=83952&isReview=true

(Accessed: 3 July 2019).

Bakker, A. *et al.* (2012) 'Reduction of hippocampal hyperactivity improves cognition in amnestic mild cognitive impairment.', *Neuron*. Cell Press, 74(3), pp. 467–474. doi: 10.1016/J.NEURON.2012.03.023.

Barnham, K. J. *et al.* (2003) 'Structure of the Alzheimer's disease amyloid precursor protein copper binding domain. A regulator of neuronal copper homeostasis.', *The Journal of Biological Chemistry*. American Society for Biochemistry and Molecular Biology, 278(19), pp. 17401–7. doi: 10.1074/jbc.M300629200.

Barthet, G. *et al.* (2018) 'Presenilin-mediated cleavage of APP regulates synaptotagmin-7 and presynaptic plasticity.', *Nature Communications*. Nature Publishing Group, 9(1), p. 4780. doi: 10.1038/s41467-018-06813-x.

Basu, J. and Siegelbaum, S. A. (2015) 'The corticohippocampal circuit, synaptic plasticity, and memory.', *Cold Spring Harbor Perspectives in Biology*. Cold Spring Harbor Laboratory Press, 7(11), p. a021733. doi: 10.1101/CSHPERSPECT.A021733.

Benilova, I., Karran, E. and De Strooper, B. (2012) 'The toxic Aβ oligomer and Alzheimer's disease: An emperor in need of clothes.', *Nature Neuroscience*. Nature Publishing Group, pp. 349–357. doi: 10.1038/nn.3028.

Benz, R. *et al.* (1978) 'Formation of large, ion-permeable membrane channels by the matrix protein (porin) of Escherichia coli.', *Biochimica et Biophysica Acta (BBA) - Biomembranes*. Elsevier, 511(3), pp. 305–319. doi: 10.1016/0005-2736(78)90269-9.

Bezprozvanny, I. (2009) 'Calcium signaling and neurodegenerative diseases.', *Trends in Molecular Medicine*. Elsevier Current Trends, 15(3), pp. 89–100. doi: 10.1016/J.MOLMED.2009.01.001.

Bezzina, C. *et al.* (2015) 'Early onset of hypersynchronous network activity and expression of a marker of chronic seizures in the TG2576 mouse model of Alzheimer's disease.', *PLOS ONE*. Edited by Y. Herault. Public Library of Science, 10(3), p. e0119910. doi: 10.1371/journal.pone.0119910.

Birks, J. S. (2006) 'Cholinesterase inhibitors for Alzheimer's disease', *Cochrane Database of Systematic Reviews*. Edited by J. S. Birks. Chichester, UK: John Wiley & Sons, Ltd, (1). doi: 10.1002/14651858.CD005593.

Bitan, G. *et al.* (2003) 'Amyloid β-protein (Aβ) assembly: Aβ 40 and Aβ 42 oligomerize through distinct pathways.', *Proceedings of the National Academy of Sciences of the United States of America*. National Academy of Sciences, 100(1), pp. 330–335. doi: 10.1073/pnas.222681699.

Bittner, T. *et al.* (2009) 'γ-secretase inhibition reduces spine density in vivo via an amyloid precursor protein-dependent pathway.', *The Journal of Neuroscience : the official journal of the Society for Neuroscience*. Society for Neuroscience, 29(33), pp. 10405–9. doi: 10.1523/JNEUROSCI.2288-09.2009.

Blum, H., Beier, H. and Gross, H. J. (1987) 'Improved silver staining of plant proteins, RNA and DNA in polyacrylamide gels.', *Electrophoresis*. John Wiley & Sons, Ltd, 8(2), pp. 93–99. doi: 10.1002/elps.1150080203.

Bode, D. C. *et al.* (2019) 'Amyloid-β oligomers have a profound detergent-like effect on lipid membrane bilayers, imaged by atomic force and electron microscopy.', *The Journal of Biological Chemistry*. American Society for Biochemistry and Molecular Biology, 294(19), pp. 7566–7572. doi: 10.1074/jbc.AC118.007195.

Bode, D. C., Baker, M. D. and Viles, J. H. (2017) 'Ion channel formation by amyloid-β 42 oligomers but not amyloid-β 40 in cellular membranes.', *The Journal of Biological Chemistry*. American Society for Biochemistry and Molecular Biology, 292(4), pp. 1404–1413. doi: 10.1074/jbc.M116.762526.

Bolte, S. and Cordelieres, F. P. (2006) 'A guided tour into subcellular colocalization analysis in light microscopy.', *Journal of Microscopy*. John Wiley & Sons, Ltd (10.1111), 224(3), pp. 213–232. doi: 10.1111/j.1365-2818.2006.01706.x.

Bookheimer, S. Y. *et al.* (2000) 'Patterns of brain activation in people at risk for Alzheimer's

disease.', *New England Journal of Medicine*. Massachusetts Medical Society, 343(7), pp. 450–456. doi: 10.1056/NEJM200008173430701.

Borg, J.-P. *et al.* (1996) 'The phosphotyrosine interaction domains of X11 and FE65 bind to distinct sites on the YENPTY motif of amyloid precursor protein.', *Molecular and Cellular Biology*. American Society for Microbiology Journals, 16(11), pp. 6229–41. doi: 10.1128/MCB.16.11.6229.

Braak, H. and Braak, E. (1991) 'Neuropathological stageing of Alzheimer-related changes.', *Acta Neuropathologica*. Springer-Verlag, pp. 239–259. doi: 10.1007/BF00308809.

Brini, M. *et al.* (2014) 'Neuronal calcium signaling: function and dysfunction.', *Cellular and Molecular Life Sciences*. Springer Basel, 71(15), pp. 2787–2814. doi: 10.1007/s00018-013-1550-7.

Burgalossi, A. *et al.* (2012) 'Analysis of neurotransmitter release mechanisms by photolysis of caged Ca2+ in an autaptic neuron culture system.', *Nature Protocols*. Nature Publishing Group, 7(7), pp. 1351–1365. doi: 10.1038/nprot.2012.074.

Capone, R. *et al.* (2012) 'All-D-enantiomer of β-amyloid peptide forms ion channels in lipid bilayers.', *Journal of Chemical Theory and Computation*. American Chemical Society, 8(3), pp. 1143–1152. doi: 10.1021/ct200885r.

Castellano, J. M. *et al.* (2011) 'Human apoE isoforms differentially regulate brain amyloid-β peptide clearance.', *Science Translational Medicine*. American Association for the Advancement of Science, 3(89), p. 89ra57. doi: 10.1126/scitranslmed.3002156.

Celone, K. A. *et al.* (2006) 'Alterations in memory networks in mild cognitive impairment and Alzheimer's disease: an independent component analysis.', *The Journal of neuroscience : the official journal of the Society for Neuroscience*. Society for Neuroscience, 26(40), pp. 10222–31. doi: 10.1523/JNEUROSCI.2250-06.2006.

Chapman, P. F. *et al.* (1999) 'Impaired synaptic plasticity and learning in aged amyloid precursor protein transgenic mice.', *Nature Neuroscience*. Nature Publishing Group, 2(3), pp. 271–276. doi: 10.1038/6374.

Chen, H.-S. V. and Lipton, S. A. (2006) 'The chemical biology of clinically tolerated NMDA receptor antagonists.', *Journal of Neurochemistry*. John Wiley & Sons, Ltd (10.1111), 97(6), pp. 1611–1626. doi: 10.1111/j.1471-4159.2006.03991.x.

Chen, M. *et al.* (2017) 'APP modulates KCC2 expression and function in hippocampal GABAergic inhibition.', *eLife*, 6. doi: 10.7554/eLife.20142.

Christensen, D. Z. *et al.* (2008) 'Transient intraneuronal Aβ rather than extracellular plaque pathology correlates with neuron loss in the frontal cortex of APP/PS1KI mice.', *Acta Neuropathologica*. Springer-Verlag, 116(6), pp. 647–655. doi: 10.1007/s00401-008-0451-6.

Cirrito, J. R. *et al.* (2005) 'Synaptic activity regulates interstitial fluid amyloid-β levels in vivo.', *Neuron*. Cell Press, 48(6), pp. 913–922. doi: 10.1016/j.neuron.2005.10.028.

Coburger, I. *et al.* (2013) 'Analysis of the overall structure of the multi-domain amyloid precursor protein (APP).', *PLoS ONE*. Edited by R. Yan. Public Library of Science, 8(12), p. e81926. doi: 10.1371/journal.pone.0081926.

Cochran, J. N., Hall, A. M. and Roberson, E. D. (2014) 'The dendritic hypothesis for Alzheimer's disease pathophysiology', *Brain Research Bulletin*. Elsevier Inc., 103, pp. 18–28. doi: 10.1016/j.brainresbull.2013.12.004.

Congdon, E. E. and Sigurdsson, E. M. (2018) 'Tau-targeting therapies for Alzheimer disease.', *Nature Reviews Neurology*. Nature Publishing Group, 14(7), pp. 399–415. doi: 10.1038/s41582-018-0013-z.

Connelly, L. *et al.* (2012) 'Atomic force microscopy and MD simulations reveal pore-like structures of all-D-enantiomer of Alzheimer's β-amyloid peptide: relevance to the ion channel mechanism of AD pathology.', *The Journal of Physical Chemistry*. American Chemical Society, 116(5), pp. 1728–1735. doi: 10.1021/jp2108126.

Corcoran, N. M. *et al.* (2010) 'Sodium selenate specifically activates PP2A phosphatase, dephosphorylates tau and reverses memory deficits in an Alzheimer's disease model.', *Journal*

of Clinical Neuroscience. Churchill Livingstone, 17(8), pp. 1025–1033. doi: 10.1016/J.JOCN.2010.04.020.

Coric, V. *et al.* (2015) 'Targeting prodromal Alzheimer disease with avagacestat: a randomized clinical trial.', *JAMA Neurology*. American Medical Association, 72(11), pp. 1324–1333. doi: 10.1001/JAMANEUROL.2015.0607.

Cribbs, D. H. *et al.* (1997) 'All-D-enantiomers of β-amyloid exhibit similar biological properties to all-L-β-amyloids.', *The Journal of Biological Chemistry*. doi: 10.1074/jbc.272.11.7431.

Dahlgren, K. N. *et al.* (2002) 'Oligomeric and fibrillar species of amyloid-β peptides differentially affect neuronal viability.', *The Journal of Biological Chemistry*. American Society for Biochemistry and Molecular Biology, 277(35), pp. 32046–32053. doi: 10.1074/jbc.M201750200.

Dahms, S. O. *et al.* (2010) 'Structure and biochemical analysis of the heparin-induced E1 dimer of the amyloid precursor protein.', *Proceedings of the National Academy of Sciences of the United States of America*. National Academy of Sciences, 107(12), pp. 5381–6. doi: 10.1073/pnas.0911326107.

Das, U. *et al.* (2013) 'Activity-induced convergence of APP and BACE-1 in acidic microdomains via an endocytosis-dependent pathway.', *Neuron*. Cell Press, 79(3), pp. 447–460. doi: 10.1016/J.NEURON.2013.05.035.

Das, U. *et al.* (2016) 'Visualizing APP and BACE-1 approximation in neurons yields insight into the amyloidogenic pathway.', *Nature Neuroscience*. Nature Publishing Group, 19(1), pp. 55–64. doi: 10.1038/nn.4188.

Davies, P. and Maloney, A. J. F. (1976) 'Selective loss of central cholinergic neurons in Alzheimer's disease.', *The Lancet*. Elsevier, 308(8000), p. 1403. doi: 10.1016/S0140-6736(76)91936-X.

Dawson, G. R. *et al.* (1999) 'Age-related cognitive deficits, impaired long-term potentiation and reduction in synaptic marker density in mice lacking the β-amyloid precursor protein.', *Neuroscience*. Pergamon, 90(1), pp. 1–13. doi: 10.1016/S0306-4522(98)00410-2.

Deane, R. *et al.* (2003) 'RAGE mediates amyloid-β peptide transport across the blood-brain barrier and accumulation in brain.', *Nature Medicine*. Nature Publishing Group, 9(7), pp. 907–913. doi: 10.1038/nm890.

Deczkowska, A. *et al.* (2018) 'Disease-associated microglia: a universal immune sensor of neurodegeneration.', *Cell*. Elsevier, pp. 1073–1081. doi: 10.1016/j.cell.2018.05.003.

Delaère, P. *et al.* (1990) 'Large amounts of neocortical βA4 deposits without neuritic plaques nor tangles in a psychometrically assessed, non-demented person.', *Neuroscience Letters*. Elsevier, 116(1–2), pp. 87–93. doi: 10.1016/0304-3940(90)90391-L.

Demuro, A., Smith, M. and Parker, I. (2011) 'Single-channel Ca2+ imaging implicates Aβ 1-42 amyloid pores in Alzheimer's disease pathology.', *Journal of Cell Biology*, 195(3), pp. 515–524. doi: 10.1083/jcb.201104133.

Deng, J. *et al.* (2015) 'Soluble amyloid precursor protein alpha inhibits tau phosphorylation through modulation of GSK3β signaling pathway.', *Journal of Neurochemistry*. John Wiley & Sons, Ltd (10.1111), 135(3), pp. 630–637. doi: 10.1111/jnc.13351.

Deshpande, A. (2006) 'Different conformations of amyloid β induce neurotoxicity by distinct mechanisms in human cortical neurons.', *The Journal of Neuroscience : the official journal of the Society for Neuroscience*, 26(22), pp. 6011–6018. doi: 10.1523/JNEUROSCI.1189-06.2006.

DeVos, S. L. *et al.* (2017) 'Tau reduction prevents neuronal loss and reverses pathological tau deposition and seeding in mice with tauopathy.', *Science translational medicine*. American Association for the Advancement of Science, 9(374), p. eaag0481. doi: 10.1126/scitranslmed.aag0481.

Diaz, J. C. *et al.* (2009) 'Small molecule blockers of the Alzheimer Aβ calcium channel potently protect neurons from Aβ cytotoxicity.', *Proceedings of the National Academy of Sciences of the United States of America*, 106(9), pp. 3348–3353. doi: 0813355106 [pii]\r10.1073/pnas.0813355106.

Dickson, D. W. *et al.* (1992) 'Identification of normal and pathological aging in prospectively studied nondemented elderly humans.', *Neurobiology of Aging*. Elsevier, 13(1), pp. 179–189. doi: 10.1016/0197-4580(92)90027-U.

Doody, R. S. *et al.* (2013) 'A phase 3 trial of semagacestat for treatment of Alzheimer's disease.', *New England Journal of Medicine*, 369(4), pp. 341–350. doi: 10.1056/NEJMoa1210951.

Drews, A. *et al.* (2016) 'Individual aggregates of amyloid beta induce temporary calcium influx through the cell membrane of neuronal cells.', *Scientific Reports*. Nature Publishing Group, 6(1), p. 31910. doi: 10.1038/srep31910.

Duyckaerts, C., Delatour, B. and Potier, M.-C. (2009) 'Classification and basic pathology of Alzheimer disease.', *Acta Neuropathologica*. Springer-Verlag, 118(1), pp. 5–36. doi: 10.1007/s00401-009-0532-1.

Esquerda-Canals, G. *et al.* (2017) 'Mouse models of Alzheimer's disease.', *Journal of Alzheimer's Disease*. IOS Press, 57(4), pp. 1171–1183. doi: 10.3233/JAD-170045.

Evangelisti, E. *et al.* (2016) 'Binding affinity of amyloid oligomers to cellular membranes is a generic indicator of cellular dysfunction in protein misfolding diseases.', *Scientific Reports*. Nature Publishing Group, 6(1), p. 32721. doi: 10.1038/srep32721.

Fanutza, T. *et al.* (2015) 'APP and APLP2 interact with the synaptic release machinery and facilitate transmitter release at hippocampal synapses.', *eLife*, 4. doi: 10.7554/eLife.09743.

De Felice, F. G. *et al.* (2009) 'Protection of synapses against Alzheimer's-linked toxins: insulin signaling prevents the pathogenic binding of Aβ oligomers.', *Proceedings of the National Academy of Sciences of the United States of America*. National Academy of Sciences, 106(6), pp. 1971–6. doi: 10.1073/pnas.0809158106.

Fellner, L. *et al.* (2016) 'Anle138b partly ameliorates motor deficits despite failure of neuroprotection in a model of advanced multiple system atrophy.', *Frontiers in Neuroscience*. Frontiers, 10(MAR), pp. 1–9. doi: 10.3389/fnins.2016.00099.

Ferguson, S. M. *et al.* (2007) 'Vesicle endocytosis requires dynamin-dependent GTP hydrolysis at a fast CNS synapse.', *Science*. American Association for the Advancement of Science, 307(5706), pp. 124–127. doi: 10.1126/science.1103631.

Ferreiro, E., Oliveira, C. R. and Pereira, C. (2004) 'Involvement of endoplasmic reticulum Ca2+ release through ryanodine and inositol 1,4,5-triphosphate receptors in the neurotoxic effects induced by the amyloid-β peptide', *Journal of Neuroscience Research*. John Wiley & Sons, Ltd, 76(6), pp. 872–880. doi: 10.1002/jnr.20135.

Fezoui, Y. *et al.* (2000) 'An improved method of preparing the amyloid β-protein for fibrillogenesis and neurotoxicity experiments.', *Amyloid*, 7(3), pp. 744–763. doi: 10.3109/13506120009146831.

Finder, V. H. *et al.* (2010) 'The recombinant amyloid-β peptide Aβ 1-42 aggregates faster and is more neurotoxic than synthetic Aβ 1-42.', *Journal of Molecular Biology*. Elsevier Ltd, 396(1), pp. 9–18. doi: 10.1016/j.jmb.2009.12.016.

Fitzjohn, S. M. *et al.* (2001) 'Age-related impairment of synaptic transmission but normal long-term potentiation in transgenic mice that overexpress the human APP695SWE mutant form of amyloid precursor protein.', *The Journal of neuroscience : the official journal of the Society for Neuroscience*. Society for Neuroscience, 21(13), pp. 4691–8. doi: 10.1523/JNEUROSCI.21-13-04691.2001.

Fogel, H. *et al.* (2014) 'APP homodimers transduce an amyloid-β-mediated increase in release probability at excitatory synapses.', *Cell Reports*. Cell Press, 7(5), pp. 1560–1576. doi: 10.1016/J.CELREP.2014.04.024.

Fol, R. *et al.* (2016) 'Viral gene transfer of APPsα rescues synaptic failure in an Alzheimer's disease mouse model.', *Acta Neuropathologica*. Springer Berlin Heidelberg, 131(2), pp. 247–266. doi: 10.1007/s00401-015-1498-9.

Fu, A. K. Y. *et al.* (2014) 'Blockade of EphA4 signaling ameliorates hippocampal synaptic dysfunctions in mouse models of Alzheimer's disease.', *Proceedings of the National Academy of Sciences of the United States of America*. National Academy of Sciences, 111(27), pp. 9959–64. doi: 10.1073/pnas.1405803111.

Galasko, D. R. *et al.* (2007) 'Safety, tolerability, pharmacokinetics, and Aβ levels after short-term administration of R-flurbiprofen in healthy elderly individuals.', *Alzheimer disease and associated disorders*, 21(4), pp. 292–9. doi: 10.1097/WAD.0b013e31815d1048.

Games, D. *et al.* (1995) 'Alzheimer-type neuropathology in transgenic mice overexpressing V717F β-amyloid precursor protein.', *Nature*. Nature Publishing Group, 373(6514), pp. 523–527. doi: 10.1038/373523a0.

Gauthier, S. *et al.* (2016) 'Efficacy and safety of tau-aggregation inhibitor therapy in patients with mild or moderate Alzheimer's disease: a randomised, controlled, double-blind, parallel-arm, phase 3 trial.', *Lancet (London, England)*. Elsevier, 388(10062), pp. 2873–2884. doi: 10.1016/S0140-6736(16)31275-2.

St. George-Hyslop, P. *et al.* (1987) 'The genetic defect causing familial Alzheimer's disease maps on chromosome 21.', *Science*. American Association for the Advancement of Science, 235(4791), pp. 885–890. doi: 10.1126/science.2880399.

Geppert, M. *et al.* (1994) 'Synaptotagmin I: A major Ca2+ sensor for transmitter release at a central synapse.', *Cell*. Cell Press, 79(4), pp. 717–727. doi: 10.1016/0092-8674(94)90556-8.

Gillman, K. W. *et al.* (2010) 'Discovery and evaluation of BMS-708163, a potent, selective and orally bioavailable γ-secretase inhibitor.', *ACS Medicinal Chemistry Letters*. American Chemical Society, 1(3), pp. 120–124. doi: 10.1021/ml1000239.

Gilman, S. *et al.* (2005) 'Clinical effects of Aβ immunization (AN1792) in patients with AD in an interrupted trial.', *Neurology*. Wolters Kluwer Health, Inc. on behalf of the American Academy of Neurology, 64(9), pp. 1553–62. doi: 10.1212/01.WNL.0000159740.16984.3C.

Gilson, V. *et al.* (2015) 'Effects of low amyloid-β (aβ) concentration on aβ 1–42 oligomers binding and GluN2b membrane expression.', *Journal of Alzheimer's Disease*. IOS Press, 47(2), pp. 453–466. doi: 10.3233/JAD-142529.

Gimbel, D. A. *et al.* (2010) 'Memory impairment in transgenic Alzheimer mice requires cellular prion protein.', *The Journal of neuroscience : the official journal of the Society for Neuroscience*. Society for Neuroscience, 30(18), pp. 6367–74. doi: 10.1523/JNEUROSCI.0395-10.2010.

Glenner, G. G. and Wong, C. W. (1984) 'Alzheimer's disease: Initial report of the purification and characterization of a novel cerebrovascular amyloid protein.', *Biochemical and Biophysical Research Communications*. Academic Press, 120(3), pp. 885–890. doi: 10.1016/S0006-291X(84)80190-4.

Goldgaber, D. *et al.* (1987) 'Characterization and chromosomal localization of a cDNA encoding brain amyloid of Alzheimer's disease.', *Science*. American Association for the Advancement of Science, 235(4791), pp. 877–80. doi: 10.1126/SCIENCE.3810169.

Gómez-Isla, T. *et al.* (1997) 'Neuronal loss correlates with but exceeds neurofibrillary tangles in Alzheimer's disease.', *Annals of Neurology*. John Wiley & Sons, Ltd, 41(1), pp. 17–24. doi: 10.1002/ana.410410106.

Gong, B. *et al.* (2004) 'Persistent improvement in synaptic and cognitive functions in an Alzheimer mouse model after rolipram treatment.', *The Journal of Clinical Investigation*. American Society for Clinical Investigation, 114(11), pp. 1624–1634. doi: 10.1172/JCI22831.

Götz, J., Bodea, L.-G. and Goedert, M. (2018) 'Rodent models for Alzheimer disease.', *Nature Reviews Neuroscience*. Nature Publishing Group, 19(10), pp. 583–598. doi: 10.1038/s41583-018-0054-8.

Goutagny, R. *et al.* (2013) 'Alterations in hippocampal network oscillations and theta-gamma coupling arise before Aβ overproduction in a mouse model of Alzheimer's disease.', *European Journal of Neuroscience*. John Wiley & Sons, Ltd (10.1111), 37(12), pp. 1896–1902. doi: 10.1111/ejn.12233.

Green, R. C. *et al.* (2009) 'Effect of tarenflurbil on cognitive decline and activities of daily living in patients with mild Alzheimer disease. A randomized controlled trial.', *JAMA*. American Medical Association, 302(23), p. 2557. doi: 10.1001/jama.2009.1866.

Grimm, M. O. W. *et al.* (2005) 'Regulation of cholesterol and sphingomyelin metabolism by amyloid-β and presenilin.', *Nature Cell Biology*. Nature Publishing Group, 7(11), pp. 1118–1123.

doi: 10.1038/ncb1313.

Guerrero-Muñoz, M. J., Castillo-Carranza, D. L. and Kayed, R. (2014) 'Therapeutic approaches against common structural features of toxic oligomers shared by multiple amyloidogenic proteins.', *Biochemical Pharmacology*. Elsevier, 88(4), pp. 468–478. doi: 10.1016/J.BCP.2013.12.023.

Guo, T., Noble, W. and Hanger, D. P. (2017) 'Roles of tau protein in health and disease.', *Acta Neuropathologica*. Springer Berlin Heidelberg, 133(5), pp. 665–704. doi: 10.1007/s00401-017-1707-9.

Gurevicius, K., Lipponen, A. and Tanila, H. (2013) 'Increased cortical and thalamic excitability in freely moving APPswe/PS1dE9 mice modeling epileptic activity associated with Alzheimer's disease.', *Cerebral Cortex*. Narnia, 23(5), pp. 1148–1158. doi: 10.1093/cercor/bhs105.

Haass, C. *et al.* (1992) 'Amyloid-β peptide is produced by cultured cells during normal metabolism.', *Nature*. Nature Publishing Group, 359(6393), pp. 322–325. doi: 10.1038/359322a0.

Haass, C. *et al.* (2012) 'Trafficking and proteolytic processing of APP.', *Cold Spring Harbor Perspectives in Medicine*, 2(5). doi: 10.1101/cshperspect.a006270.

Haass, C. and Selkoe, D. J. (1993) 'Cellular processing of β-amyloid precursor protein and the genesis of amyloid β-peptide.', *Cell*. Cell Press, 75(6), pp. 1039–1042. doi: 10.1016/0092-8674(93)90312-E.

Hardy, J. and Higgins, G. (1992) 'Alzheimer' s Disease: the amyloid cascade hypothesis.', *Science*, 256(5054), pp. 184–185. doi: 10.1126/science.1566067.

Hardy, J. and Selkoe, D. J. (2002) 'The amyloid hypothesis of Alzheimer's disease: progress and problems on the road to therapeutics.', *Science*. American Association for the Advancement of Science, 297(5580), pp. 353–6. doi: 10.1126/science.1072994.

He, W. and Barrow, C. J. (1999) 'The Aβ 3-pyroglutamyl and 11-pyroglutamyl peptides found in senile plaque have greater β-sheet forming and aggregation propensities in vitro than full-length Aβ.', *Biochemistry*. American Chemical Society, 38(33), pp. 10871–10877. doi: 10.1021/BI990563R.

He, Y. *et al.* (2019) 'Amyloid β oligomers suppress excitatory transmitter release via presynaptic depletion of phosphatidylinositol-4,5-bisphosphate.', *Nature Communications*. Nature Publishing Group, 10(1), p. 1193. doi: 10.1038/s41467-019-09114-z.

Heber, S. *et al.* (2000) 'Mice with combined gene knock-outs reveal essential and partially redundant functions of amyloid precursor protein family members.', *The Journal of Neuroscience : the official journal of the Society for Neuroscience*. Society for Neuroscience, 20(21), pp. 7951–7963. doi: 10.1523/JNEUROSCI.20-21-07951.2000.

Heras-Garvin, A. *et al.* (2018) 'Anle138b modulates α-synuclein oligomerization and prevents motor decline and neurodegeneration in a mouse model of multiple system atrophy.', *Movement Disorders*. John Wiley & Sons, Ltd. doi: 10.1002/mds.27562.

Herms, J. *et al.* (2004) 'Cortical dysplasia resembling human type 2 lissencephaly in mice lacking all three APP family members.', *The EMBO journal*. EMBO Press, 23(20), pp. 4106–15. doi: 10.1038/sj.emboj.7600390.

Herms, J. and Dorostkar, M. M. (2016) 'Dendritic spine pathology in neurodegenerative diseases.', *Annual Review of Pathology: Mechanisms of Disease*. Annual Reviews, 11(1), pp. 221–250. doi: 10.1146/annurev-pathol-012615-044216.

Herrup, K. (2015) 'The case for rejecting the amyloid cascade hypothesis.', *Nature Neuroscience*. Nature Publishing Group, 18(6), pp. 794–799. doi: 10.1038/nn.4017.

Hick, M. *et al.* (2015) 'Acute function of secreted amyloid precursor protein fragment APPsα in synaptic plasticity.', *Acta Neuropathologica*. Springer Berlin Heidelberg, 129(1), pp. 21–37. doi: 10.1007/s00401-014-1368-x.

Ho, A. and Südhof, T. C. (2004) 'Binding of F-spondin to amyloid-β precursor protein: a candidate amyloid-β precursor protein ligand that modulates amyloid-β precursor protein cleavage.', *Proceedings of the National Academy of Sciences of the United States of America*. National

Academy of Sciences, 101(8), pp. 2548–2553. doi: 10.1073/PNAS.0308655100.

Holmes, C. *et al.* (2008) 'Long-term effects of Aβ42 immunisation in Alzheimer's disease: follow-up of a randomised, placebo-controlled phase I trial.', *The Lancet*. Elsevier, 372(9634), pp. 216–223. doi: 10.1016/S0140-6736(08)61075-2.

Hong, S. *et al.* (2014) 'Soluble Aβ oligomers are rapidly sequestered from brain ISF in vivo and bind GM1 ganglioside on cellular membranes.', *Neuron*. Cell Press, 82(2), pp. 308–319. doi: 10.1016/J.NEURON.2014.02.027.

Hong, S. *et al.* (2016) 'Complement and microglia mediate early synapse loss in Alzheimer mouse models.', *Science*. American Association for the Advancement of Science, 352(6286), pp. 712–716. doi: 10.1126/science.aad8373.

Hoover, B. R. *et al.* (2010) 'Tau mislocalization to dendritic spines mediates synaptic dysfunction independently of neurodegeneration.', *Neuron*. Cell Press, 68(6), pp. 1067–1081. doi: 10.1016/J.NEURON.2010.11.030.

Hou, L. *et al.* (2004) 'Solution NMR studies of the Aβ(1−40) and Aβ(1−42) peptides establish that the Met35 oxidation state affects the mechanism of amyloid formation.', *Journal of the American Chemical Society*. American Chemical Society, 126(7), pp. 1992–2005. doi: 10.1021/JA036813F.

Hsiao, K. *et al.* (1996) 'Correlative memory deficits, Abeta elevation, and amyloid plaques in transgenic mice.', *Science (New York, N.Y.)*. American Association for the Advancement of Science, 274(5284), pp. 99–102. doi: 10.1126/science.274.5284.99.

Hsieh, H. *et al.* (2006) 'AMPAR removal underlies Aβ-induced synaptic depression and dendritic spine loss.', *Neuron*. Cell Press, 52(5), pp. 831–843. doi: 10.1016/J.NEURON.2006.10.035.

Hyman, B. T. *et al.* (2012) 'National Institute on Aging-Alzheimer's Association guidelines for the neuropathologic assessment of Alzheimer's disease.', *Alzheimer's & Dementia*. NIH Public Access, 8(1), pp. 1–13. doi: 10.1016/j.jalz.2011.10.007.

Imfeld, P. *et al.* (2013) 'Seizures in patients with Alzheimer's disease or vascular dementia: A population-based nested case-control analysis.', *Epilepsia*. John Wiley & Sons, Ltd (10.1111), 54(4), pp. 700–707. doi: 10.1111/epi.12045.

Ingelsson, M. *et al.* (2004) 'Early Aβ accumulation and progressive synaptic loss, gliosis, and tangle formation in AD brain.', *Neurology*. Wolters Kluwer Health, Inc. on behalf of the American Academy of Neurology, 62(6), pp. 925–931. doi: 10.1212/01.WNL.0000115115.98960.37.

International Clincal Trials Registry Platform. (2019) *A study comparing the safety and effects of a new compound, ACI-35 with placebo in patients with mild to moderate Alzheimer's disease*. Available at: http://www.isrctn.com/ISRCTN13033912 (Accessed: 3 July 2019).

Ittner, L. M. *et al.* (2010) 'Dendritic function of tau mediates amyloid-β toxicity in Alzheimer's disease mouse models.', *Cell*. Cell Press, 142(3), pp. 387–397. doi: 10.1016/J.CELL.2010.06.036.

Jack, C. R. *et al.* (2013) 'Tracking pathophysiological processes in Alzheimer's disease: An updated hypothetical model of dynamic biomarkers.', *The Lancet Neurology*. Elsevier, pp. 207–216. doi: 10.1016/S1474-4422(12)70291-0.

Jack, C. R. *et al.* (2018) 'NIA-AA Research Framework: toward a biological definition of Alzheimer's disease.', *Alzheimer's & Dementia*. Elsevier, 14(4), pp. 535–562. doi: 10.1016/J.JALZ.2018.02.018.

Jacobsen, J. S. *et al.* (2006) 'Early-onset behavioral and synaptic deficits in a mouse model of Alzheimer's disease.', *Proceedings of the National Academy of Sciences of the United States of America*. National Academy of Sciences, 103(13), pp. 5161–6. doi: 10.1073/pnas.0600948103.

Jan, A. *et al.* (2008) 'The ratio of monomeric to aggregated forms of Aβ40 and Aβ42 is an important determinant of amyloid-β aggregation, fibrillogenesis, and toxicity.', *The Journal of Biological Chemistry*. American Society for Biochemistry and Molecular Biology, 283(42), pp. 28176–89. doi: 10.1074/jbc.M803159200.

Jan, A., Hartley, D. M. and Lashuel, H. A. (2010) 'Preparation and characterization of toxic aβ aggregates for structural and functional studies in alzheimer's disease research.', *Nature*

Protocols. Nature Publishing Group, 5(6), pp. 1186–1209. doi: 10.1038/nprot.2010.72.

Jankowsky, J. L. *et al.* (2001) 'Co-expression of multiple transgenes in mouse CNS: a comparison of strategies.', *Biomolecular Engineering*. Elsevier, 17(6), pp. 157–165. doi: 10.1016/S1389-0344(01)00067-3.

Jawhar, S. *et al.* (2011) 'Overexpression of glutaminyl cyclase, the enzyme responsible for pyroglutamate A{beta} formation, induces behavioral deficits, and glutaminyl cyclase knock-out rescues the behavioral phenotype in 5XFAD mice.', *The Journal of Bbiological Chemistry*. American Society for Biochemistry and Molecular Biology, 286(6), pp. 4454–60. doi: 10.1074/jbc.M110.185819.

Jellinger, K. A. (2002) 'Alzheimer disease and cerebrovascular pathology: an update.', *Journal of Neural Transmission*. Springer-Verlag, 109(5–6), pp. 813–836. doi: 10.1007/s007020200068.

Jin, M. *et al.* (2011) 'Soluble amyloid β-protein dimers isolated from Alzheimer cortex directly induce Tau hyperphosphorylation and neuritic degeneration', *Proceedings of the National Academy of Sciences of the United States of America*. National Academy of Sciences, 108(14), pp. 5819–5824. doi: 10.1073/pnas.1017033108.

Kaether, C., Haass, C. and Steiner, H. (2006) 'Assembly, trafficking and function of γ-secretase.', *Neurodegenerative Diseases*. Karger Publishers, 3(4–5), pp. 275–283. doi: 10.1159/000095267.

Kam, T.-I. *et al.* (2013) 'FcγRIIb mediates amyloid-β neurotoxicity and memory impairment in Alzheimer's disease.', *The Journal of Clinical Investigation*. American Society for Clinical Investigation, 123(7), pp. 2791–2802. doi: 10.1172/JCI66827.

Kam, T. I., Gwon, Y. and Jung, Y. K. (2014) 'Amyloid beta receptors responsible for neurotoxicity and cellular defects in Alzheimer's disease.', *Cellular and Molecular Life Sciences*, 71(24), pp. 4803–4813. doi: 10.1007/s00018-014-1706-0.

Kamenetz, F. *et al.* (2003) 'APP processing and synaptic function.', *Neuron*. Cell Press, 37(6), pp. 925–937. doi: 10.1016/S0896-6273(03)00124-7.

Kang, J. *et al.* (1987) 'The precursor of Alzheimer's disease amyloid A4 protein resembles a cell-surface receptor.', *Nature*. Nature Publishing Group, 325(6106), pp. 733–736. doi: 10.1038/325733a0.

Karran, E. and De Strooper, B. (2016) 'The amyloid cascade hypothesis: are we poised for success or failure?', *Journal of Neurochemistry*. John Wiley & Sons, Ltd (10.1111), 139, pp. 237–252. doi: 10.1111/jnc.13632.

Kawahara, M. *et al.* (1997) 'Alzheimer's disease amyloid beta-protein forms Zn(2+)-sensitive, cation-selective channels across excised membrane patches from hypothalamic neurons.', *Biophysical Journal*, 73(1), pp. 67–75. doi: 10.1016/S0006-3495(97)78048-2.

Kawahara, M. *et al.* (2000) 'Alzheimer's β-amyloid, human islet amylin, and prion protein fragment evoke intracellular free calcium elevations by a common mechanism in a hypothalamic GnRH neuronal cell line TL- 275.', *The Journal of Biological Chemistry*, 275 VN-(19), pp. 14077–14083. doi: 10.1074/jbc.275.19.14077.

Kawarabayashi, T. *et al.* (2001) 'Age-dependent changes in brain, CSF, and plasma amyloid β protein in the Tg2576 transgenic mouse model of Alzheimer's disease.', *Journal of Neuroscience*. Society for Neuroscience, 21(2), pp. 372–381. doi: 10.1523/JNEUROSCI.21-02-00372.2001.

Kayed, R. *et al.* (2004) 'Permeabilization of lipid bilayers is a common conformation-dependent activity of soluble amyloid oligomers in protein misfolding diseases.', *The Journal of Biological Chemistry*. American Society for Biochemistry and Molecular Biology, 279(45), pp. 46363–6. doi: 10.1074/jbc.C400260200.

Kayed, R. *et al.* (2010) 'Conformation dependent monoclonal antibodies distinguish different replicating strains or conformers of prefibrillar Aβ oligomers.', *Molecular Neurodegeneration*. BioMed Central Ltd, 5(1), p. 57. doi: 10.1186/1750-1326-5-57.

Ke, Y. D. *et al.* (2012) 'Lessons from tau-deficient mice.', *International Journal of Alzheimer's Disease*. Hindawi, 2012, pp. 1–8. doi: 10.1155/2012/873270.

Keil, C. *et al.* (2004) 'Cloning, expression, crystallization and initial crystallographic analysis of the

C-terminal domain of the amyloid precursor protein APP.', *Acta Crystallographica Section D Biological Crystallography*. International Union of Crystallography, 60(9), pp. 1614–1617. doi: 10.1107/S0907444904015343.

Kelly, B. L. and Ferreira, A. (2006) 'β-Amyloid-induced dynamin 1 degradation is mediated by N-methyl-D-aspartate receptors in hippocampal neurons.', *The Journal of Biological Chemistry*. American Society for Biochemistry and Molecular Biology, 281(38), pp. 28079–89. doi: 10.1074/jbc.M605081200.

Kelly, B. L. and Ferreira, A. (2007) 'β-amyloid disrupted synaptic vesicle endocytosis in cultured hippocampal neurons.', *Neuroscience*. Pergamon, 147(1), pp. 60–70. doi: 10.1016/J.NEUROSCIENCE.2007.03.047.

Kelly, B. L., Vassar, R. and Ferreira, A. (2005) 'β-amyloid-induced dynamin 1 depletion in hippocampal neurons. A potential mechanism for early cognitive decline in Alzheimer disease.', *The Journal of Biological Chemistry*. American Society for Biochemistry and Molecular Biology, 280(36), pp. 31746–53. doi: 10.1074/jbc.M503259200.

Kibbey, M. C. *et al.* (1993) 'β-Amyloid precursor protein binds to the neurite-promoting IKVAV site of laminin.', *Proceedings of the National Academy of Sciences of the United States of America*. National Academy of Sciences, 90(21), pp. 10150–3. doi: 10.1073/PNAS.90.21.10150.

Kim, T. *et al.* (2013) 'Human LilrB2 is a β-amyloid receptor and its murine homolog PirB regulates synaptic plasticity in an Alzheimer's model.', *Science*. American Association for the Advancement of Science, 341(6152), pp. 1399–404. doi: 10.1126/science.1242077.

Kimura, R., Devi, L. and Ohno, M. (2010) 'Partial reduction of BACE1 improves synaptic plasticity, recent and remote memories in Alzheimer's disease transgenic mice.', *Journal of Neurochemistry*. John Wiley & Sons, Ltd (10.1111), 113(1), pp. 248–261. doi: 10.1111/j.1471-4159.2010.06608.x.

Kimura, R. and Ohno, M. (2009) 'Impairments in remote memory stabilization precede hippocampal synaptic and cognitive failures in 5XFAD Alzheimer mouse model.', *Neurobiology of Disease*. Academic Press, 33(2), pp. 229–235. doi: 10.1016/J.NBD.2008.10.006.

Kins, S. *et al.* (2006) 'Subcellular trafficking of the amyloid precursor protein gene family and its pathogenic role in Alzheimer's disease.', *Neurodegenerative Diseases*. Karger Publishers, 3(4–5), pp. 218–226. doi: 10.1159/000095259.

Klevanski, M. *et al.* (2014) 'Differential role of APP and APLPs for neuromuscular synaptic morphology and function.', *Molecular and Cellular Neuroscience*. Academic Press, 61, pp. 201–210. doi: 10.1016/J.MCN.2014.06.004.

von Koch, C. S. *et al.* (1997) 'Generation of APLP2 KO mice and early postnatal lethality in APLP2/APP double KO mice.', *Neurobiology of Aging*. Elsevier, 18(6), pp. 661–669. doi: 10.1016/S0197-4580(97)00151-6.

Koffie, R. M. *et al.* (2009) 'Oligomeric amyloid beta associates with postsynaptic densities and correlates with excitatory synapse loss near senile plaques.', *Proceedings of the National Academy of Sciences of the United States of America*. National Academy of Sciences, 106(10), pp. 4012–4017. doi: 10.1073/pnas.0811698106.

Kokubo, H. *et al.* (2005) 'Soluble Aβ oligomers ultrastructurally localize to cell processes and might be related to synaptic dysfunction in Alzheimer's disease brain.', *Brain Research*. Elsevier, 1031(2), pp. 222–228. doi: 10.1016/J.BRAINRES.2004.10.041.

Koppensteiner, P. *et al.* (2016) 'Time-dependent reversal of synaptic plasticity induced by physiological concentrations of oligomeric Aβ42: an early index of Alzheimer's disease.', *Scientific Reports*. Nature Publishing Group, 6(1), p. 32553. doi: 10.1038/srep32553.

Kuhn, P.-H. *et al.* (2010) 'ADAM10 is the physiologically relevant, constitutive alpha-secretase of the amyloid precursor protein in primary neurons.', *The EMBO journal*. EMBO Press, 29(17), pp. 3020–32. doi: 10.1038/emboj.2010.167.

Kummer, M. P. and Heneka, M. T. (2014) 'Truncated and modified amyloid-β species.', *Alzheimer's Research & Therapy*. BioMed Central, 6(3), p. 28. doi: 10.1186/alzrt258.

Kuner, P. and Hertel, C. (1998) 'NGF induces apoptosis in a human neuroblastoma cell line

expressing the neurotrophin receptor p75NTR.', *Journal of Neuroscience Research*. John Wiley & Sons, Ltd, 54(4), pp. 465–474. doi: 10.1002/(SICI)1097-4547(19981115)54:4<465::AID-JNR4>3.0.CO;2-T.

Lacor, P. N. *et al.* (2004) 'Synaptic targeting by Alzheimer's-related amyloid β oligomers.', *The Journal of Neuroscience : the official journal of the Society for Neuroscience*. Society for Neuroscience, 24(45), pp. 10191–10200. doi: 10.1523/JNEUROSCI.3432-04.2004.

Lacor, P. N. *et al.* (2007) 'Aβ oligomer-induced aberrations in synapse composition, shape, and density provide a molecular basis for loss of connectivity in Alzheimer's disease.', *The Journal of neuroscience : the official journal of the Society for Neuroscience*. Society for Neuroscience, 27(4), pp. 796–807. doi: 10.1523/JNEUROSCI.3501-06.2007.

Lambert, M. P. *et al.* (1998) 'Diffusible, nonfibrillar ligands derived from Aβ 1-42 are potent central nervous system neurotoxins', *Proceedings of the National Academy of Sciences of the United States of America*, 95(11), pp. 6448–6453. doi: 10.1073/pnas.95.11.6448.

Larson, J. *et al.* (1999) 'Alterations in synaptic transmission and long-term potentiation in hippocampal slices from young and aged PDAPP mice.', *Brain Research*. Elsevier, 840(1–2), pp. 23–35. doi: 10.1016/S0006-8993(99)01698-4.

Larson, M. *et al.* (2012) 'The complex PrPc-Fyn couples human oligomeric Aβ with pathological tau changes in Alzheimer's disease', *Journal of Neuroscience*. J Neurosci, 32(47), pp. 16857–16871. doi: 10.1523/JNEUROSCI.1858-12.2012.

Lasagna-Reeves, C. A. *et al.* (2011) 'Tau oligomers impair memory and induce synaptic and mitochondrial dysfunction in wild-type mice.', *Molecular Neurodegeneration*. BioMed Central, 6(1), p. 39. doi: 10.1186/1750-1326-6-39.

Laßek, M. *et al.* (2013) 'Amyloid precursor proteins are constituents of the presynaptic active zone.', *Journal of Neurochemistry*. John Wiley & Sons, Ltd (10.1111), 127(1), p. n/a-n/a. doi: 10.1111/jnc.12358.

Laurén, J. *et al.* (2009) 'Cellular prion protein mediates impairment of synaptic plasticity by amyloid-B oligomers.', *Nature*, 457(7233), pp. 1128–1132. doi: 10.1038/nature07761.

Lazarevic, V. *et al.* (2017) 'Physiological concentrations of amyloid β regulate recycling of synaptic vesicles via alpha7 acetylcholine receptor and CDK5/Calcineurin signaling.', *Frontiers in Molecular Neuroscience*. Frontiers, 10, p. 221. doi: 10.3389/fnmol.2017.00221.

Lee, S. H. *et al.* (2017) 'Super-resolution imaging of synaptic and extra-synaptic AMPA receptors with different-sized fluorescent probes.', *eLife*, 6. doi: 10.7554/eLife.27744.

Lesné, S. *et al.* (2006) 'A specific amyloid-β protein assembly in the brain impairs memory.', *Nature*. Nature Publishing Group, 440(7082), pp. 352–357. doi: 10.1038/nature04533.

Levy, E. *et al.* (1990) 'Mutation of the Alzheimer's disease amyloid gene in hereditary cerebral hemorrhage, Dutch type.', *Science (New York, N.Y.)*. American Association for the Advancement of Science, 248(4959), pp. 1124–6. doi: 10.1126/science.2111584.

Li, B. *et al.* (2007) 'Disruption of microtubule network by Alzheimer abnormally hyperphosphorylated tau.', *Acta Neuropathologica*. Springer-Verlag, 113(5), pp. 501–511. doi: 10.1007/s00401-007-0207-8.

Li, C. and Götz, J. (2017) 'Somatodendritic accumulation of Tau in Alzheimer's disease is promoted by Fyn-mediated local protein translation.', *The EMBO Journal*. John Wiley & Sons, Ltd, 36(21), pp. 3120–3138. doi: 10.15252/embj.201797724.

Li, S. *et al.* (2011) 'Soluble Aβ oligomers inhibit long-term potentiation through a mechanism involving excessive activation of extrasynaptic NR2B-containing NMDA receptors.', *Journal of Neuroscience*. Society for Neuroscience, 31(18), pp. 6627–6638. doi: 10.1523/JNEUROSCI.0203-11.2011.

Li, X. *et al.* (2011) 'Novel diffusion barrier for axonal retention of Tau in neurons and its failure in neurodegeneration.', *The EMBO Journal*, 30(23), pp. 4825–4837. doi: 10.1038/emboj.2011.376.

Lim, K. H. *et al.* (2007) 'Structural, dynamic properties of key residues in Aβ amyloidogenesis: implications of an important role of nanosecond timescale dynamics.', *ChemBioChem*. John Wiley

& Sons, Ltd, 8(11), pp. 1251–1254. doi: 10.1002/cbic.200700194.

Lovestone, S. *et al.* (2015) 'A phase II trial of tideglusib in Alzheimer's disease.', *Journal of Alzheimer's Disease*. IOS Press, 45(1), pp. 75–88. doi: 10.3233/JAD-141959.

Lu, J.-X. *et al.* (2013) 'Molecular structure of β-amyloid fibrils in Alzheimer's disease brain tissue.', *Cell*. Elsevier, 154(6), pp. 1257–68. doi: 10.1016/j.cell.2013.08.035.

Lue, L. F. *et al.* (1999) 'Soluble amyloid β peptide concentration as a predictor of synaptic change in Alzheimer's disease.', *The American Journal of Pathology*. Elsevier, 155(3), pp. 853–862. doi: 10.1016/S0002-9440(10)65184-X.

Luo, Y. *et al.* (2001) 'Mice deficient in BACE1, the Alzheimer's β-secretase, have normal phenotype and abolished β-amyloid generation.', *Nature Neuroscience*. Nature Publishing Group, 4(3), pp. 231–232. doi: 10.1038/85059.

Ma, T. *et al.* (2010) 'Dysregulation of the mTOR pathway mediates impairment of synaptic plasticity in a mouse model of Alzheimer's disease.', *PLoS ONE*. Edited by M. B. Feany. Public Library of Science, 5(9), p. e12845. doi: 10.1371/journal.pone.0012845.

Mairet-Coello, G. *et al.* (2013) 'The CAMKK2-AMPK kinase pathway mediates the synaptotoxic effects of Aβ oligomers through tau phosphorylation.', *Neuron*. Elsevier Inc., 78(1), pp. 94–108. doi: 10.1016/j.neuron.2013.02.003.

María Frade, J., Rodríguez-Tébar, A. and Barde, Y.-A. (1996) 'Induction of cell death by endogenous nerve growth factor through its p75 receptor.', *Nature*. Nature Publishing Group, 383(6596), pp. 166–168. doi: 10.1038/383166a0.

Martinez-Coria, H. *et al.* (2010) 'Memantine improves cognition and reduces Alzheimer's-like neuropathology in transgenic mice.', *The American Journal of Pathology*. Elsevier, 176(2), pp. 870–880. doi: 10.2353/AJPATH.2010.090452.

Martinez Hernandez, A. *et al.* (2018) 'The diphenylpyrazole compound anle138b blocks Aβ channels and rescues disease phenotypes in a mouse model for amyloid pathology.', *EMBO Molecular Medicine*. EMBO Press, 10(1), pp. 32–47. doi: 10.15252/emmm.201707825.

Masters, C. L. and Selkoe, D. J. (2012) 'Biochemistry of amyloid β-protein and amyloid deposits in Alzheimer's disease.', *Cold Spring Harbor Perspectives in Medicine*. Cold Spring Harbor Laboratory Press, 2(6), p. a006262. doi: 10.1101/CSHPERSPECT.A006262.

Matsui, T. *et al.* (2007) 'Expression of APP pathway mRNAs and proteins in Alzheimer's disease.', *Brain Research*. Elsevier, 1161, pp. 116–123. doi: 10.1016/J.BRAINRES.2007.05.050.

Mawuenyega, K. G. *et al.* (2010) 'Decreased clearance of CNS β-amyloid in Alzheimer's disease.', *Science (New York, N.Y.)*. American Association for the Advancement of Science, 330(6012), p. 1774. doi: 10.1126/science.1197623.

McKhann, G. M. *et al.* (2011) 'The diagnosis of dementia due to Alzheimer's disease: Recommendations from the National Institute on Aging-Alzheimer's Association workgroups on diagnostic guidelines for Alzheimer's disease.', *Alzheimer's & Dementia*. Elsevier Ltd, 7(3), pp. 263–269. doi: 10.1016/j.jalz.2011.03.005.

McLean, C. A. *et al.* (1999) 'Soluble pool of Aβ amyloid as a determinant of severity of neurodegeneration in Alzheimer's disease.', *Annals of Neurology*. John Wiley & Sons, Ltd, 46(6), pp. 860–866. doi: 10.1002/1531-8249(199912)46:6<860::AID-ANA8>3.0.CO;2-M.

McShane, R. *et al.* (2019) 'Memantine for dementia.', *Cochrane Database of Systematic Reviews*. John Wiley & Sons, Ltd, (3). doi: 10.1002/14651858.CD003154.pub6.

Min, S.-W. *et al.* (2015) 'Critical role of acetylation in tau-mediated neurodegeneration and cognitive deficits.', *Nature Medicine*. Nature Publishing Group, 21(10), pp. 1154–1162. doi: 10.1038/nm.3951.

Minkeviciene, R. *et al.* (2009) 'Amyloid β-induced neuronal hyperexcitability triggers progressive epilepsy.', *The Journal of neuroscience : the official journal of the Society for Neuroscience*. Society for Neuroscience, 29(11), pp. 3453–62. doi: 10.1523/JNEUROSCI.5215-08.2009.

Mitani, Y. *et al.* (2012) 'Differential effects between γ-secretase inhibitors and modulators on

cognitive function in amyloid precursor protein-transgenic and nontransgenic mice.', *The Journal of Neuroscience : the official journal of the Society for Neuroscience*. Society for Neuroscience, 32(6), pp. 2037–2050. doi: 10.1523/JNEUROSCI.4264-11.2012.

Moolman, D. L. *et al.* (2004) 'Dendrite and dendritic spine alterations in Alzheimer models.', *Journal of Neurocytology*, (33), pp. 377–387. doi: 10.1023/B:NEUR.0000044197.83514.64.

Mori, H. *et al.* (1992) 'Mass spectrometry of purified amyloid beta protein in Alzheimer's disease.', *The Journal of Biological Chemistry*. American Society for Biochemistry and Molecular Biology, 267, pp. 17082–17086. Available at: http://www.jbc.org/content/267/24/17082?ijkey=b2f76efcc88c1f6ef9f91ff13779995d7e2f0e38&keytype2=tf_ipsecsha (Accessed: 2 April 2019).

Mucke, L. *et al.* (2000) 'High-level neuronal expression of abeta 1-42 in wild-type human amyloid protein precursor transgenic mice: synaptotoxicity without plaque formation.', *The Journal of neuroscience : the official journal of the Society for Neuroscience*. Society for Neuroscience, 20(11), pp. 4050–8. doi: 10.1523/JNEUROSCI.20-11-04050.2000.

Mucke, L. and Selkoe, D. J. (2012) 'Neurotoxicity of amyloid β-protein: synaptic and network dysfunction.', *Cold Spring Harbor Perspectives in Medicine*. Cold Spring Harbor Laboratory Press, 2(7), p. a006338. doi: 10.1101/cshperspect.a006338.

Mullan, M. *et al.* (1992) 'A pathogenic mutation for probable Alzheimer's disease in the APP gene at the N–terminus of β–amyloid.', *Nature Genetics*. Nature Publishing Group, 1(5), pp. 345–347. doi: 10.1038/ng0892-345.

Müller, U. *et al.* (1994) 'Behavioral and anatomical deficits in mice homozygous for a modified β-amyloid precursor protein gene.', *Cell*. Elsevier, 79(5), pp. 755–65. doi: 10.1016/0092-8674(94)90066-3.

Müller, U. C., Deller, T. and Korte, M. (2017) 'Not just amyloid: Physiological functions of the amyloid precursor protein family.', *Nature Reviews Neuroscience*. Nature Publishing Group, 18(5), pp. 281–298. doi: 10.1038/nrn.2017.29.

Müller, U. C. and Zheng, H. (2012) 'Physiological functions of APP family proteins.', *Cold Spring Harbor Perspectives in Medicine*, 2(2). doi: 10.1101/cshperspect.a006288.

Murrell, J. *et al.* (1991) 'A mutation in the amyloid precursor protein associated with hereditary Alzheimer's disease.', *Science (New York, N.Y.)*. American Association for the Advancement of Science, 254(5028), pp. 97–9. doi: 10.1126/science.1925564.

Mutations Search | ALZFORUM (2019). Available at: https://www.alzforum.org/mutations/search?genes%5B%5D=348&diseases%5B%5D=145&keywords-entry=&keywords=#results (Accessed: 25 June 2019).

Nalbantoglu, J. *et al.* (1997) 'Impaired learning and LTP in mice expressing the carboxy terminus of the Alzheimer amyloid precursor protein.', *Nature*. Nature Publishing Group, 387(6632), pp. 500–505. doi: 10.1038/387500a0.

Narayan, P. *et al.* (2013) 'Single molecule characterization of the interactions between amyloid-beta peptides and the membranes of hippocampal cells.', *Journal of the American Chemical Society*, 135(4), pp. 1491–1498. doi: 10.1021/ja3103567.

Nilsberth, C. *et al.* (2001) 'The "Arctic" APP mutation (E693G) causes Alzheimer's disease by enhanced Aβ protofibril formation.', *Nature Neuroscience*. Nature Publishing Group, 4(9), pp. 887–893. doi: 10.1038/nn0901-887.

Nilsson, M. R. (2004) 'Techniques to study amyloid fibril formation in vitro.', *Methods*, pp. 151–160. doi: 10.1016/j.ymeth.2004.03.012.

Oakley, H. *et al.* (2006) 'Intraneuronal β-amyloid aggregates, neurodegeneration, and neuron loss in transgenic mice with five familial Alzheimer's disease mutations: potential factors in amyloid plaque formation.', *The Journal of neuroscience : the official journal of the Society for Neuroscience*. Society for Neuroscience, 26(40), pp. 10129–40. doi: 10.1523/JNEUROSCI.1202-06.2006.

Obregon, D. *et al.* (2012) 'Soluble amyloid precursor protein-α modulates β-secretase activity and amyloid-β generation.', *Nature Communications*. Nature Publishing Group, 3(1), p. 777. doi:

10.1038/ncomms1781.

Oddo, S. *et al.* (2003) 'Triple-transgenic model of Alzheimer's disease with plaques and tangles: Intracellular Aβ and synaptic dysfunction', *Neuron*. Cell Press, 39(3), pp. 409–421. doi: 10.1016/S0896-6273(03)00434-3.

Olsson, B. *et al.* (2016) 'CSF and blood biomarkers for the diagnosis of Alzheimer's disease: a systematic review and meta-analysis.', *The Lancet Neurology*. Elsevier, 15(7), pp. 673–684. doi: 10.1016/S1474-4422(16)00070-3.

Ossenkoppele, R. *et al.* (2015) 'Prevalence of amyloid PET positivity in dementia syndromes: a meta-analysis.', *JAMA*. American Medical Association, 313(19), pp. 1939–1949. doi: 10.1001/jama.2015.4669.

Ovsepian, S. V. *et al.* (2018) 'Synaptic vesicle cycle and amyloid β: biting the hand that feeds.', *Alzheimer's & Dementia*. Elsevier, 14(4), pp. 502–513. doi: 10.1016/J.JALZ.2018.01.011.

Palop, J. J. *et al.* (2007) 'Aberrant excitatory neuronal activity and compensatory remodeling of inhibitory hippocampal circuits in mouse models of Alzheimer's disease.', *Neuron*. Cell Press, 55(5), pp. 697–711. doi: 10.1016/J.NEURON.2007.07.025.

Palop, J. J. and Mucke, L. (2016) 'Network abnormalities and interneuron dysfunction in Alzheimer disease.', *Nature Reviews Neuroscience*. Nature Publishing Group, 17(12), pp. 777–792. doi: 10.1038/nrn.2016.141.

Panza, F. *et al.* (2016) 'Tau-based therapeutics for Alzheimer's disease: active and passive immunotherapy.', *Immunotherapy*. Future Medicine Ltd London, UK, 8(9), pp. 1119–1134. doi: 10.2217/imt-2016-0019.

Panza, F., Lozupone, M., Logroscino, G., *et al.* (2019) 'A critical appraisal of amyloid-β-targeting therapies for Alzheimer disease.', *Nature Reviews Neurology*. Nature Publishing Group, 15(2), pp. 73–88. doi: 10.1038/s41582-018-0116-6.

Panza, F., Lozupone, M., Dibello, V., *et al.* (2019) 'Are antibodies directed against amyloid-β (Aβ) oligomers the last call for the Aβ hypothesis of Alzheimer's disease?', *Immunotherapy*. Future Medicine Ltd London, UK, 11(1), pp. 3–6. doi: 10.2217/imt-2018-0119.

Park, D. *et al.* (2017) 'Activation of CaMKIV by soluble amyloid-β 1-42 impedes trafficking of axonal vesicles and impairs activity-dependent synaptogenesis.', *Science signaling*. American Association for the Advancement of Science, 10(487), p. eaam8661. doi: 10.1126/scisignal.aam8661.

Park, J., Jang, M. and Chang, S. (2013) 'Deleterious effects of soluble amyloid-β oligomers on multiple steps of synaptic vesicle trafficking.', *Neurobiology of Disease*. Academic Press, 55, pp. 129–139. doi: 10.1016/J.NBD.2013.03.004.

Parodi, J. *et al.* (2010) 'β-Amyloid causes depletion of synaptic vesicles leading to neurotransmission failure.', *The Journal of Biological Chemistry*, 285(4), pp. 2506–2514. doi: 10.1074/jbc.M109.030023.

Parvathy, S. *et al.* (1999) 'Cleavage of Alzheimer's amyloid precursor protein by α-secretase occurs at the surface of neuronal cells.', *Biochemistry*. American Chemical Society, 38(30), pp. 9728–9734. doi: 10.1021/BI9906827.

Perez, R. G. *et al.* (1999) 'Mutagenesis identifies new signals for β-amyloid precursor protein endocytosis, turnover, and the generation of secreted fragments, including Aβ42.', *The Journal of Biological Chemistry*. American Society for Biochemistry and Molecular Biology, 274(27), pp. 18851–6. doi: 10.1074/JBC.274.27.18851.

Petkova, A. T. *et al.* (2005) 'Self-propagating, molecular-level polymorphism in Alzheimer's beta-amyloid fibrils.', *Science*. American Association for the Advancement of Science, 307(5707), pp. 262–5. doi: 10.1126/science.1105850.

Pike, C. J. *et al.* (1991) 'In vitro aging of beta-amyloid protein causes peptide aggregation and neurotoxicity.', *Brain research*, 563(1–2), pp. 311–314. doi: 10.1016/0006-8993(91)91553-D.

Poirel, O. *et al.* (2018) 'Moderate decline in select synaptic markers in the prefrontal cortex (BA9) of patients with Alzheimer's disease at various cognitive stages.', *Scientific Reports*, 8(1), p. 938.

doi: 10.1038/s41598-018-19154-y.

Prangkio, P. *et al.* (2012) 'Multivariate analyses of amyloid-β oligomer populations indicate a connection between pore formation and cytotoxicity.', *PLoS ONE*, 7(10). doi: 10.1371/journal.pone.0047261.

Prince, M. *et al.* (2015) *World Alzheimer Report 2015. The global impact of dementia: an analysis of prevalence, incidence, cost and trends.*, *London: Alzheimer's Disease International*. Available at: https://apps.who.int/iris/bitstream/handle/10665/259615/9789241513487-eng.pdf?sequence=1 (Accessed: 14 February 2019).

Puzzo, D., Privitera, L., Leznik, E., Fà, M., Staniszewski, A., Palmeri, A. and Arancio, O. (2008) 'Picomolar amyloid-beta positively modulates synaptic plasticity and memory in hippocampus.', *The Journal of Neuroscience*. Society for Neuroscience, 28(53), pp. 14537–45. doi: 10.1523/jneurosci.2692-08.2008.

Puzzo, D., Privitera, L., Leznik, E., Fà, M., Staniszewski, A., Palmeri, A., Arancio, O., *et al.* (2008) 'Picomolar amyloid-β positively modulates synaptic plasticity and memory in hippocampus.', *The Journal of Neuroscience : the official journal of the Society for Neuroscience*. Society for Neuroscience, 28(53), pp. 1965–1975. doi: 10.1523/jneurosci.2692-08.2008.

Puzzo, D. *et al.* (2011) 'Endogenous amyloid-β is necessary for hippocampal synaptic plasticity and memory.', *Annals of Neurology*. John Wiley & Sons, Ltd, 69(5), pp. 819–830. doi: 10.1002/ana.22313.

Qin, K. *et al.* (2019) 'Anle138b prevents PrP plaque accumulation in Tg(PrP-A116V) mice but does not mitigate clinical disease.', *Journal of General Virology*. Microbiology Society, 100(6), pp. 1027–1037. doi: 10.1099/jgv.0.001262.

Quiroz, Y. T. *et al.* (2010) 'Hippocampal hyperactivation in presymptomatic familial Alzheimer's disease.', *Annals of Neurology*. John Wiley & Sons, Ltd, 68(6), pp. 865–875. doi: 10.1002/ana.22105.

Quist, A. P. *et al.* (2005) 'Amyloid ion channels: A common structural link for protein-misfolding disease.', *Proceedings of the National Academy of Sciences of the United States of America*, 102(30), pp. 10427–10432. doi: 10.1073/pnas.0502066102.

Rabizadeh, S. *et al.* (1994) 'Expression of the low-affinity nerve growth factor receptor enhances beta-amyloid peptide toxicity.', *Proceedings of the National Academy of Sciences of the United States of America*. National Academy of Sciences, 91(22), pp. 10703–6. doi: 10.1073/pnas.91.22.10703.

Research Models Search | ALZFORUM (2019). Available at: https://www.alzforum.org/research-models/search?species%5B%5D=319&diseases%5B%5D=145&genes=&types=&keywords-entry=&keywords=#results (Accessed: 9 June 2019).

Rezaei-Ghaleh, N. *et al.* (2011) 'Effect of zinc binding on β-amyloid structure and dynamics: implications for Aβ aggregation.', *Biophysical journal*. Elsevier, 101(5), pp. 1202–11. doi: 10.1016/j.bpj.2011.06.062.

Rhee, S. K., Quist, A. P. and Lal, R. (1998) 'Amyloid beta protein-(1-42) forms calcium-permeable, Zn2+-sensitive channel.', *The Journal of Biological Chemistry*. American Society for Biochemistry and Molecular Biology, 273(22), pp. 13379–82. doi: 10.1074/jbc.273.22.13379.

Rice, H. C. *et al.* (2019) 'Secreted amyloid-β precursor protein functions as a GABAB-R1a ligand to modulate synaptic transmission.', *Science*. American Association for the Advancement of Science, 363(6423), p. eaao4827. doi: 10.1126/science.aao4827.

Ring, S. *et al.* (2007) 'The secreted β-amyloid precursor protein ectodomain APPs alpha is sufficient to rescue the anatomical, behavioral, and electrophysiological abnormalities of APP-deficient mice.', *The Journal of Neuroscience : the official journal of the Society for Neuroscience*. Society for Neuroscience, 27(29), pp. 7817–26. doi: 10.1523/JNEUROSCI.1026-07.2007.

Ripamonti, S. *et al.* (2017) 'Transient oxytocin signaling primes the development and function of excitatory hippocampal neurons.', *eLife*, 6. doi: 10.7554/eLife.22466.

Ripoli, C. *et al.* (2013) 'Effects of different amyloid β-protein analogues on synaptic function.', *Neurobiology of Aging*. Elsevier Ltd, 34(4), pp. 1032–1044. doi:

10.1016/j.neurobiolaging.2012.06.027.

Ripoli, C. *et al.* (2014) 'Intracellular accumulation of amyloid-β (Aβ) protein plays a major role in Aβ -induced alterations of glutamatergic synaptic transmission and plasticity.', *The Journal of Neuroscience : the official journal of the Society for Neuroscience*. Society for Neuroscience, 34(38), pp. 12893–12903. doi: 10.1523/JNEUROSCI.1201-14.2014.

Roberson, E. D. *et al.* (2007) 'Reducing endogenous tau ameliorates amyloid β-induced deficits in an Alzheimer's disease mouse model.', *Science (New York, N.Y.)*. American Association for the Advancement of Science, 316(5825), pp. 750–4. doi: 10.1126/science.1141736.

Rossjohn, J. *et al.* (1999) 'Crystal structure of the N-terminal, growth factor-like domain of Alzheimer amyloid precursor protein.', *Nature Structural and Molecular Biology*. Nature Publishing Group, 6(4), pp. 327–331. doi: 10.1038/7562.

Roychaudhuri, R. *et al.* (2009) 'Amyloid β-protein assembly and Alzheimer disease.', *The Journal of Biological Chemistry*, 284(8), pp. 4749–4753. doi: 10.1074/jbc.R800036200.

Russell, C. L. *et al.* (2012) 'Amyloid-β acts as a regulator of neurotransmitter release disrupting the interaction between synaptophysin and VAMP2.', *PLoS ONE*. Edited by S. T. Ferreira. Public Library of Science, 7(8), p. e43201. doi: 10.1371/journal.pone.0043201.

Ryan, T. M. *et al.* (2013) 'Ammonium hydroxide treatment of Aβ produces an aggregate free solution suitable for biophysical and cell culture characterization.', *PeerJ*, p. e73. doi: 10.7717/peerj.73.

Sakono, M. and Zako, T. (2010) 'Amyloid oligomers: formation and toxicity of Aβ oligomers.', *FEBS Journal*. John Wiley & Sons, Ltd (10.1111), 277(6), pp. 1348–1358. doi: 10.1111/j.1742-4658.2010.07568.x.

Sando, R. *et al.* (2017) 'Assembly of Excitatory Synapses in the Absence of Glutamatergic Neurotransmission', *Neuron*. Cell Press, 94(2), pp. 312-321.e3. doi: 10.1016/j.neuron.2017.03.047.

Sannerud, R. *et al.* (2011) 'ADP ribosylation factor 6 (ARF6) controls amyloid precursor protein (APP) processing by mediating the endosomal sorting of BACE1.', *Proceedings of the National Academy of Sciences of the United States of America*. National Academy of Sciences, 108(34), pp. E559-68. doi: 10.1073/pnas.1100745108.

Sarlus, H. and Heneka, M. T. (2017) 'Microglia in Alzheimer's disease', *The Journal of Clinical Investigation*. American Society for Clinical Investigation, 127(9), pp. 3240–3249. doi: 10.1172/JCI90606.

Scheff, S. W., DeKosky, S. T. and Price, D. A. (1990) 'Quantitative assessment of cortical synaptic density in Alzheimer's disease.', *Neurobiology of Aging*. Elsevier, 11(1), pp. 29–37. doi: 10.1016/0197-4580(90)90059-9.

Schenk, D., Basi, G. S. and Pangalos, M. N. (2012) 'Treatment strategies targeting amyloid β-protein.', *Cold Spring Harbor perspectives in medicine*. Cold Spring Harbor Laboratory Press, 2(9), p. a006387. doi: 10.1101/cshperspect.a006387.

Scheuermann, S. *et al.* (2001) 'Homodimerization of amyloid precursor protein and its implication in the amyloidogenic pathway of Alzheimer's disease.', *The Journal of Biological Chemistry*. American Society for Biochemistry and Molecular Biology, 276(36), pp. 33923–9. doi: 10.1074/jbc.M105410200.

Schieb, H. *et al.* (2011) 'β-amyloid peptide variants in brains and cerebrospinal fluid from amyloid precursor protein (APP) transgenic mice: comparison with human Alzheimer amyloid.', *The Journal of Biological Chemistry*. American Society for Biochemistry and Molecular Biology, 286(39), pp. 33747–58. doi: 10.1074/jbc.M111.246561.

Schindelin, J. *et al.* (2012) 'Fiji: an open-source platform for biological-image analysis.', *Nature Methods*. Nature Publishing Group, 9(7), pp. 676–682. doi: 10.1038/nmeth.2019.

Seabrook, G. R. *et al.* (1999) 'Mechanisms contributing to the deficits in hippocampal synaptic plasticity in mice lacking amyloid precursor protein.', *Neuropharmacology*. Pergamon, 38(3), pp. 349–359. doi: 10.1016/S0028-3908(98)00204-4.

Sederberg, P. B. *et al.* (2006) 'Hippocampal and neocortical gamma oscillations predict memory formation in humans.', *Cerebral Cortex*. Narnia, 17(5), pp. 1190–1196. doi: 10.1093/cercor/bhl030.

Selkoe, D. J. (2002) 'Alzheimer's disease is a synaptic failure.', *Science*. American Association for the Advancement of Science, 298(5594), pp. 789–91. doi: 10.1126/science.1074069.

Selkoe, D. J. (2019) 'Alzheimer disease and aducanumab: adjusting our approach.', *Nature Reviews Neurology*. Nature Publishing Group, 15(7), pp. 365–366. doi: 10.1038/s41582-019-0205-1.

Selkoe, D. J. and Hardy, J. (2016) 'The amyloid hypothesis of Alzheimer's disease at 25 years.', *EMBO Molecular Medicine*. EMBO Press, 8(6), pp. 595–608. doi: 10.15252/emmm.201606210.

Sepulveda-Falla, D., Glatzel, M. and Lopera, F. (2012) 'Phenotypic profile of early-onset familial Alzheimer's disease caused by presenilin-1 E280A mutation.', *Journal of Alzheimer's Disease*. IOS Press, 32(1), pp. 1–12. doi: 10.3233/JAD-2012-120907.

Sepúlveda, F. J. *et al.* (2010) 'Synaptotoxicity of Alzheimer beta amyloid can be explained by its membrane perforating property.', *PLoS ONE*, 5(7), pp. 1–9. doi: 10.1371/journal.pone.0011820.

Sepúlveda, F. J. *et al.* (2014) 'Nature of the neurotoxic membrane actions of amyloid-β on hippocampal neurons in Alzheimer's disease.', *Neurobiology of Aging*. Elsevier Ltd, 35(3), pp. 472–481. doi: 10.1016/j.neurobiolaging.2013.08.035.

Serrano-Pozo, A. *et al.* (2011) 'Neuropathological alterations in Alzheimer disease.', *Cold Spring Harbor Perspectives in Medicine*. Cold Spring Harbor Laboratory Press, 1(1), pp. 1–23. doi: 10.1101/cshperspect.a006189.

Serrano-Pozo, A. *et al.* (2014) 'Mild to moderate Alzheimer dementia with insufficient neuropathological changes.', *Annals of Neurology*. John Wiley & Sons, Ltd, 75(4), pp. 597–601. doi: 10.1002/ana.24125.

Seubert, P. *et al.* (1992) 'Isolation and quantification of soluble Alzheimer's β-peptide from biological fluids.', *Nature*. Nature Publishing Group, 359(6393), pp. 325–327. doi: 10.1038/359325a0.

Sevigny, J. *et al.* (2016) 'The antibody aducanumab reduces Aβ plaques in Alzheimer's disease.', *Nature*. Nature Publishing Group, 537(7618), pp. 50–56. doi: 10.1038/nature19323.

Shankar, G. M. *et al.* (2007) 'Natural oligomers of the Alzheimer amyloid- protein induce reversible synapse loss by modulating an NMDA-type glutamate receptor-dependent signalling pathway.', *The Journal of Neuroscience : the official journal of the Society for Neuroscience*, 27(11), pp. 2866–2875. doi: 10.1523/JNEUROSCI.4970-06.2007.

Shankar, G. M. *et al.* (2008) 'Amyloid-β protein dimers isolated directly from Alzheimer's brains impair synaptic plasticity and memory.', *Nature Medicine*. Nature Publishing Group, 14(8), pp. 837–842. doi: 10.1038/nm1782.

Sharma, M., Burré, J. and Südhof, T. C. (2012) 'Proteasome inhibition alleviates SNARE-dependent neurodegeneration.', *Science translational medicine*. American Association for the Advancement of Science, 4(147), p. 147ra113. doi: 10.1126/scitranslmed.3004028.

Shipton, O. A. *et al.* (2011) 'Tau protein is required for amyloid β-induced impairment of hippocampal long-term potentiation.', *The Journal of neuroscience : the official journal of the Society for Neuroscience*. Society for Neuroscience, 31(5), pp. 1688–92. doi: 10.1523/JNEUROSCI.2610-10.2011.

Shoji, M. *et al.* (1992) 'Production of the Alzheimer amyloid-β protein by normal proteolytic processing.', *Science*. American Association for the Advancement of Science, 258(5079), pp. 126–9. doi: 10.1126/science.1439760.

Sigler, A. *et al.* (2017) 'Formation and Maintenance of Functional Spines in the Absence of Presynaptic Glutamate Release', *Neuron*. Cell Press, 94(2), pp. 304-311.e4. doi: 10.1016/j.neuron.2017.03.029.

Simakova, O. and Arispe, N. (2007) 'The cell-selective neurotoxicity of the Alzheimer's Aβ peptide is determined by surface phosphatidylserine and cytosolic ATP levels. Membrane binding is

required for Aβ toxicity.', *The Journal of Neuroscience : the official journal of the Society for Neuroscience*. Society for Neuroscience, 27(50), pp. 13719–29. doi: 10.1523/JNEUROSCI.3006-07.2007.

Sisodia, S. (1992) 'β-amyloid precursor protein cleavage by a membrane-bound protease.', *Proceedings of the National Academy of Sciences of the United States of America*. National Academy of Sciences, 89(13), pp. 6075–9. doi: 10.1073/PNAS.89.13.6075.

Siwek, M. E. *et al.* (2015) 'Altered theta oscillations and aberrant cortical excitatory activity in the 5XFAD model of Alzheimer's disease.', *Neural plasticity*. Hindawi, 2015, p. 781731. doi: 10.1155/2015/781731.

Smith, L. M. and Strittmatter, S. M. (2017) 'Binding sites for amyloid-β oligomers and synaptic toxicity.', *Cold Spring Harbor perspectives in medicine*. Cold Spring Harbor Laboratory Press, 7(5), p. a024075. doi: 10.1101/cshperspect.a024075.

Soba, P. *et al.* (2005) 'Homo- and heterodimerization of APP family members promotes intercellular adhesion.', *The EMBO Journal*. EMBO Press, 24(20), pp. 3624–3634. doi: 10.1038/sj.emboj.7600824.

Sokolow, S. *et al.* (2012) 'Preferential accumulation of amyloid-β in presynaptic glutamatergic terminals (VGluT1 and VGluT2) in Alzheimer's disease cortex.', *Neurobiology of Disease*. Academic Press, 45(1), pp. 381–387. doi: 10.1016/J.NBD.2011.08.027.

Song, D.-K. *et al.* (1998) 'Behavioral and neuropathologic changes induced by central injection of carboxyl-terminal fragment of β-amyloid precursor protein in mice.', *Journal of Neurochemistry*. John Wiley & Sons, Ltd (10.1111), 71(2), pp. 875–878. doi: 10.1046/j.1471-4159.1998.71020875.x.

Soto, C. (2003) 'Unfolding the role of protein misfolding in neurodegenerative diseases.', *Nature Reviews Neuroscience*, 4(1), pp. 49–60. doi: 10.1038/nrn1007.

Soto, C. and Pritzkow, S. (2018) 'Protein misfolding, aggregation, and conformational strains in neurodegenerative diseases.', *Nature Neuroscience*. Nature Publishing Group, pp. 1332–1340. doi: 10.1038/s41593-018-0235-9.

Sperling, R. A. *et al.* (2009) 'Amyloid deposition is associated with impaired default network function in older persons without dementia.', *Neuron*. Cell Press, 63(2), pp. 178–188. doi: 10.1016/J.NEURON.2009.07.003.

Sperling, R. A. *et al.* (2010) 'Functional alterations in memory networks in early Alzheimer's disease.', *NeuroMolecular Medicine*. Humana Press Inc, 12(1), pp. 27–43. doi: 10.1007/s12017-009-8109-7.

Spillantini, M. G. and Goedert, M. (2013) 'Tau pathology and neurodegeneration.', *The Lancet Neurology*. Elsevier Ltd, 12(6), pp. 609–622. doi: 10.1016/S1474-4422(13)70090-5.

Spires-Jones, T. and Knafo, S. (2012) 'Spines, plasticity, and cognition in Alzheimer's model mice.', *Neural plasticity*. Hindawi, 2012, p. 319836. doi: 10.1155/2012/319836.

Spires-Jones, T. L. and Hyman, B. T. (2014) 'The intersection of amyloid β and tau at synapses in Alzheimer's disease.', *Neuron*. Elsevier Inc., 82(4), pp. 756–771. doi: 10.1016/j.neuron.2014.05.004.

Spires, T. L. *et al.* (2005) 'Dendritic spine abnormalities in amyloid precursor protein transgenic mice demonstrated by gene transfer and intravital multiphoton microscopy.', *The Journal of Neuroscience : the official journal of the Society for Neuroscience*. Society for Neuroscience, 25(31), pp. 7278–87. doi: 10.1523/JNEUROSCI.1879-05.2005.

Steinbach, J. P. *et al.* (1998) 'Hypersensitivity to seizures in β-amyloid precursor protein deficient mice.', *Cell Death & Differentiation*. Nature Publishing Group, 5(10), pp. 858–866. doi: 10.1038/sj.cdd.4400391.

Stine, W. B. *et al.* (2003) 'In vitro characterization of conditions for amyloid-β peptide oligomerization and fibrillogenesis.', *The Journal of Biological Chemistry*. doi: 10.1074/jbc.M210207200.

De Strooper, B. *et al.* (1998) 'Deficiency of presenilin-1 inhibits the normal cleavage of amyloid

precursor protein.', *Nature*. Nature Publishing Group, 391(6665), pp. 387–390. doi: 10.1038/34910.

Syken, J. *et al.* (2006) 'PirB restricts ocular-dominance plasticity in visual cortex.', *Science*. American Association for the Advancement of Science, 313(5794), pp. 1795–1800. doi: 10.1126/SCIENCE.1128232.

Talantova, M. *et al.* (2013) 'Aβ induces astrocytic glutamate release, extrasynaptic NMDA receptor activation, and synaptic loss.', *Proceedings of the National Academy of Sciences of the United States of America*. National Academy of Sciences, 110(27), pp. E2518-27. doi: 10.1073/pnas.1306832110.

Tamayev, R. *et al.* (2012) 'β- but not γ-secretase proteolysis of APP causes synaptic and memory deficits in a mouse model of dementia.', *EMBO Molecular Medicine*. EMBO Press, 4(3), pp. 171–179. doi: 10.1002/emmm.201100195.

Tamayev, R., Zhou, D. and D'Adamio, L. (2009) 'The interactome of the amyloid β precursor protein family members is shaped by phosphorylation of their intracellular domains.', *Molecular Neurodegeneration*. BioMed Central, 4(1), p. 28. doi: 10.1186/1750-1326-4-28.

Tanzi, R. E. *et al.* (1987) 'Amyloid-β protein gene: CDNA, mRNA distribution, and genetic linkage near the Alzheimer locus.', *Science*. American Association for the Advancement of Science, 235(4791), pp. 880–884. doi: 10.1126/science.2949367.

Tanzi, R. E. and Bertram, L. (2005) 'Twenty years of the Alzheimer's disease amyloid hypothesis: A genetic perspective.', *Cell*. Cell Press, pp. 545–555. doi: 10.1016/j.cell.2005.02.008.

Taylor, C. J. *et al.* (2008) 'Endogenous secreted amyloid precursor protein-α regulates hippocampal NMDA receptor function, long-term potentiation and spatial memory.', *Neurobiology of Disease*. Academic Press, 31(2), pp. 250–260. doi: 10.1016/J.NBD.2008.04.011.

Tekirian, T. L. *et al.* (2002) 'Toxicity of pyroglutaminated amyloid β-peptides 3(pE)-40 and -42 is similar to that of Aβ 1-40 and -42.', *Journal of Neurochemistry*. John Wiley & Sons, Ltd (10.1111), 73(4), pp. 1584–1589. doi: 10.1046/j.1471-4159.1999.0731584.x.

Teplow, D. B. (2006) 'Preparation of amyloid β-protein for structural and functional studies.', *Methods in Enzymology*, 413(06), pp. 20–33. doi: 10.1016/S0076-6879(06)13002-5.

Terry, R. D. *et al.* (1991) 'Physical basis of cognitive alterations in Alzheimer's disease: synapse loss is the major correlate of cognitive impairment.', *Annals of Neurology*. John Wiley & Sons, Ltd, 30(4), pp. 572–580. doi: 10.1002/ana.410300410.

Thal, D. R. *et al.* (2002) 'Phases of Aβ deposition in the human brain and its relevance for the development of AD.', *Neurology*. Wolters Kluwer Health, Inc. on behalf of the American Academy of Neurology, 58(12), pp. 1791–800. doi: 10.1212/WNL.58.12.1791.

Thal, D. R. *et al.* (2015) 'Neuropathology and biochemistry of Aβ and its aggregates in Alzheimer's disease.', *Acta Neuropathologica*. Springer Berlin Heidelberg, 129(2), pp. 167–182. doi: 10.1007/s00401-014-1375-y.

Tort, A. B. L. *et al.* (2009) 'Theta-gamma coupling increases during the learning of item-context associations.', *Proceedings of the National Academy of Sciences of the United States of America*. National Academy of Sciences, 106(49), pp. 20942–7. doi: 10.1073/pnas.0911331106.

Townsend, M., Mehta, T. and Selkoe, D. J. (2007) 'Soluble Aβ inhibits specific signal transduction cascades common to the insulin receptor pathway.', *The Journal of Biological Chemistry*. American Society for Biochemistry and Molecular Biology, 282(46), pp. 33305–12. doi: 10.1074/jbc.M610390200.

Trinchese, F. *et al.* (2004) 'Progressive age-related development of Alzheimer-like pathology in APP/PS1 mice.', *Annals of Neurology*. John Wiley & Sons, Ltd, 55(6), pp. 801–814. doi: 10.1002/ana.20101.

Tsai, J. *et al.* (2004) 'Fibrillar amyloid deposition leads to local synaptic abnormalities and breakage of neuronal branches', *Nature Neuroscience*. Nature Publishing Group, 7(11), pp. 1181–1183. doi: 10.1038/nn1335.

Tycko, R. (2015) 'Amyloid polymorphism: structural basis and neurobiological relevance.',

Neuron. Elsevier, 86(3), pp. 632–645. doi: 10.1016/j.neuron.2015.03.017.

Um, J. W. *et al.* (2012) 'Alzheimer amyloid-β 42 oligomer bound to postsynaptic prion protein activates Fyn to impair neurons.', *Nature Neuroscience*. Nature Publishing Group, 15(9), pp. 1227–1235. doi: 10.1038/nn.3178.

Um, J. W. *et al.* (2013) 'Metabotropic glutamate receptor 5 is a coreceptor for Alzheimer Aβ oligomer bound to cellular prion protein.', *Neuron*. Cell Press, 79(5), pp. 887–902. doi: 10.1016/J.NEURON.2013.06.036.

US National Library of Medicine. ClinicalTrials.gov (2019a) *24 Months Safety and Efficacy Study of AADvac1 in Patients With Mild Alzheimer's Disease (ADAMANT)*. Available at: https://clinicaltrials.gov/ct2/show/NCT02579252?term=AADvac1&rank=4.

US National Library of Medicine. ClinicalTrials.gov (2019b) *A 24-Month Study to Evaluate the Efficacy and Safety of Elenbecestat (E2609) in Subjects With Early Alzheimer's Disease_ (MissionAD2)*. Available at: https://www.clinicaltrials.gov/ct2/show/NCT03036280 (Accessed: 2 July 2019).

US National Library of Medicine. ClinicalTrials.gov (2019c) *A 24-Month Study to Evaluate the Efficacy and Safety of Elenbecestat (E2609) in Subjects With Early Alzheimer's Disease (MissionAD1)*. Available at: https://www.clinicaltrials.gov/ct2/show/NCT02956486 (Accessed: 2 July 2019).

US National Library of Medicine. ClinicalTrials.gov (2019d) *A Safety, Tolerability, Pharmacokinetics, Pharmacodynamics and Preliminary Efficacy Study of TPI-287 in Alzheimer's Disease*. Available at: https://www.clinicaltrials.gov/ct2/show/NCT01966666?term=TPI+287&cond=Alzheimer+Disease&rank=1 (Accessed: 3 July 2019).

US National Library of Medicine. ClinicalTrials.gov (2019e) *A Study of CAD106 and CNP520 Versus Placebo in Participants at Risk for the Onset of Clinical Symptoms of Alzheimer's Disease (Generation S1)*. Available at: https://www.clinicaltrials.gov/ct2/show/NCT02565511?term=CNP520&rank=3 (Accessed: 2 July 2019).

US National Library of Medicine. ClinicalTrials.gov (2019f) *A Study of CNP520 Versus Placebo in Participants at Risk for the Onset of Clinical Symptoms of Alzheimer's Disease (Generation S2)*. Available at: https://www.clinicaltrials.gov/ct2/show/NCT03131453 (Accessed: 2 July 2019).

US National Library of Medicine. ClinicalTrials.gov (2019g) *A Study of Crenezumab Versus Placebo in Preclinical Presenilin1 (PSEN1) E280A Mutation Carriers to Evaluate Efficacy and Safety in the Treatment of Autosomal-Dominant Alzheimer's Disease (AD), Including a Placebo-Treated Non-Carrier Cohort.* Available at: https://clinicaltrials.gov/ct2/show/NCT01998841?term=crenezumab&rank=5 (Accessed: 2 July 2019).

US National Library of Medicine. ClinicalTrials.gov (2019h) *A Study of LY3303560 in Participants With Early Symptomatic Alzheimer's Disease*. Available at: https://www.clinicaltrials.gov/ct2/show/NCT03518073 (Accessed: 4 July 2019).

US National Library of Medicine. ClinicalTrials.gov (2019i) *A Study to Confirm Safety and Efficacy of BAN2401 in Participants With Early Alzheimer's Disease.* Available at: https://clinicaltrials.gov/ct2/show/NCT03887455?term=ban2401&draw=1&rank=1 (Accessed: 2 July 2019).

US National Library of Medicine. ClinicalTrials.gov (2019j) *A Study to Evaluate the Efficacy and Safety of ABBV-8E12 in Subjects With Early Alzheimer's Disease*. Available at: https://www.clinicaltrials.gov/ct2/show/NCT02880956 (Accessed: 4 July 2019).

US National Library of Medicine. ClinicalTrials.gov (2019k) *Clinical Trial of Solanezumab for Older Individuals Who May be at Risk for Memory Loss (A4)*. Available at: https://clinicaltrials.gov/ct2/show/NCT02008357?term=solanezumab&id=NCT02008357&rank=1 (Accessed: 2 July 2019).

US National Library of Medicine. ClinicalTrials.gov (2019l) *Dominantly Inherited Alzheimer Network Trial: An Opportunity to Prevent Dementia. A Study of Potential Disease Modifying*

Treatments in Individuals at Risk for or With a Type of Early Onset Alzheimer's Disease Caused by a Genetic Mutation (DIAN-TU). Available at: https://clinicaltrials.gov/ct2/show/NCT01760005?term=solanezumab&id=NCT01760005&rank=1 (Accessed: 2 July 2019).

US National Library of Medicine. ClinicalTrials.gov (2019m) *Efficacy and Safety Study of Gantenerumab in Participants With Early Alzheimer's Disease (AD).* Available at: https://www.clinicaltrials.gov/ct2/show/NCT03444870 (Accessed: 2 July 2019).

US National Library of Medicine. ClinicalTrials.gov (2019n) *Phase 2 Study of BIIB092 in Participants With Early Alzheimer's Disease (TANGO)*. Available at: https://clinicaltrials.gov/ct2/show/NCT03352557?term=BIIB092&cond=Alzheimer+Disease&rank=1 (Accessed: 3 July 2019).

US National Library of Medicine. ClinicalTrials.gov (2019o) *Phase 3 Study of Aducanumab (BIIB037) in Early Alzheimer's Disease (EMERGE).* Available at: https://www.clinicaltrials.gov/ct2/show/NCT02484547 (Accessed: 2 July 2019).

US National Library of Medicine. ClinicalTrials.gov (2019p) *Phase 3 Study of Aducanumab (BIIB037) in Early Alzheimer's Disease (ENGAGE)*. Available at: https://www.clinicaltrials.gov/ct2/show/NCT02477800 (Accessed: 2 July 2019).

US National Library of Medicine. ClinicalTrials.gov (2019q) *Safety, Tolerability, Pharmacokinetics, and Pharmacodynamics of IONIS-MAPTRx in Patients With Mild Alzheimer's Disease*. Available at: https://clinicaltrials.gov/ct2/show/NCT03186989?term=MAPTRx&rank=1 (Accessed: 3 July 2019).

US National Library of Medicine. ClinicalTrials.gov (2019r) *Safety and Efficacy Study of Gantenerumab in Participants With Early Alzheimer's Disease (AD).* Available at: https://www.clinicaltrials.gov/ct2/show/NCT03443973 (Accessed: 2 July 2019).

US National Library of Medicine. ClinicalTrials.gov (2019s) *Salsalate in Patients Mild to Moderate Alzheimer's Disease (SAL-AD)*. Available at: https://clinicaltrials.gov/ct2/show/NCT03277573?term=salsalate&cond=Alzheimer+Disease&rank=1 (Accessed: 3 July 2019).

Vadukul, D. M. *et al.* (2017) 'Amyloidogenicity and toxicity of the reverse and scrambled variants of amyloid-β 1-42.', *FEBS letters*. Wiley-Blackwell, 591(5), pp. 822–830. doi: 10.1002/1873-3468.12590.

Vardar, G. *et al.* (2016) 'Distinct functions of syntaxin-1 in neuronal maintenance, synaptic vesicle docking, and fusion in mouse neurons.', *The Journal of neuroscience : the official journal of the Society for Neuroscience*. Society for Neuroscience, 36(30), pp. 7911–24. doi: 10.1523/JNEUROSCI.1314-16.2016.

Vassar, R. *et al.* (1999) 'β-secretase cleavage of Alzheimer's amyloid precursor protein by the transmembrane aspartic protease BACE.', *Science*. American Association for the Advancement of Science, 286(5440), pp. 735–41. doi: 10.1126/SCIENCE.286.5440.735.

Verret, L. *et al.* (2012) 'Inhibitory interneuron deficit links altered network activity and cognitive dysfunction in Alzheimer's model.', *Cell*. Cell Press, 149(3), pp. 708–721. doi: 10.1016/J.CELL.2012.02.046.

Villemagne, V. L. *et al.* (2013) 'Amyloid β deposition, neurodegeneration, and cognitive decline in sporadic Alzheimer's disease: a prospective cohort study.', *The Lancet Neurology*. Elsevier, 12(4), pp. 357–367. doi: 10.1016/S1474-4422(13)70044-9.

Villemagne, V. L. *et al.* (2018) 'Imaging tau and amyloid-β proteinopathies in Alzheimer disease and other conditions.', *Nature Reviews Neurology*. Nature Publishing Group, 14(4), pp. 225–236. doi: 10.1038/nrneurol.2018.9.

Vodopivec, I. *et al.* (2009) 'RAGE does not affect amyloid pathology in transgenic ArcAβ mice.', *Neurodegenerative Diseases*. Karger Publishers, 6(5–6), pp. 270–280. doi: 10.1159/000261723.

Vossel, K. A. *et al.* (2013) 'Seizures and epileptiform activity in the early stages of Alzheimer's disease.', *JAMA Neurology*. American Medical Association, 70(9), p. 1158. doi: 10.1001/jamaneurol.2013.136.

Wagner, J. *et al.* (2013) 'Anle138b: A novel oligomer modulator for disease-modifying therapy of neurodegenerative diseases such as prion and Parkinson's disease.', *Acta Neuropathologica*, 125(6), pp. 795–813. doi: 10.1007/s00401-013-1114-9.

Wagner, J. *et al.* (2015) 'Reducing tau aggregates with anle138b delays disease progression in a mouse model of tauopathies.', *Acta Neuropathologica*. Springer Berlin Heidelberg, 130(5), pp. 619–631. doi: 10.1007/s00401-015-1483-3.

Walsh, D. M. *et al.* (2002) 'Amyloid-β oligomers: their production, toxicity and therapeutic inhibition.', *Biochemical Society Transactions*, 30(4), pp. 552–557. doi: 10.1042/bst0300552.

Walsh, Dominic M. *et al.* (2002) 'Naturally secreted oligomers of amyloid β protein potently inhibit hippocampal long-term potentiation in vivo', *Nature*. Nature Publishing Group, 416(6880), pp. 535–539. doi: 10.1038/416535a.

Wang, P. *et al.* (2005) 'Defective neuromuscular synapses in mice lacking amyloid precursor protein (APP) and APP-Like protein 2.', *The Journal of Neuroscience : the official journal of the Society for Neuroscience*. Society for Neuroscience, 25(5), pp. 1219–25. doi: 10.1523/JNEUROSCI.4660-04.2005.

Wang, Y. and Ha, Y. (2004) 'The X-ray structure of an antiparallel dimer of the human amyloid precursor protein E2 domain.', *Molecular Cell*. Cell Press, 15(3), pp. 343–353. doi: 10.1016/J.MOLCEL.2004.06.037.

Wang, Z. *et al.* (2009) 'Presynaptic and postsynaptic interaction of the amyloid precursor protein promotes peripheral and central synaptogenesis.', *The Journal of Neuroscience : the official journal of the Society for Neuroscience*. Society for Neuroscience, 29(35), pp. 10788–10801. doi: 10.1523/JNEUROSCI.2132-09.2009.

Wasco, W. *et al.* (1992) 'Identification of a mouse brain cDNA that encodes a protein related to the Alzheimer disease-associated amyloid beta protein precursor.', *Proceedings of the National Academy of Sciences of the United States of America*. National Academy of Sciences, 89(22), pp. 10758–62. doi: 10.1073/PNAS.89.22.10758.

Wasco, W. *et al.* (1993) 'Isolation and characterization of APLP2 encoding a homologue of the Alzheimer's associated amyloid β protein precursor.', *Nature Genetics*. Nature Publishing Group, 5(1), pp. 95–100. doi: 10.1038/ng0993-95.

Wegrzynowicz, M. *et al.* (2019) 'Depopulation of dense α-synuclein aggregates is associated with rescue of dopamine neuron dysfunction and death in a new Parkinson's disease model.', *Acta Neuropathologica*. Springer Berlin Heidelberg, pp. 1–21. doi: 10.1007/s00401-019-02023-x.

Wei, W. *et al.* (2010) 'Amyloid β from axons and dendrites reduces local spine number and plasticity.', *Nature Neuroscience*, 13(2), pp. 190–196. doi: 10.1038/nn.2476.

Weidemann, A. *et al.* (1989) 'Identification, biogenesis, and localization of precursors of Alzheimer's disease A4 amyloid protein.', *Cell*. Cell Press, 57(1), pp. 115–126. doi: 10.1016/0092-8674(89)90177-3.

Weyer, S. W. *et al.* (2014) 'Comparative analysis of single and combined APP/APLP knockouts reveals reduced spine density in APP-KO mice that is prevented by APPsα expression.', *Acta Neuropathologica Communications*. BioMed Central, 2(1), p. 36. doi: 10.1186/2051-5960-2-36.

White, A. R. *et al.* (1999) 'Copper levels are increased in the cerebral cortex and liver of APP and APLP2 knockout mice.', *Brain Research*. Elsevier, 842(2), pp. 439–444. doi: 10.1016/S0006-8993(99)01861-2.

WHO (2017a) *Dementia.*, *Dementia. World Health Organization*. Available at: https://www.who.int/en/news-room/fact-sheets/detail/dementia (Accessed: 13 February 2019).

WHO (2017b) *Global action plan on the public health response to dementia 2017 - 2025.*, *Geneva: World Health Organization.* World Health Organization. doi: Licence: CC BY-NC-SA 3.0 IGO.

WHO (2018) *Towards a dementia plan: a WHO guide.*, *WHO*. World Health Organization. Available at: https://www.who.int/mental_health/neurology/dementia/policy_guidance/en/ (Accessed: 13 February 2019).

Wiessner, C. *et al.* (2011) 'The second-generation active Aβ immunotherapy CAD106 reduces

amyloid accumulation in APP transgenic mice while minimizing potential side effects.', *Journal of Neuroscience*. Society for Neuroscience, 31(25), pp. 9323–9331. doi: 10.1523/JNEUROSCI.0293-11.2011.

de Wilde, M. C. *et al.* (2016) 'Meta-analysis of synaptic pathology in Alzheimer's disease reveals selective molecular vesicular machinery vulnerability.', *Alzheimer's & Dementia*. Elsevier, 12(6), pp. 633–644. doi: 10.1016/J.JALZ.2015.12.005.

Willem, M. *et al.* (2015) 'η-Secretase processing of APP inhibits neuronal activity in the hippocampus.', *Nature*. Nature Publishing Group, 526(7573), pp. 443–447. doi: 10.1038/nature14864.

Winblad, B. *et al.* (2012) 'Safety, tolerability, and antibody response of active Aβ immunotherapy with CAD106 in patients with Alzheimer's disease: randomised, double-blind, placebo-controlled, first-in-human study.', *The Lancet Neurology*. Elsevier, 11(7), pp. 597–604. doi: 10.1016/S1474-4422(12)70140-0.

Wischik, C. M. *et al.* (1996) 'Selective inhibition of Alzheimer disease-like tau aggregation by phenothiazines.', *Proceedings of the National Academy of Sciences of the United States of America*. National Academy of Sciences, 93(20), pp. 11213–8. doi: 10.1073/pnas.93.20.11213.

Wu, H.-Y. *et al.* (2010) 'Amyloid beta induces the morphological neurodegenerative triad of spine loss, dendritic simplification, and neuritic dystrophies through calcineurin activation.', *The Journal of neuroscience : the official journal of the Society for Neuroscience*. Society for Neuroscience, 30(7), pp. 2636–49. doi: 10.1523/JNEUROSCI.4456-09.2010.

Xia, D., Li, C. and Götz, J. (2015) 'Pseudophosphorylation of Tau at distinct epitopes or the presence of the P301L mutation targets the microtubule-associated protein Tau to dendritic spines.', *Biochimica et Biophysica Acta (BBA) - Molecular Basis of Disease*. Elsevier, 1852(5), pp. 913–924. doi: 10.1016/J.BBADIS.2014.12.017.

Xiao, Y. *et al.* (2015) 'Aβ(1–42) fibril structure illuminates self-recognition and replication of amyloid in Alzheimer's disease.', *Nature Structural and Molecular Biology*. Nature Publishing Group, 22(6), pp. 499–505. doi: 10.1038/nsmb.2991.

Yan, Y. and Wang, C. (2006) 'Aβ42 is more rigid than Aβ40 at the C terminus: implications for Aβ aggregation and toxicity.', *Journal of Molecular Biology*. Academic Press, 364(5), pp. 853–862. doi: 10.1016/j.jmb.2006.09.046.

Yang, L. *et al.* (2009) 'Amyloid precursor protein regulates Cav1.2 L-type calcium channel levels and function to influence GABAergic short-term plasticity.', *The Journal of Neuroscience : the official journal of the Society for Neuroscience*. Society for Neuroscience, 29(50), pp. 15660–15668. doi: 10.1523/JNEUROSCI.4104-09.2009.

Yang, Y. *et al.* (2015) 'Amyloid-β Oligomers May Impair SNARE-Mediated Exocytosis by Direct Binding to Syntaxin 1a', *Cell Reports*. Cell Press, 12(8), pp. 1244–1251. doi: 10.1016/j.celrep.2015.07.044.

Zempel, H. *et al.* (2010) 'Aβ oligomers cause localized Ca2+ elevation, missorting of endogenous tau into dendrites, tau phosphorylation, and destruction of microtubules and spines.', *The Journal of Neuroscience : the official journal of the Society for Neuroscience*. Society for Neuroscience, 30(36), pp. 11938–11950. doi: 10.1523/JNEUROSCI.2357-10.2010.

Zempel, H. *et al.* (2013) 'Amyloid-β oligomers induce synaptic damage via Tau-dependent microtubule severing by TTLL6 and spastin', *EMBO Journal*. EMBO J, 32(22), pp. 2920–2937. doi: 10.1038/emboj.2013.207.

Zhang, Y. *et al.* (1996) 'The lipid compositions of different regions of rat brain during development and aging', *Neurobiology of Aging*. Elsevier, 17(6), pp. 869–875. doi: 10.1016/S0197-4580(96)00076-0.

Zhao, G. *et al.* (2010) 'γ-secretase composed of PS1/Pen2/Aph1a can cleave notch and amyloid precursor protein in the absence of nicastrin.', *The Journal of Neuroscience : the official journal of the Society for Neuroscience*. Society for Neuroscience, 30(5), pp. 1648–56. doi: 10.1523/JNEUROSCI.3826-09.2010.

Zhao, W.-Q. *et al.* (2008) 'Amyloid beta oligomers induce impairment of neuronal insulin

receptors.', *The FASEB Journal*. Federation of American Societies for Experimental Biology, 22(1), pp. 246–260. doi: 10.1096/fj.06-7703com.

Zheng, H. *et al.* (1995) 'β-Amyloid precursor protein-deficient mice show reactive gliosis and decreased locomotor activity.', *Cell*, 81(4), pp. 525–31. Available at: http://www.ncbi.nlm.nih.gov/pubmed/7758106 (Accessed: 11 April 2019).

Zhou, L. *et al.* (2017) 'Tau association with synaptic vesicles causes presynaptic dysfunction.', *Nature Communications*. Nature Publishing Group, 8(1), p. 15295. doi: 10.1038/ncomms15295.

Zou, C. *et al.* (2016) 'Amyloid precursor protein maintains constitutive and adaptive plasticity of dendritic spines in adult brain by regulating D-serine homeostasis.', *The EMBO Journal*. EMBO Press, 35(20), pp. 2213–2222. doi: 10.15252/embj.201694085.

Acknowledgements

I would like to make use of this very important moment for me to say thank you and feel grateful.

First, I would like to thank Prof. Christian Griesinger for believing in me from day one in Buenos Aires, opening doors for me and for trusting me with our beloved anle project. He was and is a constant fuel for curiosity and motivation in my lab work.

I also wish to say thank you to Prof. JeongSeop Rhee, who constantly supported me, at every moment in the day (or the night!) at the setup. Thank you for believing that I could be an electrophysiologist, for teaching me to be patient but work hard, and for always having a word of wisdom and support.

I would like to thank also Prof. Nils Brose for letting me be part of his Lab, in which I grew as a person and as a scientist. Many of the lessons I learnt during my PhD, I learnt them from him.

I also want to thank Prof. Ralf Heinrich, for his commitment during the Thesis Committee Meetings, and also for the time and career advice. It was good to know that there was someone always on my side at the University.

I would also like to take the chance to say thank you to the members of the Extended Examination Board, Prof. Tiago Outeiro, Prof. Luis Pardo and Prof. Christine Stadelmann. Thank you for your time, your flexibility and because each of you at different moments in my PhD had a word of support and was always willing to help me.

I wish to thank the collaborators during this study: Prof. Tiago Outeiro, Prof. Luis Pardo, Prof. Roland Benz and members of his lab, Prof. Olaf Jahn and Thomas Liepold, Uwe Pleßmann and Prof. Henning Urlaub, Sergey Ryazanov, Kris Runge and Dr. Nasrollah Rezaei-Ghalleh from the NMR-based Structural Biology department, and Ben Cooper, Lydia Bickford and Ali Shaib from the Molecular Neurobiology department. Thanks for your time, for always being open for questions and discussion and for your invaluable contribution to this project.

I also want to thank Prof. Dieter Heineke, from the Dean’s Office for his help with my thesis presentation.

I would like to thank specially Anja Guenther for her excellent technical support, for being open to teaching me cell culture techniques and many more lab tasks, and also for her kind company during my work at the setup.

I would like to also acknowledge the technical support of the members of the Synapse Physiology group in the Molecular Neurobiology department, HongJun Rhee and ChungKu Lee, for their help with primary cultures, and also for the long hours trying to get “one more cell” side to side at the setup.

I would like to acknowledge the support of some colleagues without whom this thesis would still be a blank page: Fran and Ali, for supporting and encouraging me in the most difficult times, Cordelia, for always asking, even when she did not have a second of free time, she made that second to ask how all was going.

I would like to specially thank the people who corrected this manuscript: Erinn (and Blob), James and Damian. A big thank you for helping me to improve my writing and to sharpen my view as a scientist.

I would also like to thank all the members of the Molecular Neurobiology department, present or former who had an impact in this project and in my life during my PhD, in particular Nandhini, Riikka, Silvia, Dennis and James. A big thank you for all that I learnt from you and with you. Mary and Sünke, Sofia and Kerstin, thank you for the moments shared. And all the friends and colleagues who made the everyday Lab life easier and better: Ben, Olga, Hugo, Bekir, Julia, Nati, Peter, Manu, Aisha, Ahmed, Heba, Noa, Theo, Sven, Dilja, Öyküm, Jennifer.

In addition, I would like to acknowledge the support of my friends in Germany and in Argentina: Noe, Colo, Eu, Nati, Fede, Sün, Alonso and Andrés. Special thanks to the fantastic Running group: Erinn, Silvia, Lydia and Julia. Also, a big thank you to my volleyball team, who supported me throughout my PhD: thank you, my dear Closed group!

Finally, I would like to specially thank my family and acknowledge their support and efforts to give me the chance of pursuing my dreams: my mum Graciela, my dad Gustavo, my brothers Fede and Ger, and also a special thanks to Maria José, Tani, Cale and Dani.

I dedicate this work first to my partner Pablo, who makes me a better person every day.

Dedico este trabajo a mi compañero Pablo, quien me hace una mejor persona cada día.

I also dedicate this Thesis to my grandparents, Coco and Nora, Alcides and Laura, Mary and Alberto. You made me who I am.

Dedico ésta tesis a mis abuelitos Coco y Nora, Alcides y Laura, Mary y Alberto. Ustedes me hicieron quien soy.